12-2008

Accelerated Thermal Aging of Fe-Zeolite SCR Catalysts on an Engine Bench

Adam Lamar Foster
University of Tennessee - Knoxville

To the Graduate Council:

I am submitting herewith a thesis written by Adam Lamar Foster entitled "Accelerated Thermal Aging of Fe-Zeolite SCR Catalysts on an Engine Bench." I have examined the final electronic copy of this thesis for form and content and recommend that it be accepted in partial fulfillment of the requirements for the degree of Master of Science, with a major in Mechanical Engineering.

Ke Nguyen, Major Professor

We have read this thesis and recommend its acceptance:

Bruce G. Bunting, Todd J. Toops, J. Roger Parsons

Accepted for the Council:
Carolyn R. Hodges

Vice Provost and Dean of the Graduate School

(Original signatures are on file with official student records.)

To the Graduate Council:

I am submitting herewith a thesis written by Adam Lamar Foster entitled "Accelerated Thermal Aging of Fe-Zeolite SCR Catalysts on an Engine Bench." I have examined the final electronic copy of this thesis for form and content and recommend that it be accepted in partial fulfillment of the requirements for the degree of Master of Science, with a major in Mechanical Engineering.

Ke Nguyen
Major Professor

We have read this thesis and
Recommend its acceptance:

Bruce G. Bunting

Todd J. Toops

J. Roger Parsons

Accepted for the Council:

Carolyn R. Hodges
Vice Provost and Dean of the Graduate School

(Original signatures are on file with official student records.)

ACCELERATED THERMAL AGING OF IRON-ZEOLITE SCR CATALYST ON AN ENGINE BENCH

A Thesis

Presented for the

Master of Science

Degree

The University of Tennessee, Knoxville

Adam Lamar Foster

December 2008

DEDICATION

To my wife, Julie, and my father, Raynard, for their love, support and inspiration

ACKNOWLEDGEMENTS

I would like thank my advisor, Dr. Ke Nguyen, for his encouragement, patience and insight throughout the duration of this project, without which this work would not have been possible. I would also like to express my gratitude to my co-advisors, Dr. Todd Toops and Dr. Bruce Bunting, for their technical knowledge, wisdom and guidance as well as my other graduate committee member Dr. J. Roger Parsons for his valued feedback. Within Oak Ridge National Laboratory, I want to thank Dr. Roberta A. Miesner, Dr. Jim Szibits, Scott Eaton, Vitaly Prikohdko and Adam Youngquist for their individual contributions to not only my project, but also my technical growth and confidence. In additions I want to express my appreciation to my laboratory colleague, Nathan Ottinger, for his support and friendship during this project.

Lastly, I want to thank the U.S. Department of Energy (DOE), Office of Energy Efficiency and Renewable Energy/FreedomCAR and Vehicle Technologies Program for their financial support of this research.

ABSTRACT

Selective catalytic reduction (SCR) of NO_x with urea/NH_3 is a leading candidate to the impending more stringent emissions regulations for diesel engines. Currently, there is no consensus on the durability and the deactivation mechanisms associated with zeolite-based SCR catalysts, nor is there an established protocol for rapidly aging zeolite-based SCR catalysts that replicates the catalyst deactivation associated with field service. A 517 cc single-cylinder, naturally-aspirated direct injection (NA/DI) diesel engine is used to perform accelerated thermal aging on Fe-zeolite SCR catalysts. The engine is fitted with an exhaust aftertreatment system consisting of a DOC, a SCR catalyst and a DPF. Accelerated aging protocol established for the SCR catalyst utilizes high temperature exhaust gases during the active regeneration of the DPF. Accelerated aging is carried out at exhaust gas temperatures of 650, 750 and 850°C at the SCR inlet and at a gas hourly space velocity (GHSV) of approximately 40,000 h^{-1}. The engine is maintained at 1500 rpm and supplemental fuel is injected upstream of the DOC to alter the temperature of the aftertreatment system. The aged Fe-zeolite SCR catalysts are evaluated for NO_x performance in a bench-flow reactor and characterized by multiple surface characterization techniques for materials changes.

The NO_x performance of the front sections of the engine-aged catalysts is severely degraded. BET surface area measurements of the engine-aged catalyst indicate a severe reduction of catalyst surface area in the front sections of the catalysts aged at 750 and 850°C. However, the catalyst aged at 650°C has a catalyst surface area similar to that of a fresh catalyst; thereby ruling out reduction of catalyst surface area as the sole cause of the catalyst deactivation seen in the front sections of the engine-aged catalysts. The similar shape of the NO_x conversion profiles observed with these catalyst sections even at different aging temperatures indicates some type of catalyst poisoning; however, the cause of catalyst degradation in these catalyst sections is not identified in this investigation.

There is a good relationship between the NO_x performance and catalyst aging temperature for the rear sections of the engine-aged catalysts – NO_x performance decreases with increasing aging temperature. XRD patterns and NO oxidation experiments reveal evidence of

zeolite dealumination in the engine-aged catalysts. BET surface area measurements show that catalyst surface area decreases with increasing aging temperature, which further supports the suggestion of zeolite dealumination as the cause of catalyst deactivation in the rear sections of the engine-aged catalysts.

A comparison between the engine-aged and field-aged catalysts is conducted to assess the validity of the implemented accelerated thermal aging protocol in replicating the aging conditions observed in the field-aged catalyst. Bench-flow reactor evaluation is used to determine the NO_x performance of the engine-aged and field-aged catalysts, and in depth surface studies are used to determine the deactivation mechanisms associated with each type of catalyst aging. SEM micrographs and BET surface area measurements of the aged catalysts show that the deactivation mechanism associated with catalyst aging is primarily physical damage to the zeolite washcoat for both the field-aged and engine-aged catalysts. Furthermore, X-ray diffraction and NO oxidation experiments identify zeolite dealumination as the underlying cause of the washcoat degradation. Finally, BFR evaluation shows that the NO_x performance of the catalyst aged at 750°C for approximately 50 hours compares very well to that of the field-aged catalyst with a service life of 3 years. It is concluded that accelerated thermal aging on the engine bench is successful in bringing about similar catalyst changes to those seen with the field-aged catalyst.

TABLE OF CONTENTS

LIST OF TABLES

LIST OF FIGURES

CHAPTER 1 INTRODUCTION

This chapter presents the rationales which motivate the present study of Fe-Zeolite selective catalytic reduction (SCR) catalysts. Section 1.1 contains an overview of the benefits and problems associated with the use of diesel engines for both transportation and utility applications. Current and future emissions regulations for diesel engines are discussed in Section 1.2. A brief review of the current NO_x abatement technologies for meeting the ever increasingly stringent emissions regulations is given in Section 1.3. Finally, an overview of the objectives of the current investigation is presented in Section 1.4

1.1 Overview

Diesel engines encompass a large percentage of power producing devices worldwide. The majority of diesel engines are used in automotive applications. A study conducted in 1995 by Mori estimated that 67 million of the 640 million automobiles worldwide were powered by diesel engines [2]. Although spark ignition (SI) engines make up the vast majority of the vehicle population, diesel engines have received considerable interest in recent years due to their inherent high fuel efficiency and durability. Typical SI engines are designed for a 100,000 mile lifetime, while diesel engines are typically expected to last as long as 500,000 miles, and some heavy-duty diesel engines are targeted to achieve as much as 1 million miles. The SI engines use a throttle and operate at a stoichiometric air/fuel ratio, which leads to a significant amount of unburned hydrocarbon emissions. Diesel engines, on the other hand, are un-throttled and have much higher compression ratios with a lean air/fuel ratio, which results in a higher percentage of fuel consumed during each power stroke. Therefore, diesel engines produce more energy per volume of fuel. The benefits of the diesel engines have made them a popular choice in many heavy-duty applications [3]. As evidenced in Figure 1.1, diesel engines power more than 90% of the world's buses, trains and freight trucking services [4].

Aside from the economic advantages, the use of diesel engines also has an environmental impact. The production of green-house gases from the burning of fossil fuels is the main cause of global warming. According to the EPA, total U.S. emissions have grown 16.3% between 1990 and 2005. Green-house gas emissions such as CO_2 from transportation activities rose by 32%

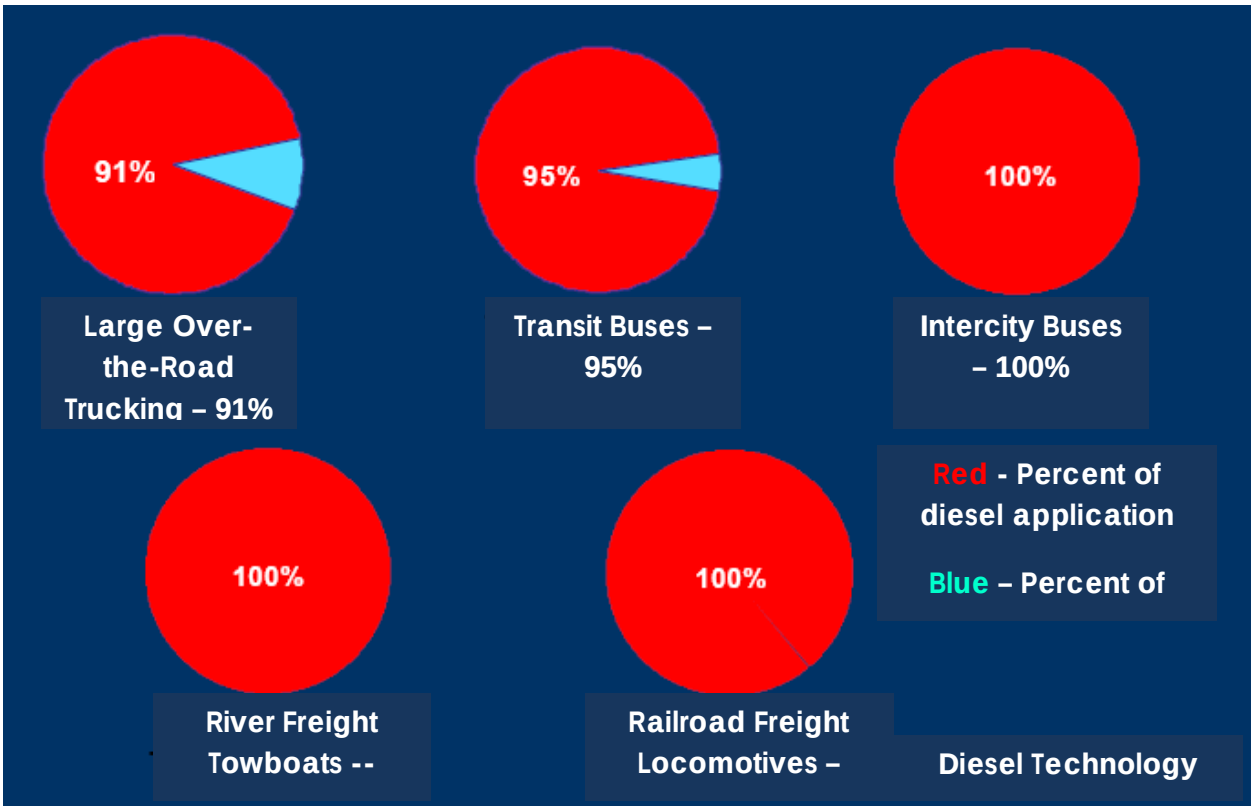

Figure 1-1. Percentage of diesel engine usage in heavy-duty applications [4]

over the same time period. As the largest source of U.S. green-house gas emissions, CO_2 from fossil fuel combustion has accounted for approximately 77% of global warming potential (GWP) weighted emissions since 1990 [5]. As a result of the increasing amount of CO_2 in the atmosphere, the Intergovernmental Panel on Climate Change (IPCC) estimates that the Earth's surface is warming at a rate of approximately 0.32°F/decade (0.18ºC/decade). Also the top ten warmest years have all occurred since 1990. It is projected that the average surface temperature of the Earth is likely to increase by 2 to 11.5ºF (1.1 to 6.4ºC) by the end of the 21st century [6]. Figure 1.2 shows projected global surface warming trends as a function of both time and estimated CO_2 emissions.

Since lean-burn engines use less fuel, and thus producing less CO_2, they are quickly becoming a transportation alternative to help ease the burden of CO_2 emissions. However, there are drawbacks to the utilization of lean-burn diesel engines when compared to SI engines. Diesel

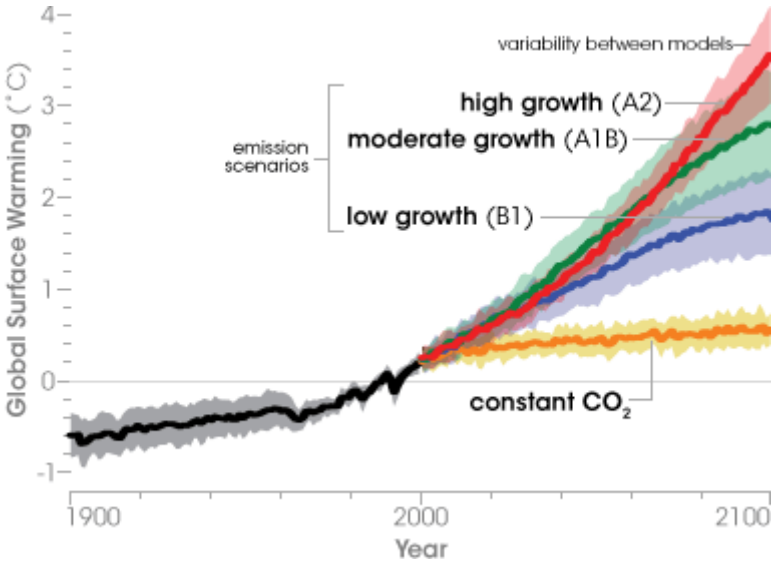

Figure 1-2. Estimated future global warming trends [5]

engines produce large amounts of nitrogen oxides (NO_x) and particulate matter (PM). NO_x is a major contributor to smog and acid rain, while PM is linked to thousands of excess deaths and health problems [7, 8].

1.2 Emissions Regulations

Emissions regulations for diesel engines first took effect in the U.S. in the 1970's with the Clean Air Act (CAA). Due to the increasing usage of fossil fuels and their subsequent burning, increasingly stringent regulations were placed on harmful emissions which are unwanted by-products from the combustion of these fossil fuels: HC, CO, SO_x, PM and NO_x [3]. The U.S. Congress first passed the CAA in 1963 to reduce smog and air pollution. Major amendments to the CAA were made in 1970 and 1990. The 1990 Amendment put into action a schedule for all sources of air-born pollution to meet emissions standards by deadlines set forth in the amendment [9]. Initially, NO_x emissions regulations could be met solely by optimizing the combustion processes for low NO_x production. Modifications to the combustion chamber and high pressure fuel injection are effective for PM reduction. Similarly, combustion control and exhaust gas recirculation (EGR) can reduce NO_x. Through EGR, lower flame temperature is achieved by reducing the oxygen concentration and increasing the thermal capacity of the

burning mixture, resulting in lower NO_x formation. Figure 1.3 illustrates the combustion concept for low PM and NO_x. However as the EGR rate increases; the combustion process slows down considerably, resulting in an increase in PM. As a result, the SOF (Soluble Organic Fraction) oxidation catalyst, which was effective in oxidizing the soluble organic components of PM and reducing overall PM, was introduced to the market in the early 1990s [2].

With the recent passing of stricter legislation, the development of sophisticated aftertreatment devices has become essential in keeping exhaust gas emissions within the allowable limits. In conjunction with emissions standards, durability requirements have been added to current regulations, requiring aftertreatment devices to perform effectively over a lifetime of 100,000 miles or more. The EPA emissions standards for heavy-duty diesel engines model year 1987-1998 are listed in Figure 1.4. The emissions standards for heavy-duty diesel engines model year 2007 or later are as follows: 0.20 g/bhp-hr of NO_x, 0.01 g/bhp-hr of PM and 0.14 g/bhp-hr of non-methane hydro-carbons (NMHC). Compliance with the emissions standards must be demonstrated over the useful life of the engine, which is shown in Table 1 for heavy-

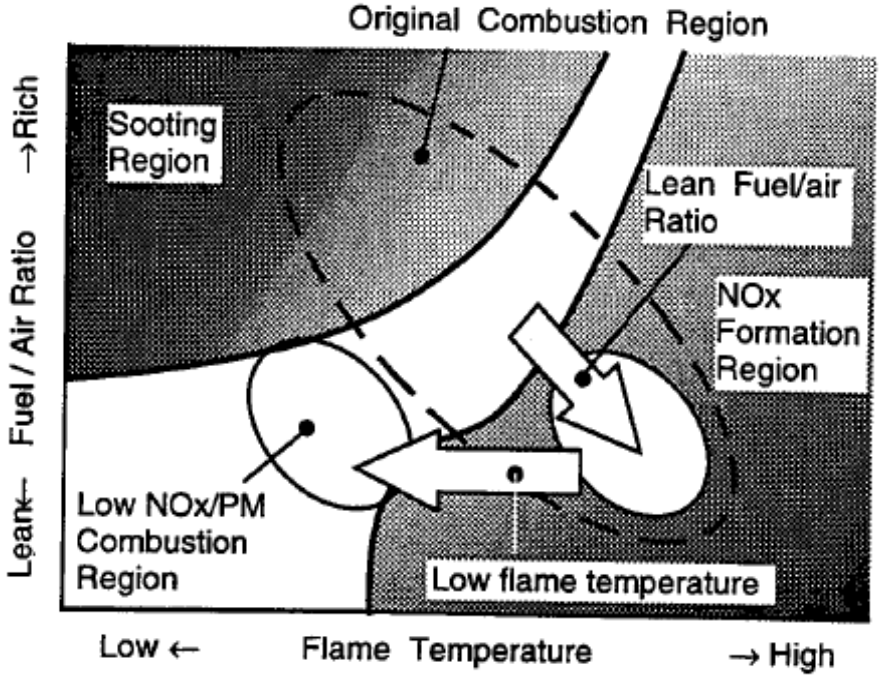

Figure 1-3. Combustion concepts for low PM and low NOx [2]

Year	HC	CO	NO_x	PM
Heavy-Duty Diesel Truck Engines				
1988	1.3	15.5	10.7	0.6
1990	1.3	15.5	6	0.6
1991	1.3	15.5	5	0.25
1994	1.3	15.5	5	0.1
1998	1.3	15.5	4	0.1
Urban Bus Engines				
1991	1.3	15.5	5	0.25
1993	1.3	15.5	5	0.1
1994	1.3	15.5	5	0.07
1996	1.3	15.5	5	0.05*
1998	1.3	15.5	4	0.05*
* - in-use PM standard 0.07				

Figure 1-4. EPA emissions standards for heavy-duty diesel engines of model year 1987-1998 (g/bhp-hr) [9]

duty diesel engines of model year 1987 - 2003. By the model year 2007, durability requirements increased to 10 years or 110,000 miles for light heavy-duty diesel engines (LHDDE), 10 years or 185,000 miles for medium heavy-duty diesel engines (MHDDE) and 10 years or 435,000 miles for heavy heavy-duty diesel engines (HHDDE) [9].

Two sets of standards have been defined for light-duty vehicles in the 1990 amendment to the CAA: Tier 1 and Tier 2 standards. Tier 1 standards were published in the summer of 1991 and phased-in progressively from 1994 to 1997. The standards applied to all new light-duty vehicles (LDV), such as passenger cars and light-duty trucks. The standards applied to vehicles model year 2004 or later are summarized in Figure 1.5. Tier 2 standards were adopted in December of 1999 with a phase-in implementation schedule from 2004 to 2009. Under the Tier 2 regulations, the same emissions standards applied to all vehicle weight categories. The regulations are structured into eight permanent and 3 temporary certification levels or "certification bins", and an average fleet standard NO_x emission. Vehicle manufacturers have the choice to certify vehicles to any of the available bins. Once fully implemented in 2009, the average NO_x emissions of the entire light-duty vehicle fleet sold by each manufacturer have to meet the average NO_x standard of 0.07 g/mile. The Tier 2 standards are summarized in Figure 1.6 [9].

Table 1. Useful life of heavy-duty diesel engines as defined by the U.S. federal government for diesel engines of model year 1987 – 2003 [9]

Type	years	mileage
LHDDE	8	110,000
MHDDE	8	185,000
HHDDE	8	290,000

Category	50,000 miles/5 years						100,000 miles/10 years[1]					
	THC	NMHC	CO	NOx† diesel	*NOx gasoline*	PM	THC	NMHC	CO	NOx† diesel	*NOx gasoline*	PM
Passenger cars	0.41	0.25	3.4	1	*0.4*	0.08	-	0.31	4.2	1.25	*0.6*	0.1
LLDT, LVW <3,750 lbs	-	0.25	3.4	1	*0.4*	0.08	0.8	0.31	4.2	1.25	*0.6*	0.1
LLDT, LVW >3,750 lbs	-	0.32	4.4	-	*0.7*	0.08	0.8	0.4	5.5	0.97	*0.97*	0.1
HLDT, ALVW <5,750 lbs	0.32	-	4.4	-	*0.7*	-	0.8	0.46	6.4	0.98	*0.98*	0.1
HLDT, ALVW > 5,750 lbs	0.39	-	5	-	*1.1*	-	0.8	0.56	7.3	1.53	*1.53*	0.12

1 - Useful life 120,000 miles/11 years for all HLDT standards and for THC standards for LDT
† - More relaxed NOx limits for diesels applicable to vehicles through 2003 model year

Abbreviations:
LVW - loaded vehicle weight (curb weight + 300 lbs)
ALVW - adjusted LVW (the numerical average of the curb weight and the GVWR)
LLDT - light light-duty truck (below 6,000 lbs GVWR)
HLDT - heavy light-duty truck (above 6,000 lbs GVWR)

Figure 1-5. Tier 1 emission standards applicable to vehicles of model year 2004 or later (g/mile) [9]

Bin#	Intermediate life (5 years / 50,000 mi)					Full useful life				
	NMOG*	CO	NOx	PM	HCHO	NMOG*	CO	NOx†	PM	HCHO
Temporary Bins										
11 MDPV[c]						0.28	7.3	0.9	0.12	0.032
10[a,b,d,f]	0.125 (0.160)	3.4 (4.4)	0.4	-	0.015 (0.018)	0.156 (0.230)	4.2 (6.4)	0.6	0.08	0.018 (0.027)
9[a,b,e,f]	0.075 (0.140)	3.4	0.2	-	0.015	0.090 (0.180)	4.2	0.3	0.06	0.018
Permanent Bins										
8[b]	0.100 (0.125)	3.4	0.14	-	0.015	0.125 (0.156)	4.2	0.2	0.02	0.018
7	0.075	3.4	0.11	-	0.015	0.09	4.2	0.15	0.02	0.018
6	0.075	3.4	0.08	-	0.015	0.09	4.2	0.1	0.01	0.018
5	0.075	3.4	0.05	-	0.015	0.09	4.2	0.07	0.01	0.018
4	-	-	-	-	-	0.07	2.1	0.04	0.01	0.011
3	-	-	-	-	-	0.055	2.1	0.03	0.01	0.011
2	-	-	-	-	-	0.01	2.1	0.02	0.01	0.004
1	-	-	-	-	-	0	0	0	0	0

* for diesel fueled vehicle, NMOG (non-methane organic gases) means NMHC (non-methane hydrocarbons)
† average manufacturer fleet NOx standard is 0.07 g/mi for Tier 2 vehicles

a - Bin deleted at end of 2006 model year (2008 for HLDTs)
b - The higher temporary NMOG, CO and HCHO values apply only to HLDTs and MDPVs and expire after 2008
c - An additional temporary bin restricted to MDPVs, expires after model year 2008
d - Optional temporary NMOG standard of 0.195 g/mi (50,000) and 0.280 g/mi (full useful life) applies for
e - Optional temporary NMOG standard of 0.100 g/mi (50,000) and 0.130 g/mi (full useful life) applies for
f - 50,000 mile standard optional for diesels certified to bins 9 or 10

Figure 1-6. Tier 2 emission standards applicable to vehicles model year 2009 or later (g/mile) [9]

1.3 Aftertreatment Technology

Current diesel aftertreatment systems are focused on reducing four components of exhaust emissions: unburned hydrocarbons, CO, PM and NO_x. Unburned hydrocarbons and CO in the exhaust gases are oxidized using a diesel oxidation catalyst (DOC). For control of PM, a diesel particulate filter (DPF) is used to filter the PM suspended in the exhaust gas stream and subsequently burn it. Currently, there are three NO_x abatement technologies which are used to remove NO_x from diesel exhaust: HC-lean NO_x catalysts (LNCs), lean NO_x traps (LNTs) and selective catalytic reduction (SCR) catalysts.

HC-LNCs consist of a porous, high surface area support such as zeolites or alumina impregnated with either Cu or Pt particles providing active sites, on which NO_x is reduced with HC's. Under normal diesel operating conditions HC's are not sufficiently present in the exhaust stream. Therefore in some HC-LNC systems a small amount of fuel or HC is injected into the exhaust upstream of the catalyst. Depending on the system design and vehicle application, HC-LNC technology can achieve only 10% to 25% NO_x reduction efficiencies, which does not meet today's emissions standards. Since the HC's used to reduce NO_x do not produce any mechanical energy, HC-LNC's typically operate at a fuel penalty of approximately 3%. Also, the additional fuel consumption results in slightly higher CO_2 emissions [10].

LNT's present a promising technology for the abatement of NO_x under lean conditions. The catalyst possesses dual functionality, a storage function in the form of a basic metal oxide, typically BaO or K_2O, and a NO_x reduction component, typically composed of Pt or Rh, dispersed on γ-Al_2O_3. Under lean conditions NO is oxidized to NO_2 over Pt and stored on the basic metal oxide in the form of nitrites or nitrates. Periodically, the exhaust gases are switched to reducing conditions, i.e., rich conditions, and the stored NO_x in the form of nitrites or nitrates is released and reduced to N_2 over the precious metal sites. While the LNT is capable of achieving NO_x reduction efficiencies of 90% or more, catalyst durability remains a crucial issue. Susceptibility to sulfur poisoning is the single most important factor in determining the LNT's effective lifetime. The NO_x storage medium of the LNT has a greater affinity for SO_x than NO_x, and the resulting sulfate is more stable than the stored nitrates. The stored sulfate can only be removed from the LNT at high temperatures ($T \geq 650°C$). Such required high temperature can lead to sintering of Pt particles, surface area loss, and solid state reactions between the various

components in the washcoat, which ultimately affect the durability of the LNT [11].

SCR systems first appeared in large scale power plants in the 1970's, where they are used to remove NO_x from the flue gas of boilers. These catalysts consist of a substrate made from various ceramic materials and a catalytically active component consisting of base metal oxides such as Vn_2O_5 and WO_3 supported on TiO_2 [12]. Unlike LNT's, periodic switching between a lean and rich phase is not required, and NO_x is continuously converted to N_2 and H_2O over the SCR catalyst with the use of ammonia as a reducing agent. Depending on the operating temperature these systems have been shown to reduce NO_x by 70% to 90%. Although metal oxide SCR catalysts are effective, they are not ideal for automotive applications. Miller found that base metal catalysts commonly operate at temperatures ranging from 350 to 450ºC and lack high thermal durability [13], which make them susceptible to damage when being used in conjunction with a DPF, which requires periodically high temperature regeneration. They also have a high catalyzing potential to oxidize SO_2 to SO_3, which can be damaging to the catalyst's acidic properties. Furthermore, SO_3 can react with NH_3 to form ammonium sulfate and ammonium bisulfate, both of which are harmful to the catalyst [12, 13].

Zeolite SCR catalysts have been developed out of the need for a more durable SCR catalyst for automotive applications. Zeolites are crystalline aluminosilicates containing pores and cavities of molecular dimensions. These catalysts have the potential to operate at significantly higher temperatures than metal oxide-based SCR catalysts, with the ability to withstand long term operational temperatures as high as 650ºC. Zeolites also have a lower potential for the oxidation of SO_2 to SO_3 [16].

Zeolites have an open pore structure that can accommodate a wide variety of cations as shown in Figure 1.7. The positive ions can readily be exchanged for other cations. Cu and Fe-Zeolites are some of the more popular zeolite-based catalysts. The catalysts are typically produced by ion exchanging Fe^{3+} and Cu^{2+} ions onto the H^+ of the parent zeolite [18]. The resulting Fe or Cu-zeolite is washcoated onto a honeycomb-like ceramic monolith.

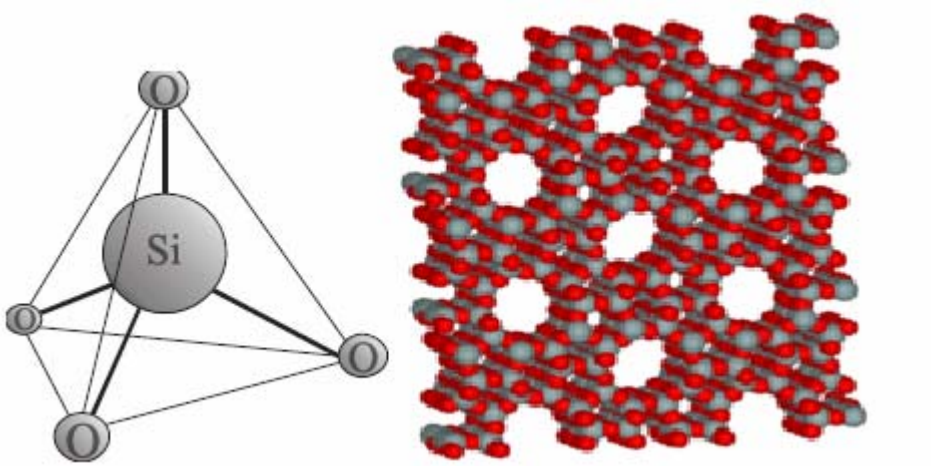

Figure 1-7. The micro-porous molecular structure of a zeolite [17]

1.4 Scope of Investigation

In previous studies, thermal aging of Fe-zeolite SCR catalysts was carried out using hydrothermal aging on a bench-flow reactor. SCR catalysts are seldom used by themselves instead they are used as part of an aftertreatment system, consisting of a DOC, a SCR catalyst and a DPF. Therefore, the objective of the current investigation is to determine the deactivation mechanisms and durability of a commercially-available Fe-Zeolite SCR catalyst by performing accelerated thermal aging of SCR catalysts in conjunction with a DOC and DPF using a small single-cylinder diesel engine.

The engine used in this study is a 517 cc, naturally aspirated direct injection (NA/DI) single-cylinder Hatz diesel engine. Aging is achieved by increasing the exhaust temperature during DPF regenerations. Three different temperatures are used to age the SCR catalysts: 850°C for 13 aging cycles, 750°C for 50 aging cycles and 650°C for 31 aging cycles. There are less aging cycles at 650 and 850°C because of problems that arose during aging at these temperatures. While operating the engine at a constant speed of 1500 RPM, the exhaust temperature is increased by injecting supplemental fuel into the exhaust upstream of the DOC. The flow rate of supplemental fuel is adjusted until the temperature at the inlet of the SCR catalyst reaches the target aging temperature. After each aging cycle the NO_x conversion of the engine-aged Fe-Zeolite SCR catalyst is evaluated at an exhaust temperature of approximately 300°C. To minimize NH_3 slip an α ratio of NH_3 to NO equal to 0.6 is used during on-engine NO_x

conversion evaluations.

In addition to engine aging, hydrothermal aging of Fe-Zeolite SCR catalysts using the CLEERS aging protocol is also performed on a bench-flow reactor [1]. The hydrothermal aging is used to study the effect of sulfur poisoning on the durability of Fe-zeolite SCR catalysts. The catalyst is aged for 64 hrs with NO_x reduction performance evaluated after every 16 hours of aging.

Due to cycle-to-cycle variations both temperature and composition of the engine's exhaust gases can vary considerably, which necessitates the use of the bench flow reactor in evaluating the NO_x performance of fresh, accelerated engine-aged, hydrothermally-aged and field-aged Fe-zeolite SCR catalysts. The composition of the simulated exhaust gases and evaluation temperatures used for BFR testing are recommended by the CLEERS protocol for steady-state evaluation of SCR catalysts.

Cross-Cut Lean Exhaust Emissions Reduction Simulations (CLEERS) is an R&D focus project, whose overall objective is to promote development of improved computational tools for simulating realistic full-system performance of lean-burn engines and associated emissions control devices [1]. All aging and performance evaluations using the BFR are conducted in accordance with CLEERS protocols. This is done so that the data collected during this study can be compared to other data collected in the same manner.

Materials characterization of both fresh and aged Fe-zeolite SCR catalysts are performed using a number of surface characterization techniques including scanning electron microscopy (SEM), electron probe microanalysis (EPMA), X-ray diffraction (XRD) and BET surface area measurement. SEM is used to examine the change in surface morphology. EPMA is used to detect the migration, agglomeration and contaminations of the SCR washcoat as a result of aging. X-ray diffraction (XRD) is used to identify changes in the structure of the zeolite and the formation of new iron oxides due to aging. Finally, BET is used to measure the surface area per gram of the SCR catalysts.

It is expected that this work will provide a valuable engineering tool for the development of new catalyst formulations and provide additional insight into the deactivation mechanisms of thermally-aged Fe-zeolite SCR catalysts. The additional knowledge of the thermal durability of Fe-zeolite SCR catalysts gained should contribute to the improvement of current technology by

increasing the useful lifetime of these catalysts. Also, the results of accelerated thermal aging should contribute to the development of an engine-based accelerated aging protocol for SCR-DPF systems that successfully replicates typical “on-road” conditions.

CHAPTER 2 LITERATURE REVIEW

SCR catalysts can be divided into three basic groups. Noble metals, like platinum were first considered for the SCR of NO_x. They operate well at low temperatures, but the selectivity is poor at high temperatures. The second type is metal oxides. Among the various metal oxide mixtures, those based on vanadia supported on titania are most common. These catalysts are effective for the SCR of NO_x at temperatures between 350 and 450°C, but they lose selectivity at high temperatures, due to enhanced NH_3 oxidation. For application in a wider temperature range, zeolite-based catalysts have been developed, which are active for SCR of NO_x at temperatures up to 600°C [26]. Among these, Cu-exchanged and Fe-exchanged zeolites have been widely studied for SCR of NO_x using NH_3 as a reducing agent. This chapter contains an overview of selective catalytic reduction of NO_x emissions from diesel exhaust using Fe-zeolite catalysts. A discussion of SCR operating principles and Fe-Zeolite catalyst composition is presented in Sections 2.1 and 2.2, respectively. Section 2.3 focuses on catalyst durability and deactivation mechanisms associated with catalyst aging.

2.1 SCR Operating Principles

NO_x abatement is achieved via the SCR reaction between NO_x and ammonia (NH_3) which reduces NO_x to N_2 and H_2O according to the following global reactions.

$$4NH_3 + 4NO + O_2 \rightarrow 4N_2 + 6H_2O \quad (2.1)$$

$$4NH_3 + 3NO_2 \rightarrow 3.5N_2 + 6H_2O \quad (2.2)$$

$$4NH_3 + 2NO + 2NO_2 \rightarrow 4N_2 + 6H_2O \quad (2.3)$$

As reviewed by Miller, the rates of these reactions vary greatly, with Reaction 2.3 being the fastest, followed by Reactions 2.1 and 2.2 [13-15]. As can be seen in Reaction 2.3 the fastest reaction requires an equimolar amount of NO and NO_2. However, typical exhaust gas from a lean-burn engine is comprised of approximately 90% NO and 10% NO_2, therefore it is beneficial to oxidize a fraction of NO to NO_2, typically by an oxidation catalyst, in order for the SCR

reaction to proceed according to Reaction 2.3. It is important that the ratio of NO_2 to NO does not become greater than one, since the reaction with NH_3 and NO_2 is the slowest [13, 19]. At temperatures greater than 400°C traditional metal oxide catalysts have the potential to produce nitrous oxide via reaction 2.4.

$$4NH_3 + 4NO + 3O_2 \rightarrow 4N_2O + 6H_2O \quad (2.4)$$

If the temperature is increased higher than 550°C there is a direct oxidation of NH_3 to NO, which limits the amount of NO_x reduction.

$$4NH_3 + 5O_2 \rightarrow 4NO + 6H_2O \quad (2.5)$$

Some SCR catalysts can also produce undesired intermediates at low temperatures. For example, below 120°C ammonium nitrate can be formed by Reaction 2.6, and ammonium

$$2NH_3 + 2NO_2 \rightarrow NH_4NO_3 + N_2 + H_2O \quad (2.6)$$

nitrate is known to be very unstable, decomposing explosively at temperatures above 60°C. There are a host of other unwanted side reactions than can occur as the result of oxygen content, catalyst composition, and temperature [13]. One of the major drawbacks to the use of vanadia-based SCR catalysts in automotive applications is the narrow range of conditions for which desirable reactions occur.

Fe-Zeolite catalysts are regarded as an alternative to the established vanadia-based catalysts, because they could function at temperatures up to 600°C without the risk of emitting volatile vanadyl species, and there are no disposal problems associated with zeolite based catalysts [19, 20]. Besides good thermal durability Fe-zeolites for NH_3 SCR show a high selectivity towards the desired products N_2 and H_2O, even at elevated temperatures. Malmberg et al. measured no N_2O at catalyst temperatures ranging from 150 to 400°C, while using a Fe-Zeolite catalyst for NO_x abatement studies [21]. With vanadia-based SCR catalysts it is generally accepted that the SCR reaction occurs according to the Eley-Ridel mechanism, where NH_3 is strongly absorbed on the surface sites of the catalyst and reacts with gas phase NO_x [12]. However, a different reaction mechanism is proposed for Fe-Zeolite catalysts. It is suggested that the iron present in Fe-Zeolite is responsible for the oxidation of NO to NO_2, while the main

purpose of the Brønsted acid sites in the zeolite is to bind NH_3 to the catalyst surface [21].

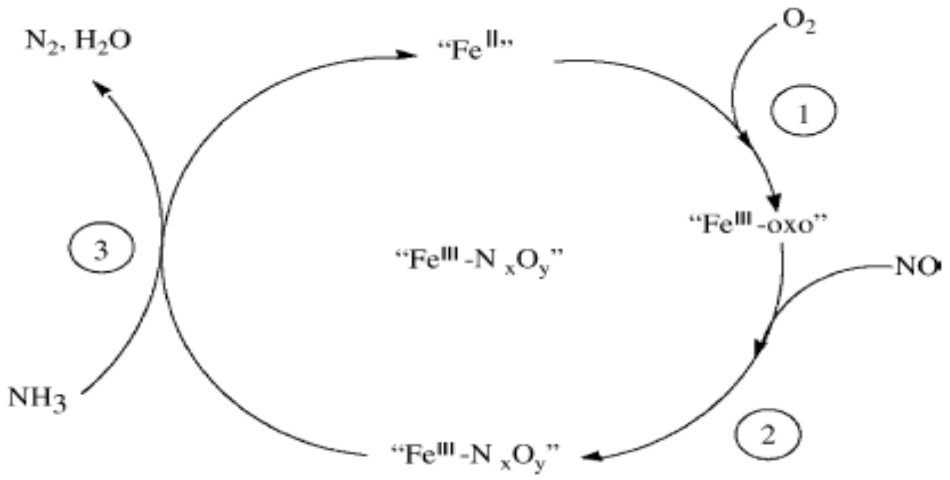

Figure 2-1. Fe2+/Fe3+ redox cycle for the oxidation of NO [15]

According to Delahay et al., the oxidation of NO follows a Fe^{2+}/Fe^{3+} redox cycle. Reactions 2.7 through 2.9 and Figure 2.1 illustrate the redox process. In this cycle Fe^{II} is oxidized by O_2 to form a Fe^{III} oxo ($Fe^{III}O$) species. The extra-framework oxygen then reacts with NO to form a surface NO_2 intermediate bound to iron. Finally, the later species reacts with NH_3 to form water and nitrogen with concomitant reduction of Fe^{III} to Fe^{II} species [17].

$$NO + Fe^{III}"O" \rightarrow Fe^{III}"O"-NO \tag{2.7}$$

$$Fe^{III}"O"-NO \rightarrow Fe^{II} + NO_2^{\uparrow} \tag{2.8}$$

$$Fe^{II} + \frac{1}{2}O_2 \rightarrow Fe^{III}"O" \tag{2.9}$$

Several investigators agree that both NO and NO_2 participate in NO_x reduction and that NH_4NO_2 is a key intermediate [16, 21-23]. Sun et al. have proposed a reaction mechanism for the SCR of NO_x over a Fe-Zeolite catalyst shown in Reactions 2.10 through 2.13, where "S" signifies a catalytic site.

$$S - NO + \frac{1}{2}O_2 \rightarrow S - NO_2 \quad (2.10)$$

$$S - NO_2 + S - NO \rightarrow S - N_2O_3 - S \quad (2.11)$$

$$S - N_2O_3 + 2S - NH_3 + H_2O \rightarrow 2S - NH_4NO_2 + S \quad (2.12)$$

$$S - NH_4NO_2 \rightarrow N_2 + H_2O + S \quad (2.13)$$

Spectroscopic studies conducted by Sun et al. confirmed the formation of NH_4^+ ions on the Brønsted acid sites of a Fe-Zeolite catalyst during NH_3 adsorption tests [23]. Further investigation revealed evidence of the formation of NO_2 followed by N_2O_3 and NH_4NO_2, when a NH_3-doped catalyst was exposed to a flow of NO and O_2.

It is known that the addition of NO_2 to the feed gas increases the SCR activity of metal-promoted zeolite catalysts especially at temperatures below 400°C [20]. Figure 2.2 compares the NO_x abatement performance of hydrothermally-aged Fe-zeolite catalysts with and without NO_2 in the feed gas. Therefore it is generally agreed upon that the SCR reaction mechanism includes the oxidation of NO to NO_2, and that it is the rate determining step in the SCR process [18-20, 23, 24]. Using NO oxidation experiments, Delahay et al. found a good correlation between the

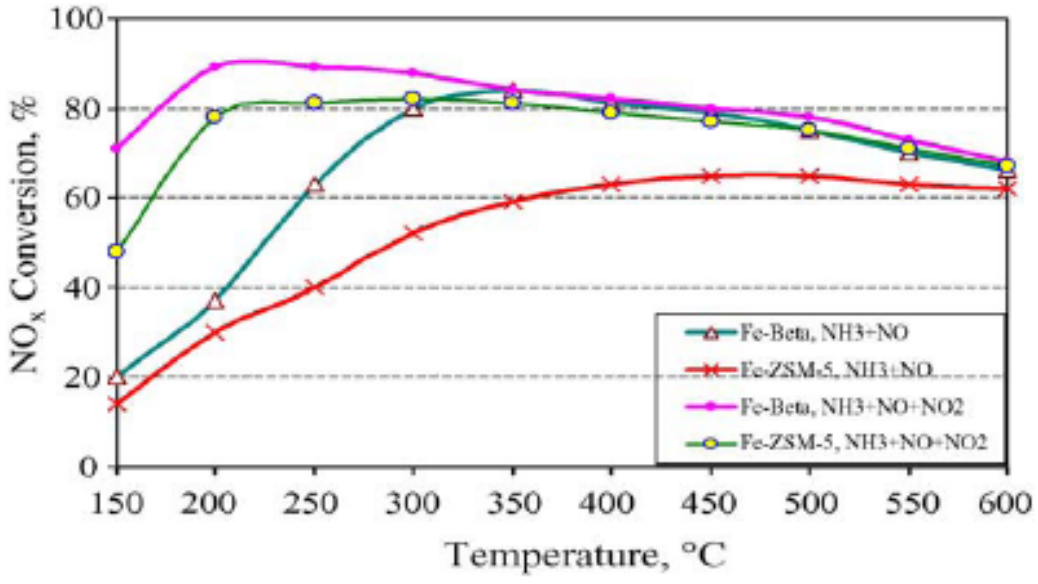

Figure 2-2. NOx conversion of hydrothermally-aged Fe-beta and Fe-ZSM-5 in the presence and absence of NO2. Conditions: 600ppm NO + 400ppm NO_2 or 1000ppm NO and 1000ppm NH_3, 8% H_2O, 10% O_2 and balance with N_2 [18]

activity for the oxidation of NO and the SCR of NO by NH_3 [18], however the oxidation activity was two to three times less than the SCR activity. Therefore it is suggested that NO_2 strongly absorbs on the catalyst surface before rapidly reacting with NO and NH_3 to form N_2 and H_2O, which explains low NO oxidation in comparison to high NO reduction.

2.2 Catalyst Composition

A washcoated honeycomb monolith is a commonly used configuration for SCR catalysts. The configuration provides a high surface to volume ratio and a low pressure drop across the catalyst [27]. The monolith substrate is usually made of a high temperature ceramic material, such as cordierite. Cordierite mainly consists of kaolin ($Al_2O_3 \cdot 2SiO_2 \cdot 2H_2O$), talc ($3MgO \cdot 4SiO_2 \cdot H_2O$) and alumina ($Al_2O_3$) and it has a low coefficient of thermal expansion, high temperature stability, desirable porosity and excellent resistance to oxidation [28]. The surface of the monolith is washcoated with a layer of high surface area material, in this case zeolite. Zeolites are crystalline aluminosilicates containing pores and cavities of molecular dimensions and they are extensively used as shape-selective solid acid catalysts in many industrial processes. Factors such as framework type and Si/Al_2 ratio determine the catalytic properties of the material. The framework acidity can be modified by variation of the Si/Al_2 ratio of the zeolite or by substitution of Al by other trivalent elements. The acidity increases as the ratio of Si/Al_2 decreases. The acid properties of zeolites are considered as an important factor in controlling the catalytic activity of chemical reactions. It is assumed that SCR activity is enhanced by the surface acidity of catalysts. [20]. It is generally accepted that NH_3 strongly bonds to Brønsted acid sites within the zeolite structure, generating NH_4^+ ions [22]. Therefore the NH_3 activation capacity of a zeolite catalyst is increased by increasing the acidity of the zeolite.

After being impregnated onto the monolith, an active cation such as Cu or Fe is added to the zeolite. It has been shown that zeolites alone are not very active for the SCR of NO_x [18, 22]. Figure 2.3 compares the de-NO_x performance of a zeolite (ZSM-5) before and after the addition of the active cation Fe. The cation is typically inserted into the zeolite framework by ion

exchange at acid sites, such as $FeCl_3$ vapor sublimation, ion exchange from an aqueous solution or solid-state ion exchange [18] While all methods produce highly active catalysts, those catalysts prepared by $FeCl_3$ vapor sublimation appear to be the most active for the SCR of NO_x with NH_3 [16]. $FeCl_3$ is sublimed into the cavities of H-zeolite, where it reacts chemically with the acid sites according to the reaction:

$$H^+ + FeCl_3 \rightarrow \left[FeCl_2\right]^+ + HCl \qquad (2.14)$$

After all the protons are replaced by $[FeCl_2]^+$, the sample is then washed with water and calcined in a flow of O_2 at high temperature. With this kind of preparation a Fe/Al ratio of approximately one is obtained [22, 29].

Aqueous ion exchange is achieved by submerging the NH_4^+ form of the zeolite (NH_4-Zeolite) into a $Fe(NO_3)_3$ aqueous solution. The pH of the slurry is kept between 3.0 and 3.5, while the solution is stirred for at least 24 hrs. The solid is then dried and calcined in air at temperatures between 500 and 600°C [18]. Another common technique for producing Fe-Zeolites utilizes Fe(III)acetylacetonate, $Fe(C_5H_8O_2)_3$. H-Zeolite is added to a toluene solution containing an appropriate amount of $Fe(C_5H_8O_2)_3$. The solution is stirred for at least 24 hrs, after which the solvent is removed by evaporation under vacuum. Then the solids are dried and calcined in air. It is expected to obtain an ion exchange ratio (Fe/Al) of approximately one with this method [17]. Although, $FeCl_3$ sublimation has been shown to produce the most active

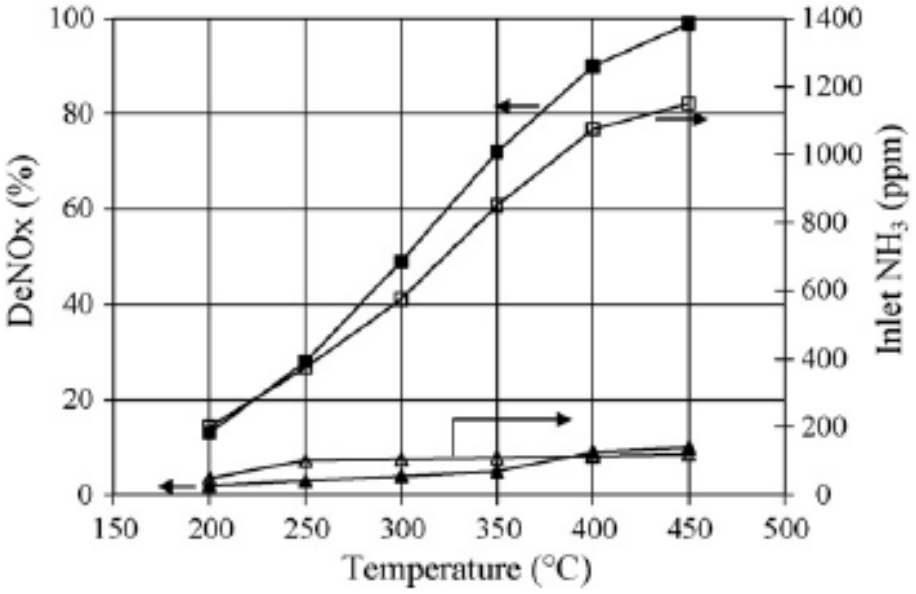

Figure 2-3. De-NOx activity (closed symbol) and inlet ammonia (open symbol) of (■) Fe-ZSM5 and (▲) H-ZSM5 with 1000ppm inlet NO [22]

catalysts, this method is hard to perform on a large scale. Therefore aqueous ion exchange with $Fe(NO_3)_3$ or $Fe(C_5H_8O_2)_3$ is a more practical technique for manufacturing large amounts Fe-Zeolite catalysts, which are highly active for the SCR reactions of NO_x with NH_3. These are some of the typical procedures for producing zeolite-based SCR catalysts; however, there are other techniques and methods that are not listed here.

When the ion exchange ratio is low more acid sites are free for NH_3 adsorption and cations are finely dispersed. If the ion exchange ratio is too high, there is a risk of having extra "out of framework" cations (Fe^{3+}) and metal oxide clusters, such as Fe_2O_3, which can be active for NH_3 oxidation [20]. It is believed that Fe loadings corresponding to an ion exchange ratio of one are ideal for achieving maximum catalyst performance.

2.3 Catalyst Durability

During operation, the activity of SCR catalysts declines. As discussed by Herman, there are physical and chemical causes for the loss of activity [30]. Physically, loss of the catalyst activity can occur by erosion caused by ash particles in the exhaust gases. The ash particles can also be lodged in the pores of the catalyst, thereby blocking appreciable portions of the catalyst's

surface from the exhaust gas, as well as increasing NH_3 slippage. For some catalysts, thermal cycling leads to loss of active catalytic surface sites via sintering. Catalyst activity can also be decreased by poisoning through the adsorption of gaseous components in the exhaust gas, such as SO_2 or SO_3 that can subsequently form ammonium bi-sulfates upon reaction with NH_3 and water vapor.

Devadas et al. preformed hydrothermal aging on Fe-ZSM5 catalysts to gain a better understanding of durability [19]. The Fe-ZSM5 catalyst monoliths were aged for 50 hrs at 650°C in 5% O, 10% O_2 and N_2 balance. The fresh and aged catalysts were evaluated for NO_x abatement performance with 1000 ppm NO, 10% O_2, 5% H_2O, 0 – 1200 ppm NH_3 and N_2 balance in the feed gas. The ratio of NH_3/NO_x was varied from 0 to 1.2 to quantify the NO_x conversion over each catalyst at 10ppm NH_3 slip. Figure 2.4 compares the performance of the fresh and aged Fe-Zeolite SCR catalysts at 10ppm NH_3 slip. It is observed that aging the catalyst resulted in an absolute decrease in NO_x reduction of approximately 10% over the entire temperature range, proving the good hydrothermal stability of the catalyst. No N_2O could be

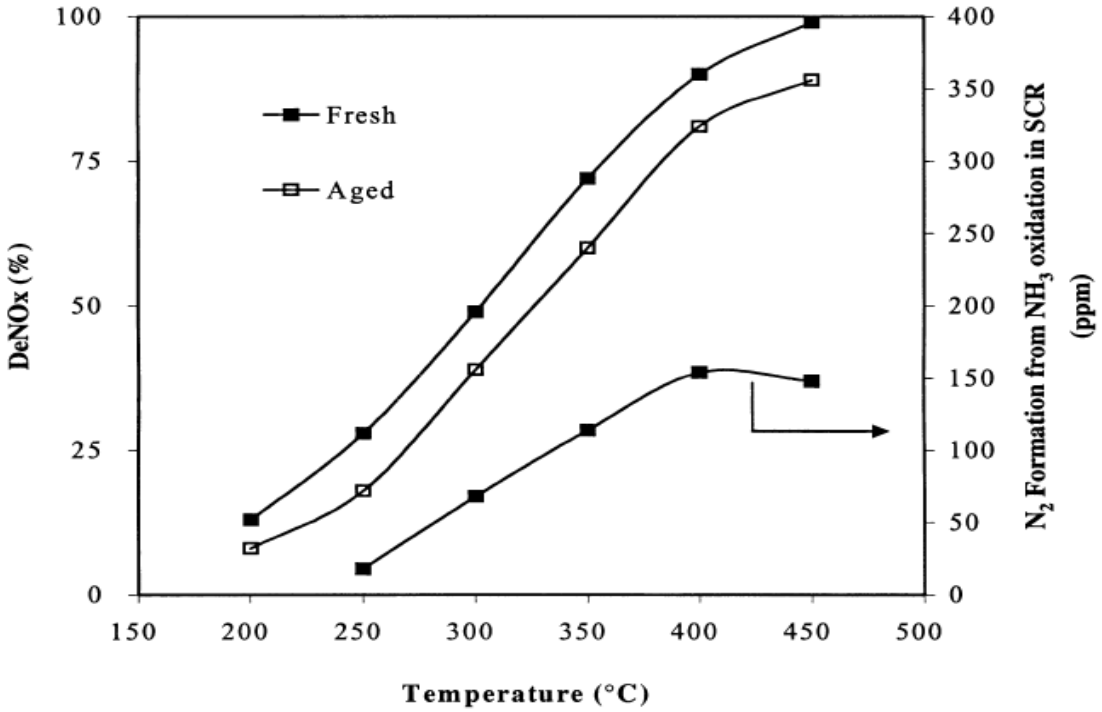

Figure 2-4. DeNOx activity of fresh (■) and aged (□) Fe-ZSM-5 and N2 formation from NH3 oxidation at 10 ppm NH3 slip [19]

detected at all temperatures for both the fresh and aged catalyst. N_2 formation by NH_3 oxidation increased with temperature, reaching a maximum at 400°C. Figure 2.5 shows the NO_x conversion activity at 10ppm NH_3 slip for the fresh and aged Fe-ZSM5 monoliths when an equimolar amount of NO and NO_2 are present in the feed mixture. The activity of both catalyst were enhanced tremendously at low temperatures (T<400°C). The loss in activity over the aged catalyst was only about 3%; however, the production of N_2O increased at all temperatures [19].

Rahkamaa-Tolonen et al. conducted a study on an assortment of metal promoted zeolite catalysts [20]. From the group of zeolites examined (Fe, Cu, Ag and H), Fe and Cu-zeolites achieved high NO conversion (>90%) over a large temperature range (300 - 600°C). A comparison between Cu and Fe-Zeolite catalysts showed that Cu containing zeolites produced higher levels of N_2O than Fe-containing zeolites. This indicates that selectivity to N_2 is higher over Fe-containing zeolites. Hydrothermal aging was performed for 20 hrs at 600°C with 10% H_2O in air. After aging , the maximum NO_x conversions were lower and occurred at higher

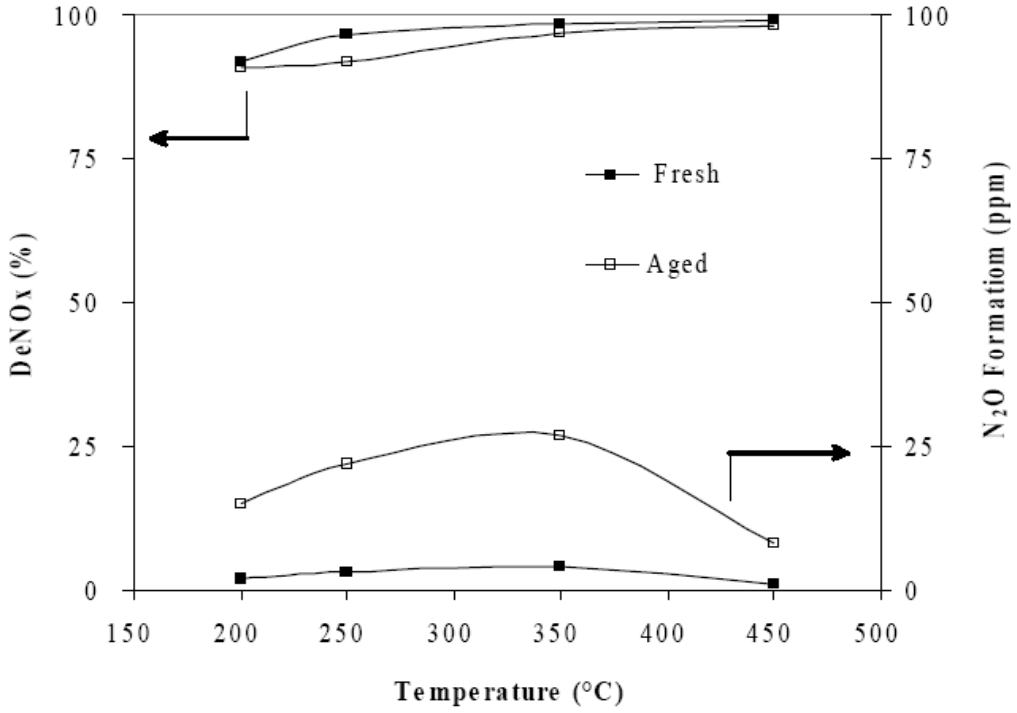

Figure 2-5. DeNOx activity and N2O formation of fresh (■) and aged (□) Fe-ZSM-5 monoliths at 10ppm NH3 slip (NOin = 500ppm, NO2,in = 500ppm)[19]

temperatures. Meanwhile, catalytic activity increased above 450°C. The addition of NO_2 to the inlet flow increased the activity of the hydrothermally aged catalysts by 5 to 10%.

According to Rahkamaa-Tolonen [20], the acidity of zeolites decreases after hydrothermal aging. This is caused by a decrease in surface area and dealumination. NH_3 adsorption tests revealed a decrease of NH_3 adsorption capacity in the aged catalysts, indicating a loss of surface acidity. This could explain the observed increase in NO_x conversion at high temperatures. The decrease in NH_3 adsorption due to dealumination results in a decline of NH_3 oxidation at high temperature resulting in increased NO_x conversion. It is concluded that hydrothermal aging modifies the acid properties of zeolites. The higher the acidity retention, the better the hydrothermal stability for SCR activity.

There is a general consensus that the deactivation of Fe-Zeolite SCR catalysts during hydrothermal-aging is directly related to zeolite dealumination [31-33]. Dealumination is the

process in which the Al^{3+} ion in the SiO_2-Al_2O_3 tetrahedral framework migrates out of the structure. This leads to irreversible deactivation and in extreme cases, collapse of the crystalline structure [31]. Liu found that hydrothermal aging at 700°C had a significant effect on the performance of Fe exchange zeolite SCR catalysts including ammonia storage, NH_3 oxidation by O_2 and NH_3-SCR reactions, which are all related to Brønsted acid sites. In particular, the results showed a good agreement between ammonia oxidation and SCR performance degradation, implying that hydrothermal aging leads to the loss of active sites (Brønsted acid sites) from zeolite dealumination [31].

Guinest et al. [34] quantified the concentration of acid sites in H-beta zeolites before and after dealumination using infrared spectroscopy (IR) measurements of pyridine sorption. Zeolite dealumination was induced by treatment with HCl solution. Samples with various Si/Al ratios were obtained by using HCl solutions of various concentrations ($0.1\text{-}1.5_M$) at various temperatures (30-100°C) and for various times (5min-6hrs). From the results they concluded that dealumination had a direct impact on the concentration of Brønsted acid sites. Comparison of the IR studies showed that an increase in the Si/Al ration from 10 to 35 resulted in a twofold decrease in Brønsted acid sites.

Park et al. [32] found a good correlation between catalyst surface area and aging temperature. Four different Cu-Zeolite catalysts were examined; each with a different ion exchange level. An aging temperature of 800°C caused severe reduction in surface area of all the catalysts, especially in those with ion exchange ratios greater than one (over-exchanged) [32]. This indicates that high ion exchange ratios weaken the crystallinity of the zeolite. Zhdanov et al. found that high-silica zeolites like those used in catalytic applications begin to breakdown structurally between 800 and 1000°C [35], depending on Si/Al_2 ratio and method of preparation. In general, thermal stability increased with increasing Si/Al_2 ratio, while the additions of active cations like Fe and Cu decreased thermal stability [32, 35]. All the zeolites tested by Zhdanov et al. experienced severe dealumination and became wholly or largely amorphous converting to cristobalite (a high temperature phase of quartz, SiO_2), when heated above 1000°C.

Park et al. also found that XRD patterns of hydrothermally aged Cu-zeolite revealed the formation of bulk CuO. It is believed that aging reduces the number of active Cu^{2+} species in the catalyst via the transfer of Cu^{2+} to a crystalline CuO. Park concluded that the observed catalyst

deactivation from hydrothermal aging was attributed to a combination of factors including a decreased number of active acid sites, formation of bulk CuO, redistribution/sintering of Cu^{2+} sites and structural degradation of the zeolite support [32].

It appears that the main cause of catalyst deactivation in zeolite-based SCR catalysts is dealumination and structural degradation of the zeolite. Loss of active acid sites, decrease in surface area and sintering of active cations can all be directly or indirectly related to structural degradation of the zeolite lattice and dealumination. Therefore, thermal stability of the zeolite at temperatures experienced during normal engine operation and active regeneration of the diesel particulate filter is one of the vital factors for SCR catalyst selection and application.

CHAPTER 3 EXPERIMENTAL APPARATUS AND PROCEDURES

This chapter describes the experimental apparatus and procedure used in the present investigation, the formulation and physical dimensions of Fe-zeolite SCR catalyst samples, and the testing protocols used in evaluating catalyst performance. Also included is a brief description of characterization techniques. Section 3.1 is an overview of the bench-flow reactor and its components. Section 3.2 describes the engine bench used for accelerated aging the Fe-zeolite SCR catalysts. Section 3.3 discusses the catalysts used for the study. Finally, Section 3.4 offers a detailed overview of the various characterization techniques used throughout the study.

3.1 Bench-Flow Reactor

3.1.1 Overall Description of the Bench-Flow Reactor System

The bench-flow reactor (BFR) is located at the University of Tennessee, where it has been used by Eaton, Kim and Smith [3, 36 and 37]. A photograph and a schematic of the BFR are shown in Figures 3.1 and 3.2, respectively. The setup consists of five main components: a steam generator, a SCR tubular reactor, a simulated diesel exhaust gas introduction system, a gas analyzer bench and a data acquisition (DAQ) system. Simulated diesel exhaust gases used during SCR catalyst performance evaluations are composed of 5% CO_2, 14% O_2, 5% H_2O, 350ppm NO_x, varying amounts of NH_3 and N_2 balance. The alpha ratio ($\alpha = [NH_3]/[NO_x]$) was varied from 0.5 to 1.2 by changing the concentration of NH_3 between 175ppm and 420ppm in the simulated exhaust gases. A gas hourly space velocity (GHSV) of 30,000 h^{-1} is used during performance evaluations. The gas hourly space velocity is defined by Eq. 3.1,

$$GHSV = \frac{Q}{V_s} \tag{3.1}$$

where Q is the total volumetric flow rate of the simulated diesel exhaust gases at STP, and V_s is the volume of space in which gas flows through the catalyst i.e., the catalyst channels. Hydrothermal aging of SCR catalysts is also carried out in the bench-flow reactor at a GHSV of

Figure 3-1. Photograph of bench-flow reactor system

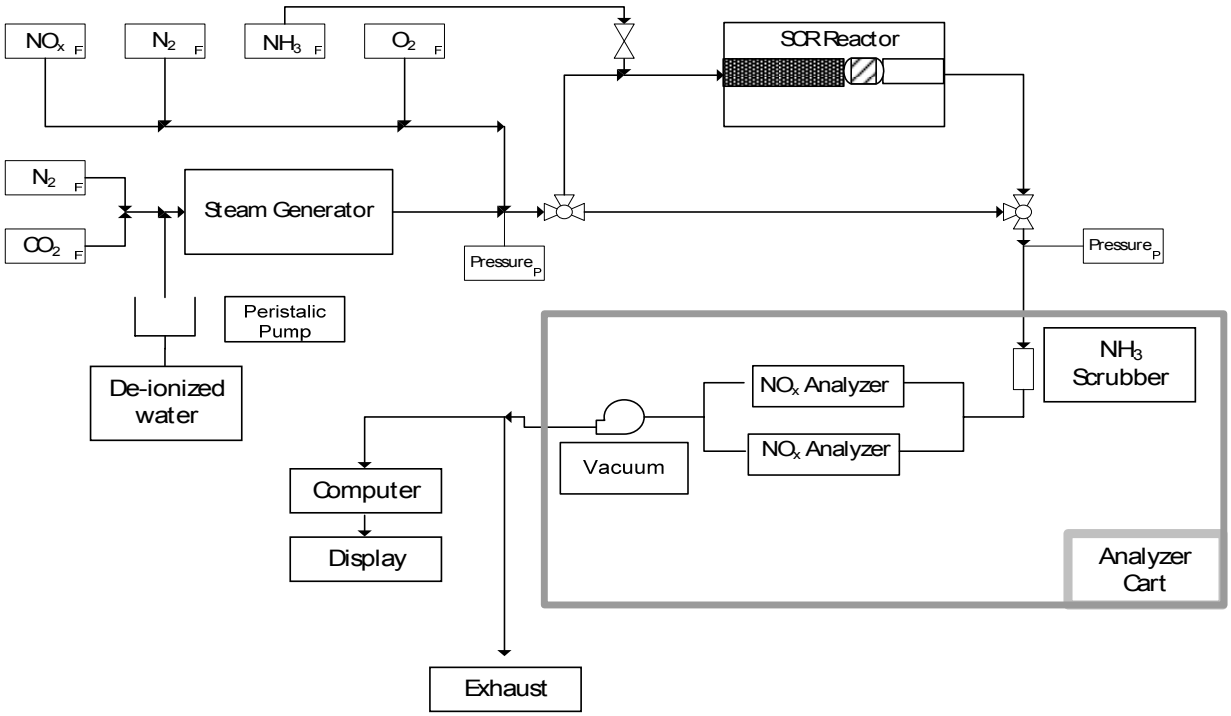

Figure 3-2. Schematic of bench-flow reactor system

$30{,}000h^{-1}$. With one notable exception the composition of the simulated exhaust gases used during hydrothermal aging is similar to that used during performance evaluation, but with 28ppm SO_2 instead of NO_x and NH_3. The volumetric flow rate of each gas component is controlled with mass flow controller (MFC). Steam is introduced into the system through a steam generator into which de-ionized water is injected using a peristaltic pump.

N_2 and CO_2 are used as carrier gases for sweeping water vapor from the steam generator into the BFR system. The remaining gases, consisting of O_2, NO_x and SO_2, are introduced into the system at the exit of the steam generator. Once mixed, the gases pass through either the SCR reactor or the reactor bypass line. The reactor bypass line allows the measurement of the simulated diesel exhaust gases at the SCR inlet conditions. A three-way valve is used to switch between the SCR reactor and the bypass line. NH_3 is introduced before the SCR reactor through a separate heated line, which is maintained at 200°C to prevent the formation of ammonium nitrates. Backpressure and pressure-drop across the SCR reactor are monitored with two pressure transducers located at the inlet and outlet.

The SCR monolith samples of 2.0 cm in diameter are core-drilled from fresh, field-aged and engine-aged SCR catalysts. The sample is inserted inside a quartz tubular reactor, which in turn is placed inside a Lindberg Minimite tubular furnace. Heated sample lines are used throughout the system to both preheat the simulated exhaust gases and ensure no water condensation is occurring in the system. The inlet portion of the reactor tube is filled with 5 mm diameter Pyrex™ beads for effective preheating and mixing of the simulated diesel exhaust gases before entering the SCR catalyst.

Five Omega type-K thermocouples are used to measure the inlet and exit gas temperatures as well as the internal SCR temperatures as shown in Figure 3.3. Two thermocouples, 1.6 mm in diameter, are located approximately 5 mm from the inlet and exit of the SCR catalyst and measure the inlet and exit simulated diesel exhaust gas temperature. The remaining three thermocouples of 0.51 mm in diameter are placed at ¼, ½, and ¾ of the catalyst length. These thermocouples are used to measure the axial temperature distribution in the SCR catalyst.

An analyzer bench is used to measure the concentrations of NO and total NO_x in the

simulated diesel exhaust gases. The gases are drawn through the bench flow system by a vacuum

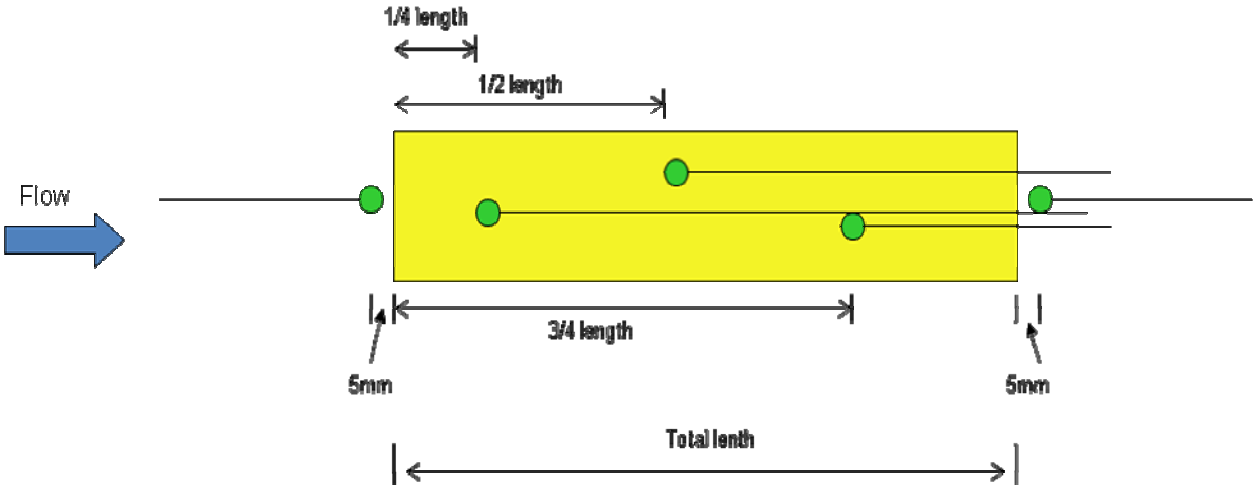

Figure 3-3. Thermocouple locations inside SCR catalyst sample

pump and enter the analyzer bench, described in Section 3.1.2.6, from either the reactor bypass or reactor sample lines.

Pressure, temperature and analyzers signals from the BFR are acquired and stored using a LabVIEW-based DAQ system. A virtual control panel is used as a user interface to both monitor and control the BFR during operation. The control panel allows the user to control the MFCs and displays real-time data. The user can save data at any point during BFR operation and write to files created by LabVIEW on the hard drive.

*3.1.2 **Mechanical Components***

3.1.2.1 Mass Flow Controllers

Mass flow controllers (MFCs) are used to regulate the flow rate of the simulated diesel exhaust gases entering the BFR. MFCs are located in the instrumentation cart described in section 3.1.3, and are controlled by a LabVIEW generated virtual control panel. The flow rate of each gas component is controlled by a MFC, which is solely dedicated to that particular gas species. Since the MFCs are calibrated with N_2 gas, the flow rate of other gases can be expressed in terms of the flow rate of N_2 via a correction factor, also referred to as K factor, which corrects for difference in molecular weight of the gas of interest and that of N_2. Lab view controls the

MFCs by varying the input voltage between 0 and 5v to correspond with the desired flow rate. Each MFC has a different linear response to the supplied voltage. Therefore, an internal feedback system is utilized to ensure correct flow rates. The concentrations of both NO_x and NH_3 in N_2 are small, so the K factor for the gas mixture is very close to that of pure N_2. The gas concentrations of the various gas cylinders used in this study are: 1% NO in N_2, 5000 ppm NO and 5000 ppm NO_2 in N_2, 5% NH_3 in N_2, 500 ppm SO_2 in N_2, 100% O_2, 100% CO_2 and 100% N_2.

3.1.2.2 Peristaltic Pump

A Masterflex™ peristaltic pump is used to inject de-ionized water into the steam generator. The pump allows for continuous water injection creating a constant concentration of water vapor leaving the steam generator. The peristaltic pump, shown in Figure 3.4, can achieve flow rates between 0.1 and 580 cc/min. The peristaltic pump is used to inject de-ionized water into the steam generator where it is vaporized and swept away by carrier gases.

3.1.2.3 Steam Generator

The steam generator consists of a Lindberg heavy-duty tube furnace, shown in Figure 3.5, and a 1.26 cm OD stainless steel tube in which liquid water evaporates into steam. The stainless steel tube sits in the tube furnace and the front 1.5 cm of the tube is packed with quartz wool while the rest is filled with glass beads. The tube is connected to a Swagelok union tee fitting. One end of the fitting is connected to a 0.64 cm OD heated line that delivers carrier gases to sweep the water vapor out of the steam generator and into the BFR system. A 0.16 cm OD steel tube is inserted through the Swagelok fitting leaving one end buried inside the quarts wool, while the other end is connected to the PVC tube carrying liquid water from the peristaltic pump. Incoming water is absorbed in the quartz wool where it evaporates and is swept away by carrier gases. The steam generator is maintained at 300°C to ensure complete water evaporation before entering the SCR reactor.

3.1.2.4 SCR Reactor

The SCR reactor consists of a 44.5 cm long quartz tube, reactor end fittings and Pyrex™ beads. The quartz tube has an ID and OD of 2.22 cm and 2.54 cm, respectively. The Pyrex™ beads are 5 mm in diameter and take up the first half of the reactor tube to enhance heating and

mixing of the simulated exhaust gases. Shown in Figure 3.6 is a reactor end fitting, which

Figure 3-4. Peristaltic pump used to inject de-ionized water into steam generator

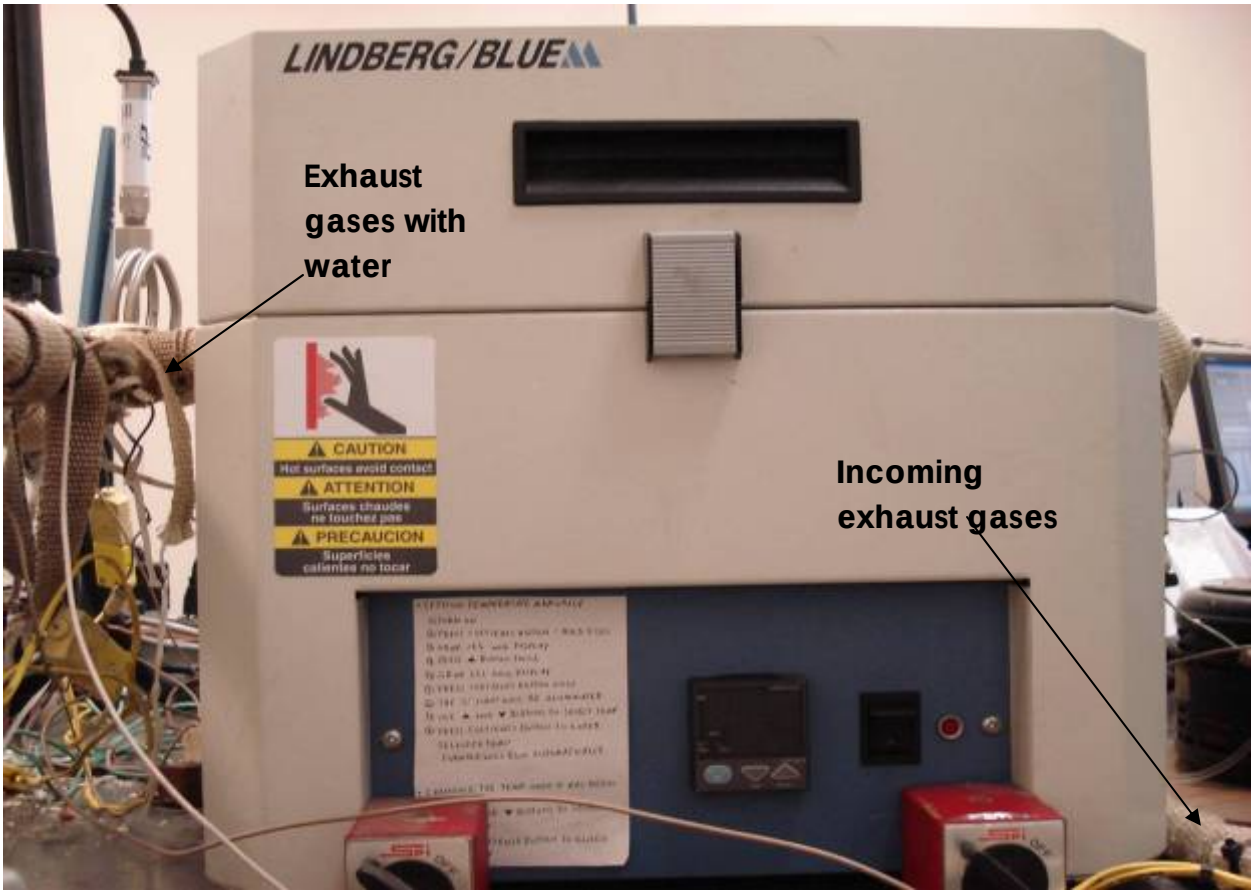

Figure 3-5. Steam generator used in bench-flow reactor system

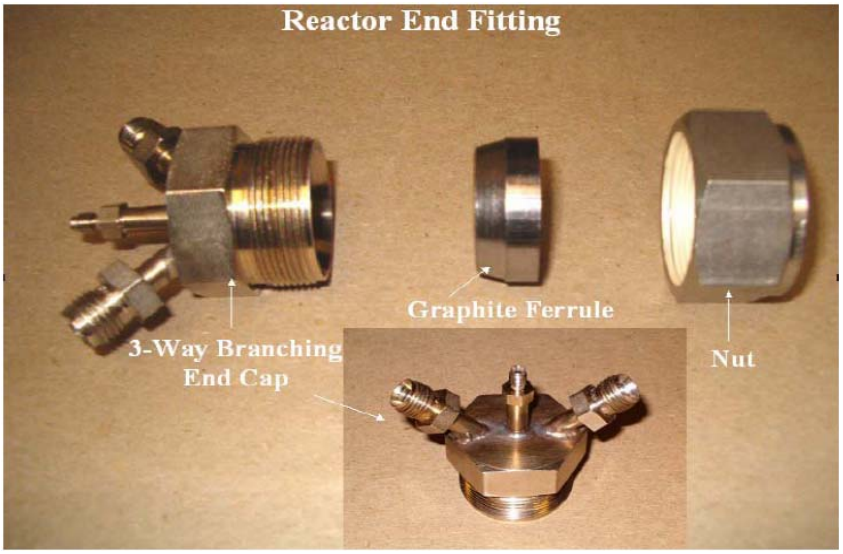

Figure 3-6. Reactor end cap with three welded Swagelok fittings served as thermocouple wells

consists of a 2.54 cm reactor end cap and tube fittings. Three Swagelok fittings are welded to the end cap, of which two are used as thermocouple wells and gas enters the remaining one.

Graphite ferrules are used to create a compression seal between the quartz tube and the reactor fitting. Graphite is used because it can withstand the high temperatures encountered in the SCR reactor; however, these ferrules do need to be replaced about once every six months. Prior to inserting in the tubular reactor the Fe-zeolite catalyst sample is wrapped in FiberFrax^{TM} glass wool to prevent gas slippage around the catalyst's circumference. Thermocouples are positioned within the SCR catalyst as shown in Figure 3.3 in Section 3.1.1. A Lindberg electric furnace, Model TF55035A-1 with a maximum operating temperature of 1100°C is used to maintain the catalyst temperature at the desired value. The furnace is equipped with a feedback control to ensure that the temperature in the middle of the furnace is kept within 1ºC of the preset temperature. Figure 3.7 is a photograph showing the SCR reactor inside the Lindberg furnace.

3.1.2.5 Analyzer Bench

The analyzer bench consists of five different gas analyzers, a vacuum pump, a NH_3 trap and cartridge filters. Before entering the gas analyzers the simulated diesel exhaust gases are sent through a NH_3 scrubber to remove any remaining NH_3 from the gas stream, and cartridge filters

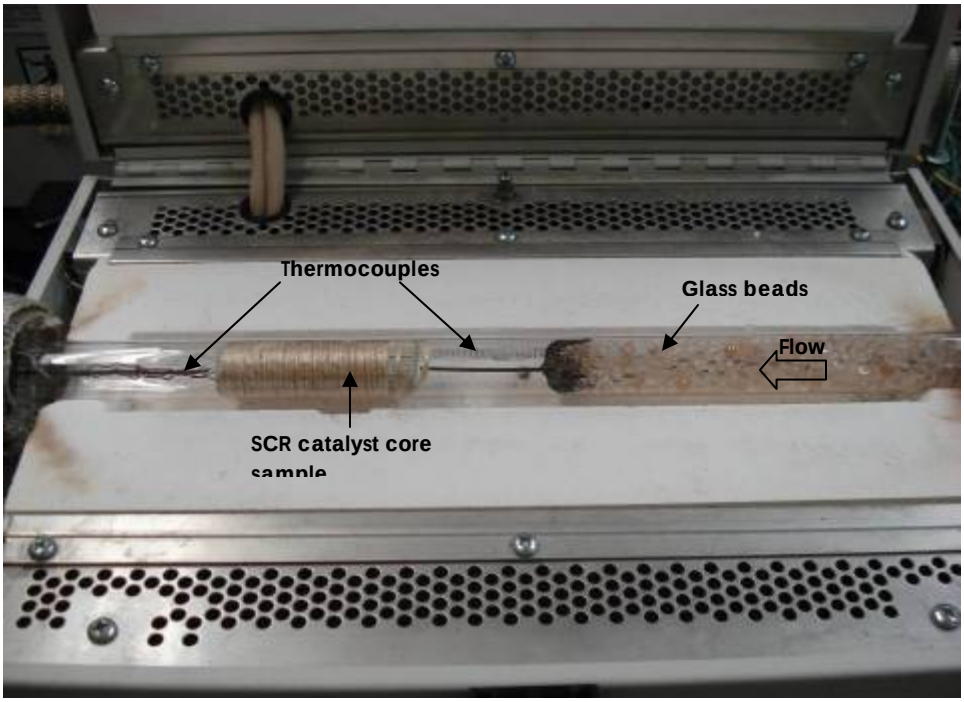

Figure 3-7. SCR reactor placed inside Lindberg furnace

for removing contaminations. The analyzer matrix switches, shown in Figure 3.8, is located on the control panel for the analyzer bench and allows the user to select which analyzers to use. For SCR evaluations only two NO_x analyzers are used; one for measuring NO_x and the other NO. The switch matrix is wired to three-way solenoid valves that regulate the flow to each analyzer. An analyzer is selected by placing its respective switch on "sample" allowing gas to flow into the analyzer for measurement.

A throttling valve and pressure regulator on the control panel regulate the flow rate and pressure of the simulated diesel exhaust gases in the analyzer bench. The pressure inside the analyzer bench is regulated to 1.63 bar (9 psig), while a pressure of 1.08 bar (1 psig) is maintained at the inlet of the SCR reactor. Gases that are not extracted for analysis are exhausted through the exhaust vent.

3.1.3 Instrumentation and Displays

All of the control and monitoring devices used during operation of the BFR are located in

the instrumentation cabinet. Pressure indicators, temperature controllers, power switches, DAQ

Figure 3-8.Analyzer bench control panel

terminal blocks and gas inlet connectors are located on the front panel of the cabinet. The DAQ system mounted at the bottom of the cabinet is wired to the monitoring equipment and PC. MFCs, switching valves and power supplies are also housed inside the cabinet, and are accessible through the back panel.

Two Cole-Parmer pressure transducers Model 07356-50 are used to monitor the pressure at the inlet and exit of the SCR reactor. The pressure transducers have a linear operating range of 0 to 2.05 bar (29.7 psig). Since pressure transducers are susceptible to thermal damage, stainless steel tubing shaped into a helix is used to cool the simulated diesel exhaust gas mixture before it reaches the transducers.

Six Omega type-K thermocouples are used to monitor temperatures in the SCR reactor. One thermocouple located just downstream of the steam generator is used as a feedback signal for the heat tape temperature controller that regulates the heated sample line leading to the SCR reactor. The other five thermocouples are positioned inside the SCR reactor as described in section 3.1.1. Two thermocouples, 1.6 mm in diameter and 31.0 cm long are positioned at the inlet and exit of the SCR catalyst to measure gas temperatures. The three thermocouples located

inside the catalyst are each 31.0 cm in length and 0.51 mm in diameter. The small diameter of the thermocouples allows them to be inserted inside the catalyst channels for monitoring the temperatures inside the SCR catalyst. During BFR operation, real-time temperature measurements are displayed on the virtual control panel.

An Athena Model – XT16 temperature controller is used to control the temperature of a heavy-insulated Samox heating tape, whose function is to pre-heat the simulated diesel exhaust gases entering the SCR reactor. The heating tape has a maximum operating temperature of 760°C. The temperature controllers using a 120 VAC power supply can be programmed to provide a constant heating rate.

*3.1.4 **Gas Analyzers***

Only two NO_x analyzers are used in the present investigation: one to measure NO and the other total NO_x. A Horiba chemiluminescence analyzer Model CLA-220 and a California Analytical Instruments chemiluminescence analyzer Model 400-HCLD are used to measure total NO_x and NO concentrations, respectively. The analyzers measure the light emissions from the chemiluminescent reaction between NO and O_3 (ozone), which is directly proportional to the concentration of NO. For the purpose of measuring total NO_x, both analyzers are equipped with an NO_2 to NO converter, giving each analyzer the ability to measure either NO or total NO_x.

*3.1.5 **Data Acquisition System***

The purpose of the data acquisition system (DAQ) is to acquire, display and save all data collected during operation of the BFR as well as control the MFCs. The DAQ consists of a Dell personal computer (PC), data acquisition boards, shielded BNC adapter chassis, terminal blocks and LabVIEW software. All thermocouple signals are gathered in a National Instruments Model TC-2095 terminal block and sent through a National Instruments Model SCXI-1102 signal amplifier. A National Instruments Model PXI-6040E DAQ card converts the analog signals into digital signals and sends them to the PC through a National Instruments Model PXI-8330 PCI card. Pressure transducer and gas analyzer signals are collected and conditioned by a National Instruments Model TBX-68 terminal block and sent directly to the PC to be displayed in LabVIEW. MFC signals are gathered using a National Instruments Model BNC-2090 connector

block and routed through a National Instruments Model PXI-6040E PCI card for data sampling and display. Finally, the signals are sent to the PC through the National Instruments Model PXI-8330 PCI card. All of the data are displayed in the LabVIEW generated virtual control panel shown in Figure 3.9, where the user can monitor and control the BFR system.

3.1.6 ***Bench-Flow Reactor Operation***

3.1.6.1 Start-up Procedures

The gas analyzers are turned on and allowed to reach steady state operating conditions. Once the NO_x analyzers have warmed up to operating temperature; they are calibrated using span and zero gases. For proper use of the MFCs, the exit pressure from the gas cylinders is regulated down to 1.72 bar (25 psig).

Once all equipment is operational, the BFR is brought to an operating temperature of 200°C by flowing only N_2 through the bypass line at a GHSV to be used during evaluation. The

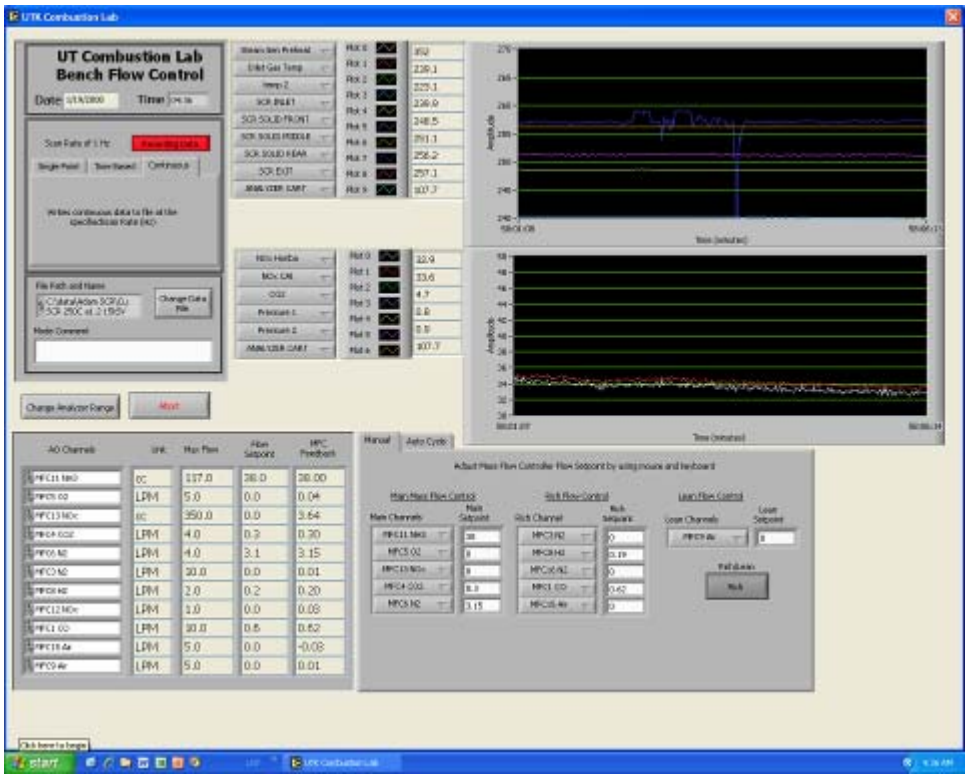

Figure 3-9. LabVIEW control panel used to monitor and control bench-flow reactor

exhaust fan and vacuum pump are turned on to provide sample pressure to the analyzers. De-ionized water is injected into the steam generator and allowed to reach steady-state at the GHSV to be used during evaluation. The mixture of inert N_2 and water vapor is sent through the system for approximately ten minutes, during which a BFR pressure of approximately 1.08 bar (1 psig) is achieved by adjusting the throttling valve on the front of the analyzer bench.

3.1.6.2 NO_x performance evaluations

Prior to performance evaluation all fresh SCR catalyst samples are de-greened to allow the catalysts to achieve stable and reproducible levels of activity. De-greening is only necessary for fresh catalysts, because aged catalysts are stable. De-greening is carried out by exposing the catalyst to a gas mixture of 5% H_2O, 14% O_2 and N_2 at a GHSV of 30,000 h^{-1} while maintaining a catalyst temperature of 600°C for 4 hours. NO_x conversion evaluations are performed using a simulated diesel exhaust gas mixture consisting of 5% H_2O, 5% CO_2, 14% O_2, 350ppm NO_x, varying amounts of NH_3 and N_2 balance at a GHSV of 30,000 h^{-1}. The alpha ratio ($\alpha = [NH_3]/[NO_x]$) is varied from 0.5 to 1.2 by changing the concentration of NH_3 between 175ppm and 420ppm in the simulated exhaust gases. Before starting an SCR evaluation, a gas mixture containing 5% H_2O, 5% CO_2, 14% O_2, 350ppm NO_x and N_2 balance is sent through the reactor bypass line to measure the SCR reactor inlet conditions and ensure a concentration of 350ppm NO_x. NH_3 is never sent through the reactor bypass line to avoid damage to the gas analyzers. To account for any NH_3 slip that may take place during SCR evaluation, all gases entering the analyzer bench pass through an NH_3 trap that removes any residual NH_3, which is known to interfere with NO_x measurements. The catalyst temperature is varied from 200°C to 600°C in 100°C increments during evaluation. It is costly to flow these gases through the BFR for extended periods of time; therefore a mixture of 5% H_2O, 14% O_2 and N_2 is used to heat up the catalyst to the desired temperatures. Once the SCR catalyst temperature has come to steady-state, the flow is switched to the simulated diesel exhaust gas mixture.

The catalyst temperature is controlled by adjusting the reactor furnace setting. The heat tape that pre-heats the simulated diesel exhaust gases is maintained at 250°C to ensure that none of the NH_3 oxidizes before reaching the reactor furnace. Temperature and NO_x concentration data are collected until the concentration of NO_x exiting the SCR reactor changes by two ppm or

less in a span of five minutes. The steady-state NO_x concentration is used to determine NO_x conversion via Eq. 3.2.

$$\frac{NO_{x,inlet} - NO_{x,outlet}}{NO_{x,inlet}} \times 100\% \qquad 3.2$$

Once the catalyst temperature and SCR reactor exit NO_x concentration have come to steady-state, the gas composition is switched back to H_2O, O_2 and N_2 for the next evaluating temperature.

3.2 Engine Bench for Accelerated Thermal Aging

3.2.1 Overall Description of Engine Bench System

The engine bench used for this study is located at the Fuels, Engines and Emissions Research Center of the National Transportation Research Center (NTRC) and has been described in detail previously by Eaton [3]. This setup was used in a series of aging and poisoning research studies [3, 38] that preceded this one. The engine bench (fig. 3.10) consists of four main components: a small single-cylinder diesel engine, an electric drive motor, an aftertreatment system and an emissions analyzer bench. The engine is a 517 cc Hatz diesel engine which was chosen to minimize expenses and mechanical difficulties associated with full-scale testing. A Baldor electric drive motor is attached to the engine with a flexible shaft coupling and both are bolted to a metal table top. The table is isolated in a test cell with vented exhaust duct and forced air circulation.

The aftertreatment system consists of a diesel oxidation catalyst (DOC), an ammonia/exhaust mixer, an SCR catalyst and a diesel particulate filter (DPF). The diesel oxidation catalyst is used to oxidize unburned hydrocarbons while the DPF is used to remove soot from the engine exhaust. The ammonia/exhaust mixer mixes injected NH_3 with the oncoming engine exhaust prior to entering the SCR catalyst. Although, the DOC and DPF are not in the focus of this study, they are essential to the SCR aging process, which is discussed in Section 3.2.5.3. The SCR catalysts used in this study are 15.2 cm in length and 7.62 cm in diameter. The engine load controller consists of an actuator connected to the engine's fuel

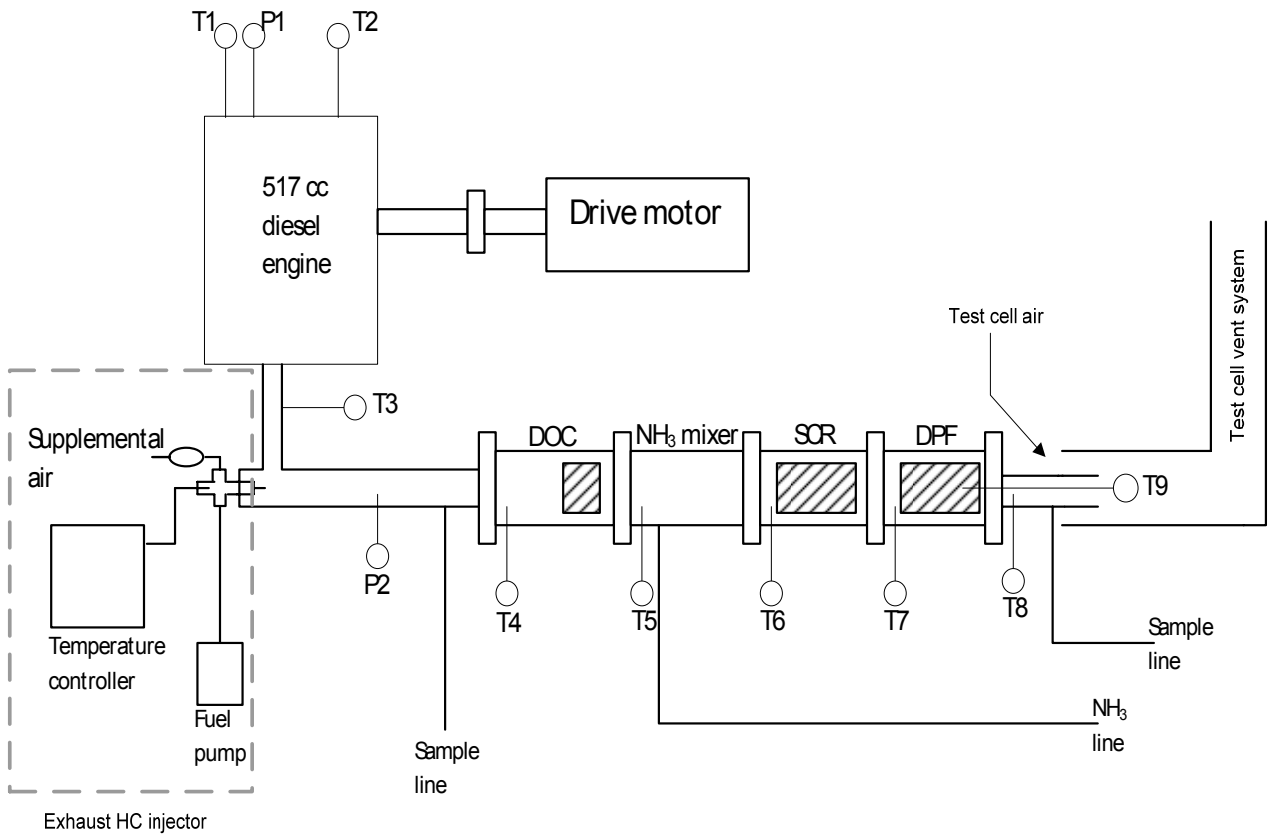

T1	Inlet Air
T2	Oil Sump
T3	Exhaust Manifold
T4	DOC Inlet gas
T5	DOC Exit gas
T6	SCR Inlet gas
T7	SCR Exit/DPF Inlet gas
T8	DPF Exit gas
T9	DPF Internal
P1	Oil Pressure
P2	Exhaust Pressure

Figure 3-10. Schematic of engine bench used for accelerated thermal aging

regulator. The actuator position is controlled with the use of LabView. The Engine Bench system used for accelerated thermal aging is shown in Figure 3.11.

Exhaust gas temperatures are measured at five different locations along the aftertreatment system with type-K thermocouples. The engine exhaust temperature is measured with a thermocouple positioned approximately 0.3m from the engine exhaust manifold. A thermocouple placed approximately 9.0 cm from the front of the DOC is used to measure the DOC inlet gas temperature. The DOC exit gas temperature is measured using a thermocouple located approximately 1.5 cm from the rear of the DOC. Thermocouples are placed about 1.5 cm from the inlet and exit of the SCR catalyst to measure the inlet and exit SCR gas temperatures. The fifth thermocouple positioned approximately 1.5 cm downstream of the DPF is used to measure the exit gas temperature. Finally, a thermocouple with a diameter of 1.6 mm is placed approximately 5.0 cm into the rear of the DPF to measure the internal DPF temperature. Two pressure transducers located near the exhaust manifold are used to measure the back pressure from the aftertreatment system. The back pressure is monitored to identify clogs in the aftertreatment system as well as monitor the progress of active DPF regenerations. One of the pressure transducers measures the absolute pressure while the other the gauge pressure. Since the aftertreatment system exits to an open collection system, these pressures represent total aftertreatment system pressure drop. Each catalyst is mounted in a 7.62 cm diameter can. Before being placed in the cans, the catalysts are wrapped in a vermiculite-coated fiber mat which provides insulation and prevents gas slippage around the catalysts' circumference. The exhaust pipe is wrapped in insulation to minimize heat losses from the aftertreatment system.

A high temperature three-way switching valve is used to sample exhaust gases, either directly from the engine or from the exit of the aftertreatment system. Two heated cartridge filters are used to remove any carbonaceous matter from the sample gases. One cartridge filter is placed immediately after the three-way valve and the other at the inlet to the analyzer bench. The sample gases are transported to the analyzer bench through a heated sample line. The analyzer bench, shown in Figure 3.12, is used to measure the volumetric concentration of NO, NO_x, CO_2, CO, O_2 and total hydrocarbons. Water vapor is removed from the sample gases that pass through the infrared analyzer to prevent condensation from forming inside the analyzer. Condensed water is collected in a water trap and pumped out of the system through a peristaltic pump.

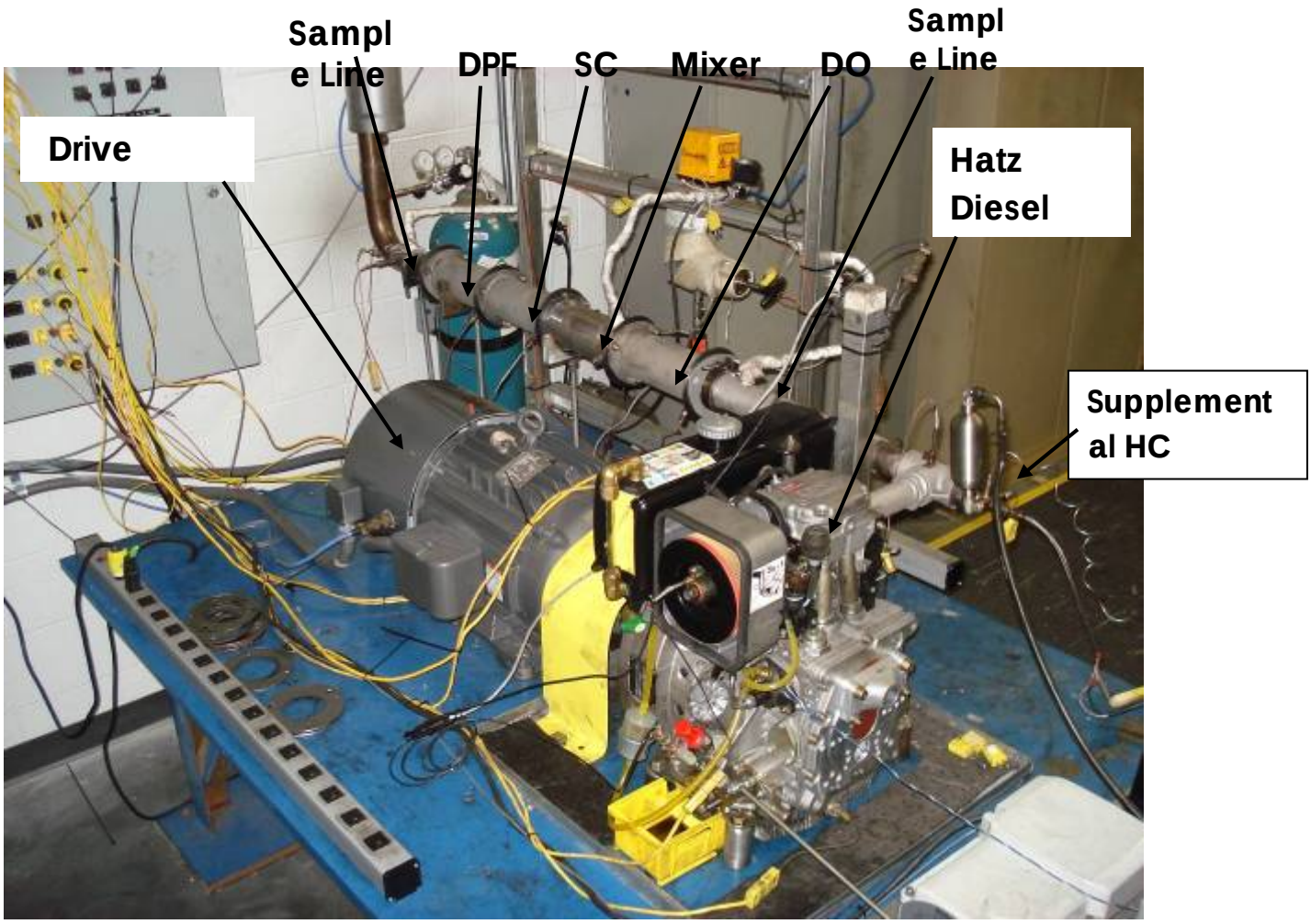

Figure 3-11. Engine bench components

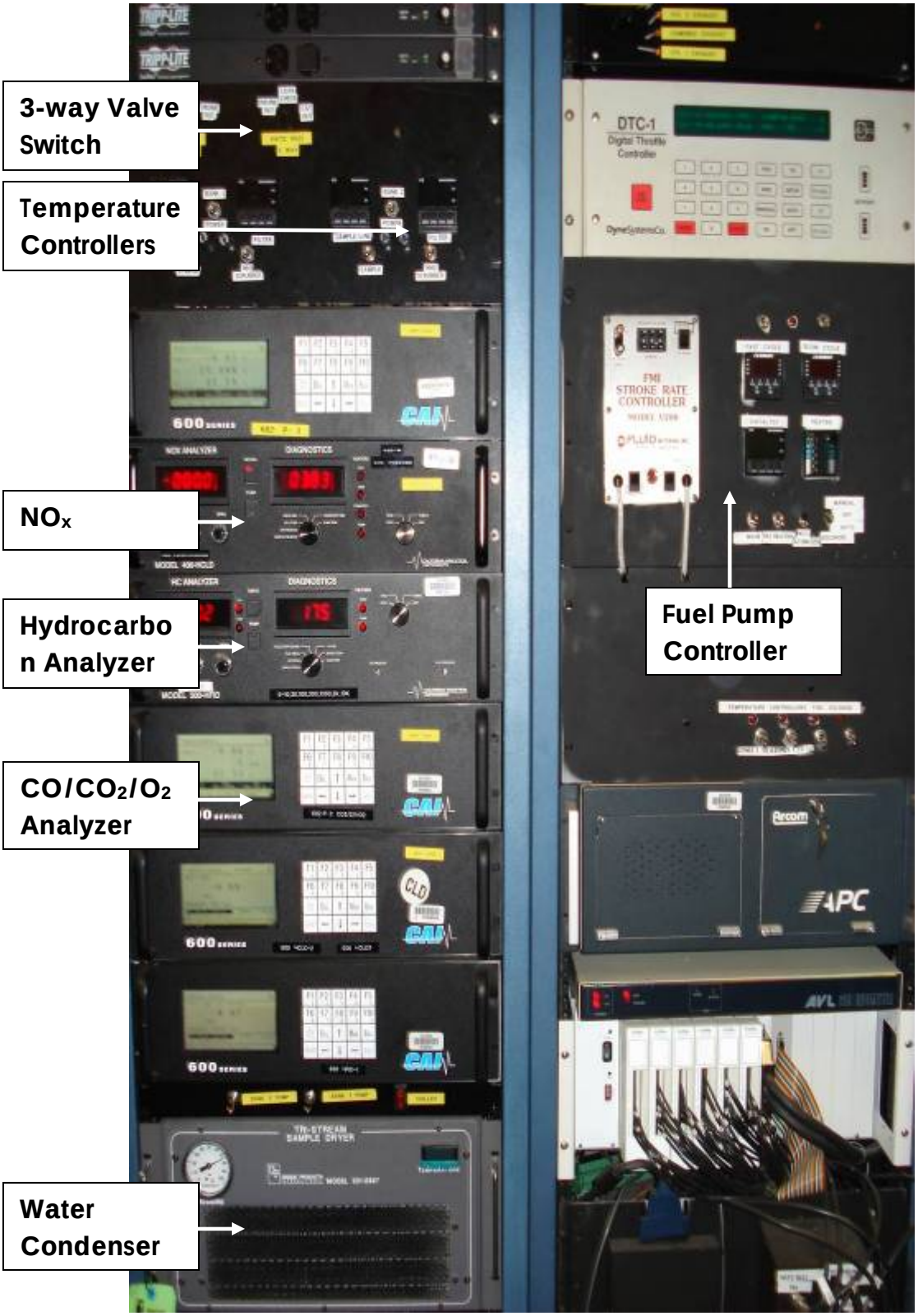
3-way Valve Switch
Temperature Controllers
NO_x
Hydrocarbon Analyzer
$CO/CO_2/O_2$ Analyzer
Water Condenser
Fuel Pump Controller
DTC-1
FMI STROKE RATE CONTROLLER
600
CAI
APC
AVL

Figure 3-12. Photograph of analyzer bench used in engine bench system

Soot collected on the DPF is burned off during the cyclical DPF regenerations used to age the SCR catalyst. This is accomplished by raising the temperature of the DPF to the combustion temperature of the soot. A fuel injection system is used to atomize fuel and inject it into the engine exhaust immediately downstream of the exhaust manifold. The injected fuel ignites as it passes through the DOC, raising the temperature of the exhaust gases. Temperatures throughout the aftertreatment system are controlled during the DPF regenerations by regulating the flow rate of the injected fuel. Although the DPF may not be completely loaded with soot, a simulated DPF regeneration is conducted after each SCR performance evaluation to raise the temperature of the SCR inlet gas to the desired aging temperature. The fuel injection system works by pumping diesel fuel from a reservoir onto a cartridge heater using a FMI Lab pump. The fuel is vaporized by the cartridge heater maintained at 375°C and swept away by compressed air as a carrier gas at a flow rate of 1000 cc/min.

*3.2.2 **Mechanical Components***

3.2.2.1 Diesel Engine

The engine used in this investigation is a naturally aspirated, direct injection (NA/DI), type 1D50Z Hatz diesel engine. The engine is a 517cc single-cylinder engine that is capable of producing 7.0 kW at 2700 RPM. An electric induction drive motor is used to start the engine and maintain an engine speed of 1500 RPM during testing. A constant engine speed allows for a nearly constant gas hourly space velocity (GHSV) through the SCR catalyst. A photograph of the engine is shown in Figure 3.13.

3.2.2.2 Drive Motor

A Baldor three-phase electric induction motor is used to start and motor the diesel engine. The drive motor is capable of absorbing/delivering 15 hp at 1765 RPM and can control engine speed to 4000 RPM. The electric motor, show in Figure 3.14, is controlled by a Vector drive variable frequency conversion unit. It is programmed to maintain an engine speed of 1500 RPM, allowing the engine to operate at various loads to alter the exhaust temperatures during testing by

changing the engine throttle controller.

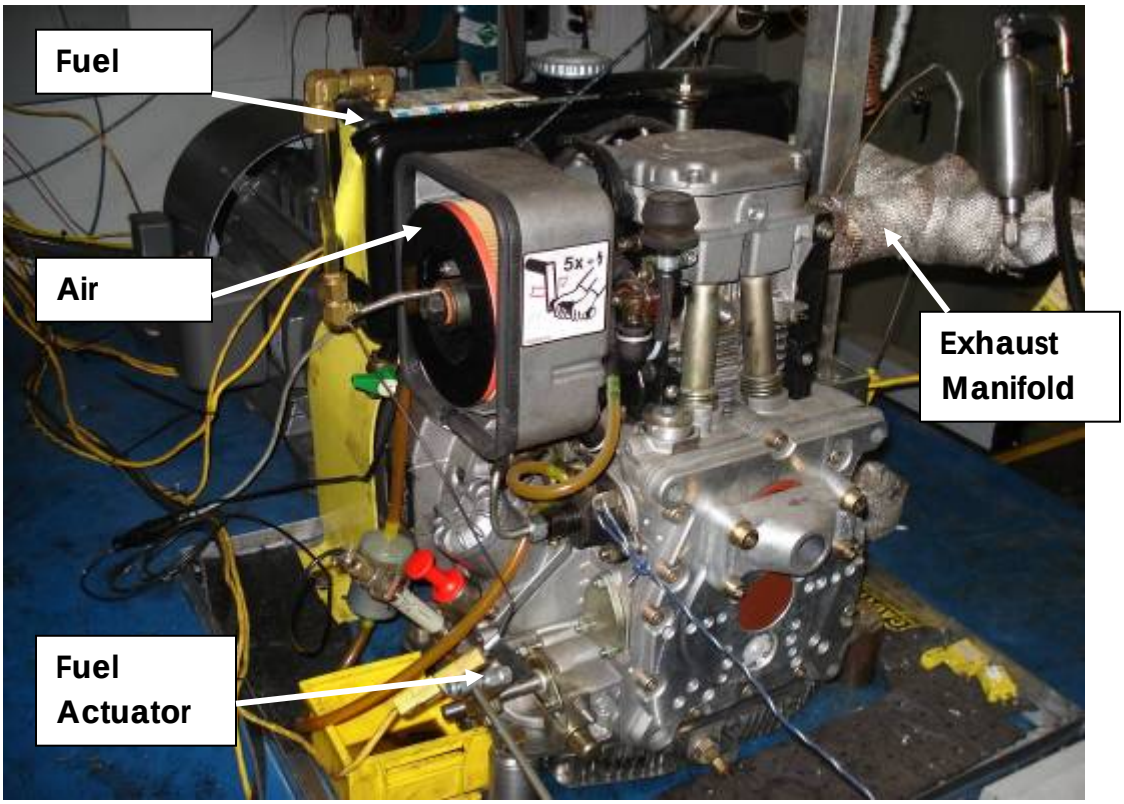

Figure 3-13. Hatz diesel engine used for accelerated aging of SCR catalysts

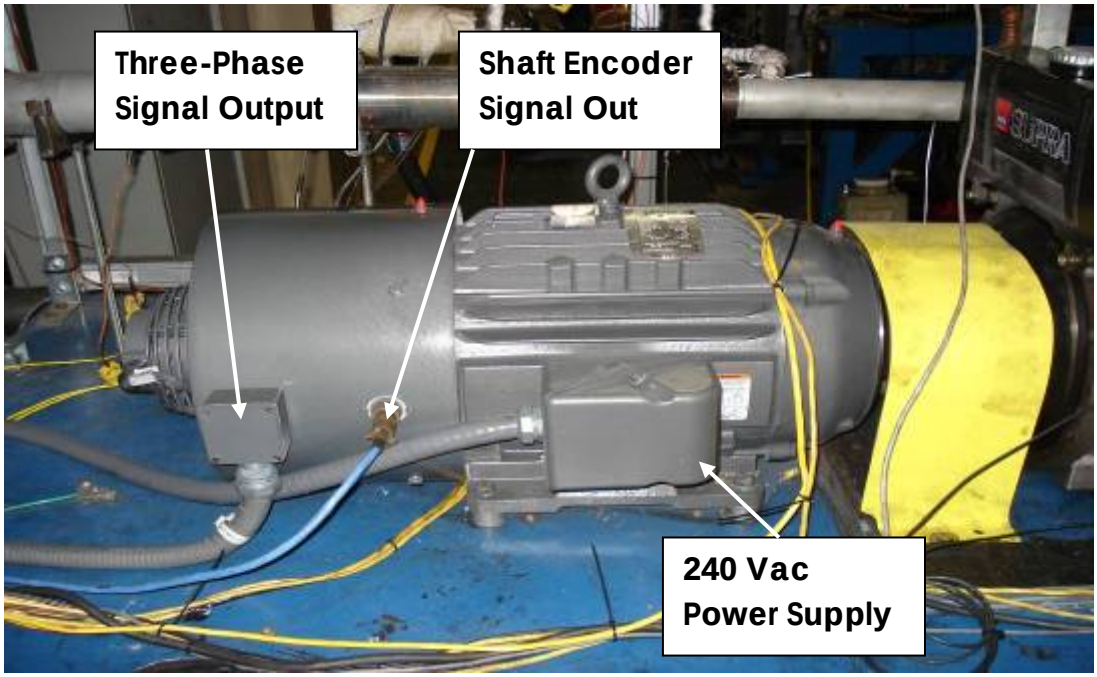

Figure 3-14. Electric drive motor used to start and motor diesel engine

3.2.2.3 Engine Load Controller

An external controller is used to control the amount of fuel that is being injected into the combustion chamber in the engine. The controller consists of a Honeywell Process Solutions Herculine 2000 series rotary actuator, wired to a PLC that communicates with the LabView program. Using the virtual control panel, the user is able to adjust the position of the actuator, which is connected to the fuel governor of the engine. The actuator mounted on the engine bench with the engine is shown in Figure 3.15.

3.2.2.4 Supplemental Fuel Pump

A FMI lab pump model RHU is used to inject atomized fuel into the engine exhaust to raise the temperature of the SCR catalyst during active DPF regenerations. The FMI lab pump is rated at 90 Vdc and 0.41 amps and delivers fuel to a cartridge heater where it is atomized and entrained by supplemental air to be injected into the exhaust where it is carried into the DOC. A picture of the supplemental fuel injection system is shown in Figure 3.16. The flow rate of fuel can be varied to alter the exhaust temperatures during active DPF regenerations. In this investigation, the desired temperature of the SCR inlet gas determines the amount of fuel

injected. The pump is capable of producing flow rates between 0 and 180 ml/min, and it is controlled by a FMI model V200 stroke rate controller. The stroke rate controller is located on the front of the analyzer bench, where the user is able to enter the desired percentage of full flow.

3.2.2.5 Exhaust HC Injection System

A five-way union used to inject supplemental fuel for DPF regeneration is installed approximately 0.3m downstream of the exhaust manifold, which can be seen in Figure 3.17. The fuel is pumped through a 1/16" stainless steel tube into the fitting. The fuel is atomized using a ¼" cartridge heater and swept into the exhaust stream using supplemental air. There is an anti-blowback chamber to prevent fuel from being pushed back into the air line by the pressure spikes that occur with each engine stroke. The cartridge heater is equipped with an internal thermocouple wired to an external temperature controller which is adjusted to maintain a cartridge heater temperature of approximately 375°C.

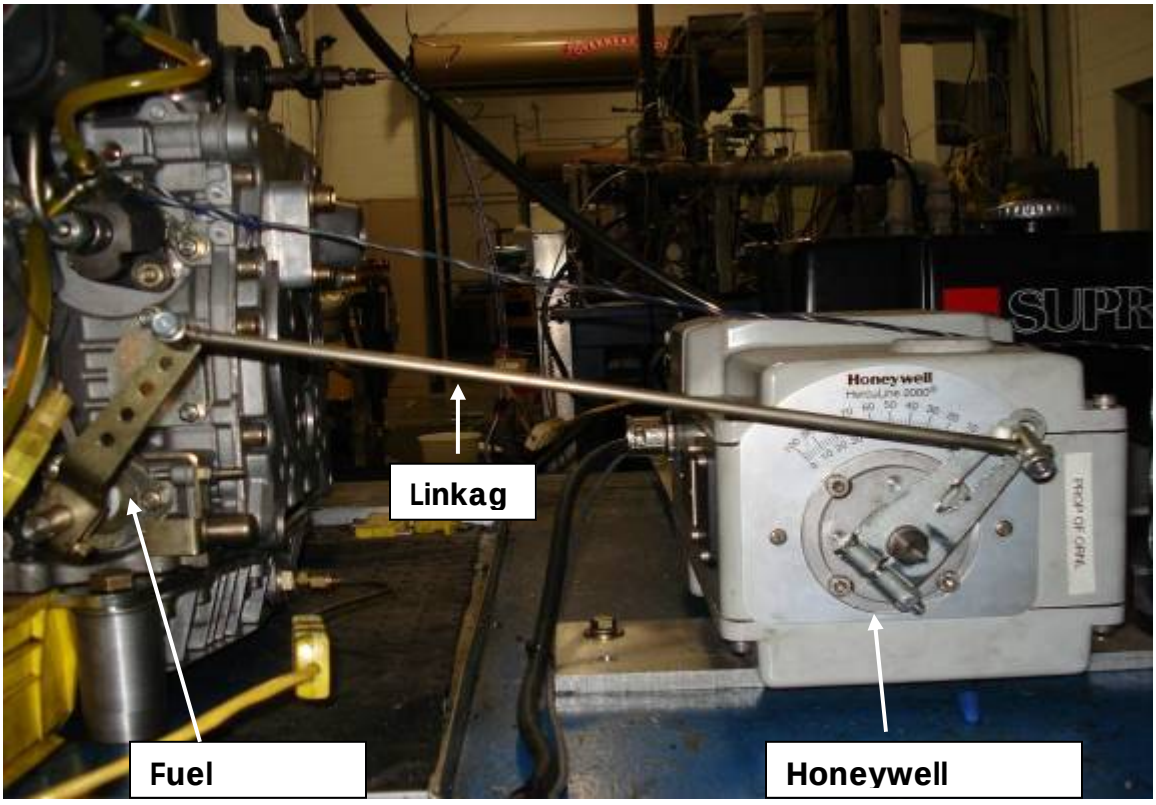

Figure 3-15. Photograph of engine load controller

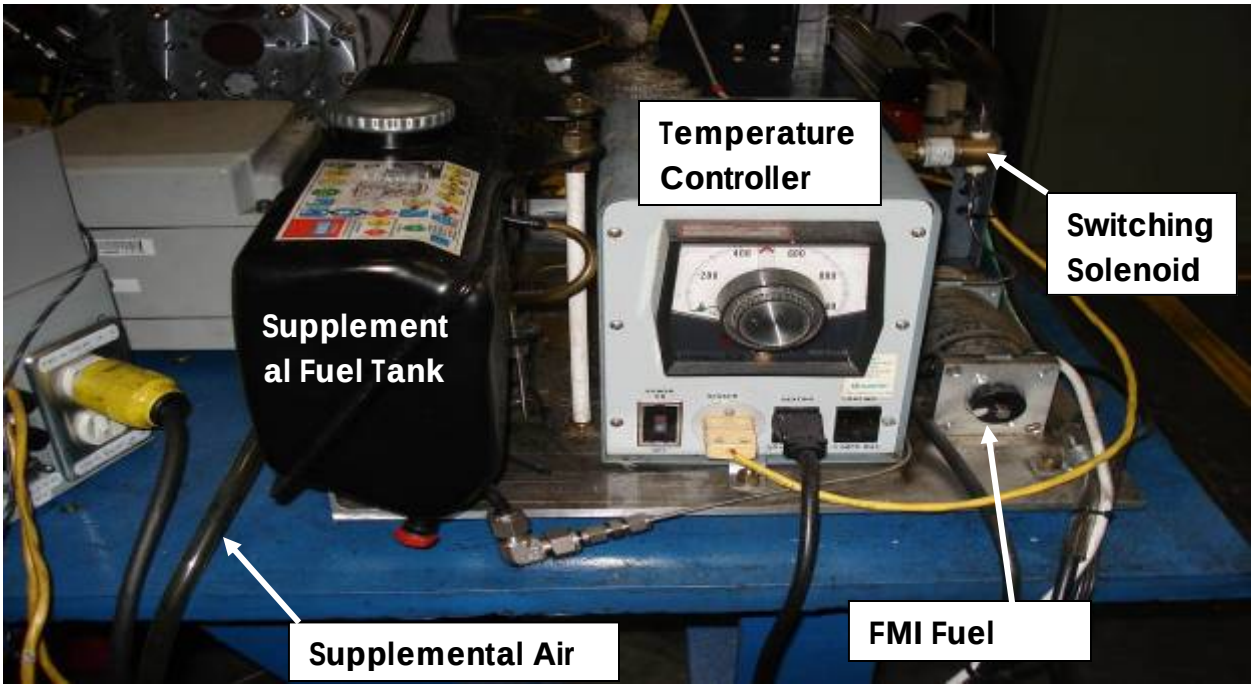

Figure 3-16. Supplemental fuel pump and temperature controller

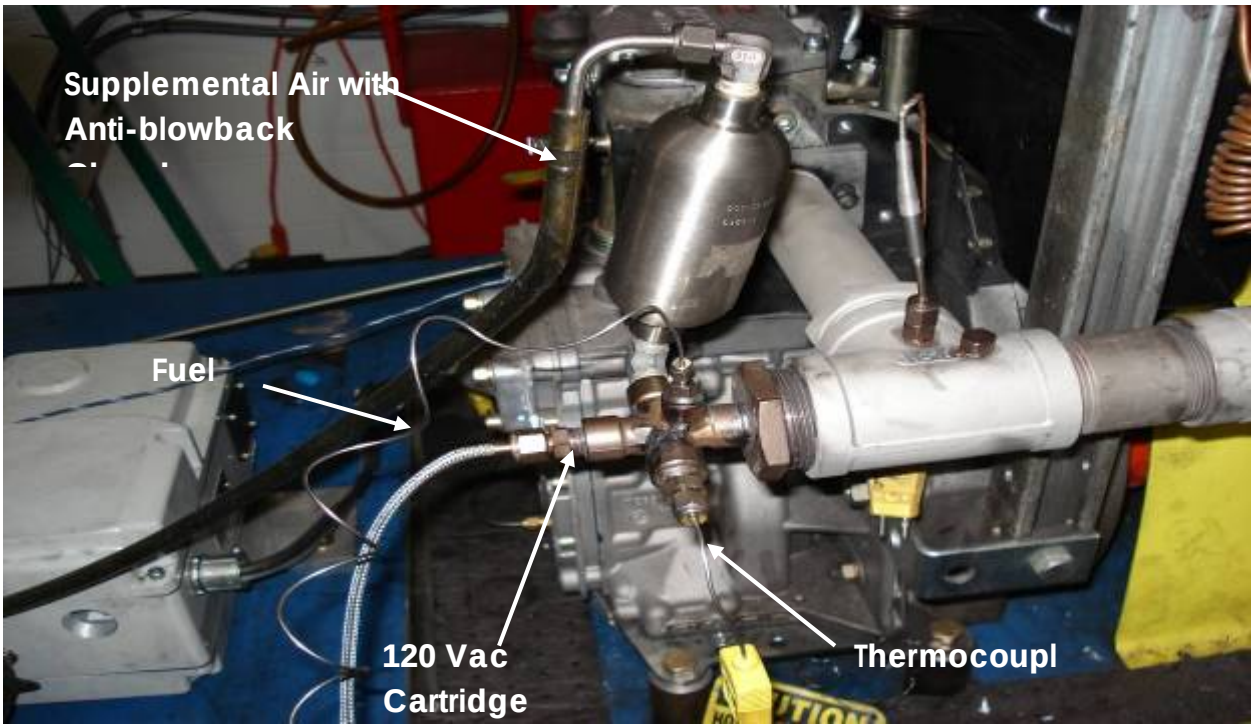

Figure 3-17. Exhaust HC injection system

3.2.2.6 NH_3 Injection System

The NH_3 injection line is connected to the front of the NH_3/exhaust mixer via a bore through Swagelok fitting. The NH_3 injection line consists of approximately 1.5m of Teflon tubing, 0.5m of stainless steel tubing and a solenoid valve separating the two sections. The 5% NH_3 in N_2 mixture is carried from a Teledyne Hastings mass flow controller through the Teflon tubing and into the NH_3/exhaust mixer via stainless steel tubing. The stainless steel section is heated with a heat tape maintained at 200°C to pre-heat the NH_3/N_2 mixture. The solenoid valve was installed to prevent backflow of the exhaust gases into the Teflon section of the ammonia injection line. When the NH_3 injection is turned on, the flow rate of the NH_3/N_2 mixture is regulated by a mass flow controller, which is controlled by a Teledyne Hastings HPS-100 Power Supply that is located next to the PC in the control room.

*3.2.3 **Instrumentation and Displays***

There are three pressure transducers employed in the engine bench. An Omega model PX61 pressure transducer is mounted to the engine block to measure lube oil pressure. The other two pressure transducers, an Omega model PX PX611 and an Omega model PX177 are used to measure absolute and gage pressures, respectively. The back pressure reading is used to monitor the engine and aftertreatment system operating conditions.

Five temperature controllers are used to control the temperature of the heated sample lines and heat tapes in the engine bench. Two of the Omega model CN 79000 temperature controllers are used to control the heat tapes that heat the stainless steel sample lines shown in Figure 3.12. Two other controllers are used to heat gaseous NH_3 and the cartridge filter located just downstream of the three way switching valve. The remaining temperature controller is an Omega model CN 77000 that is used to control the heated sample line that carries the sample gases from the three-way switching valve to the analyzer bench. All of the temperature controllers are set to 200°C.

*3.2.4 **Data Acquisition System***

The data acquisition system (DAQ) is used to monitor and store data generated during operation of the engine bench. The major components of the DAQ consist of a PC with LabView

8.2, terminal blocks, a PLC, patch cables, adapters and data acquisition boards. Within the test cell is an instrumentation cabinet which houses the PLC, terminal blocks and data acquisition boards. The instrumentation cabinet supplies power to the pressure transducers and measures voltage signals from the thermocouples and pressure transducers. Each instrument is connected to a terminal block where the analog signals are converted to digital signals using a National Instruments cFP-2120 Compact Field Point controller. The digital feed is connected to the building local area network (LAN) through a CAT-6 ethernet cable where it can be accessed by any computer with the associated LabView executable.

The LabView program used for acquiring and storing data from the engine bench is named "Hatz User interface2". There are two user interface windows within the LabView program: the "Data Monitoring" window and the "Time-elapsed Graphs" window. The "Data Monitoring" window, shown in Figure 3.18, displays system data in numerical form and allows the user to calibrate channels, vary data saving parameters and add mode comments. From the "Time-elapsed Graphs" window, the user is able to select and monitor real-time data on four customizable charts with drop-down menus. A screen capture of the "Time-elapsed Graphs" menu is shown in Figure 3.19.

*3.2.5 **Accelerated Aging Engine Bench System Operation***

3.2.5.1 Engine Start-up Procedure

At the beginning of each day of testing a visual safety inspection is conducted on the engine bench and surrounding area. The gas analyzers are calibrated with span and zero gases and all temperature controllers are turned on, so the various heated components can warm up. The engine's oil level is checked and the fuel tank is filled. Once, all of the components have reached operating conditions and it has been deemed safe to operate the engine, the overhead exhaust fans and ventilation supply air are turned on. The drive motor is turned on and begins to motor the engine at 1500 rpm. The engine speed can be varied via the velocity control knob located on the drive motor control console, but is maintained at 1500 rpm for this study. The engine load controller is set to provide an approximate exhaust temperature of 350°C and this load setting is maintained throughout the experiment.

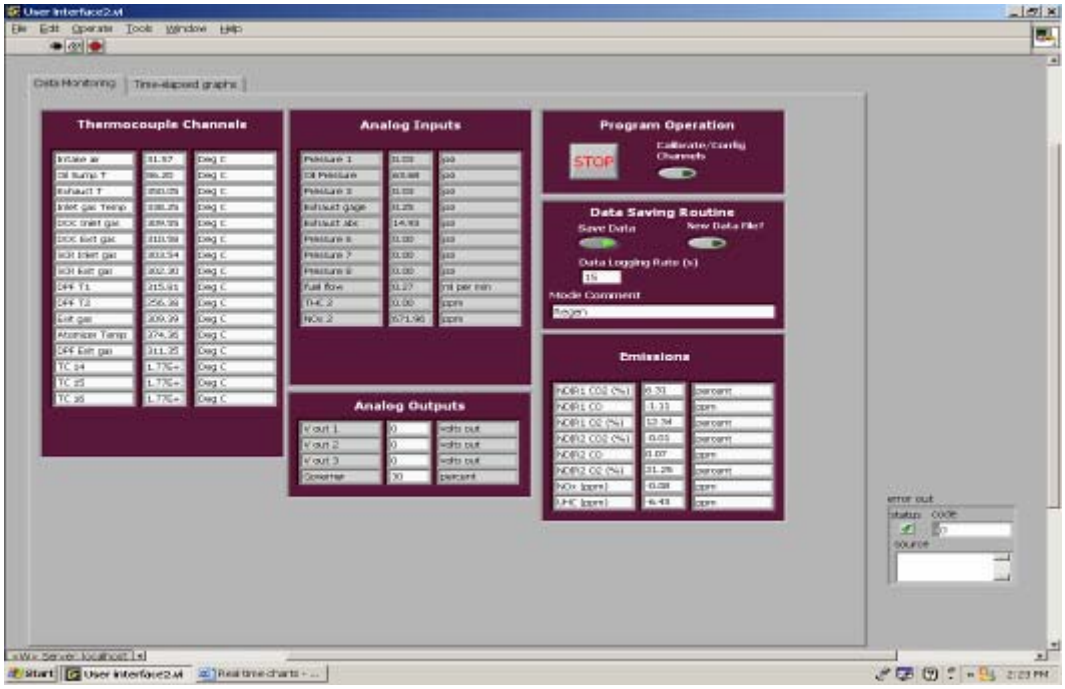

Figure 3-18. LabView user interface "data monitoring" window

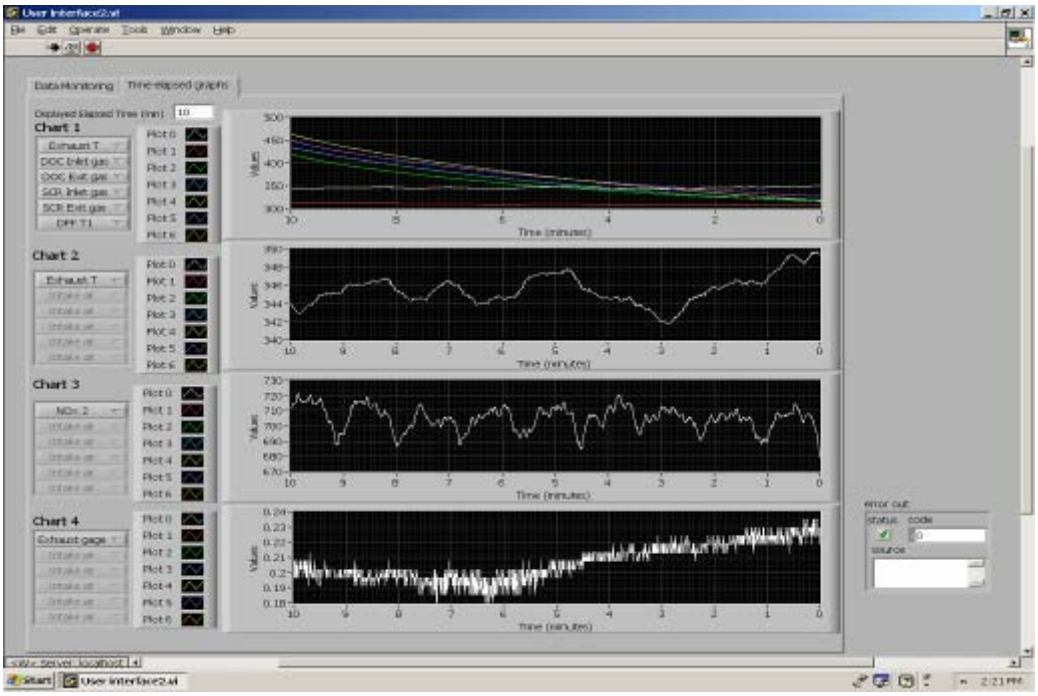

Figure 3-19. LabView user interface "time-elapsed graphs" window

3.2.5.2 Engine Bench NO_x Reduction Evaluation

After each aging cycle (DPF regeneration), the NO_x performance of the SCR catalyst is evaluated. After regeneration is completed the aftertreatment system temperatures stabilizes for twenty minutes. Once the after treatment system has reached normal operating temperatures, three different NO_x measurements are taken: concentration of NO at the DPF exit, concentration of NO at the DOC inlet and concentration of total NO_x at the DOC inlet. The three-way switching valve makes it possible to select sampling either from the inlet or exit of the aftertreatment system. NH_3 is injected into the system at a ratio of NH_3 to NO_x of 0.6 ($\alpha = 0.6$) over the SCR catalyst. Using the concentration of NO_x at the inlet to the aftertreatment system, the flow rate of NH_3 gas is calculated to be 60% of the incoming concentration of NO_x. This is accomplished using a spreadsheet that requires desired α ratio and NO_x concentration as inputs. This low alpha ratio is chosen to ensure that no ammonia slip occurs. With the addition of NH_3, the concentrations of NO and total NO_x are measured at the exit of the aftertreatment system. The engine-based NO_x performance evaluation is used to track aftertreatment system performance as the aging progresses.

3.2.5.3 DPF Active Regeneration

The SCR catalyst is aged by periodically performing active DPF regeneration at elevated temperatures. During the regenerations the DPF and SCR catalysts are cleaned of soot collected during engine operation. This is achieved by increasing the catalyst and DPF temperatures with supplemental fuel injected into the exhaust upstream of the DOC. The fuel flow rates are calibrated and adjusted to provide specific SCR catalyst temperatures. The entire regeneration cycle lasts twenty-five minutes. Catalyst and filter temperatures are constantly monitored and fuel flow rates are adjusted to achieve desired SCR inlet gas temperature.

3.3 Experimental Catalysts and Filters

The DOC, SCR catalyst and DPF used in this investigation are commercially available and used in mainly heavy-duty diesel engine applications. The SCR catalyst used in this study came from one of two sources: fresh SCR catalysts straight from the manufacturer and a field-

aged SCR catalyst that was removed from a diesel transit bus after three years of operation. The

Table 2. Experimental catalyst and filter specifications

	DOC	SCR			DPF
Aging mechanism	engine bench-aged	field-aged	BFR-aged	engine bench-aged	Engine bench-aged
Substrate material	cordierite	cordierite	cordierite	cordierite	cordierite
cpsi	400	300	400	400	200

formulation and design of these catalysts have been superseded by newer designs, based in part on some of the issues identified in the field-aged parts. The field-aged catalyst was cut into three sections: front, middle and rear. The fresh catalysts are used to determine the extent of deactivation experienced by the field-aged catalyst, and to compare lab-aged with field-aged catalysts. The SCR catalysts used in this study consist of a Fe-Zeolite washcoat supported on a cordierite substrate. A detailed description of the catalysts and DPFs used in this study is provided in Table 2. All of the catalyst and filters are manufactured by Catalytic Solutions, Inc. of Oxnard California and the cordierite substrates are provided by NGK Automotive Ceramics, Inc.

*3.3.1 **BFR-aged SCR Catalysts***

In addition to engine aging some fresh SCR catalyst cores are also hydrothermally-aged on a bench-flow reactor according to CLEERS [1] aging protocol. A gas flow of 5% H_2O, 5% CO_2, 14% O_2, 28 ppm SO_2 and N_2 balance is used while the catalyst temperature is maintained at 670°C. After de-greening for four hours the NO_x performance of the fresh SCR catalyst is determined at a GHSV of 30,000 h^{-1}. The catalyst is then aged for a total of sixty-four hours with NO_x performance evaluated every 16 hours of hydrothermal aging.

*3.3.2 **Engine-Aged SCR Catalysts***

Fe-Zeolite SCR catalysts are aged on the engine bench by raising the catalyst temperature during DPF regenerations. Supplemental fuel is injected into the exhaust upstream of the DOC. The excess fuel combusts as it passes through the DOC, thus raising the temperature of the SCR catalyst and DPF located downstream. Fuel flow rates are calibrated to achieve a maximum SCR inlet gas temperature during the regenerations. The fuel flow rate is increased stepwise in five-minute increments until the targeted aging temperature is reached. In such a manner uncontrolled DPF regeneration is avoided, preventing rapid soot oxidation, which can lead to DPF temperatures in excess of 1200°C. Table 3 lists the nominal aging temperatures and the corresponding number of DPF aging cycles. Table 4 shows the number of temperature steps and the corresponding time duration required to reach the nominal aging temperature. There are less aging cycles at 650 and 850°C because of problems that arose during aging at these temperatures.

3.4 Characterization Techniques

In this study, a number of surface characterization techniques are used to identify physical and chemical changes to the Fe-zeolite SCR catalysts as the result of aging. In this section the underlying theory of each characterization technique is briefly described as well as the equipment and sample preparation. Electron Probe Microanalysis (EPMA) is discussed in Section 3.4.1. X-ray Diffraction (XRD) is detailed in Section 3.4.2 and Scanning Electron Microscope (SEM) is presented in Section 3.4.3. Finally, BET surface area measurement is discussed in Section 3.4.4.

3.4.1 Electron Probe Microanalysis

Electron Probe Microanalysis (EPMA) is used for SCR catalyst materials characterization and produces both elemental and spatial information. Information is acquired by collecting X-rays emitted from a sample when probed by a high-energy electron beam. The X-ray detectors and accompanying software map the location of the washcoat components and identify any migration that has occurred during aging.

A finely-focused beam of electrons impinges on the surface of the sample in an ultra high vacuum (UHV) chamber. The collisions impart energy to the electrons of the sample's atoms,

inducing an energized state. As a result energy is released in the form of X-ray radiation as the electrons "relax" back to a lower energy state. The amount of energy released during the

Table 3. SCR catalysts aged on engine bench

SCR catalyst	Nominal Aging Temperature (°C)	Aging Cycles
1	850	13
2	750	50
3	650	31

Table 4.Temperature steps and time duration required to reach nominal aging temperature

		Maximum temperature obtained during temperature step (°C)		
Temperature step	Duration of temperature step (min.)	Aging at 650°C	Aging at 750°C	Aging at 850°C
1	5	390	390	390
2	5	480	475	540
3	5	560	600	710
4	10 min.	650°C	750°C	850°C

relaxation process is equal to the amount of energy consumed during the excitation process. Since each element possesses unique states of energy, elements can be identified from the wavelengths of the X-ray radiation released during the relaxation process.

The Cameca Model SX-52 EPMA device used for this study is shown in Figure 3.20 and is located at the University of Tennessee. The device consists of five wavelength-dispersive spectrometers, a high resolution energy dispersive solid state detector and an electron optical column which produces a high-energy electron beam. The electron beam is produced by a self-biasing LaB_6 cathode with double aperture beam regulation with a 0.5 to 300 nA beam current.

The X-ray spectrometers have a range between 0.22 and 0.83 sine-theta with a 40° X-ray takeoff angle and $1x10^{-5}$ sine-theta resolution. The solid-state energy dispersive detector is an Xflash 2000 detector with a resolution of less than of 159 eV at 1000 counts/s and 170 eV at 30,000 counts/s. The resolution of the detection area is approximately 2 um in diameter and the detector

Figure 3-20. Cameca electron probe microanalysis instrument

is capable of identifying elements between Sodium and Uraniumm. The EPMA setup is not capable of obtaining quantitative results for elements that are lighter than Sodium.

Line-scans and elemental maps are obtained for each of the catalysts used in the investigation. Line-scans are a trace of elemental concentrations of Mg, Al, Si, P, S, Zn, Fe, Zr, Ca, Ce and O at a cross-section of the washcoat. The scans are used to plot out element concentrations as a function of distance into the washcoat. Element maps are rastered areas of the SCR catalyst in which X-ray data is collected and discretized to produce an image showing the locations of each element [38-40].

Sample preparation for EPMA is somewhat of a delicate process, and it can affect the accuracy of the results. The manner in which EPMA is conducted requires that the sample be perfectly flat and smooth, and much care is taken to ensure that the samples are as flat and smooth as possible. Cross-sections cut from the SCR catalysts are placed in molds and embedded

with a resin, which is specially formulated to fill pore sizes smaller than 1 μm. The epoxy-embedded samples are then degassed in vacuum prior to curing. Once cured the samples are cross-sectioned with a diamond saw, removing the rough top surface. The samples are then polished to a 1μm finish. The resulting area for analysis is approximately 2.5 cm in diameter and contains between 20 and 70 channels.

3.4.2 ***Powder X-ray Diffraction***

X-ray diffraction makes use of the phenomenon known as Bragg reflections to determine the chemical compounds present in a powder sample. When a crystalline structure is bombarded with monochromatic X-ray radiation of wavelength λ, Bragg reflections are produced due to atomic lattice spacing that acts as a three-dimensional grating that diffracts the incident X-rays at specific angles. Reflections occur according to Bragg's law:

$$n\lambda = 2d\sin(\theta) \tag{3.3}$$

Where n is the order of the reflection, λ is the wavelength of the incident X-rays, d is the atomic spacing between atoms and θ is the incident angle between the surface and the X-ray beam. If the sample does not contain characteristic crystalline distances in its crystal structure then Bragg's law is not followed and no predictable X-ray reflections will be produced.

In typical XRD devices, an incident X-ray beam made up of monochromatic X-rays of a prescribed wavelength is directed towards a sample. A pattern is produced by measuring the angle and intensity of the reflected X-rays with the use of a rotating arm detector. The pattern consists of a series of peaks located at angles at which the X-rays are reflected and an intensity that corresponds to the strength of the X-rays with each corresponding wavelength. Since the spacing between atomic layers in a compound's crystalline structure is unique, the angle of diffraction can be used to determine the compound present in the powder sample. The total amount of X-ray signal diffracted at a certain angle is proportional to the concentration of the corresponding compound present in the sample and is observable in the XRD patterns where the concentration is proportional to the area under the corresponding peaks [38, 40].

In this study, approximately 1.0 g of zeolite washcoat is scraped from the substrate and ground into a fine powder. The waschoat is removed from the cordierite substrate to eliminate, as

much as possible, interference from the crystalline structure in the cordierite. The material is placed on a zero background carbon plate of approximately 3.8 cm in diameter. Scans are taken using a Philips wide-angle XRD, located at Oak Ridge National Laboratories (ORNL) with a CuKα radiation source over a 2° angle of 5-75° in a scan mode of 0.02° in 2s. The XRD patterns obtained are used to determine changes in the chemical composition of the Fe-Zeolite SCR catalyst due to aging. A photograph of the wide-angle XRD instrument is shown in Figure 3.21.

Figure 3-21. Wide-angle X-ray diffractometer

3.4.3 Scanning Electron Microscopy/ Energy Dispersive X-ray Spectroscopy

Scanning electron microscopy and energy dispersive X-ray spectroscopy are very similar in operation to EPMA. A high-energy electron beam is focused onto a sample, which is under UHV. The incident beam induces the release of high-energy electrons and X-ray radiation. An electron/X-ray detector counts the number of incident particles on the detector for each discretized area of the sample. The computer interprets the total number of counts and allocates

the numerical value to an image generating routine, which produces and displays an image based on the relative electron/X-ray intensities.

Two forms of electron information are produced by this method, secondary electrons and backscattered electrons. Secondary electrons are emitted from the top surface atoms in the sample being analyzed. They are the primary source of information yielding surface topography and morphology. Backscattered electrons are incident electrons that have been reflected into the detector. The intensity of the reflected electrons is directly proportional to the atomic number of the elements present in the sample.

Electron dispersive X-ray spectroscopy (EDS) is used to determine the concentration of the elements present in the top few atomic layers of the sample. X-rays emitted from the surface are unique to the element from which they originated. By detecting the energy of the emitted X-rays, an energy spectra can be produced from which elements can be identified [34, 35, 36].

In the current study, SCR washcoat surface topography is evaluated using a Leo 1525 field emission SEM outfitted with a Link Oxford EDS detector. The device is located at the University of Tennessee and shown in Figure 3.22. Cube-shaped SCR catalyst samples are cut from the catalysts so that the visible surface area is approximately 1 mm^2. The samples are coated with a 3 nm layer before evaluation. The gold coating electrically grounds the samples to enhance the resolution of the SEM pictures, while retaining elemental information for EDS.

3.4.4 ***BET Surface Area Measurements***

BET theory is a well known rule for the physical adsorption of gas molecules on a solid surface and is the foundation of an analytical technique used for measuring the specific surface area of a material. The letters B.E.T. are used in recognition of Stephen Brunauer, Paul Hugh Emmet and Edward Teller, who published the first article on BET theory in 1938 [41]. The measurement is an extension of the Langmuir theory, which describes monolayer molecular adsorption. The Langmuir theory states that the adsorption of gas molecules on a solid surface is a function of concentration or partial pressure of the gas when the temperature remains constant. BET extends the theory from monolayer adsorption to multilayer adsorption with the following three hypotheses. Gas molecules physically adsorb on a solid in layers, with no interaction between each adsorption layer and the Langmuir theory can be applied to each layer. The resulting BET equation is expressed as 3.4.

$$\frac{1}{\upsilon[(P_o/P)-1]}=\frac{c-1}{\upsilon_m c}\left(\frac{P}{P_o}\right)+\frac{1}{\upsilon_m c} \tag{3.4}$$

P and P_o are the equilibrium and saturation pressures of the adsorbates at the temperature of adsorption, υ is the adsorbed gas quantity, υ_m is the monolayer adsorbed gas quantity and c is the BET constant which is calculated with Equation 3.5.

Figure 3-22. Scanning electron microscope with energy dispersive spectrometry detector

$$c = \exp\left(\frac{E_1 - E_L}{RT}\right) \tag{3.5}$$

E_1 is the heat of adsorption for the first layer and E_L is that for the second and higher layers. Equation 3.4 is an adsorption isotherm and can be plotted as a straight line with $1/\upsilon[(P/P_o)-1]$ on the y-axis and $\varphi = P/P_o$ on the x-axis as shown in Figure 3.23. This plot is called a BET plot. The value of the slope A and the y-intercept I are used to calculate the monolayer absorbed gas quantity υ_m and the BET constant c.

$$\upsilon_m = \frac{1}{A + I} \tag{3.6}$$

$$c = 1 + \frac{A}{I} \tag{3.7}$$

A total surface area S_{total} and specific surface area S are calculated with Equations 3.8 and 3.9. Where N is Avogadro's number (6.022×10^{23} mol^{-1}), s is the adsorption cross-section, V is the molar volume of adsorbent gas and a is the molar weight of the adsorbed species.

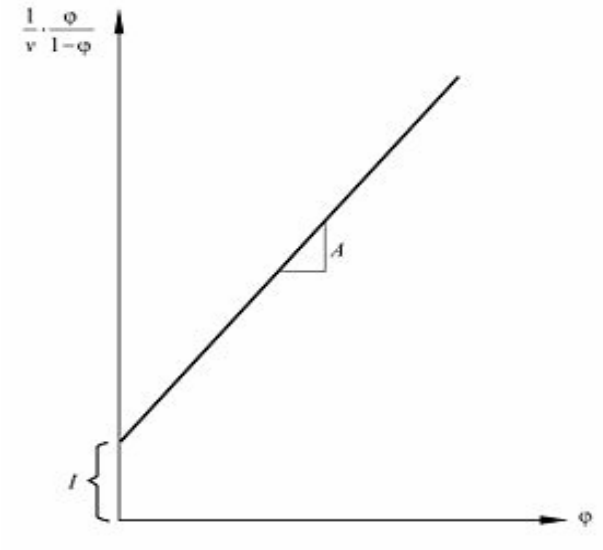

Figure 3-23. BET Plot

$$S_{Total} = \frac{(\upsilon_m Ns)}{V} \tag{3.8}$$

$$S = \frac{S_{Total}}{a} \tag{3.9}$$

The sample preparation is similar to that of X-ray diffraction except both the washcoat and substrate are used in this technique. Approximately 0.2 g is obtained from a catalyst core. The sample, containing washcoat and substrate is crushed and sifted through a 500 μm screen and any remaining sample larger than 500 um is re-ground using a medicine bowl to ensure it passes through the screen. The contribution of the high surface area washcoat to molecule adsorption is much greater than the low surface area of the cordierite substrate. Before being loaded in a micro-reactor to take adsorption measurements, the sample is weighed. The mass of the sample has a large impact on the accuracy of the results, therefore it is important to take care when measuring the mass of the sample. The micro-reactor is located at the Fuels, Engines and Emissions Research Center of Oak Ridge National Laboratories (ORNL) at the National Transportation Research Center.

CHAPTER 4 RESULTS AND DISCUSSION

This chapter consists of a presentation and discussion of the results obtained from the present study—effect of thermal aging on the performance of Fe-Zeolite SCR catalysts. Section 4.1 discusses BFR NO_x performance evaluations and materials characterization of fresh and field-aged Fe-zeolite SCR catalysts. Section 4.2 addresses SCR performance degradation and material changes resulting from accelerated thermal aging. Finally, in Section 4.3 a comparison between field-aged and accelerated engine-aged catalysts is given, from which the validity of implemented accelerated thermal aging protocol in replicating the aging conditions observed in the field-aged catalyst is assessed.

4.1 Fresh and Field-Aged Fe-Zeolite SCR Catalysts

The field-aged Fe-zeolite SCR catalyst, obtained from Catalytic Solutions, Inc, was taken off a European bus after three years of field service and sliced into three sections: front, middle and rear. Fresh catalysts of the same formulation, referred hereafter as Fe-SCR-1 are also provided by Catalytic Solutions. These catalyst samples shown on the left side of Figure 4.1 are used solely for NO_x performance evaluation in the bench-flow reactor. Since Fe-SCR-1 catalysts are no longer commercially available, Catalytic Solutions provided fresh catalyst bricks of similar formulation, referred to as Fe-SCR-2, which are used for accelerated thermal aging in a small engine bench. The Fe-SCR-2 formulation is very similar, but newer, compared to the Fe-SCR-1 formulation. Catalyst cored samples obtained from these bricks are shown on the right side of Figure 4.1.

4.1.1 Bench-Flow Reactor Evaluation

Prior to evaluation, fresh catalyst samples are “degreened” for 4 hours at 600°C with a gas composition consisting of 5% CO_2, 5% H_2O, 14% O_2, and N_2 balance at a gas hourly space velocity of 30,000h^{-1}, as prescribed by the CLEERS protocol [1]. Since field-aged catalysts have already achieved stable and reproducible levels of activity, “de-greening” is only necessary for

fresh catalysts. Evaluation experiments are performed at 200, 300, 400, 450, 500 and 600°C (5%

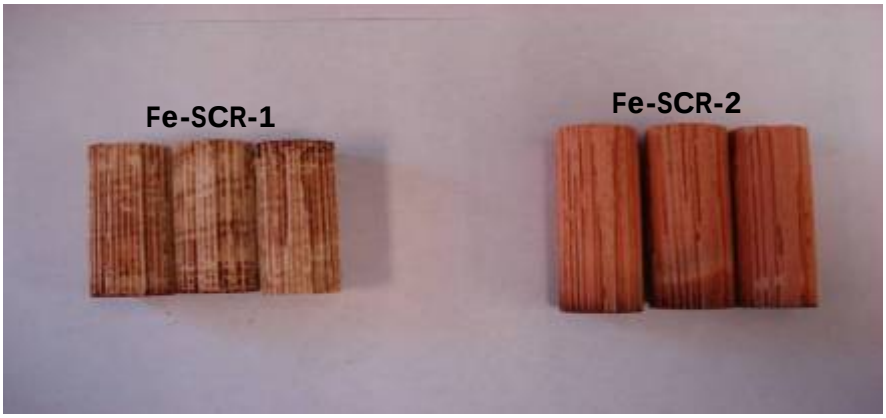

Figure 4-1. Fresh Fe-Zeolite SCR catalyst samples

CO_2, 5% H_2O, 14% O_2, 350ppm NO_x, varying amounts of NH_3 and N_2 balance) and a gas hourly space velocity of 30,000 h^{-1}.

Figures 4.2 and 4.3 show the temperature history at different locations and the axial temperature profiles in the fresh Fe-SCR-2 Fe-zeolite catalyst during NO_x performance evaluation at 300°C. The temperature histories show the temperature at different locations during performance evaluation, whereas the axial temperature profiles show the progression of the thermal front inside the catalyst. Two distinguished features are observed in the figures. First, steady state temperatures are achieved at each location in the catalyst. Second, the temperatures in the rear-half are higher than those in the front-half; the magnitude of the temperature difference increases with increasing evaluation temperature as can be seen in Figure 4.4.

In order to avoid gas phase oxidation of NH_3, the SCR pre-heat temperature is maintained at 250°C, regardless of evaluation temperature. This results in a large temperature variation within the tube furnace at evaluation temperatures greater than 250°C. As can be seen in Figures 4.2 and 4.3, the temperature in the front-half the SCR never quite reaches the nominal evaluating temperature of 300°C.

Figures 4.5 and 4.6 show the temperature history and axial temperature profile during NO_x performance evaluation at 600°C. From Figure 4.5 it is seen that the temperature variation within the SCR catalyst is much greater at 600°C. Figure 4.4 shows the difference between the SCR inlet

and SCR exit gas temperatures at each of the evaluation temperatures. It is seen that the temperature difference across the SCR catalyst increases with increasing evaluation temperature.

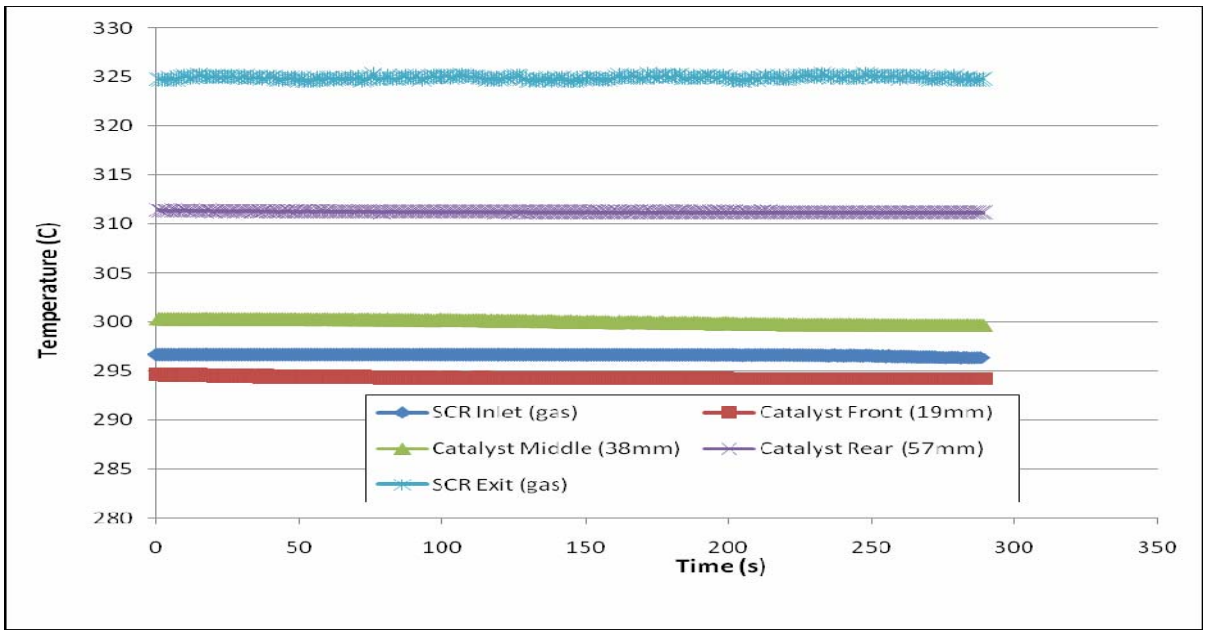

Figure 4-2. Fresh Fe-SCR-2 catalyst temperatures during NOx performance evaluation at 300°C; evaluated with 5% H_2O, 5% CO_2, 14% O_2, 350 ppm NO, 350 ppm NH_3 (α = 1), N_2 balance, GHSV = 30,000 h^{-1}

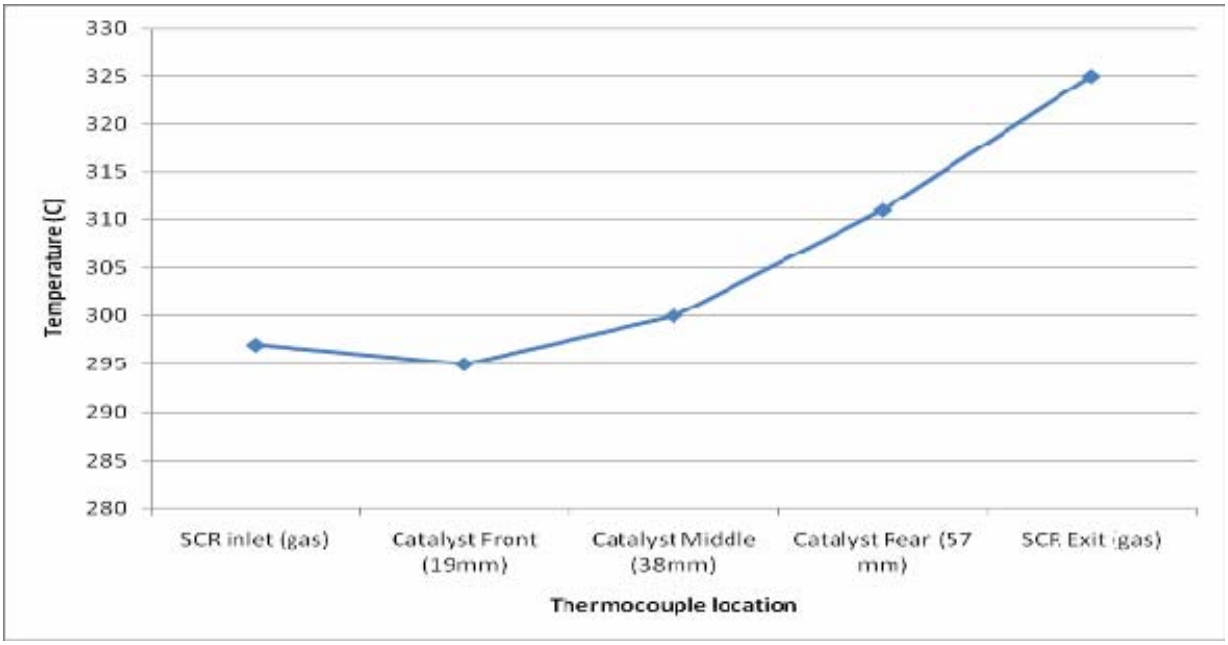

Figure 4-3. Axial temperature profile of fresh Fe-SCR-2 catalyst during NOx performance

evaluation at 300°C; evaluated with 5% H_2O, 5% CO_2, 14% O_2, 350 ppm NO, 350 ppm NH_3 ($\alpha = 1$), N_2 balance, GHSV = 30,000 h^{-1}

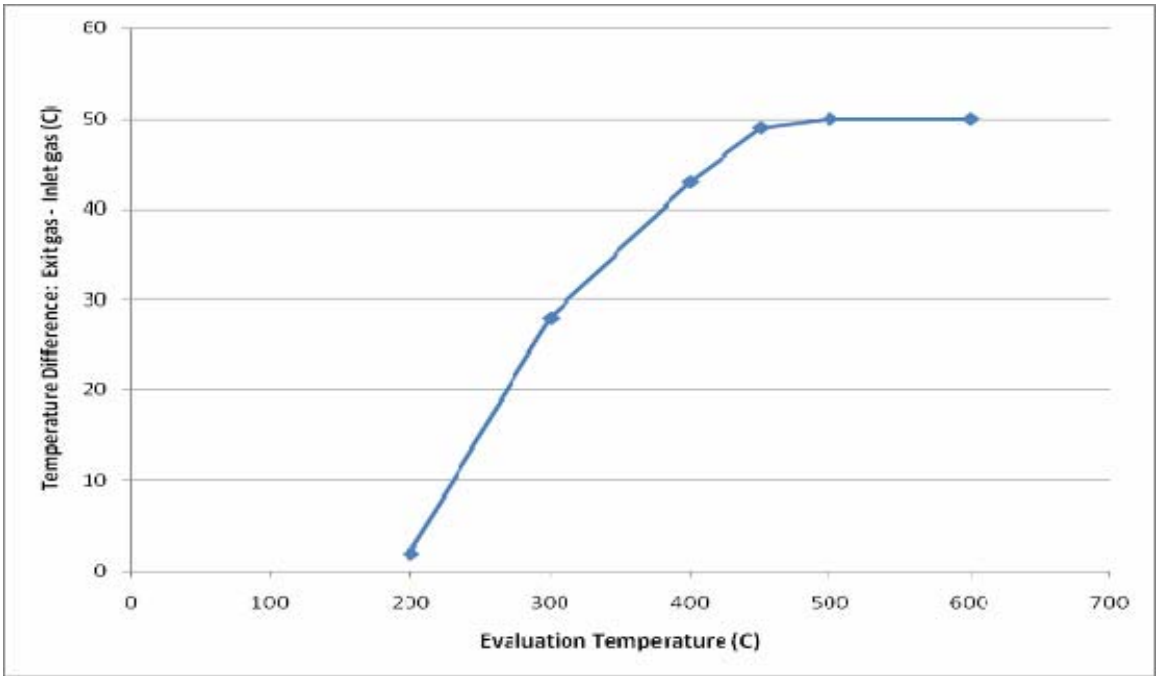

Figure 4-4. SCR Exit gas – SCR Inlet gas temperature difference at different evaluation temperatures

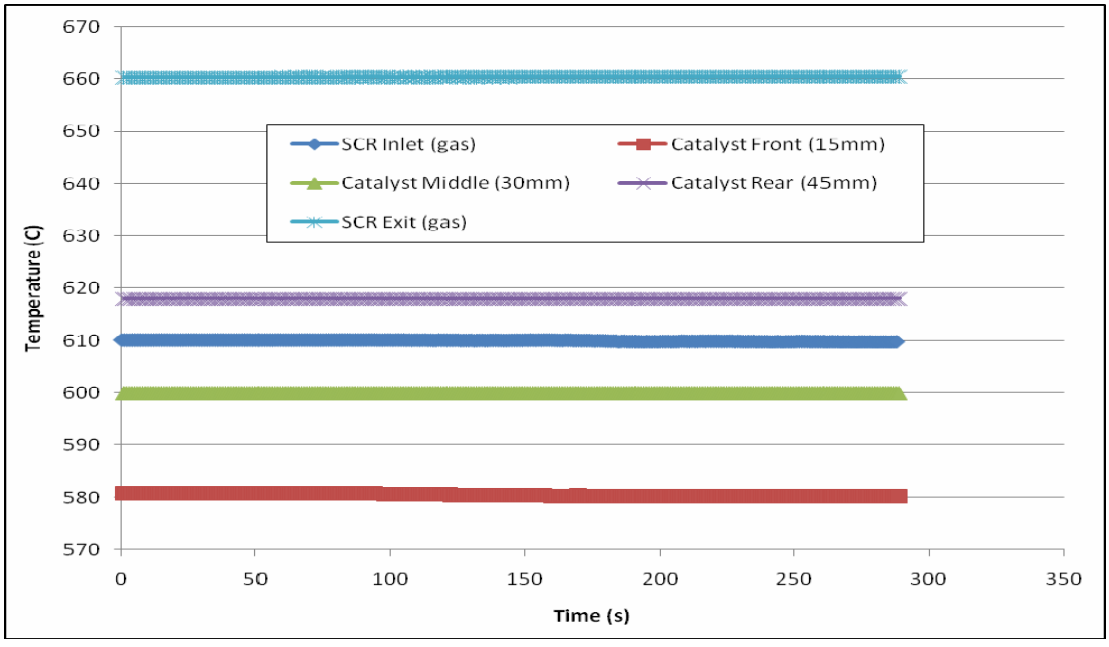

Figure 4-5. Fresh Fe-SCR-2 catalyst temperatures during NOx performance evaluation at 600°C; evaluated with 5% H_2O, 5% CO_2, 14% O_2, 350 ppm NO, 350 ppm NH_3 (α = 1), N_2 balance, GHSV = 30,000 h^{-1}

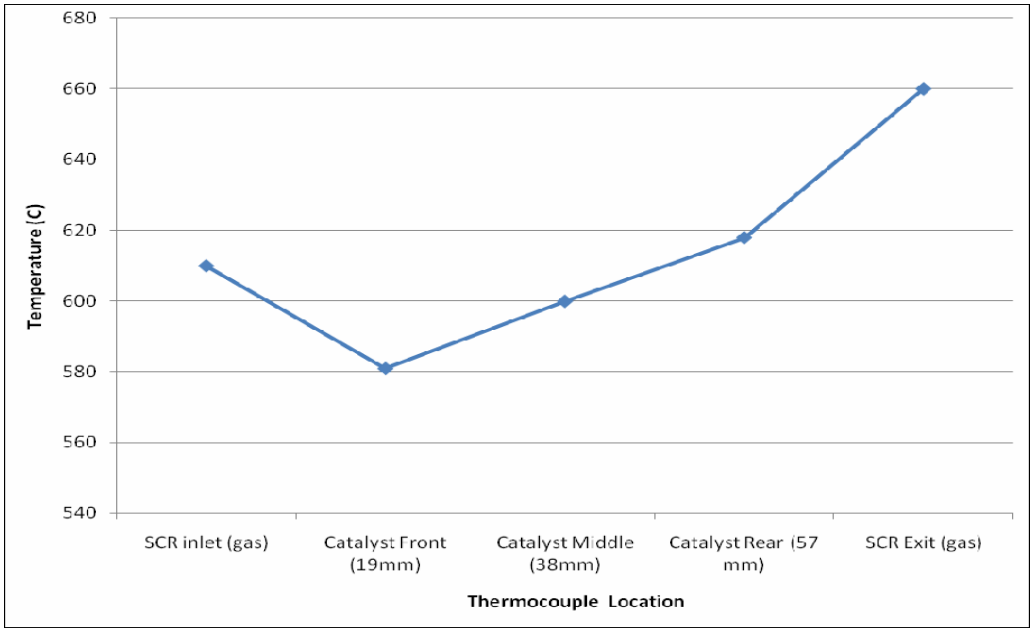

Figure 4-6. Axial temperature profile of fresh Fe-SCR-2 catalyst during NOx performance evaluation at 600°C; evaluated with 5% H_2O, 5% CO_2, 14% O_2, 350 ppm NO, 350 ppm NH_3 (α = 1), N_2 balance, GHSV = 30,000 h^{-1}

This is due to larger temperature variation within the tube furnace at higher temperature settings. The same general trend is observed in the temperature histories at other nominal evaluating temperatures of 200, 400, 450 and 500°C (see Figures AA.1 to AA.4 in appendix A).

The effect of α and evaluation temperature on the NO_x conversion of fresh Fe-SCR-1 and Fe-SCR-2 catalysts are shown in Figures 4.7 and 4.8, respectively. It can be seen from thesefigures that NO_x conversion is a strong function of α. With higher α ratios more NH_3 is available in the simulated exhaust gases to reduce NO_x; and consequently the higher the α ratio the higher the NO_x conversion. High NO_x conversion (>70%) is achieved over a temperature range of 300 to 500°C with both catalyst formulations at α = 1 with maximum NO_x conversion occurring between 400 and 500°C. NO_x reduction appears to be diffusion-limited between 300 and 500°C, because it is not a function of temperature in this range. NO_x conversion increases with increasing temperature

in the temperature range of 200 to 300°C, indicating that NO_x reduction is kinetically-limited in this temperature range. On the other hand NO_x conversion decreases at temperatures higher than 500°C. as a result of direct oxidation of NH_3 in the gas phase.

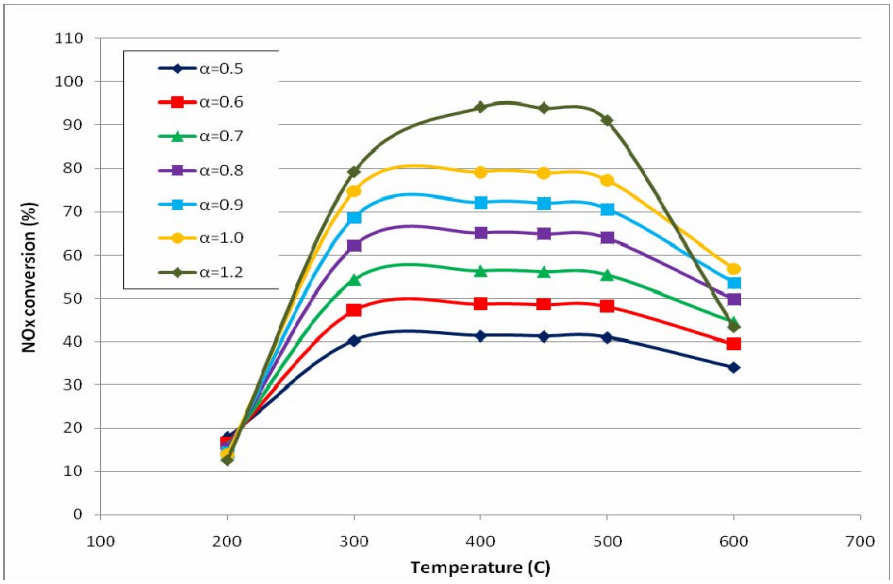

Figure 4-7. Effect of temperature on NOx conversion of fresh Fe-SCR-1 catalyst at different values of α (α = 0.5 – 1.2); evaluated with 5% CO_2, 5% H_2O, 14% O_2, 350 ppm NO, 175 – 350 ppm NH_3, N_2 balance, GHSV = 30,000 h^{-1}

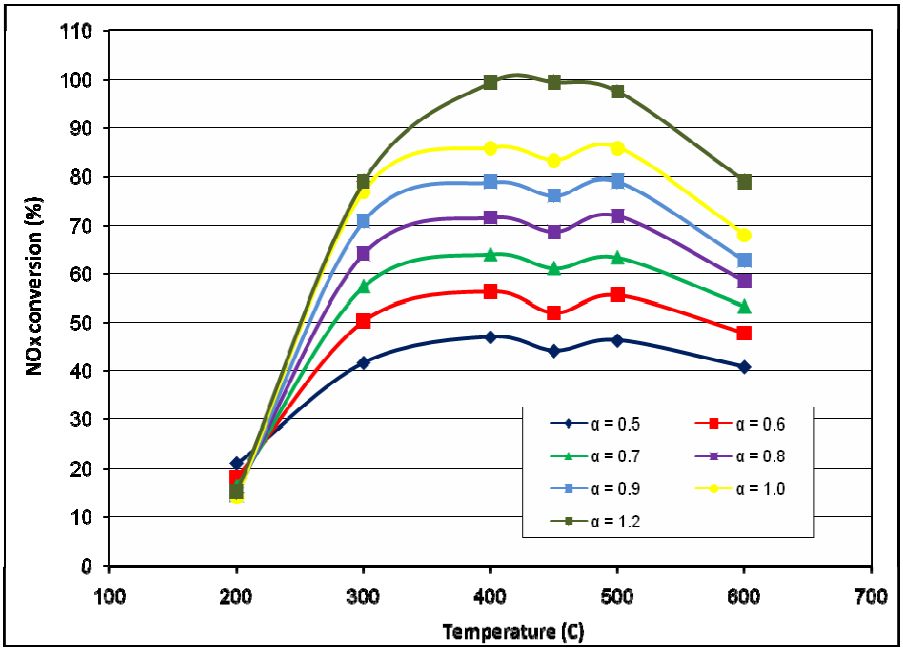

Figure 4-8. Effect of temperature on NOx conversion of fresh Fe-SCR-2 catalyst at different values of α (α = 0.5 – 1.2); evaluated with 5% CO_2, 5% H_2O, 14% O_2, 350 ppm NO, 175 – 350 ppm NH_3, N_2 balance, GHSV = 30,000 h^{-1}

When and α ratio of 1.0 is used in the feed gas, a maximum NO_x conversion of 85% with the Fe-SCR-2 catalyst and 79% with Fe-SCR-1 catalyst is achieved. Although the global equation for the SCR of NO with NH_3 (Eq. 2.1) states an equimolar amount of NO and NH_3 (α = 1) is needed in the feed gas to obtain complete reduction of NO, an α ratio of 1.2 was needed to achieve NO_x conversions greater than 90%. Devedas et al. obtained similar results with Fe-ZSM5 SCR catalysts [19]. They suggested that a constant amount (12%) of NH_3 is consumed by oxidation to N_2 over the entire temperature range, making it necessary to overdose the catalyst with NH_3. NH_3 oxidation was not monitored during this study, because a FTIR analyzer was not available for use in the BFR.

Figure 4.9 shows NO_x conversions of fresh and field-aged catalysts at an α ratio of 1.0. The front section of the field-aged catalyst experiences severe degradation as evidenced by low NO_x conversion over the entire temperature range of 200 to 600°C with a maximum NO_x conversion of approximately 30% occurring at 300°C. There is significant deactivation in the middle and rear sections of the field-aged catalyst at temperatures lower than 400°C. The middle and rear sections retain high conversion (>70%) between 400 and 500°C; however, at300°C NO_x conversion has decreased from 75% in fresh catalyst to 39% over the middle section and to 50% over the rear section of the field-aged catalyst.

It is well known that the addition of NO_2 in the exhaust gas improves the NO_x reduction efficiency of Fe-Zeolite SCR catalysts, especially below 400°C [20, 21]. According to the global equation for the SCR reaction between NO, NO_2 and NH_3 (Eq. 2.3), an equimolar amount of NO and NO_2 is needed to obtain the best NO_x conversion over a Fe-Zeolite catalyst. Figure 4.10 is a comparision of the NO_x conversions of the fresh and field-aged Fe-SCR-1 catalysts with and without NO_2 in the feed gas. The addition of NO_2 greatly enhances the NO_x performance of the fresh and field-aged catalysts below 400°C. At 200°C, the NO_x conversion increases by about 70% for the fresh and field-aged catalysts. This suggests that NO_x conversion at 200°C is strongly related to the concentration of NO_2 in the evaluation gases. Above 300°C the addition of NO_2 to the feed gas has the opposite effect on NO_x conversion. With the exception of the front section of the field-aged catalyst, the addition of NO_2 to the feed gas causes a slight decrease in NO_x conversion at temperatures between 400 and 500°C in the fresh and field-aged catalysts. For the rear section of the field-aged catalyst there is about a 10% decrease in NO_x conversion. The

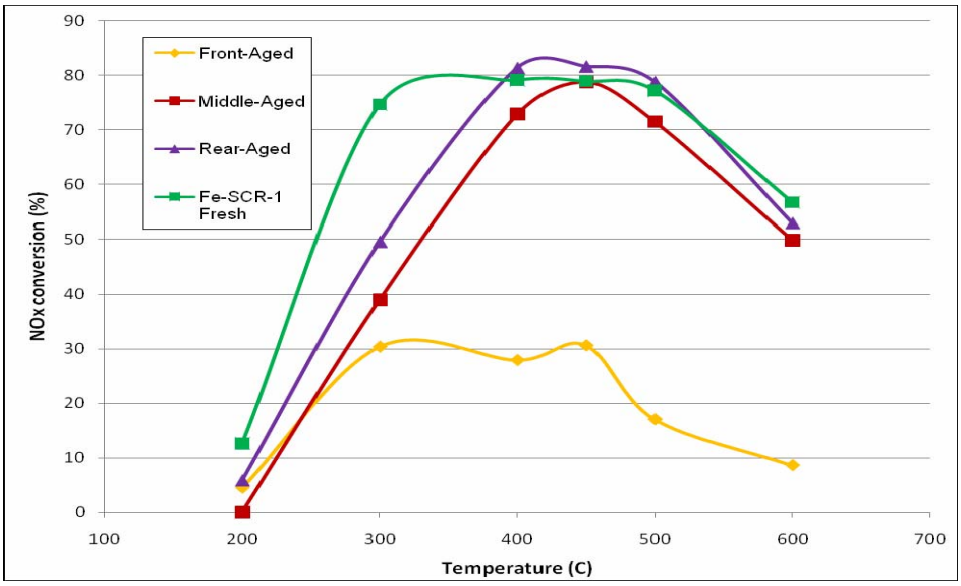

Figure 4-9. Effect of temperature on NOx conversion of fresh and field-aged Fe-SCR-1 catalysts at α = 1.0; evaluated with 5% CO_2, 5% H_2O, 14% O_2, 350 ppm NO, 350 ppm NH_3, N_2 balance, GHSV = 30,000 h^{-1}

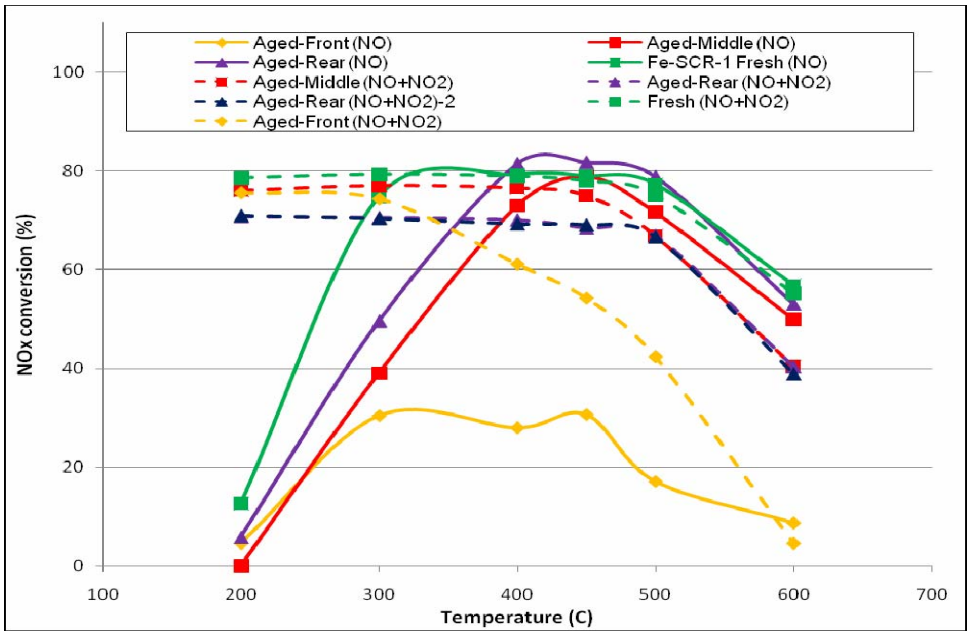

Figure 4-10. Effect of temperature on NOx conversion of fresh and field-aged Fe-SCR-1 catalysts; evaluated with 5% CO_2, 5% H_2O, 14% O_2, 175 or 350 ppm NO, 0 or 175 ppm NO_2, 350 ppm NH_3 (α = 1.0), N_2 balance, GHSV = 30,000 h^{-1}

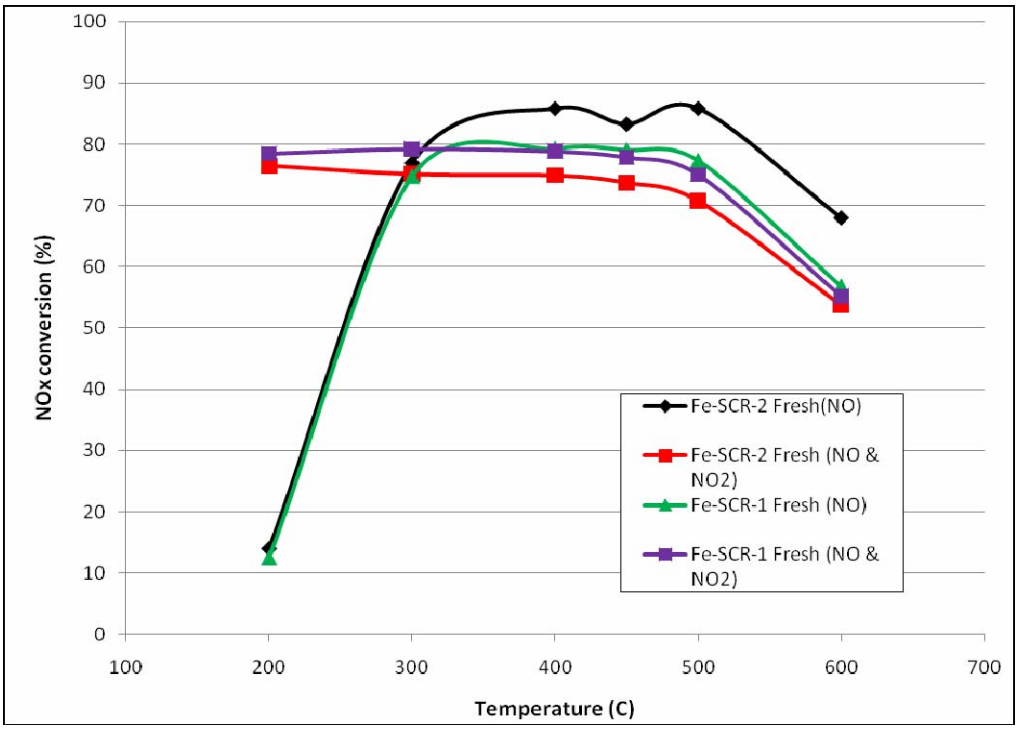

Figure 4-11. Effect of temperature on NOx conversion of fresh Fe-SCR-1 and Fe-SCR-2; evaluated with 5% CO_2, 5% H_2O, 14% O_2, 175 – 350 ppm NO, 0 – 175 ppm NO_2, 350 ppm NH_3 (α = 1.0), N_2 balance, GHSV = 30,000 h^{-1}

NO_x performance evaluation is repeated with this catalyst section to confirm the measured decrease of NO_x conversion.

NO_x conversion efficiencies of the two fresh catalysts, with and without the addition of NO_2 in the gas stream, are shown in Figure 4.11. The addition of only 175 ppm NO_2 increases the NO_x conversion by almost 70% at 200°C for both Fe-SCR-1 and Fe-SCR-2 fresh catalysts—again showin a large increase in NO_x performance at 200°C. While adding NO_2 has no affect at temperatures greater than 200°C for the Fe-SCR-1 formulation, there is approximately a 10% decrease in NO_x coversion at all temperatures greater than 300°C with the Fe-SCR-2 formulation. This is probably a result of slightly different catalyst formulations.

NO oxidation experiments are conducted with the fresh and field-aged SCR catalysts and the results are shown in Figure 4.12. NO oxidation over fresh and field-aged Fe-SCR-1 catalysts increases with temperature until reaching a maximum at 500°C. Similarly, NO oxidation over fresh Fe-SCR-2 catalyst increases with temperature until it reaches a maximum at 450°C. The

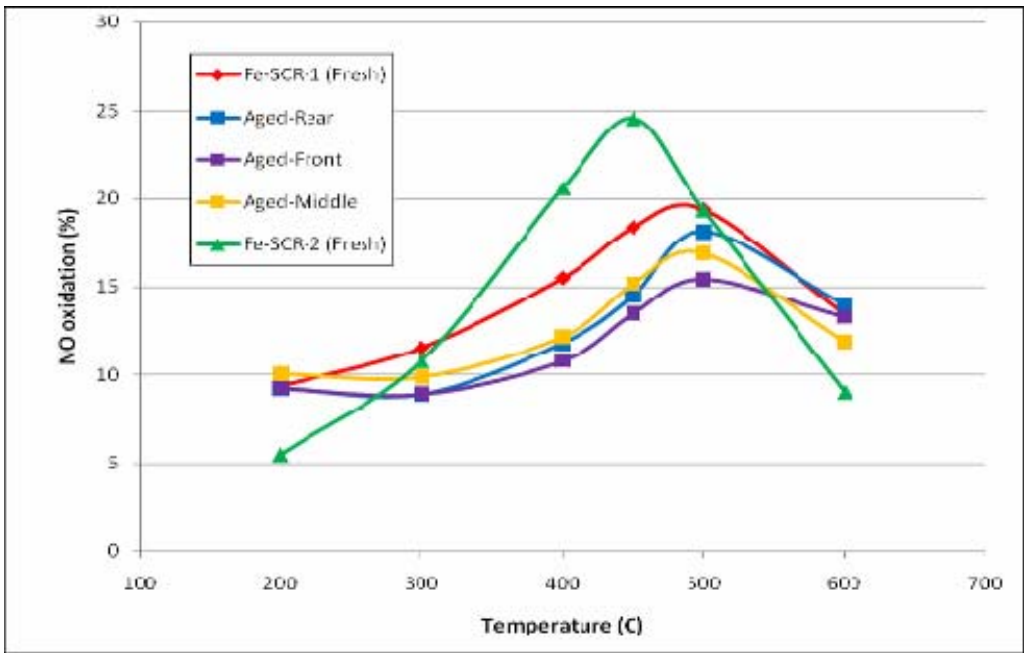

Figure 4-12. Effect of temperature on NO oxidation of fresh and field-aged Fe-SCR-1; evaluated with 5% CO_2, 5% H_2O, 14% O_2, 350 ppm NO ($\alpha = 0$), N_2 balance, GHSV = 30,000 h^{-1}

fresh Fe-SCR-1 catalyst has a maximum NO oxidation of approximately 19%, while the fresh Fe-SCR-2 catalyst has a maximum NO oxidation of approximately 25%. Higher NO oxidation with the Fe-SCR-2 formulation may lead to a ratio of NO_2/NO that is greater than one when a mixture of NO and NO_2 is in the feed gas. This would result in NO_x reduction taking place according to Eq. 2.2, the slowest of the three SCR reactions, which might explain the observed decrease in NO_x conversion above 300°C with the fresh Fe-SCR-2 catalyst when 175 ppm NO_2 is added to the feed gas.

Oxidation activity decreases in the field-aged catalyst, with the front section measuring the lowest activity, followed by the middle and rear sections. It is believed that NO oxidation to NO_2 is an important step in the SCR process [18-20, 23, 24], and it occurs over active Fe sites in the zeolite washcoat [22]. Thus, the results in Figure 4.12 seem to indicate that the active Fe sites in the field-aged catalyst have been reduced considerably.

The X-ray diffraction patterns shown in Figure 4.13 reveal the presence of Fe_2O_3 in the washcoat of the field-aged catalyst; however, it is not detected in the fresh Fe-SCR-1 sample. The formation of Fe_2O_3 in the field-aged catalyst may from the oxidation of active iron cations in

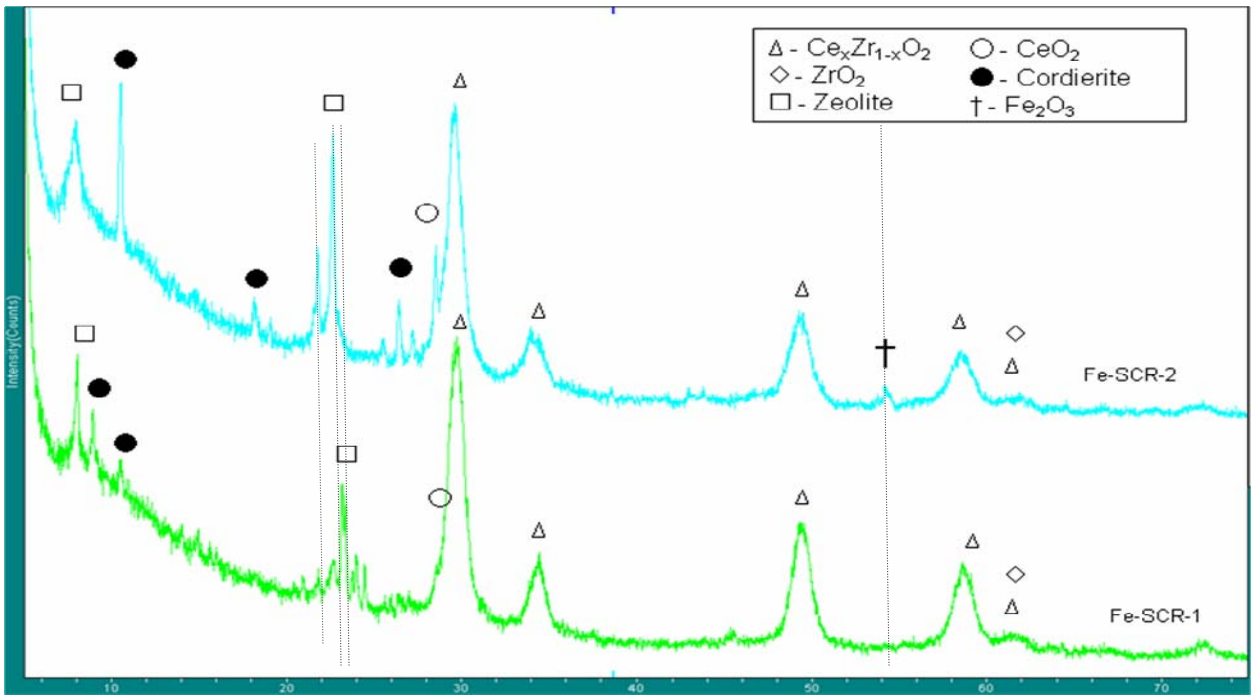

Figure 4-13. X-ray diffraction patterns of fresh Fe-SCR-1 and Fe-SCR-2 catalysts

the zeolite washcoat, which according to Devadas et al. [22] would leave less active sites for NO oxidation and, thus a reduction in overall catalytic performance.

4.1.2 ***Material Characterizations***

X-ray diffraction is used to detect the disappearance and formation of new compounds in the Fe-zeolite catalysts. Figure 4.13 shows the X-ray diffraction patterns of the fresh Fe-SCR-1 and Fe-SCR-2 samples. The two formulations differ in two ways. First, the zeolite in Fe-SCR-2 is different than that in Fe-SCR-1 as can be seen clearly in the X-ray diffraction patterns in the range of 2□ between 20 and 26°. Secondly, Fe_2O_3 is detected in the X-ray diffraction patterns of Fe-SCR-2 at 2□ of 55°. This indicates that the fresh Fe-SCR-2 catalyst may contain extra "out of framework" Fe_2O_3, which may give rise to the reddish color, seen in Figure 4.1.

Figure 4.14 shows XRD patterns of fresh Fe-SCR-1 catalyst and the three sections of field-aged catalyst. Fe_2O_3 peaks are discernable in the field-aged X-ray diffraction patterns, indicating that active Fe cations in the fresh catalyst have formed Fe_2O_3 clusters in the aged samples. According to Park et al. [33], as the zeolite structure collapses active cations are freed and they can form oxide clusters such as Fe_2O_3. Al_2O_3 peaks are discernable in the XRD patterns of the front section of the field-aged catalyst. The formation of Al_2O_3 indicates zeolite dealumination, in which Al^{3+} ions migrate out of the zeolite structure and form Al_2O_3 [34]. When comparing the XRD patterns in the region of 2Θ between 15 and 26°, it is clear that aging has affected the structure of the zeolite in the field-aged catalyst and the effects of aging are more prominent in the front section. Overall, aging has changed the structure of the zeolite in the field-aged catalyst and caused the formation of Fe_2O_3. The effects of aging are pronounced in the front section of the field-aged catalyst because the formation of Al_2O_3 implies that dealumination has occurred.

Electron Probe Microscopic Analysis (EPMA) reveals structural damage to the Zeolite washcoat of the field-aged catalyst. Figures 4.15 to 4.19 show elemental maps of fresh and field-aged catalysts. The washcoat of the front section of the field-aged catalyst is delaminated from the substrate, as can be seen in Figure 4.15; therefore, it is difficult to determine the material changes that have taken place as a result of field service other than structural degradation of the washcoat. The elemental maps of the middle and rear sections of the field-aged Fe-SCR-1 catalyst show a significant amount of sulfur present in the washcoat, as seen in Figures 4.16 and

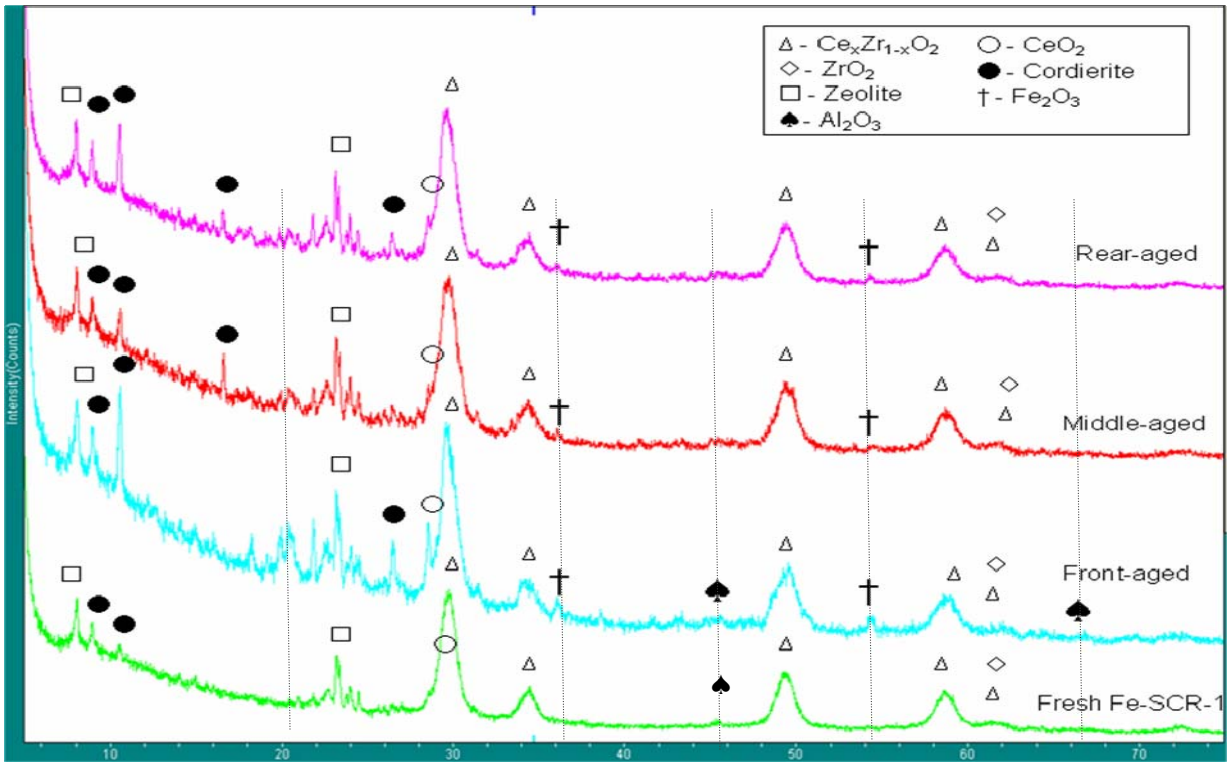

Figure 4-14. X-ray diffraction patterns of fresh and field-aged Fe-SCR-1 catalysts

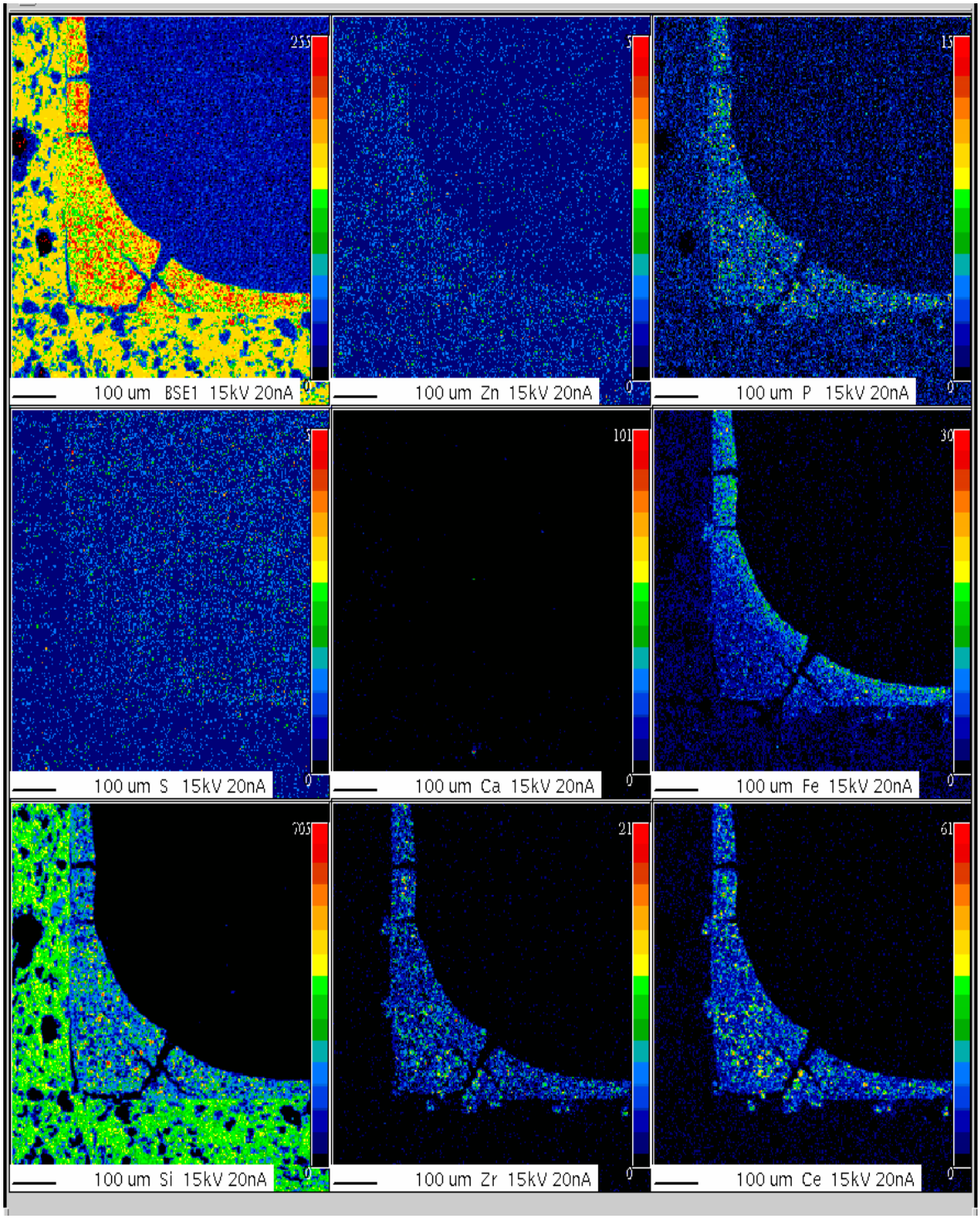

Figure 4-15. Elemental maps of fresh Fe-SCR-1 catalyst

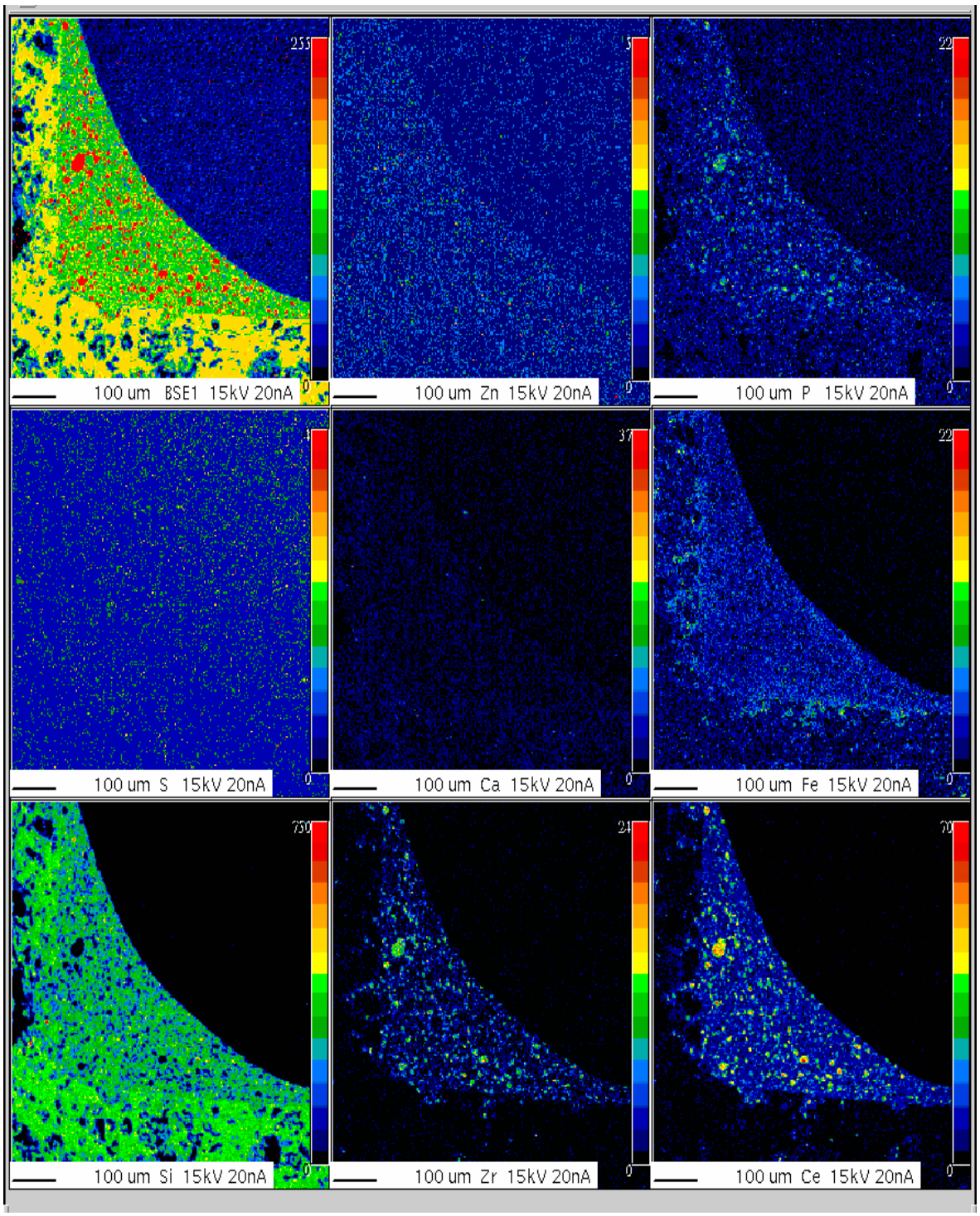

Figure 4-16. Elemental maps of fresh Fe-SCR-2 catalyst

4.17. The sulfur is most likely from the diesel fuel used by the bus and penetrates into the washcoat in the form of sulfates. Cracks in the washcoat can be seen in the element maps of the fresh and field-aged Fe-SCR-1 catalysts, however the element maps of the fresh Fe-SCR-2 catalyst do not show any cracking. When comparing the Fe-SCR-1 catalyst samples, there is more severe cracking in the field-aged sections, and the beginning of washcoat delamination can be seen in the middle and rear sections.

Trace amounts of phosphorus are detected in both fresh and field-aged catalysts. The presence of phosphorus might indicate poisoning from lube oil- derived species, but that is not the case here since there is a comparable amount of phosphorus present in both fresh and aged samples. Calcium and zinc are other lube oil-derived species that can contribute to catalyst poisoning, however only negligibles amounts of both elements are detected by EPMA in all of the catalyst samples. Since silicon is the main constituent of zeolite, it is not surprising to find a large amount of silicon in the washcoat. A cerium-zirconium mixed oxide ($Ce_xZr_{1-x}O_2$) is present in the washcoat as an oxygen storage material, which explains the large amount of cerium and zirconium detected by EPMA. Finally, the element maps show that Fe is well dispersed throughout the washcoat of each of the catalysts.

High magnification micrographs, taken with a Scanning Electron Microscope (SEM), are used to confirm the damage of the washcoat in the field-aged catalyst. SEM micrographs of fresh and field-aged catalysts are shown in Figures 4.20 to 4.24. There appears to be no delamination or structural damage to the washcoat of the fresh Fe-SCR-1 catalyst. Also, no cracks are visible in the SEM micrographs of the washcoat, which is contrary to the elemental maps from EPMA. Similarly, the SEM micrographs of the fresh Fe-SCR-2 catalyst show no structural damage to the washcoat, however unlike Fe-SCR-1 the shape of the washcoat is not symmetric in the channels of the catalyst, but somewhat distorted. The Fe-SCR-2 catalysts are laboratory samples and may not have been made with as much precision as production catalysts. Figure 4.22 confirms that the washcoat is delaminated from the substrate in many places and there are severe crackings throughout the front section of the field-aged Fe-SCR-1 catalyst. The SEM micrograph of the middle section of the field-aged catalyst shows damages to the structure of the washcoat, but not to the extent of the front section (Figure 4.23). The micrograph shows cracking and the

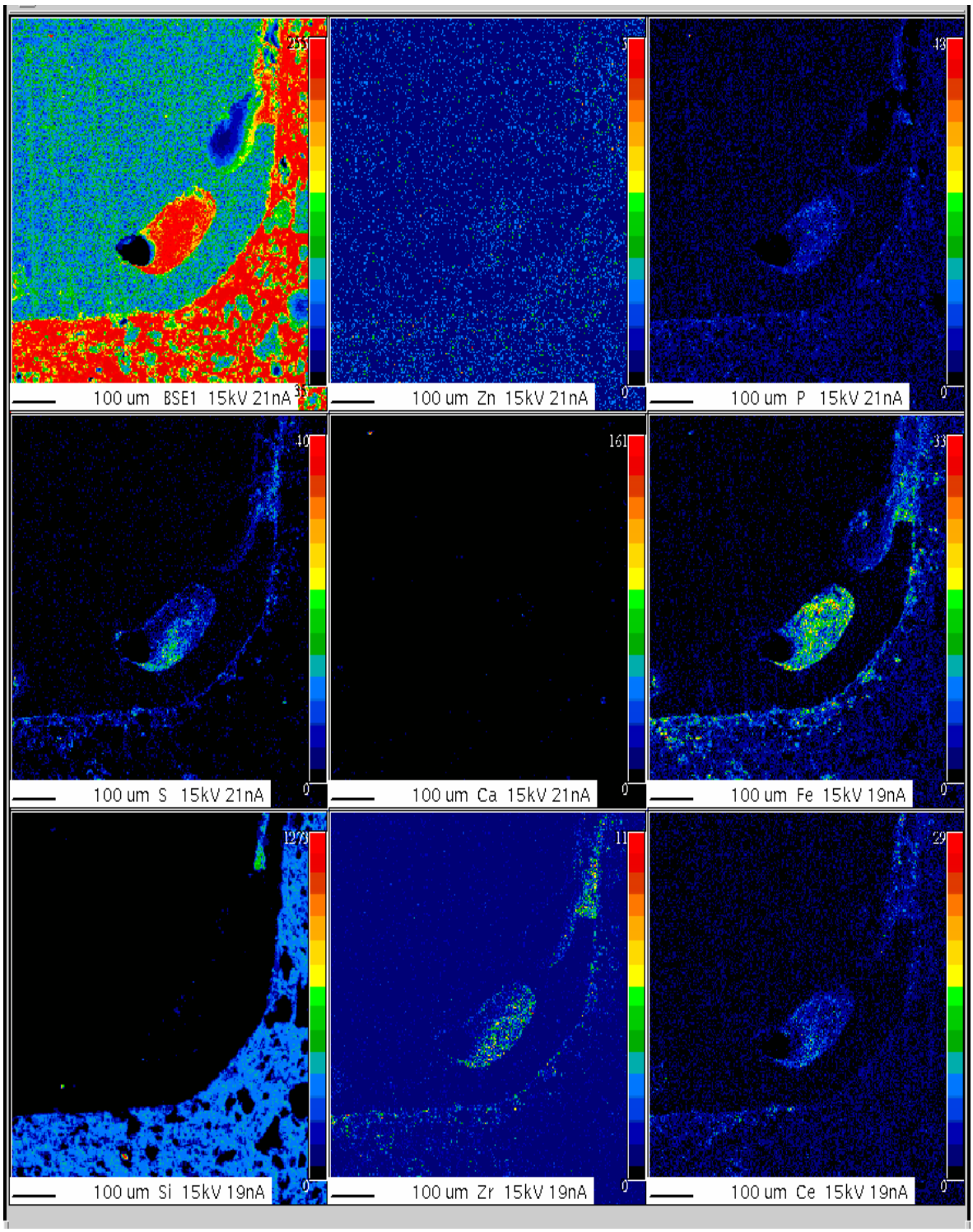

Figure 4-17. Elemental maps of front section of field-aged Fe-SCR-1 catalyst

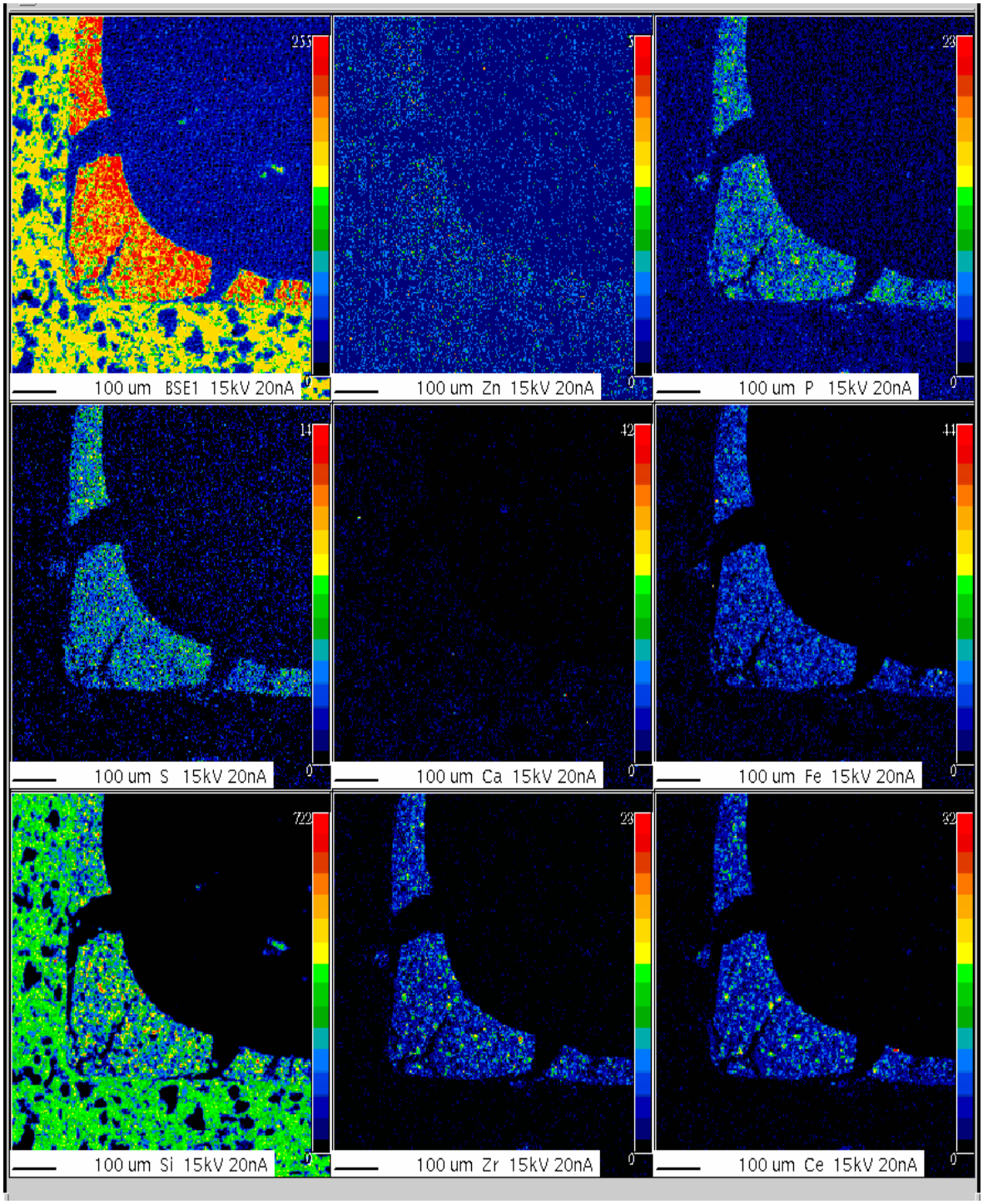

Figure 4-18. Elemental maps of middle section of field-aged Fe-SCR-1 catalyst

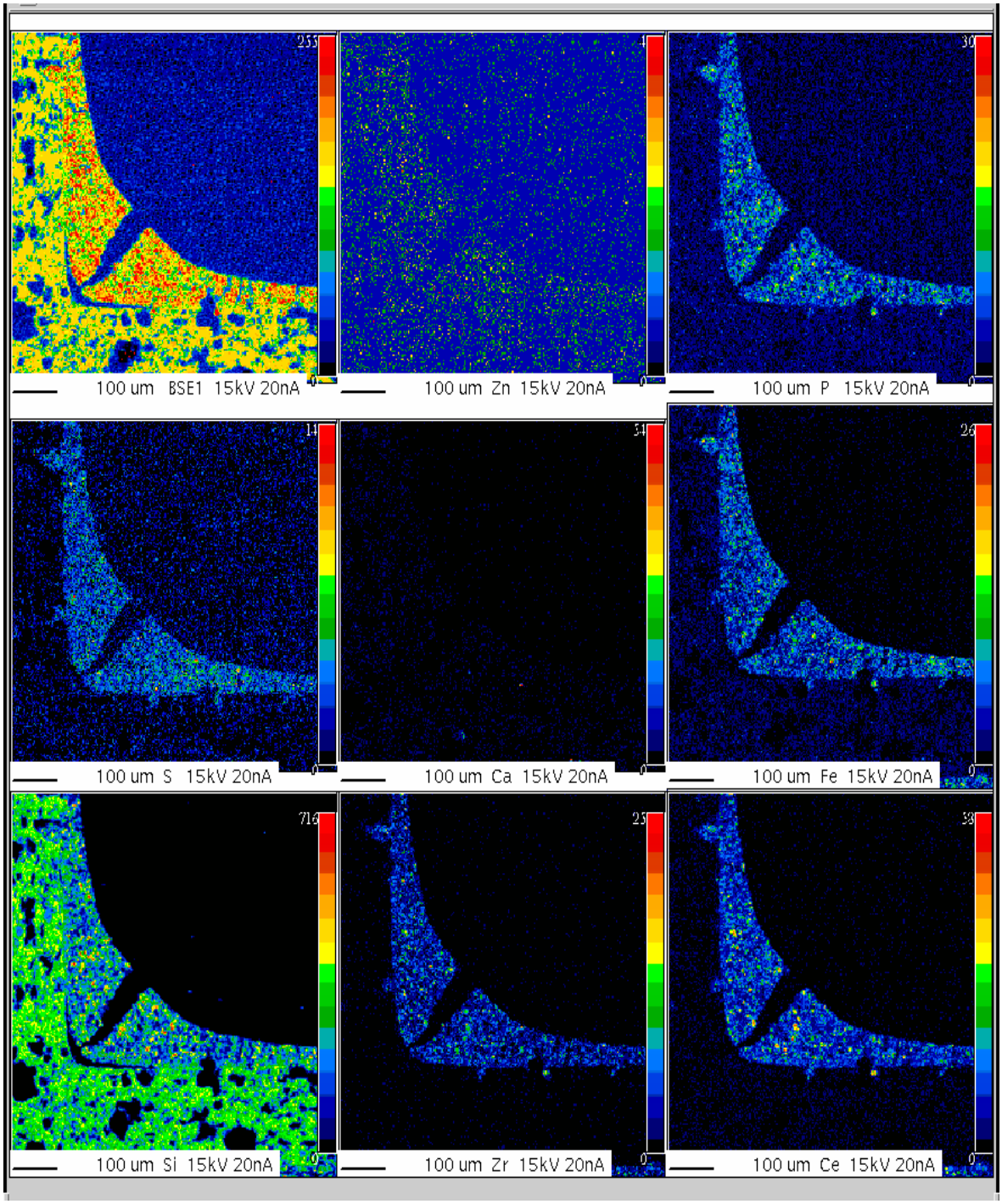

Figure 4-19. Elemental maps of rear section of field-aged Fe-SCR-1 catalyst

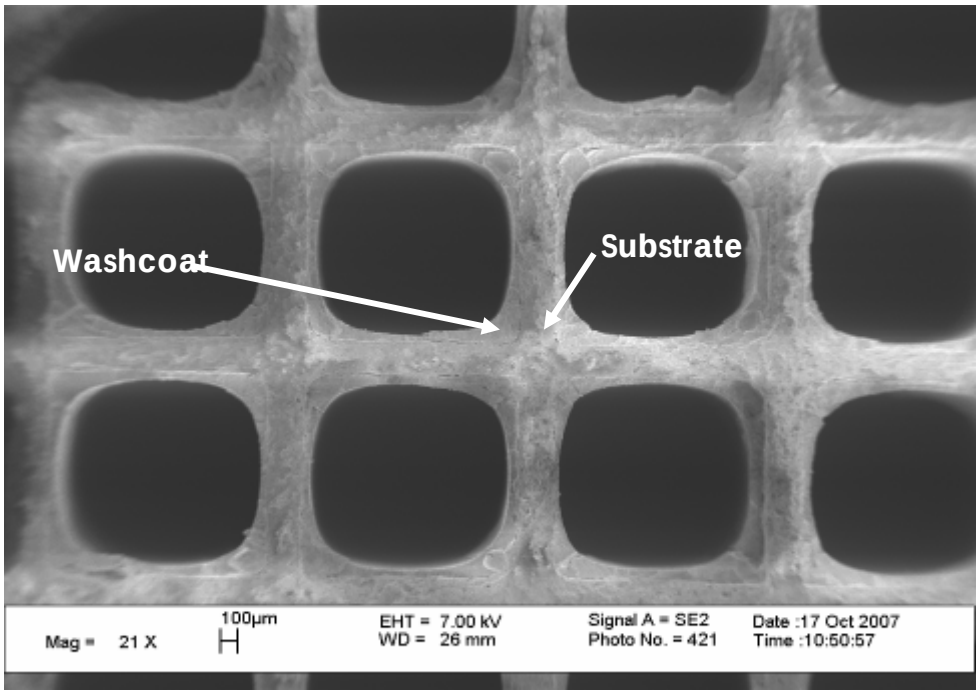

Figure 4-20. SEM micrograph of fresh Fe-SCR-1 catalyst

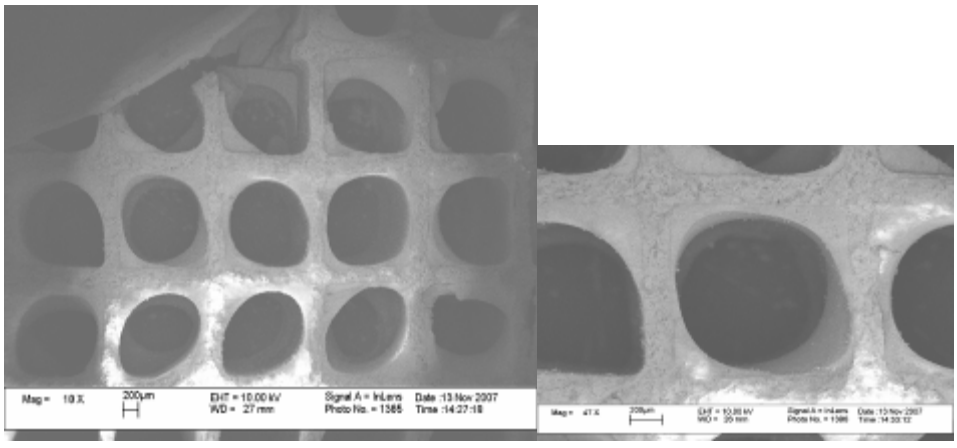

Figure 4-21. SEM micrographs of fresh Fe-SCR-2 catalyst

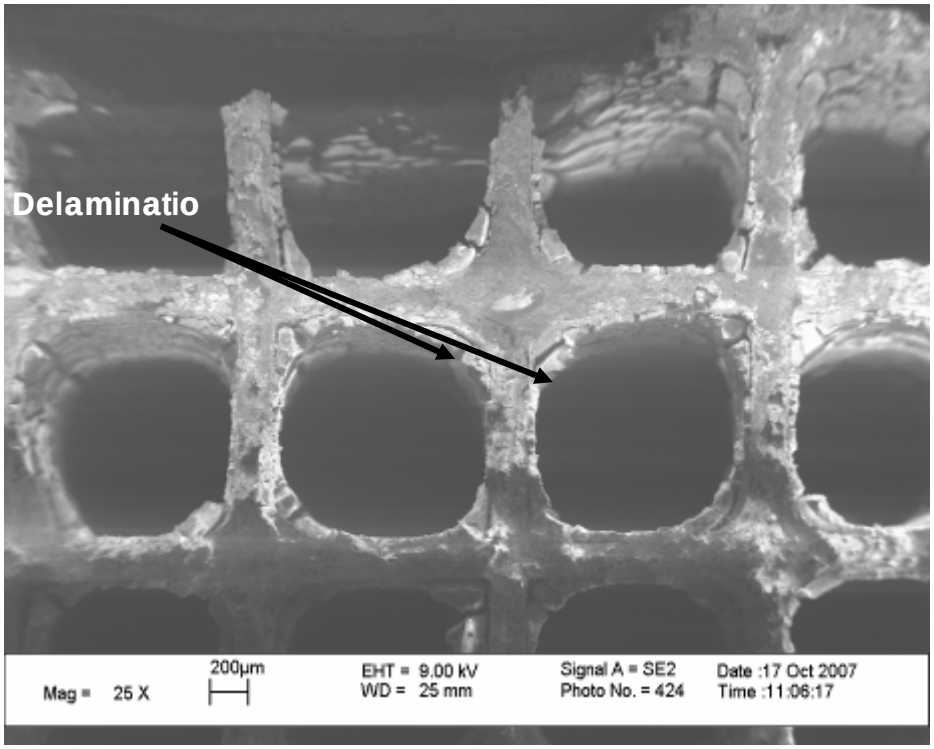

Figure 4-22. SEM micrograph of front section of field-aged Fe-SCR-1 catalyst

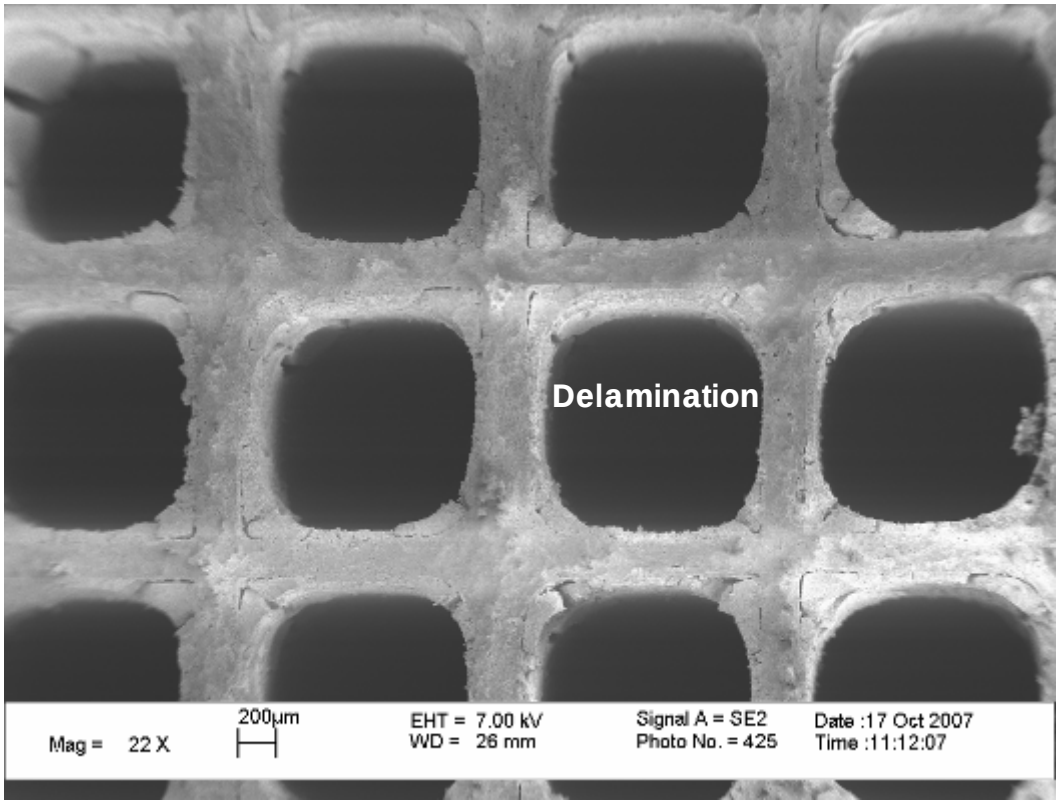

Figure 4-23. SEM micrograph of middle section of field-aged Fe-SCR-1 catalyst

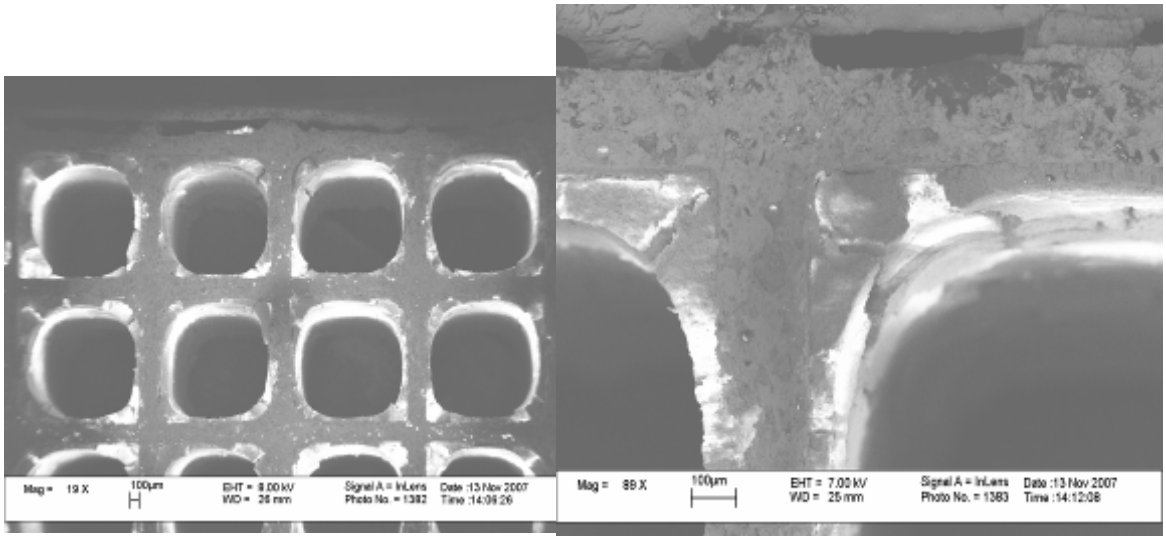

Figure 4-24. SEM micrographs of rear section of field-aged Fe-SCR-1

beginning of delamination, however the damage is not as severe as the front section. Finally, the rear section of the field-aged catalyst, shown in Figure 4.24, appears to be glowing. This glowing effect is called "charging", which is due to the catalyst being an insulator and not very conductive. The gold coating applied to the SEM samples provides a conductive layer and reduces the charging effect; however, it is still difficult to obtain clear images with some catalyst samples. The micrograph on the right side of Figure 4.24 shows that the rear section has also experienced cracking, however there is no evidence of delamniation and the cracking is not as severe as those observed in the front section of the catalyst. The SEM micrographs confirm that the field-aged Fe-SCR-1 catalyst has suffered strutural degredation, with the front section experiencing the most severe damage.

The surface area of the fresh and field-aged catalysts is measured with an Ar pulse BET method. The results are shown in Figure 4.25. It is necessary to note that these are surface area measurements of the zeolite washcoat and cordierite substrate. The substrate is a much less porous material than zeolite with an approximate surface area of 1 m^2/g and therefore will lower the surface area measurements significantly. The surface area of fresh Fe-SCR-2 catalyst is almost $20m^2/g$ more than that of fresh Fe-SCR-1 catalyst. This could be attributed to different

catalyst formulations, or the Fe-SCR-2 catalysts may have a thicker washcoat layer, as can be seen in Figures 4.20 and 4.21. Since the front section of the field-aged catalyst is severely degraded, its surface area of 18m^2/g is much less than that of fresh Fe-SCR-1 catalyst of 38m^2/g. The middle and rear sections of the field-aged catalyst also have degraded, but not as severely as the front section, resulting in surface areas of 22 and 29m^2/g, respectively. Park et al [30]. found similar results with a Cu-Zeolite SCR catalyst. Hydrothermal-aging at 800°C resulted in a severe reduction of catalyst surface area. Park attributes the loss of surface area to structural degradation of the zeolite support.

The deactivation mechanism associated with the field-aged Fe-zeolite SCR catalyst is primarily physical changes in the zeolite washcoat, such as loss of active iron sites and reduction of catalyst surface areas. Figure 4.26 shows there is a good relationship between NO_x performance at 300°C and catalyst surface area of the fresh and field-aged catalysts. The front section of the field-aged catalyst has the worst NO_x conversion, which is expected due to severe damage to the washcoat in this section of the field-aged catalyst. The middle and rear sections of the field-aged catalyst show some deactivation during BFR evaluation. However, these sections

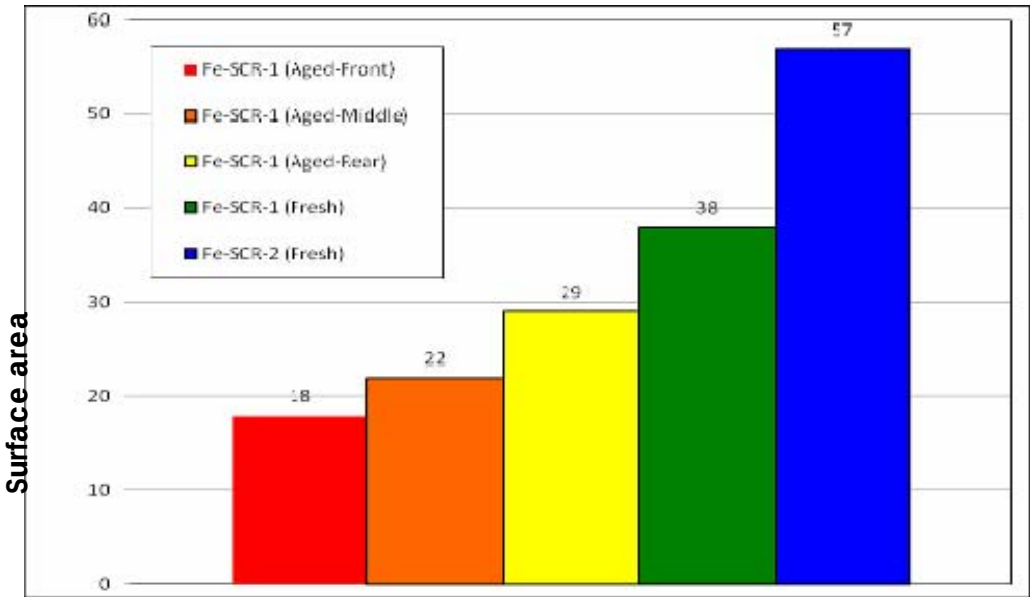

Figure 4-25. BET surface area measurements of fresh and field-aged catalysts

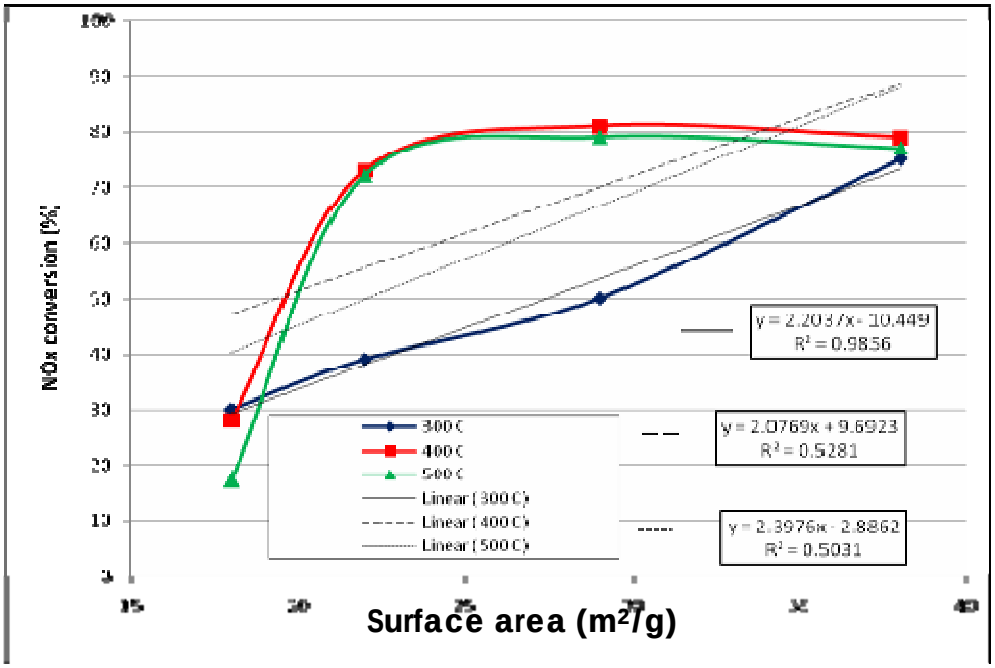

Figure 4-26. NOx conversion with 350ppm NO as a function of catalyst surface area

still perform much better than the front section of the field-aged catalyst, which is supported by the SEM micrographs and surface area measurements of these catalyst sections. From the correlation coefficients in Figure 4.26, it is seen that the relationship between NO_x performance and catalyst surface area is not as strong at 400 and 500°C.

There is a general consensus that the deactivation of Fe-Zeolite SCR catalysts is directly related to zeolite dealumination [31-33]. Dealumination is the process in which the Al^{3+} ion in the SiO_2-Al_2O_3 tetrahedral framework migrates out of the zeolite structure. This leads to irreversible deactivation, a collapse of the crystalline structure and a loss of catalyst surface area [34]. As the crystalline structure breaks down active iron cations are freed from the zeolite framework to form Fe_2O_3, resulting in reduced NO oxidation activity and a decrease in overall catalytic performance. Although, decrease in surface area and deterioration of the zeolite washcoat are indicative of zeolite dealumination, the extent of dealumination is not quantified here. In future work characterization techniques, such as IR and NMR, should be used to identify the state of the Al atoms in the zeolite and thus quantify the amount of zeolite dealumination that has occurred.

4.2 Accelerated Thermal Aging

Three Fe-SCR-2 catalysts were aged on an engine bench under accelerated thermal aging conditions. The accelerated thermal aging protocol established for the SCR catalysts utilizes high temperature exhaust gases generated for the active regeneration of the DPF. The bench-mounted engine (Figure 3.11) is fitted with an exhaust aftertreatment system consisting of a DOC, a SCR and a DPF. Accelerated aging is carried out due to the periodic regeneration of the DPF at exhaust gas temperatures of 650, 750 and 850°C at the SCR inlet. Also included are the results of hydrothermal-aging on a BFR with 28ppm SO_2 in the feed gas. Hydrothermal-aging was performed at a catalyst temperature of 670°C. Due to the temperature variation along the catalyst, the middle of the catalyst was maintained at 670°C during aging. A gas compostion of 5% CO_2, 5% H_2O, 14% O_2, 28ppm SO_2 and N_2 balance was used during hydrothermal aging at a gas hourly space velocity of 30,000 h^{-1}, as prescribed by the CLEERS protocol [1].

4.2.1 ***Hydrothermal-Aging***

A Fe-SCR-2 catalyst sample was aged for sixty-four hours with NO_x performance evaluated after every sixteen hours of aging. Figure 4.27 shows catalyst temperatures during hydrothermal aging at a nominal aging temperature of 670°C. Due to the large temperature variation along the SCR catalyst, which is the result of inefficient pre-heat and temperature variation within the tube furnace, the nominal aging temperature is taken to be the temperature at the middle of the SCR catalyst. Figure 4.28 shows the effect of temperature on the NO_x conversion of the hydrothermally-aged Fe-SCR-2 catalyst at an α of 1.0. Deactivation is minimal at evaluation temperatures of 400, 450 and 500°C and more significant at evaluation temperatures of 200, 300 and 600°C. NO_x conversion decreases from 15 to 9% at 200°C, from 76 to 69% at 300°C, and from 62 to 56% at 600°C. It is apparent that hydrothermal-aging has minimal impact on the NO_x conversion efficiency of the Fe-SCR-2 catalyst. Devadas et al. obtained similar results after 50 hours of hydrothermal-aging with a Fe-ZSM5 SCR catalyst [19].

Figure 4.29 shows the NO_x conversion of the hydrothermally-aged and fresh Fe-SCR-2 catalysts with an equimolar amount of NO and NO_2 in the gas mixture. As observed previously the addition of NO_2 in the gas stream has enhanced the NO_x performance of Fe-SCR-2 catalyst at low temperatures, specifically at 200°C, but not at high temperatures. A difference in activity of approximately 3% is obtained at evaluation temperatures of 300, 400, 450 and 500°C. Only at 600°C is the difference in NO_x conversion significant (9%).

Figure 4.30 shows NO oxidation activity of the fresh and hydrothermally-aged Fe-SCR-2 catalysts. While hydrothermal aging NO_x performance remains unaffected, does appear to have a bigger impact on NO oxidation. Maximum NO oxidation decreases from 25 to 17% with the hydrothermally-aged catalyst and it occurs at an evaluation temperature of 500°C instead of 450°C. This indicates that hydrothermal-aging reduces the number of active iron sites in the zeolite washcoat.

Hydrothermal aging has a small effect on the NO_x performance of the Fe-SCR-2 catalyst, and a more significant impact on the NO oxidation. As seen in Figure 4.30 it appears that hydrothermally-aged and field-aged catalysts exhibit similar NO oxidation behavoir, which suggests that hydrothermal aging reduces the number of active Fe sites in the washcoat causing a reduction in NO oxidation activity.

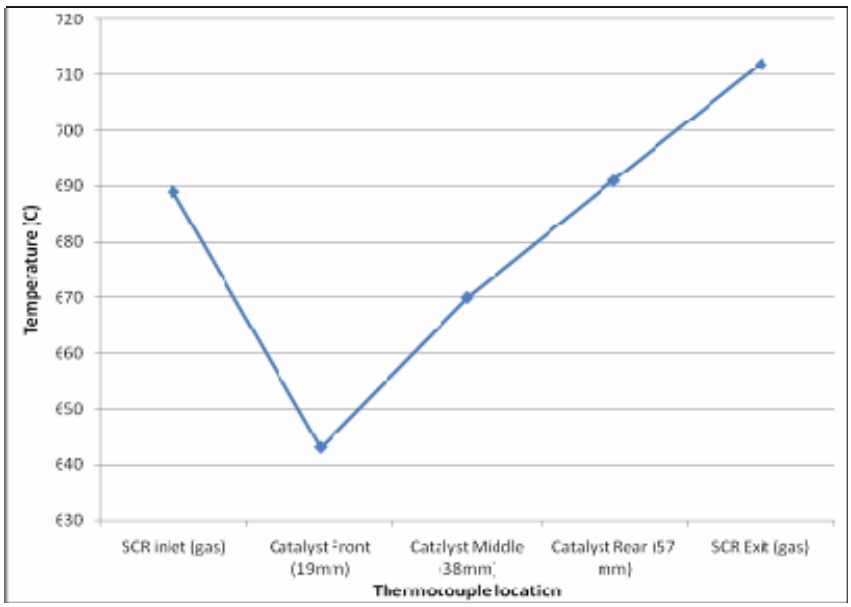

Figure 4-27. Catalyst temperatures during hydrothermal aging; aged with 5% H2O, 5% CO2, 14% O2, 28 ppm SO2, N2 balance, GHSV = 30,000 h-1

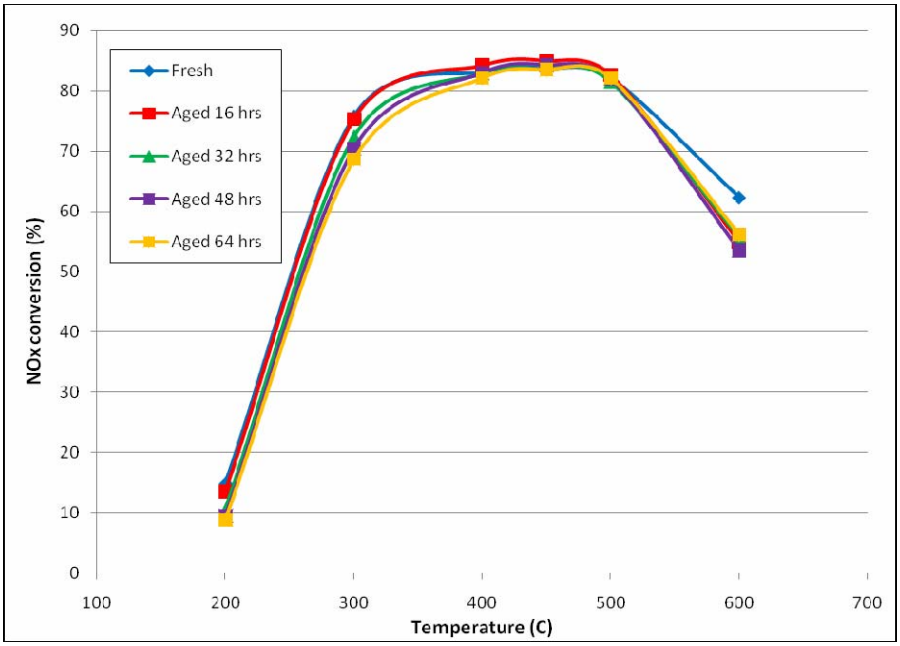

Figure 4-28. Effect of temperature on NOx conversion of hydrothermally-aged Fe-SCR-2 catalyst; evaluated with 5% CO_2, 5% H_2O, 14% O_2, 350 ppm NO, 350 ppm NH_3 (α = 1.0), N_2 balance, GHSV = 30,000 h^{-1}

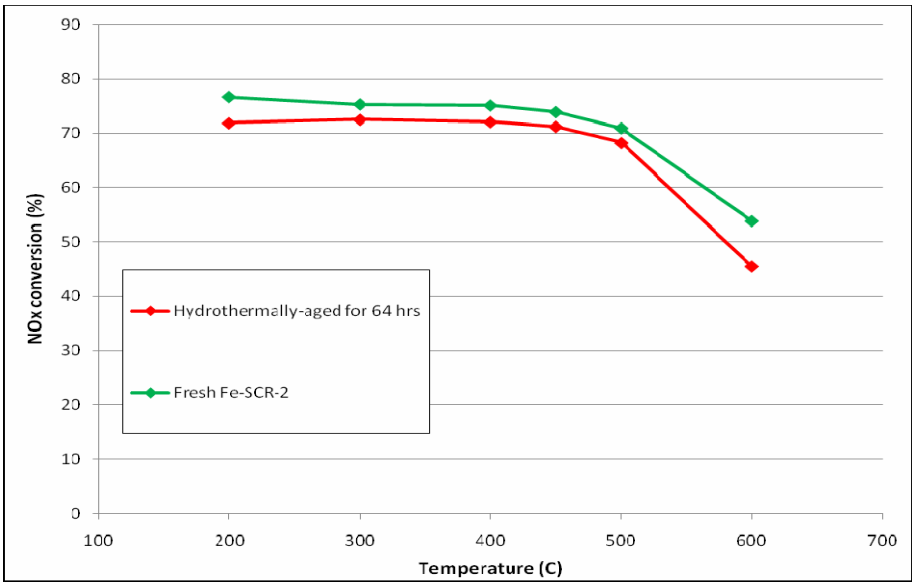

Figure 4-29. Effect of temperature on NOx conversion of fresh and hydrothermally-aged Fe-SCR-2 catalysts; evaluated with 5% CO_2, 5% H_2O, 14% O_2, 175 ppm NO, 175 ppm NO_2, 350 ppm NH_3 (α = 1.0), N_2 balance, GHSV = 30,000 h^{-1}

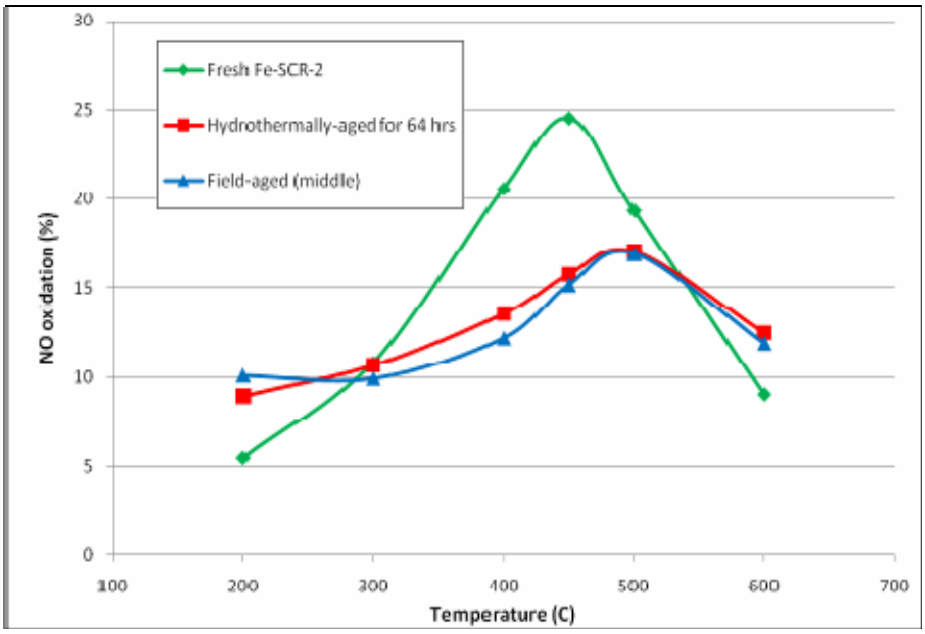

Figure 4-30. Effect of temperature on NO oxidation of fresh and hydrothermally-aged Fe-SCR-2 catalyst; evaluated with 5% CO_2, 5% H_2O, 14% O_2, 350 ppm NO, N_2 balance, GHSV = 30,000 h^{-1}

4.2.2 Accelerated Thermal Aging on the Engine Bench

A Fe-SCR-2 SCR catalyst is aged for 31 cycles (31 active DPF regenerations) at an SCR inlet gas temperature of 650°C. Atomized diesel fuel is injected into the exhaust upstream of the DOC. The flow rate of atomized fuel is varied to obtain target aging temperatures in the aftertreatment system during active DPF regeneration. Figure 4.31 shows typical aftertreatment system temperatures during aging at 650°C. Since the temperature profiles are repeatable, the SCR catalyst is experiencing the same aging conditions during each DPF regeneration. The gas temperature at the inlet of the SCR catalyst is approximately 100°C higher than the exit of SCR catalyst. Thus, the front-half of the SCR catalyst is experiencing more severe aging than the rear-half.

The NO_x performance of the engine-aged catalyst is evaluated at the end of each DPF regeneration cycle or aging cycle. After completing a regeneration, the aftertreatment system is allowed to cool for twenty minutes. The nominal temperature of the SCR catalyst during NO_x performance evaluations on the engine bench is approximately 300°C. As can be seen in Figure 4.31 this nominal temperature varies slightly with each cycle. Once the aftertreatment system has reached normal operating conditions, three NO_x measurements are taken: NO at the DOC inlet and DPF exit, and NO+NO_x at the DOC inlet. NH_3 is injected into the SCR catalyst inlet at a ratio of NH_3 to NO_x of 0.6 ($\alpha = 0.6$). This α ratio is chosen to ensure that no NH_3 slip occurs. With the addition of NH_3, the concentrations of NO and NO+NO_x are measured at the DPF exit. Figure 4.32 shows the NO_x measurements taken during NO_x performance evaluation and engine aging at 650°C. The NO_x measurements show that the aftertreatment system achieves approximately 60% NO oxidation, most of which occurs over the DOC. When NH_3 is injected upstream of the SCR catalyst, the NO_x emissions decreases from approximately 700 ppm NO_x to approximately 350 ppm NO_x at the DPF exit, resulting in an approximate NO_x reduction of 50%. Finally, the concentration of NO is measured to be approximately 175 ppm NO at the DPF exit while still injecting NH_3 upstream of the SCR catalyst. This indicates that about 50% of the NO_x that is not reduced by the aftertreatment system is NO. Similar to the exhaust gas temperature there is cycle-to-cylce variation of NO_x emissions from the diesel engine, which makes it difficult to accurately identify small changes in the

NO_x performance of the aftertreatment system during engine aging. Changes in NO_x performance can be attributed to variation of engine emissions.

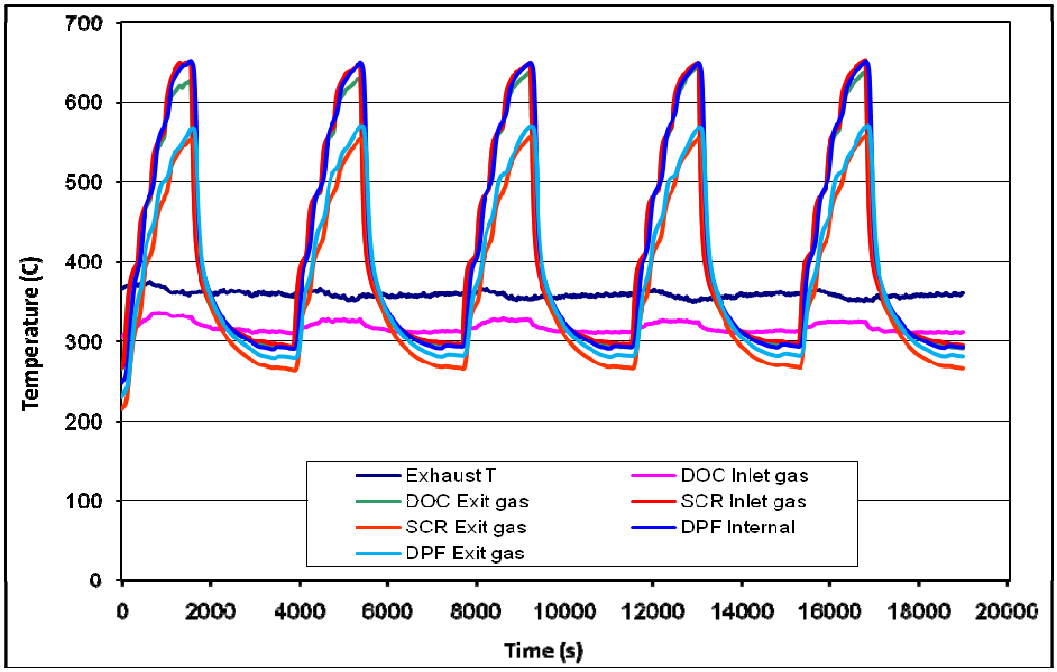

Figure 4-31. Aftertreatment system temperatures during accelerated thermal aging on engine bench at 650°C

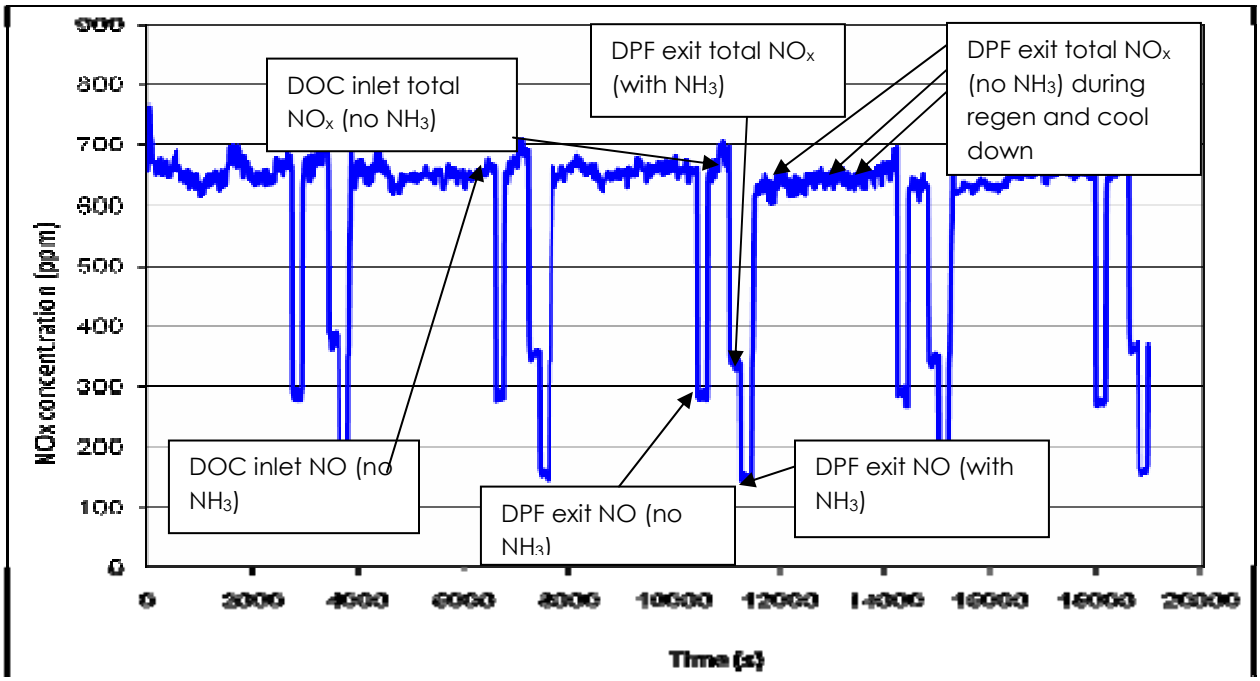

Figure 4-32. NOx emissions during accelerated thermal aging on engine bench at 650°C

Figure 4.33 shows the effect of number of aging cycles on the NO_x performance of the aftertreatment system during accelerated thermal aging at 650°C. NO_x conversion is defined as the amount of NO_x converted as a percentage of total NO_x concentration at the aftertreatment inlet. NO conversion is defined as the amount NO converted as a percentage of the total NO concentration at the aftertreatment exit. And NO oxidation is defined as the amount of NO oxidized as a percentage of the total NO concentration at the aftertreatment inlet.

Overall, NO and NO_x performance appear to decrease with aging time, however it is difficult to determine the extent of aging on the catalyst's performance due to the large cycle- to-cycle variation of the NO_x performance. There is also a large variation in NO oxidation, which makes it difficult to determine any changes in the system's NO oxidation activity. Straight lines are fitted to the data that show NO_x performance and NO conversion slightly decreasing with increasing aging time; however, the coefficient of determination (R^2) is low for each set of data, which implies that the linear relationship does not account very well for the variability in the data. Aging was discontinued after 31 cycles due to backpressure problems in the aftertreatment system. The DOC system used for aging at 650°C consists of two individual DOCs mounted in tandem. As aging progressed debris from the DOCs caused by vibration and abrasion was carried downstream of the aftertreatment system. Consequently, as the aging progressed the DPF became clogged with the DOC debris and degraded insulation, causing an irreversible drastic increase in back pressure.

A second test is conducted at 750°C for 50 cycles and Figure 4.34 shows typical aftertreatment system temperatures during accelerated thermal aging. The temperature profiles are again repeatable, so the SCR catalyst is experiencing similar aging conditions during each aging cycle. The SCR catalyst inlet temperature is approximately 90°C higher than the exit temperature.

Figure 4.35 shows NO_x measurements taken during aging at 750°C. The NO_x emissions behavior of the engine is similar to aging at 650°C. Nevertheless, Nominal NO_x emissions from the engine are approximately 800 ppm NO_x, compared to 750 ppm NO_x during aging at 650°C. Since the operation of the engine is not altered to achieve different aging temperatures, rather the fuel injection rate upstream of the DOC is varied, it is not expected to produce different NO_x emissions at the various aging temperatures. Therefore, it appears that there is day-to-day variation as well as cycle-to-cycle variation of NO_x emissions from the engine.

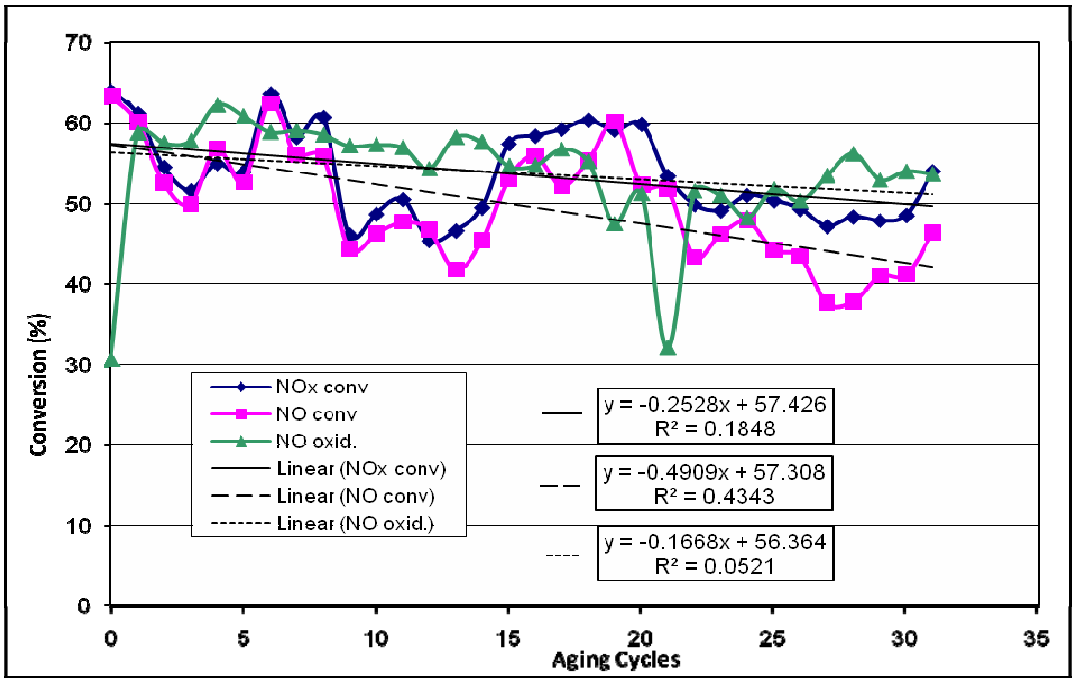

Figure 4-33. Aftertreatment system NOx performance during accelerated thermal aging on engine bench at 650°C

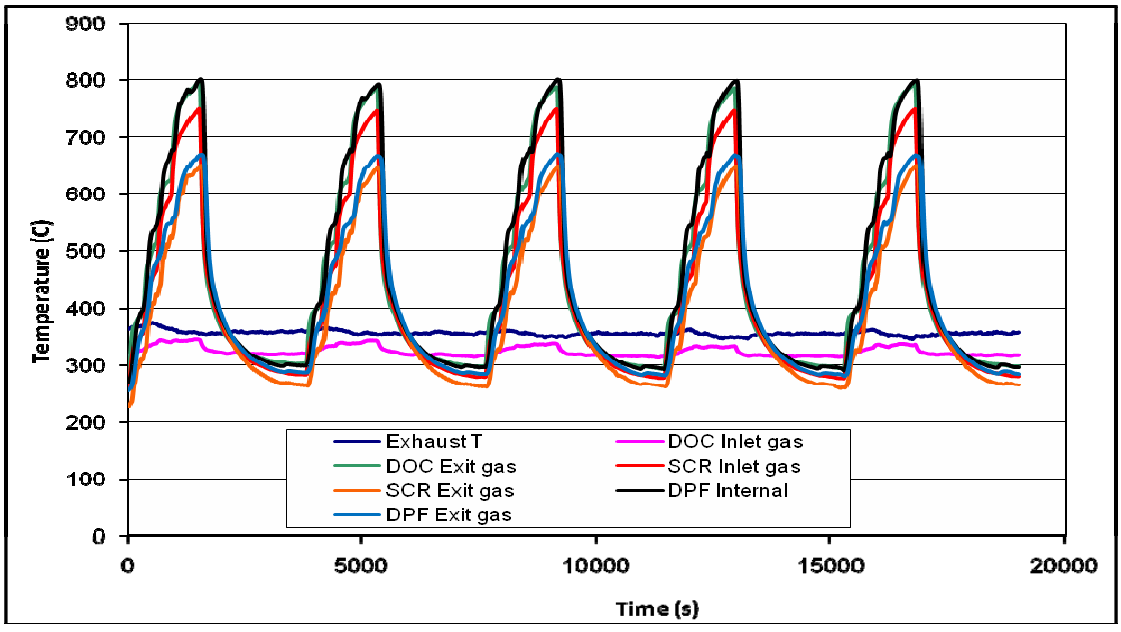

Figure 4-34. Aftertreatment system temperatures during accelerated thermal aging on engine bench at 750°C

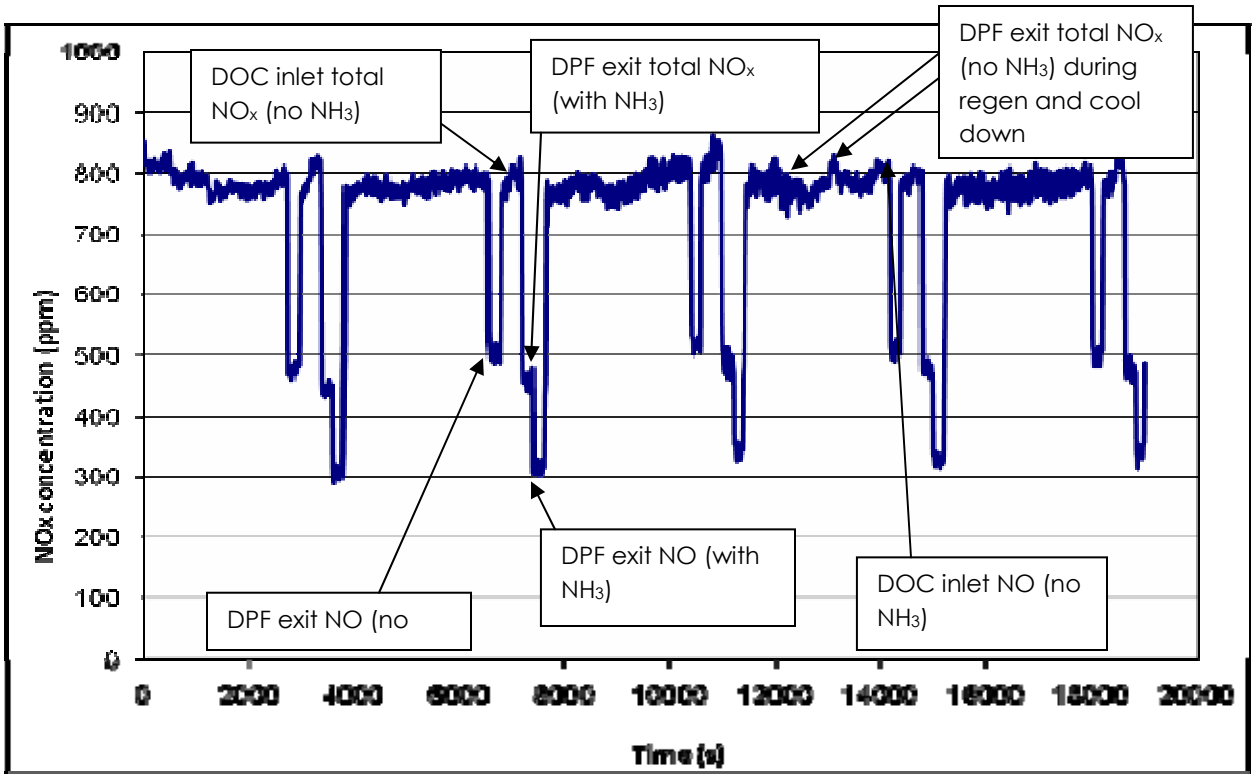

Figure 4-35. NOx emissions during accelerated thermal aging on engine bench at 750°C

Figure 4.36 shows the NO_x performance of the aftertreatment system measured at approximately 300°C between the accelerated thermal aging cycles at 750°C. The nominal NO_x conversion appears to be about 10% lower than the NO_x performance of the catalyst aged at 650°C. This could be due to higher NO_x emissions during aging at 750°C. According to the trend lines fitted to the data, NO_x performance appears to be slightly increasing with aging time. However, the corralation coefficents for NO_x conversion (0.303) and NO conversion (0.215) are very small, indicating that there is not a good relationship between NO_x The cycle-to-cycle variation of NO_x makes it difficult to identify any changes in catalytic performance. On the other hand, NO oxidation does appear to be steadily decreasing with aging time. The trend line fitted to the NO oxidation data shows a good correlation between NO oxidation and aging cycles with a correlation coefficient of 0.896. Since NO oxidation occurs over the DOC, the SCR catalyst and the DPF, a decline in the NO oxidation activity could be attributed to the deactivation of any one or all three of the aftertreatment system components.

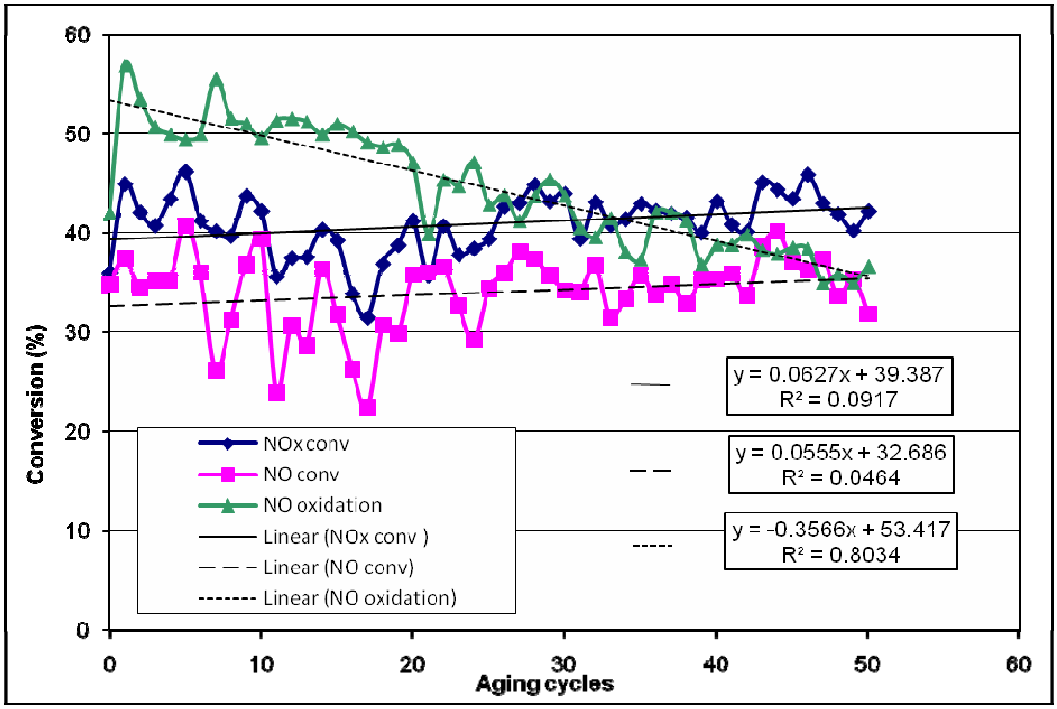

Figure 4-36. Aftertreatment system NOx performance during accelerated thermal aging on engine bench at 750°C

The last Fe-SCR-2 SCR catalyst is aged for 13 cycles at an SCR inlet gas temperature of 850°C. Figure 4.37 shows typical aftertreatment system temperatures during aging at 850°C. There is a similar trend seen here with aging at 650 and 750°C. There is an axial temperature variation of approximately 50°C along the SCR catalyst. The lower temperature difference across the SCR catalyst seen with aging at 850°C could be a result of increased convective heat tranfer at the elevated aging temperature. Higher gas velocities at elevated temperatures result in a higher convective heat transfer coefficient .

Figure 4.38 shows NO_x measurments taken during aging at 850°C. NO_x emissions trends are similar to aging at 650 and 750°C. Again, it appears that there is variation of NO_x emissions among the different aging temperatures as well as cycle to cycle variation.

Figure 4.39 shows the effect of number of aging cycles on the NO_x performance of the aftertreatment system during accelerated aging at 850°C. An increase in NO_x conversion is observed after 10 aging cycles, however, this is due to a leak at a flange junction in the exhaust system. Graphite gaskets used to seal flange connections degraded from exposure to high temperatures causing a leak to develop, resulting in an effective increase of α ratio. The catalyst

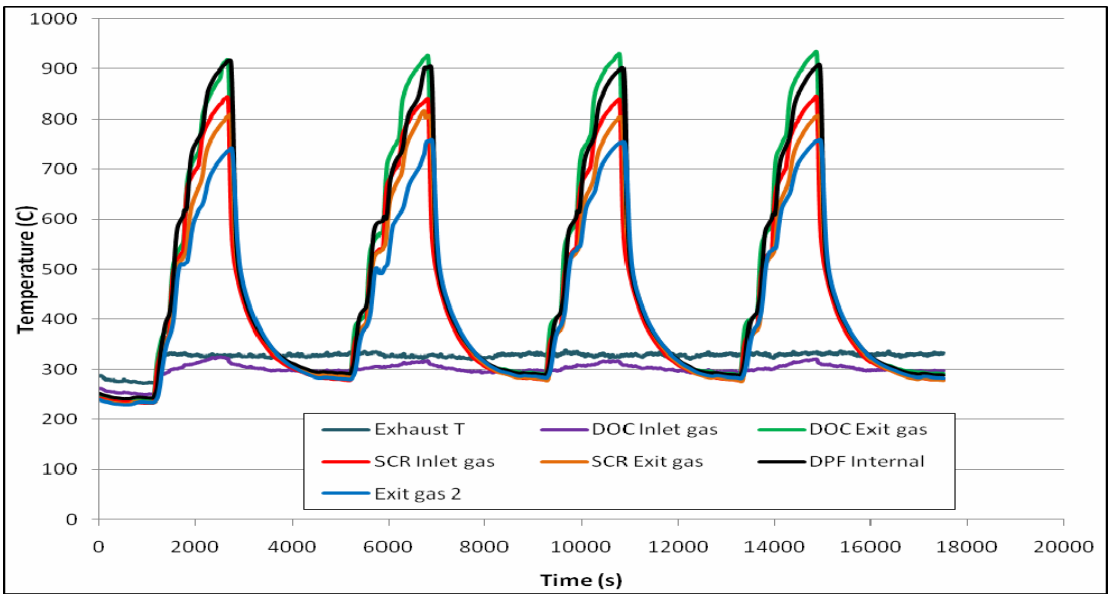

Figure 4-37. Aftertreatment system temperatures during accelerated thermal aging

on engine bench at 850°C

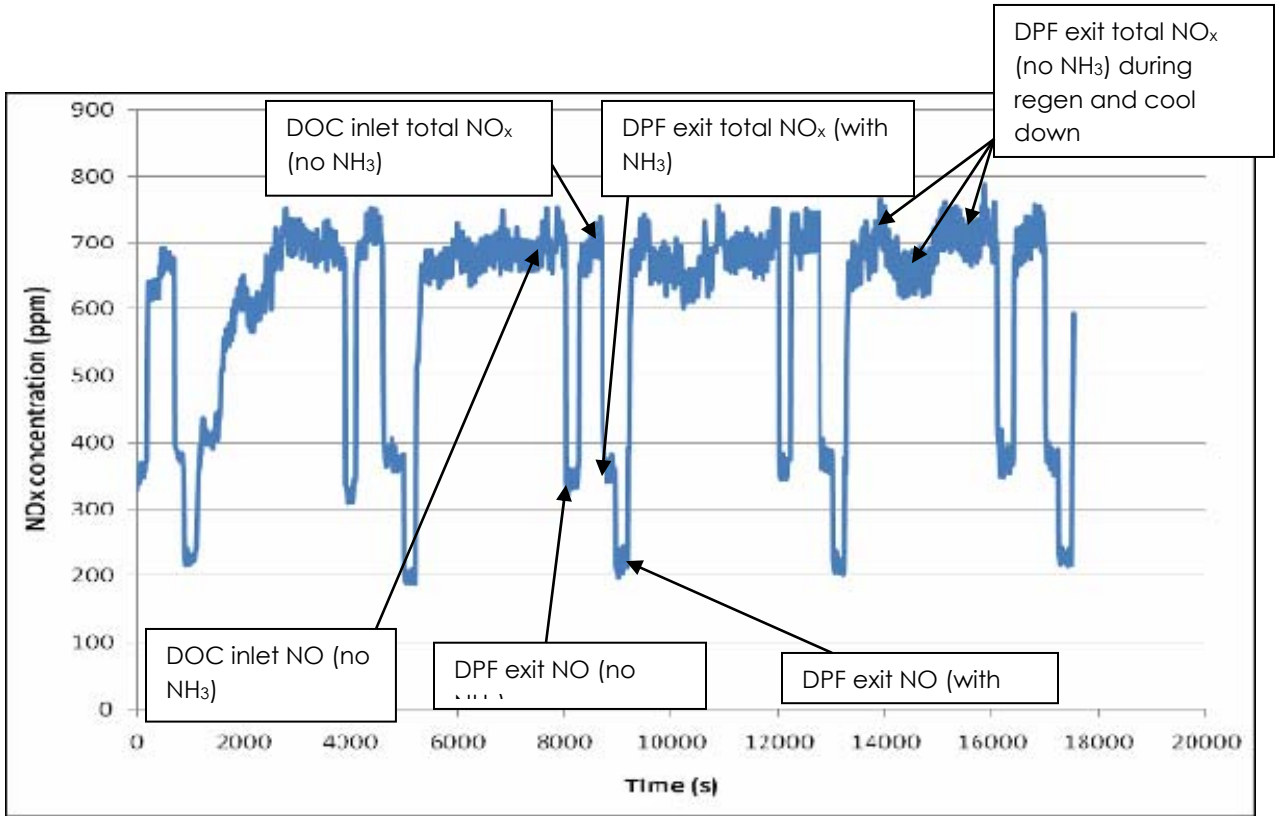

Figure 4-38. NOx emissions during accelerated thermal aging on engine bench at 850°C

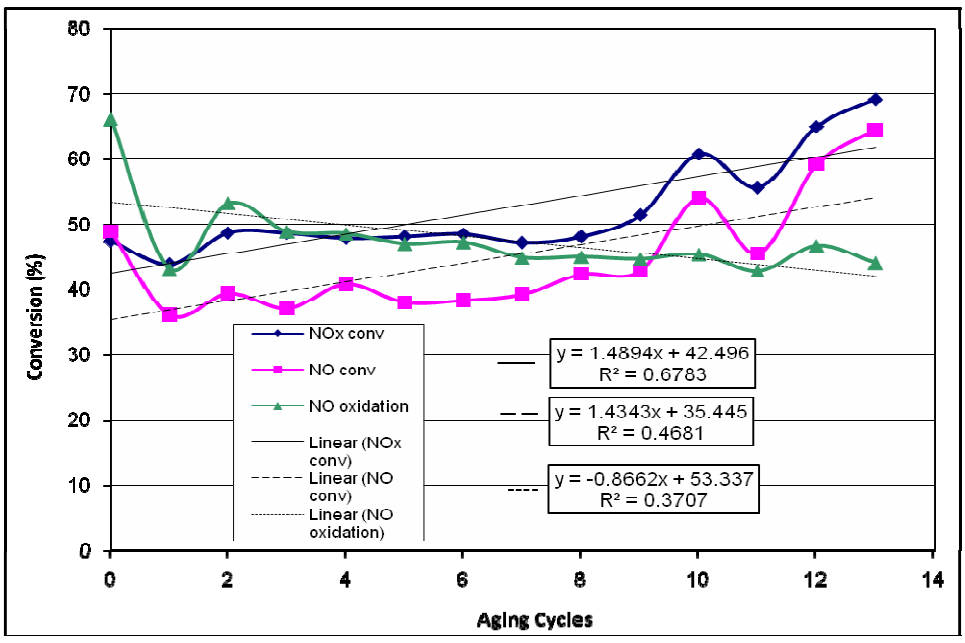

Figure 4-39. Aftertreatment system NOx performance during accelerated thermal aging on engine bench at 850°C

insulation used to hold the catalysts in place also degraded from exposure to high temperatures,causing insulation material to build up at the front of the DPF. The system backpressure began to increase after 10 aging cycles, and aging was discontinued after 13 aging cycles. If further work is done at 850°C, the gasket and insulation problems will need to be solved.

*4.2.3 **Bench-Flow Reactor Evaluation***

Due to cycle-to-cycle variations of the composition and the temperature of the engine's exhausts gases the BFR is used to evaluate the NO_x performance of the engine-aged catalysts. After aging the catalyst is sectioned into two halves before being evaluated on the BFR. The catalyst samples are evaluated with 5% H_2O, 5% CO_2, 14% O_2, 350ppm NO_x and 350ppm NH_3 ($\alpha = 1$), as prescribed by the CLEERS protocol for steady-state evaluation of SCR catalysts.

Figure 4.40 shows NO_x conversions of the front sections ofthe engine-aged Fe-SCR-2 catalysts with 350 ppm NO in the feed gas. The front sections of the aged catalysts are severely degraded as in the case of field-aged catalyst. On the other hand the rear sections of the aged catalysts still maintain the typical "bell-shaped" profile exhibited by fresh catalysts as seen in Figure 4.41. NO_x conversion over the front sections of the engine-aged catalysts increases with temperature from 200 to 300°C and then decreases at higher evaluation temperatures. It is expected that the catalyst aged at 650°C would perform well because of lower aging temperature; however, this is not the case as can be seen clearly in Figure 4.41 when comparing the front sections of the aged catalysts. The catalyst aged at 850°C exhibits the worst NO_x performance followed by the catalysts aged at 650 and 750°C. The similar shape of the NO_x conversion profiles of the front sections even at different aging temperatures seem to suggest that not only is the structure of the zeolite severly degraded, but that there may be some type of poisoning occurring in this section of the engine-aged catalysts.

While the rear sections of the engine-aged catalysts maintain the typical "bell-shaped" profile for NO_x conversion as seen in Figure 4.41, the effects from aging are still observed. Accelerated thermal aging at 850°C causes a severe decline of NO_x performance. The maximum

NO_x conversion has decreased from 85% with a fresh sample to 45% over the engine-aged sample. The rear sections of the catalysts aged at 650 and 750°C both show signs of aging at

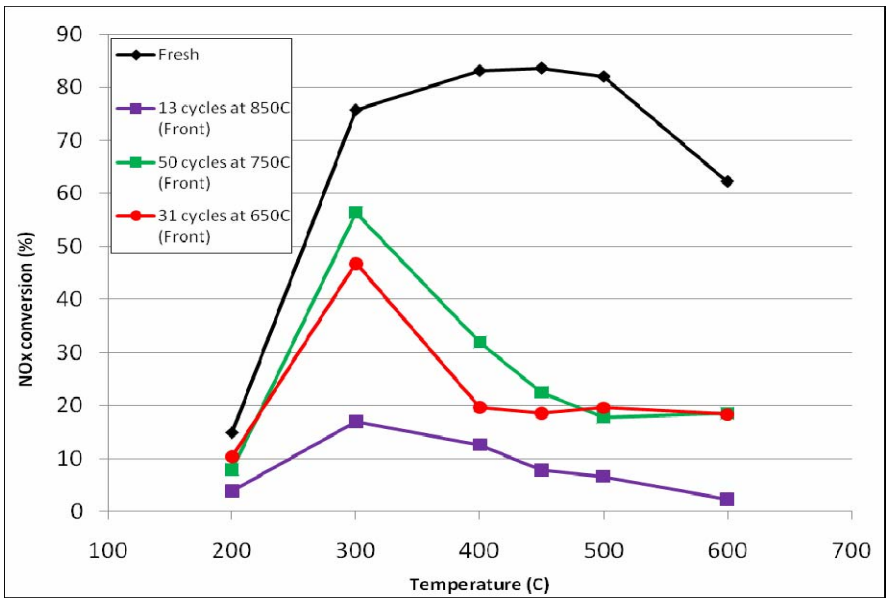

Figure 4-40. Effect of temperature on NOx conversion of front sections of engine-aged Fe-SCR-2 catalysts; evaluated with 5% CO_2, 5% H_2O, 14% O_2, 350 ppm NO, 350 ppm NH_3 (α = 1.0), N_2 balance, GHSV = 30,000 h^{-1}

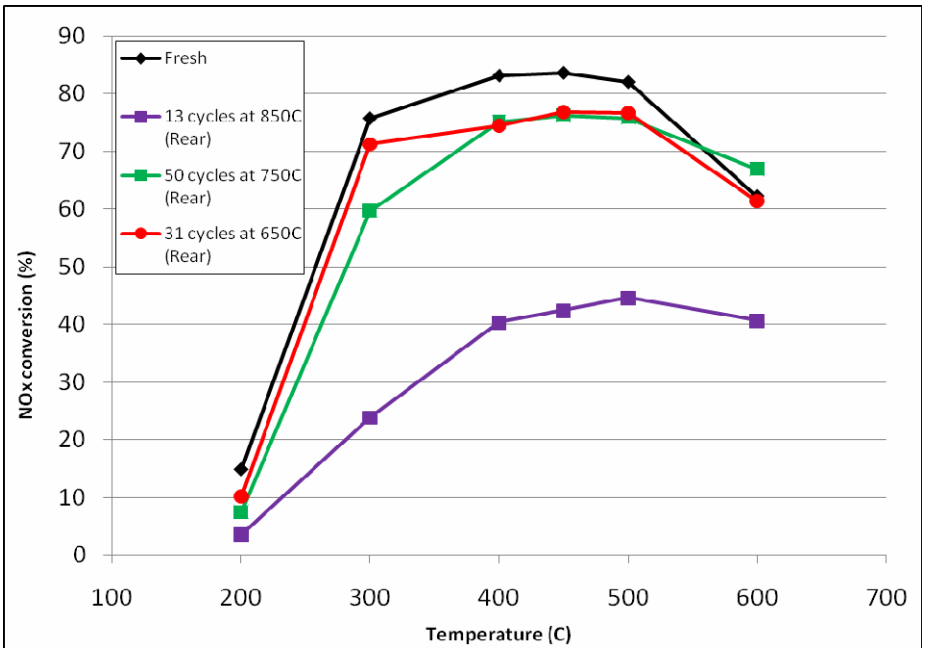

Figure 4-41.Effect of temperature on NOx conversions of rear sections of engine-aged

Fe-SCR-2 catalysts; evaluated with 5% CO_2, 5% H_2O, 14% O_2, 350 ppm NO, 350 ppm NH_3 (α = 1.0), N_2 balance, GHSV = 30,000 h^{-1}

evaluation temperatures between 400 and 500°C with maximum NO_x converisons of 77% and 76%, respectively. Although, the two catalysts show similar NO_x performance between 400 and 500°C, the effects of aging stand out more with the catalyst aged at 750°C. While the catalystaged at 750°C shows a NO_x conversion of 60% at an evaluation temperature of 300°C, the catalyst aged at 650°C has a NO_x conversion of 71%. There is a good connection between aging temperature and NO_x performance with the rear sections of the engine-aged catalysts. The catalysts aged at 650°C performs the best followed closely by the catalyst aged at 750°C, and then there is significant deactivation observed with the catalyst aged at 850°C even though aging only lasted 13 cycles. It is difficult to compare the performance of the front sections of the engine-aged catalysts with the rear sections because of the severe deactivation seen in the front sections of the engine-aged catalysts.

The NO_x performances of the front sections of the engine-aged Fe-SCR-2 catalysts with an equimolar amount of NO and NO_2 in the evaluation gases are shown in Figure 4.42. The addition of NO_2 to the feed gas greatly enhances the NO_x performance of the front sections of the engine-aged catalysts, especially at low temperature (<400°C). At an evaluation temperature of 300°C the NO_x performance of the catalyst aged at 850°C increases from 17% to 74%, whereas that of the catalysts aged at 650 and 750°C increases from 47% to 75% and 56% to 75%, respectivley. The NO_x performance of the front sections of the engine-aged catalysts is similar to that of the field-aged catalyst. NO_x conversion is high (>60%) at 200 and 300°C, before decreasing at higher evaluation temperatures.

The addition of NO_2 to the feed gas also enhances the performance in the rear sections of the engine-aged catalysts. The catalyst deactivation associated with aging at 650 and 750°C seen in Figure 4.41 is no longer seen in Figure 4.43. The NO_x conversions of the two catalyst sections are almost identical to that of a fresh Fe-SCR-2 catalyst. NO_x conversion over the catalyst aged at 850°C increases over the entire temperature range, however, catalyst deactivation is still observed with this catalyst section. Although aging was only performed for 13 cycles, the effects of aging are more pronounced in the catalyst aged at 850°C. It appears that deactivation is strongly related to aging temperature.

According to previous studies the oxidation of NO to NO_2 is an important step in the selective catalytic reduction of NO by NH_3 [18-20, 23, 24]. Figure 4.44 shows the NO oxidation

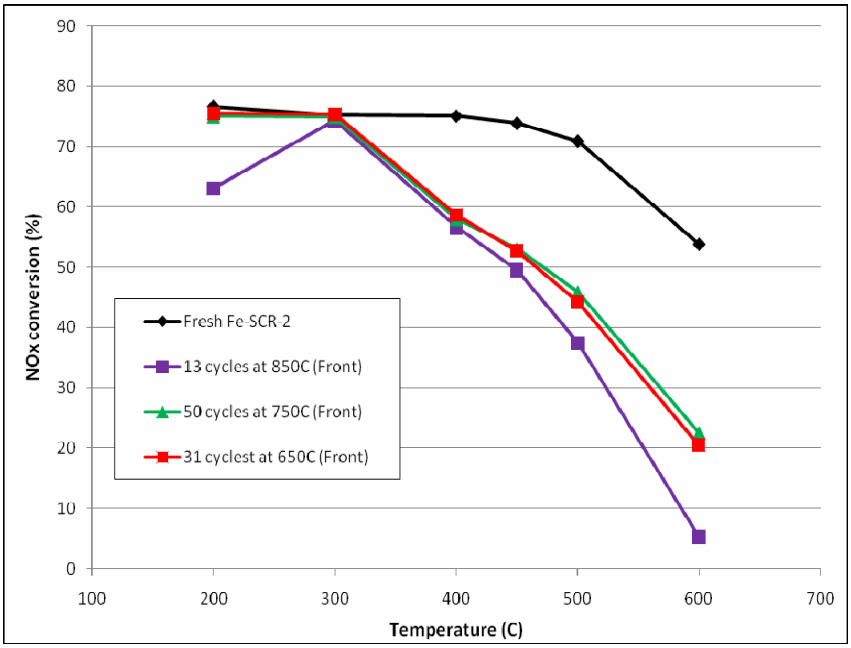

Figure 4-42. Effect of temperature on NOx conversion of front sections of engine-aged Fe-SCR-2 catalysts; evaluated with 5% CO_2, 5% H_2O, 14% O_2, 175 ppm NO, 175 ppm NO_2, 350 ppm NH_3 (α = 1.0), N_2 balance, GHSV = 30,000 h^{-1}

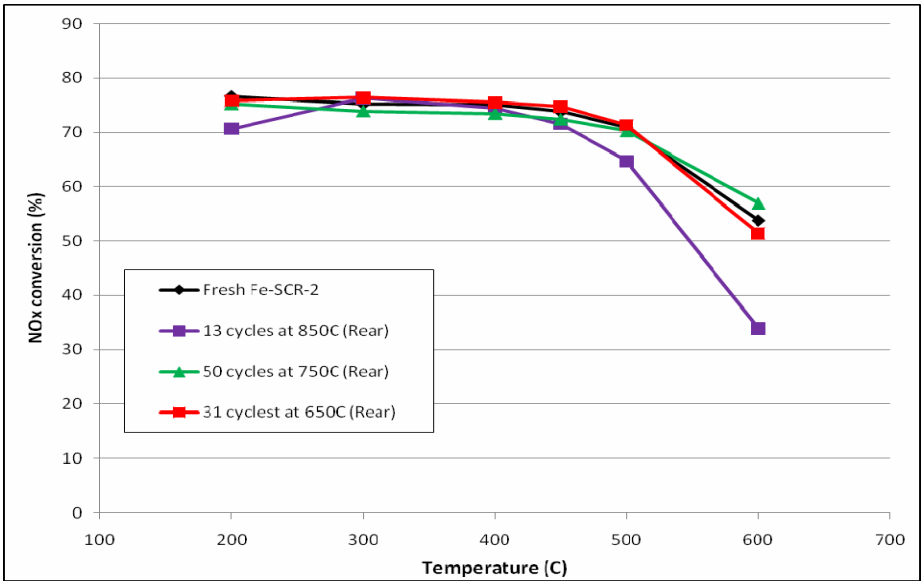

Figure 4-43. Effect of temperature on NOx conversion of rear sections of engine-aged Fe-SCR-2 catalysts; evaluated with 5% CO_2, 5% H_2O, 14% O_2, 175 ppm NO, 175 ppm NO_2, 350 ppm NH_3 (α = 1.0), N_2 balance, GHSV = 30,000 h^{-1}

activities of the egine-aged Fe-SCR-2 catalysts as a function of temperature. NO oxidation decreases with increasing aging temperature. The fresh catalyst has the greatest NO oxidation activity with 25% NO oxidation at 450°C, followed by those aged at 650°C, 750°C and 850°C. The front section of the catalyst aged at 850°C exhibits the worst NO oxidation activity with only a maximum of 10% NO oxidized. As NO oxidation activity decreases, peak NO oxidation shifts from 450°C to 500°C. It is also seen that the rear section of each catalyst shows higher NO oxidation than the front section of the same catalyst.

Bench-flow reactor evaluation of the rear sections of the engine-aged Fe-SCR-2 catalysts reveals a strong link between catalyst deactivation and aging temperature. The catalyst aged at 650°C exhibits the best overall performance followed closely by the catalyst aged at 750°C. The catalyst aged at 850°C exhibits the worst overall performance. Aging at 850°C causes significant deactivation as evidenced by the catalytic performance shown in Figures 4.40 to 4.44. It has been suggested that active Fe sites in the zeolite washcoat are responsible for NO oxidation to NO_2

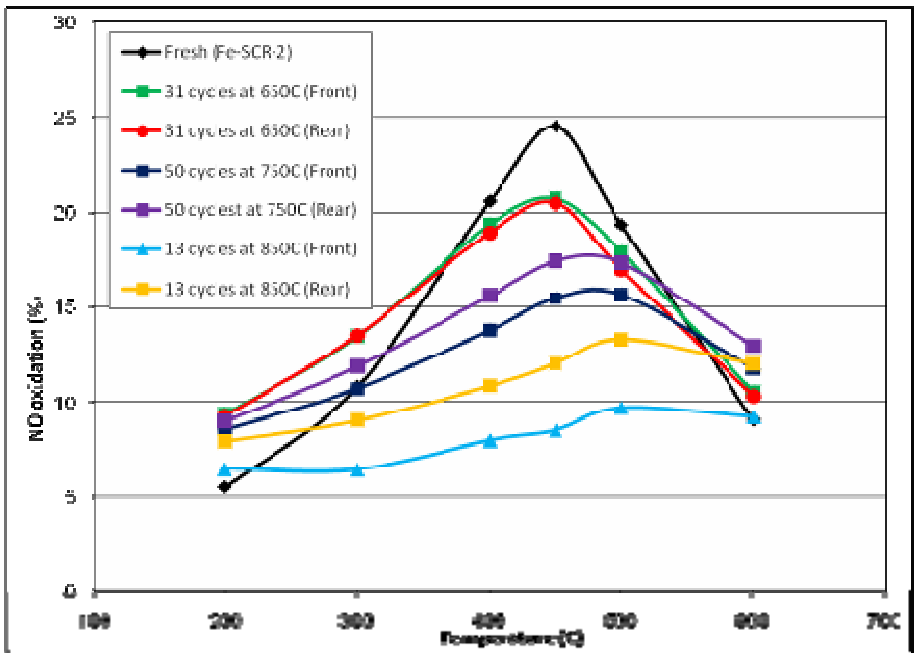

Figure 4-44. Effect of temperature on NO oxidation of engine-aged Fe-SCR-2 catalysts; evaluated with 5% CO_2, 5% H_2O, 14% O_2, 350 ppm NO ($\alpha = 0$), N_2 balance, GHSV = 30,000 h^{-1}

[22]. Therefore, it could be argued that aging decreases the number of active Fe sites in the zeolite, causing a decrease in NO oxidation activity, and a decrease in NO_x conversion, which is seen with the engine-aged catalysts. This argument is supported by improved NO_x conversion of the rear sections of the engine-aged catalysts when NO_2 is added to the feed gas. The addition of NO_2 to the evaluation gases appears to compensate for the absence of active Fe sites. Since, extensive surface characterization has not been completed, the underlying deactivation mechanism, which is responsible for the degradation of NO_x performance in the front sections of the engine-aged catalysts, has not been determined.

Others have found that dealumination is the primary source of catalyst deactivation in zeolite-based SCR catalysts [31-33]. Al^{3+} cations migrate out of the SiO_2-Al_2O_3 tetrahedral framework, resulting in destruction of the zeolite structure. Dealumination affects catalytic performance in many ways. There is a reduction in catalyst surface area, making it difficult for reactants to be adsorbed onto the active acid sites (Brønsted and Fe) in the zeolite. As the zeolite structure breaks down active Fe cations are lost due to the formation of Fe_2O_3 in conjunction with a reduction of Brønsted acid sites caused by dealumination. As can be seen later material characterization and surface studies of the field-aged Fe-SCR-1 catalyst do indeed reveal severe structural damage to the zeolite washcoat, zeolite dealumination and the loss of active Fe sites to the formation of Fe_2O_3.

Due to the fact that SCR catalysts are seldom used by themselves, it is important to understand how the other components of the aftertreatment system affect the system's overall NO_x performance. It is seen that the aged Fe-SCR-2 catalysts maintain good NO_x conversion when there is an equimolar amount of NO and NO_2 in the evaluation gases. The degradation of NO_x performance is nearly fully recovered in the rear sections of the engine-aged catalysts and NO_x performance is greatly enhanced in the front sections of the catalysts. Consequently, the lifetime of the catalysts can be extended greatly with the use of a DOC mounted upstream of the Fe-zeolite SCR catalyst, whose function is to oxidize some of NO to NO_2 in the exhaust gases. Therefore as the SCR catalyst is aged the ability of the DOC to oxidize NO to NO_2 becomes

essential to the NO_x performance of the aftertreatment system. The DOCs used for accelerated thermal aging are evaluated for NO oxidation and the results are presented in Figure 4.45. It appears that both aging time and aging temperature has an effect on DOC performance. The

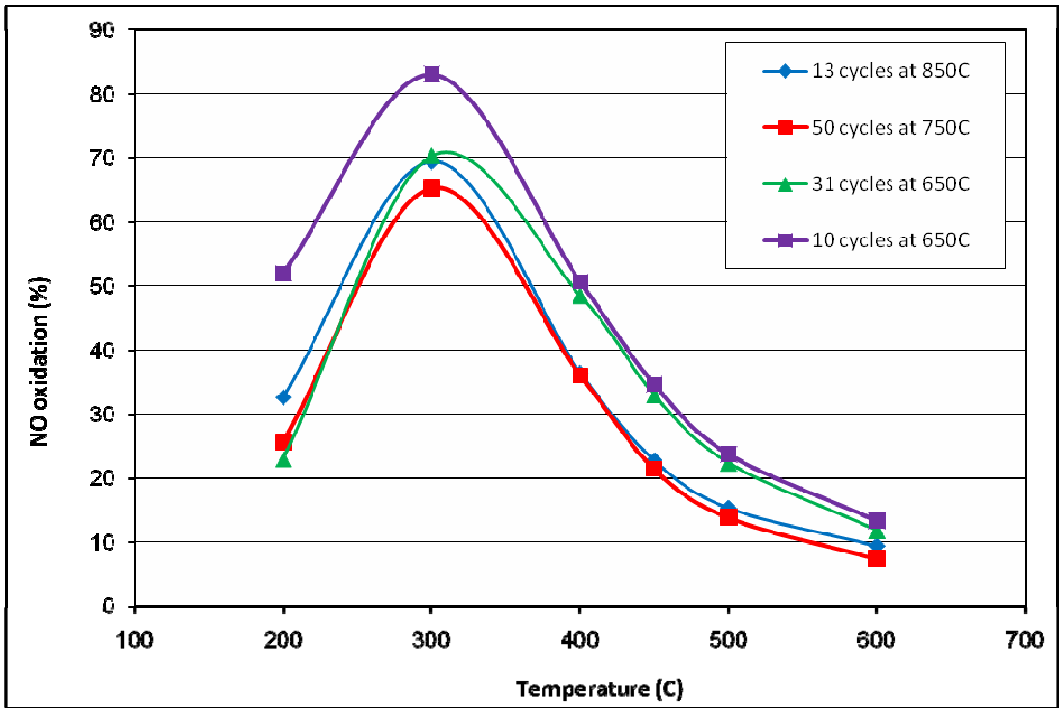

Figure 4-45. NO oxidation activity of DOC catalysts used during accelerated thermal aging; evaluated with 5% CO_2, 5% H_2O, 14% O_2, 350 ppm NO ($\alpha = 0$), N_2 balance, GHSV = 30,000 h^{-1}

DOC used for 10 cycles at 650°C shows the best NO oxidation performance, followed by the DOCs used for 31 cycles at 650°C and 13 cycles at 850°C, respectively. The DOC used for 50 cycles at 750°C exhibits the worst NO oxidation performance. Although BFR evaluation reveals differences in NO oxidation activity, none of the DOC samples show severe deactivation. This indicates that even the aftertreatment system used for aging the SCR catalyst at 850°C could still achieve good NO_x conversion.

4.2.4 ***Materials Characterization***

Due to the limited availability of fresh catalysts, X-ray diffraction is only performed at the

end of aging. X-ray diffraction patterns of the engine-aged Fe-SCR-2 catalysts reveal that accelerated thermal aging results in zeolite dealumination, formation of iron oxides and changes in physical structures of the zeolite support. Bench-flow evaluation of the hydrothermally-aged catalyst shows little evidence of catalyst deactivation, except for a decrease of NO oxidation activity. The XRD patterns of the hydrothermally-aged catalyst in the BFR, shown in Figure 4.46, reveal the formation of Fe_2O_3, which indicates a reduction of active iron sites and decreased NO oxidation activity. The formation of Al_2O_3 is also observed in the catalyst washcoat, which indicates zeolite dealumination. While catalyst deactivation is not observed with this catalyst, the XRD patterns show that zeolite dealumination and formation of Fe_2O_3 have occurred during hydrothermal aging.

Figure 4.47 shows the XRD patterns of the catalysts aged at 650°C for 31 cycles. The XRD patterns of the front and rear sections of the catalyst aged at 650°C look similar to that of the hydrothermally-aged catalyst. Fe_2O_3 and Al_2O_3 are detected in the engine-aged catalyst indicating that both zeolite dealumination and a reduction of active iron sites has occurred during accelerated thermal aging at 650°C.

The XRD patterns of the catalysts aged at 750 and 850°C are shown in Figures 4.48 and 4.49, respectively. Fe_2O_3 and Al_2O_3 are detected in the engine-aged catalysts, however, unlike the hydrothermally-aged catalyst there is a significant decrease of the intensity of the zeolite peaks, indicating a breakdown in zeolite structure in the engine-aged catalyst washcoat. The breakdown in zeolite structure would result in reduced catalyst surface area, which is confirmed by BET measurements presented in Figure 4.65. The breakdown of zeolite structure is further confirmed by the presence of Si peaks detected in the XRD patterns of Figures 4.48 and 4.49. Two distinguishing features are observed in the XRD patterns of the rear section of the catalyst aged at 750°C for 50 cycles shown in Figure 4.48. First, the intensity of the zeolite peaks are reduced considerably, whereas the intensity of the SiO_2 increases. Second, the appearance of Si, Al and Fe as well as Al_2O_3, FeO and Fe_2O_3 peaks is seen in the XRD patterns. On the contrary, Si, Al, Fe and FeO are not detected in the washcoat of the rear section of the catalyst aged for 13 cycles at 850°C. The lack of these peaks in the catalyst aged at 850°C mightbe due to sample preparation. For example, the amount of sample used for each XRD scan might be varied and consequently that of cordierite in the samples. Since, XRD patterns of cordierite are very pronounced they can overshadow the peaks of other materials making them difficult to identify.

While, the NO_x performance of the front sections of the engine-aged catalysts suggest that there may be some type of poisoning occurring in these catalyst sections, the XRD patterns do not show the presence of any compounds that are not also present in the rear sections of the engine-aged catalysts.

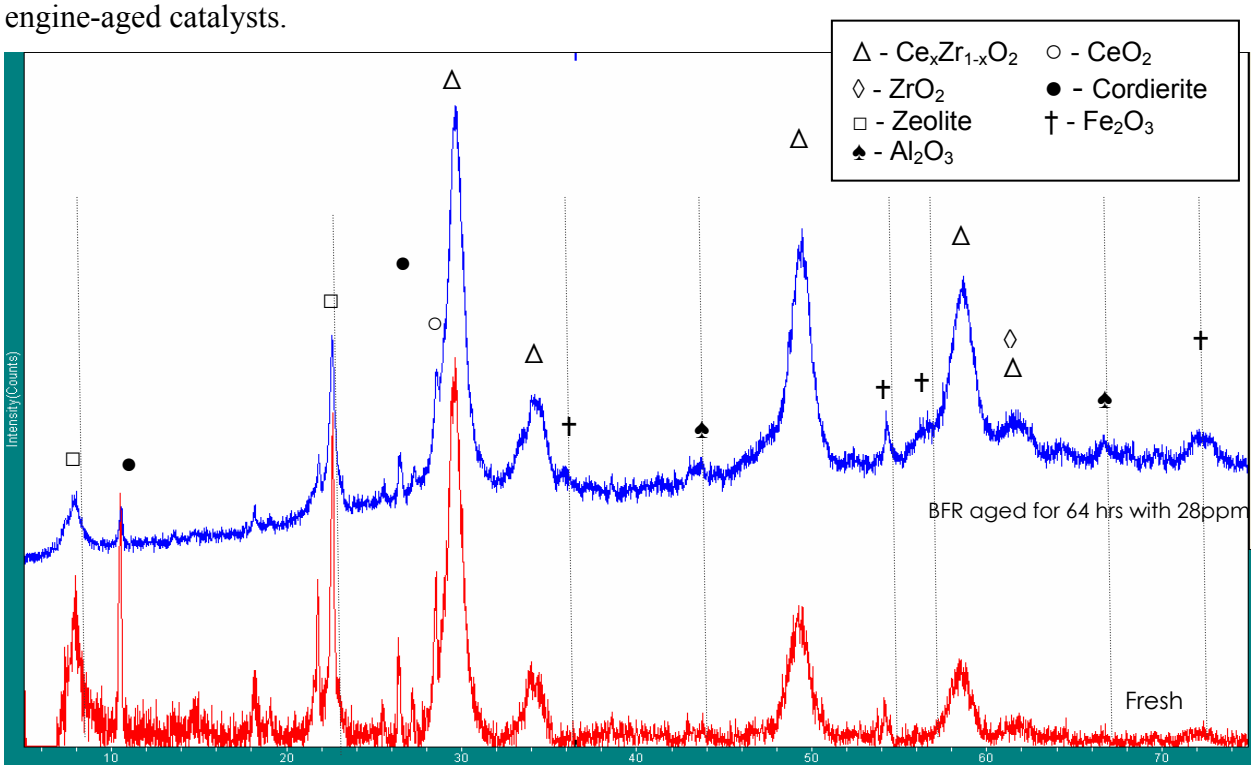

Figure 4-46. X-ray diffraction patterns of fresh and hydrothermally-aged Fe-SCR-2 catalysts

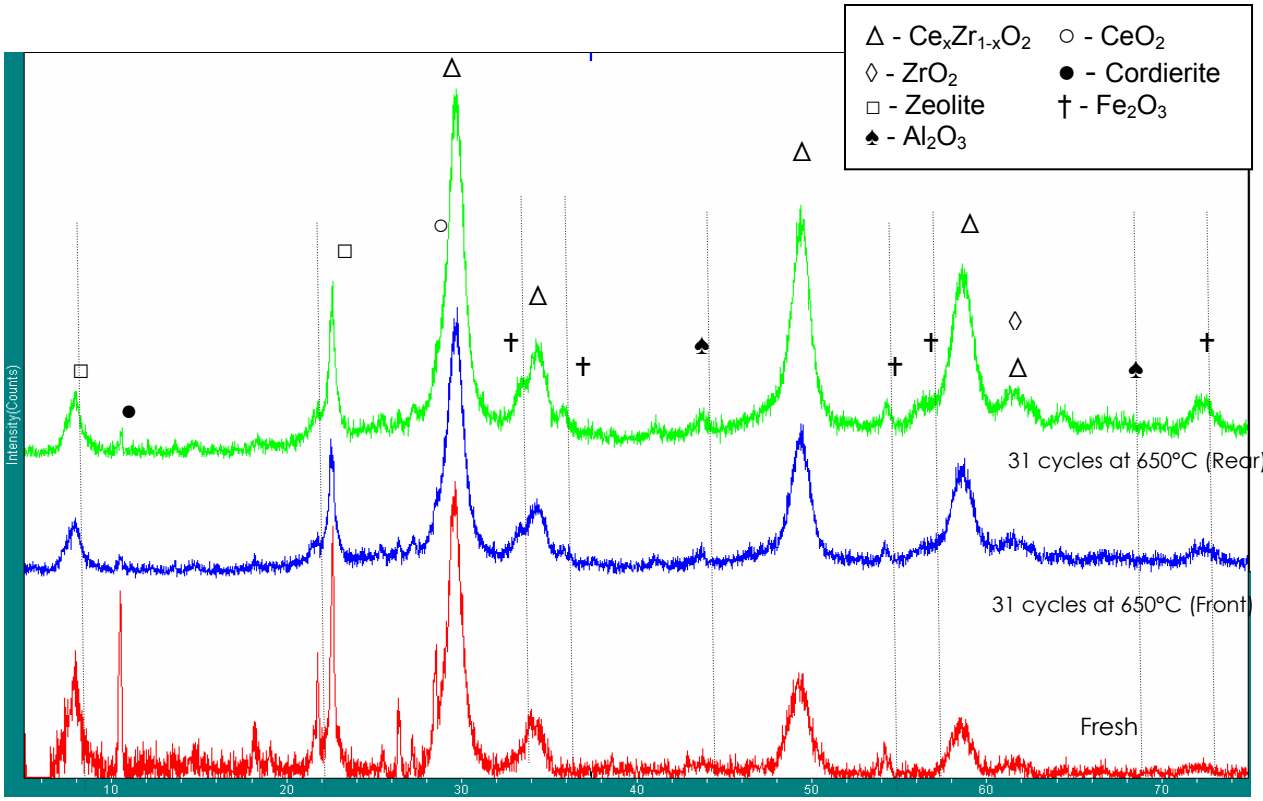

Figure 4-47. X-ray diffraction patterns of fresh and engine-aged (31 cycles at 650°C) Fe-SCR-2 catalysts

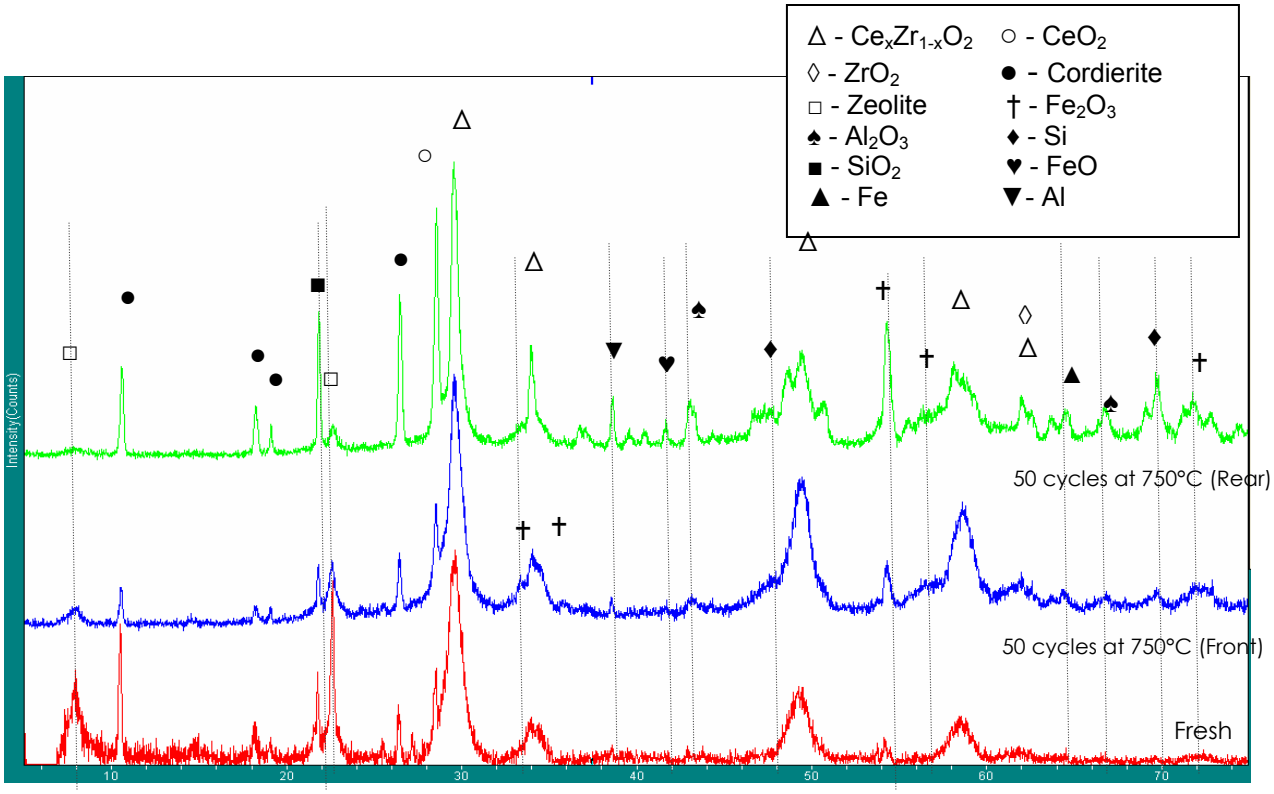

Figure 4-48. X-ray diffraction patterns of fresh and engine-aged (50 cycles at 750°C) Fe-SCR-2 catalysts

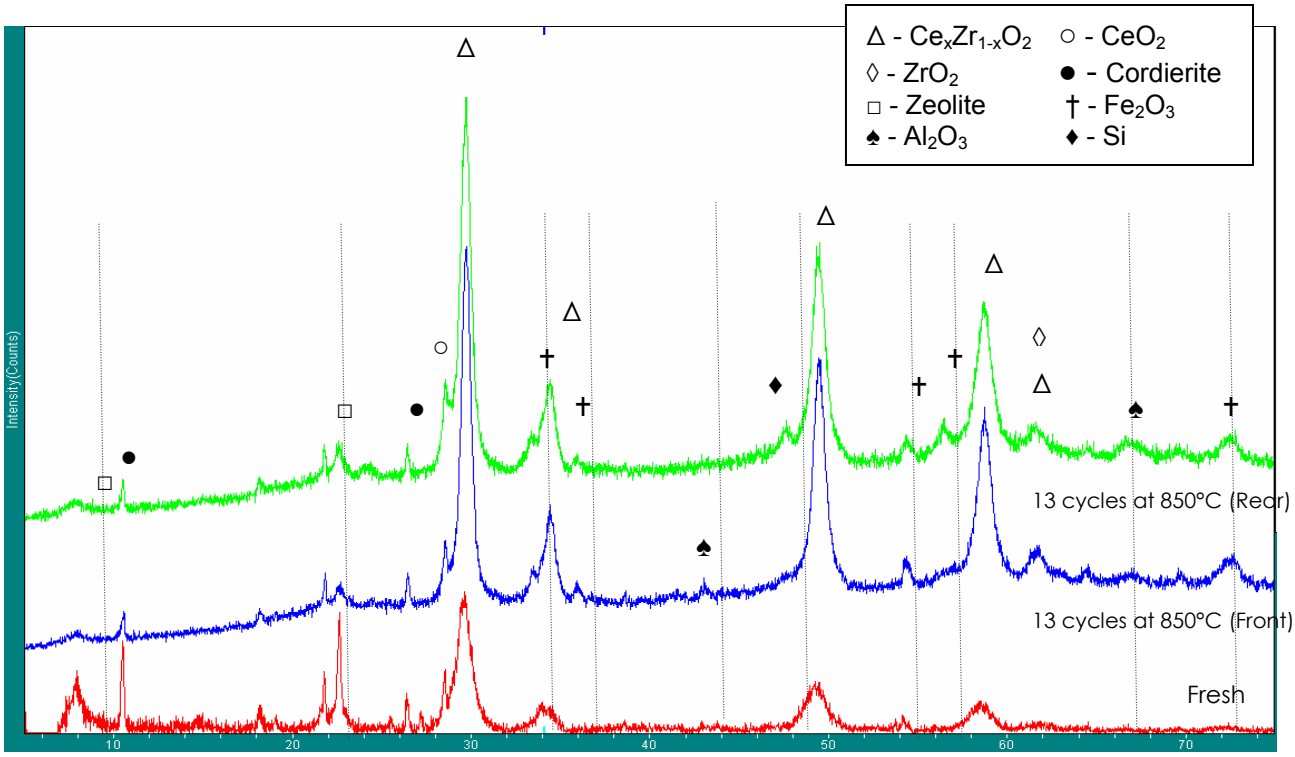

Figure 4-49. X-ray diffraction patterns of fresh and engine-aged (13 cycles at 850°C) Fe-SCR-2 catalysts

The elemental maps of the accelerated thermally-aged Fe-SCR-2 catalysts are shown in Figures 4.50 to 4.57. Cracks in the washcoat of the catalysts aged at 750 and 850°C are clearly visible in Figures 4.54, 4.56 and 4.57. As a result of higher aging temperature cracking is more severe in the catalyst aged at 850°C. Trace amount of phosphorus is detected in the washcoat of both fresh and accelerated thermally-aged catalysts. Unlike the field-aged catalyst, there is not a significant amount of sulfur detected in the washcoat of the Fe-SCR-2 aged catalysts. This may be due to the use of a low sulfur (15ppm) diesel fuel during engine-aging and the relatively short time these catalysts were aged, resulting in less tota fuel exposure. BFR-aging uses a concentration of 28ppm SO_2 in the feed gas. The elemental maps show that the Fe-SCR-2 catalysts do not appear to absorb sulfur at concentrations during aging. Calcium and zinc are also oil-derived species that can contribute to catalyst posisoning, but negligible amounts of both are detected by EPMA in all of the catalyst samples.

Fe is well-dispersed in the washcoat of the fresh and aged Fe-SCR-2 catalysts. Silicon is the main constituent of zeolite, therefore it is not surprising to see a large concentration of silicon present in the washcoat of the catalysts. A cerium-zirconium mixed oxide ($Ce_xZr_{1-x}O_2$) is present in the washcoat as an oxygen storage material, which explains the large amount of cerium and zirconium detected by EPMA.

As seen with the field-aged catalyst, the EPMA elemental maps do not reveal any significant differences in elemental make up of the fresh and aged Fe-SCR-2 catalysts. This Indicates that poisoning or loss of a washcoat component is not the cause of performance losses. The elemental maps of the front sections of the engine-aged catalysts do not reveal any changes from accelerated thermal aging that would suggest an explanation to the severe degradation seen with these catalyst sections. It could be argued that the poor activity seen with the front section of the field-aged catalyst is simply due to deterioration of the washcoat However that does not appear to be the case with the engine-aged catalysts aged at 650 and 750°C. X-ray diffraction and EPMA do not show evidence of lube-oil poisoning, but these catalyst samples perform poorly during BFR evaluation.

A scanning electron microscope (SEM) is used to obtain high magnification micrographs of the accelerated thermally-aged Fe-SCR-2 catalysts. The SEM micrographs of the hydrothermally-aged catalyst shown in Figure 4.59, looks similar to that of the fresh catalyst

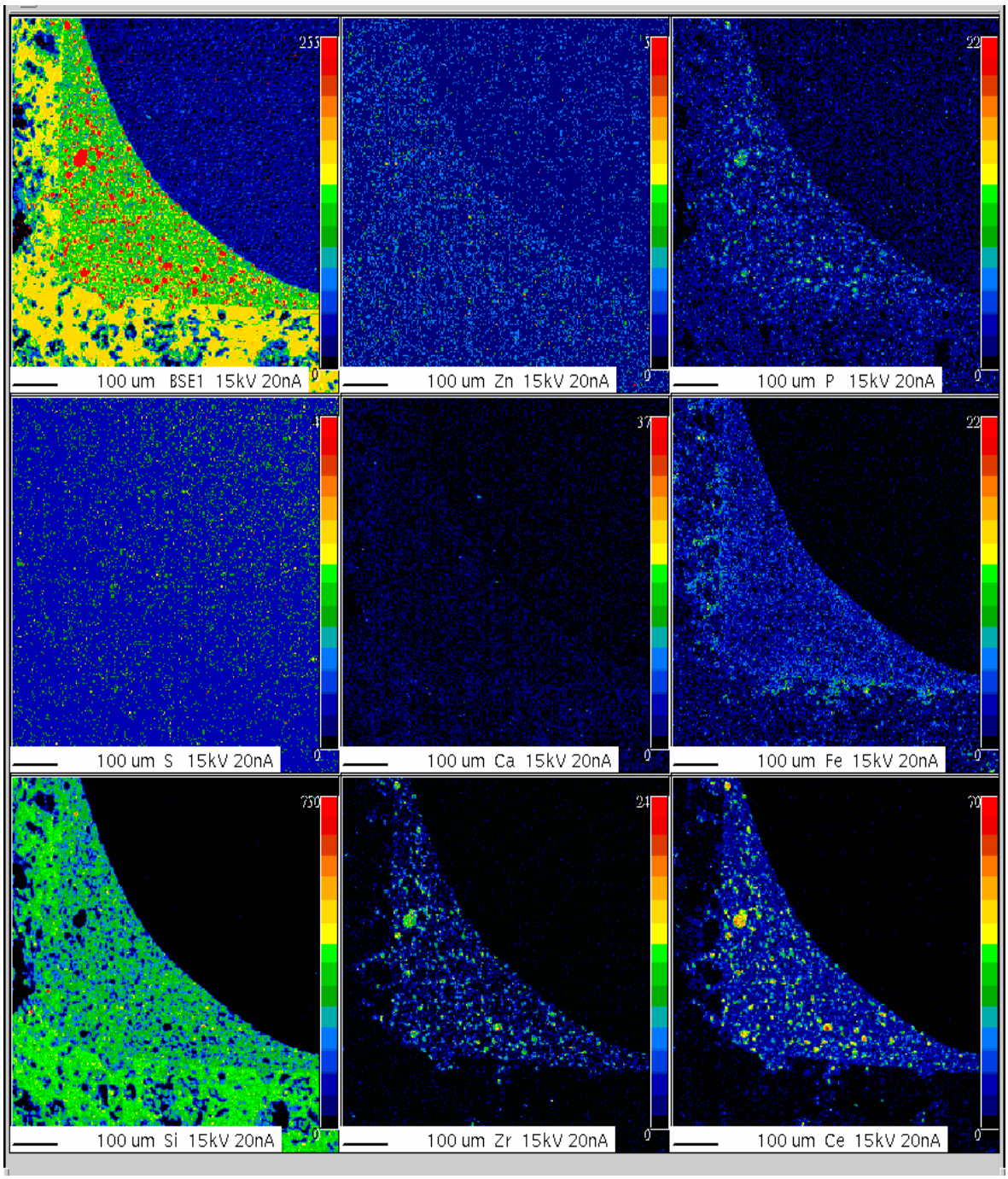

Figure 4-50. Element maps of fresh Fe-SCR-2 catalyst

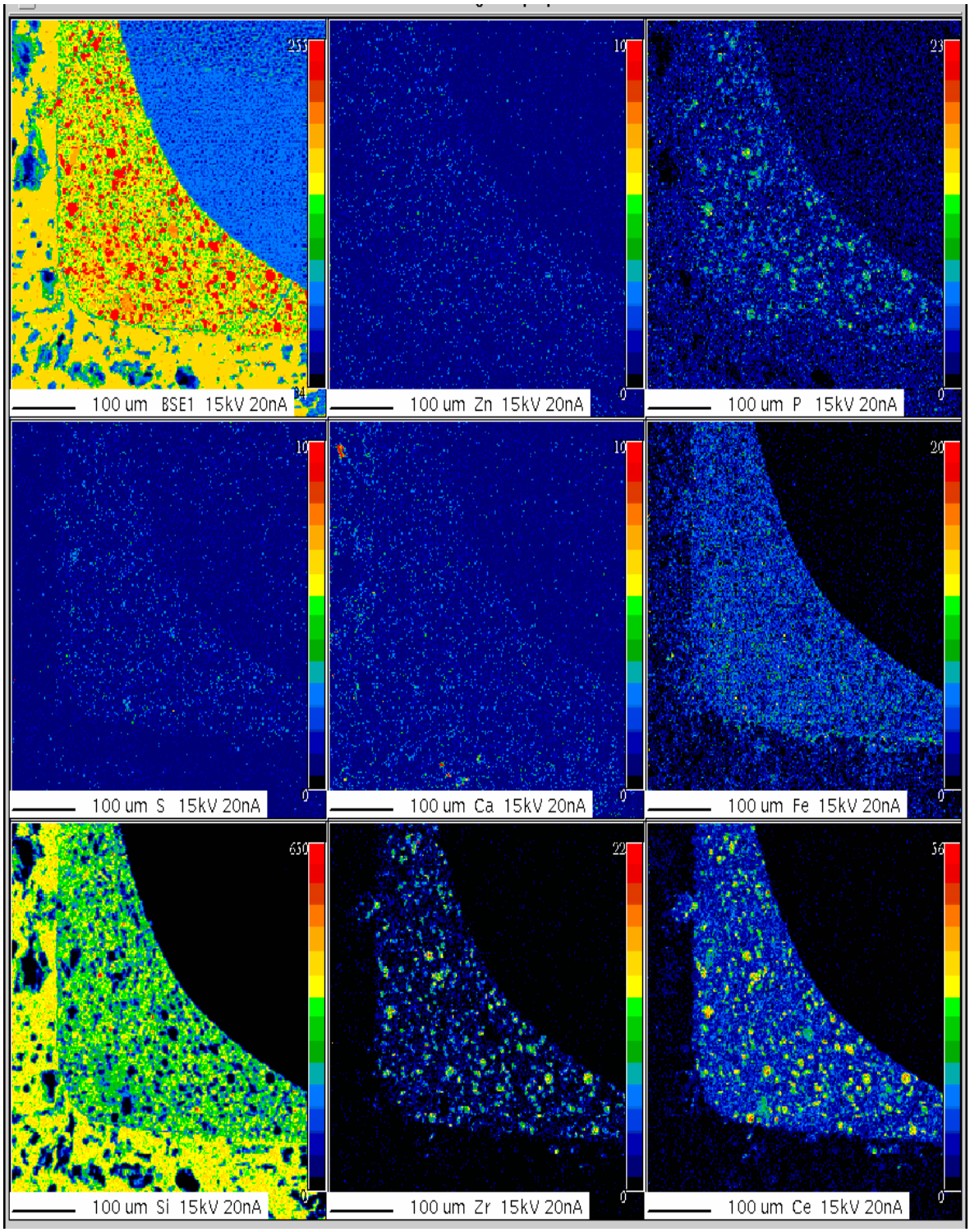

Figure 4-51. Element maps of hydrothermally-aged Fe-SCR-2 catalyst

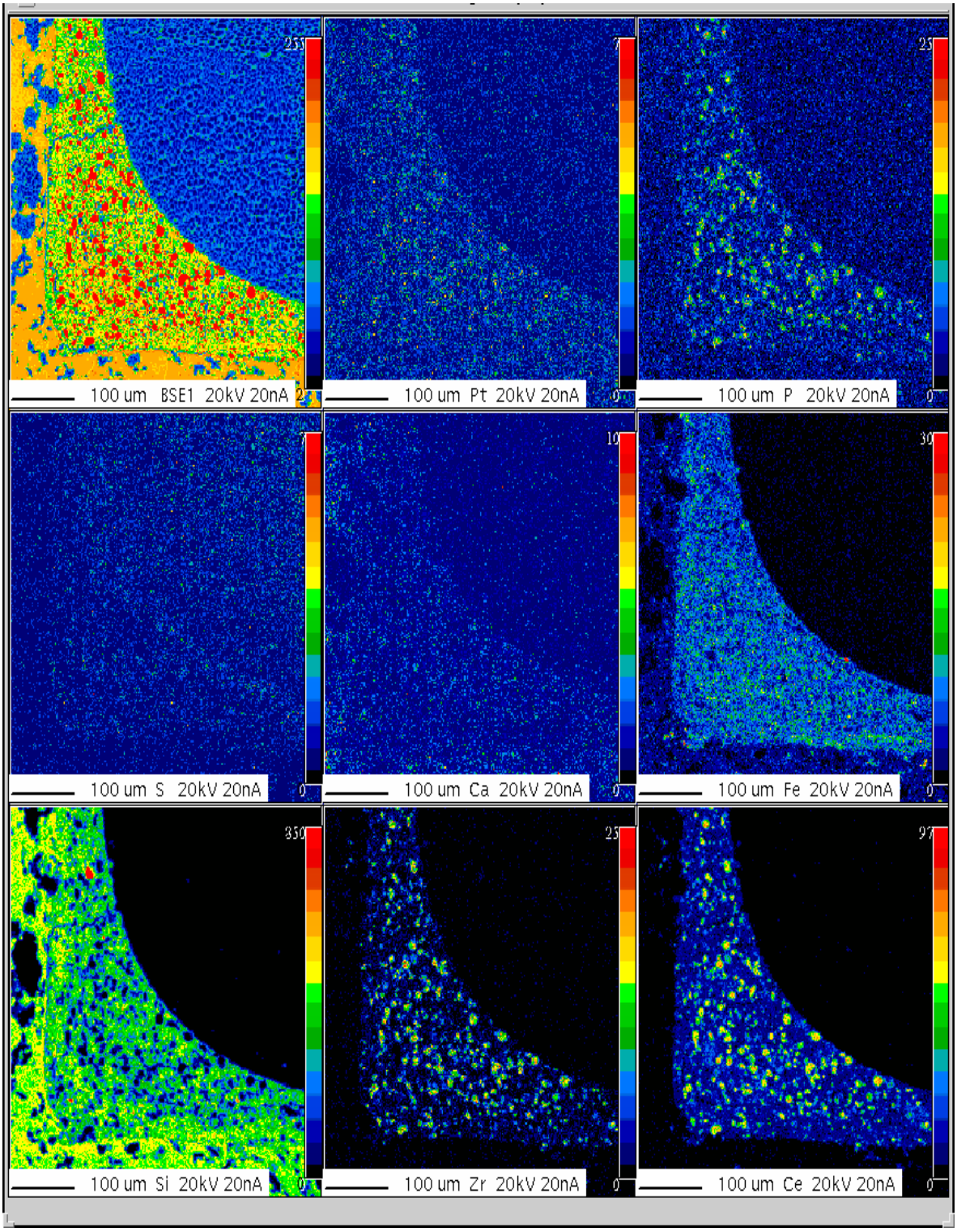

Figure 4-52. Element maps of front section of Fe-SCR-2 catalyst aged at 650°C for 31 cycles

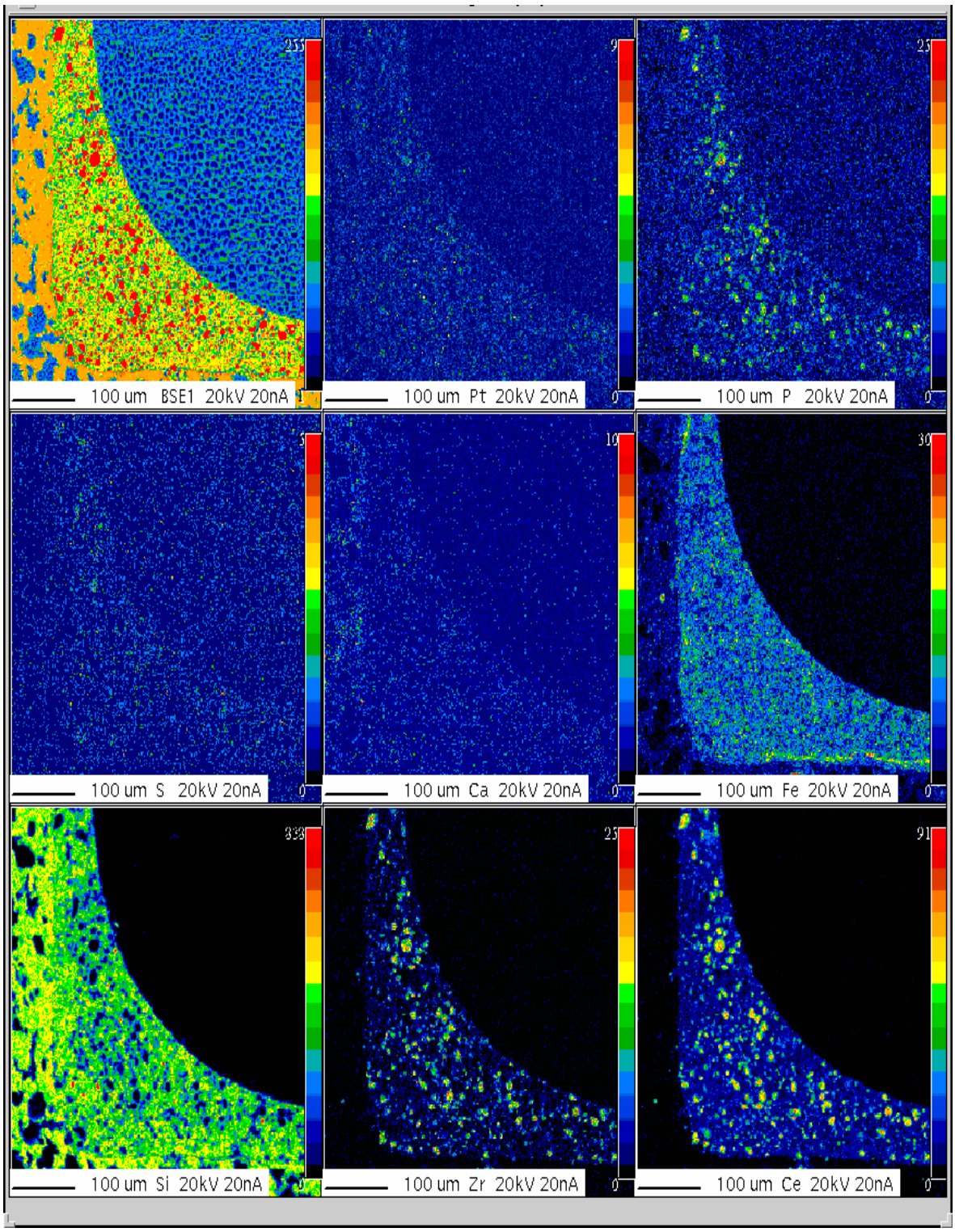

Figure 4-53. Element maps of rear section of Fe-SCR-2 catalyst aged at 650°C for 31 cycles

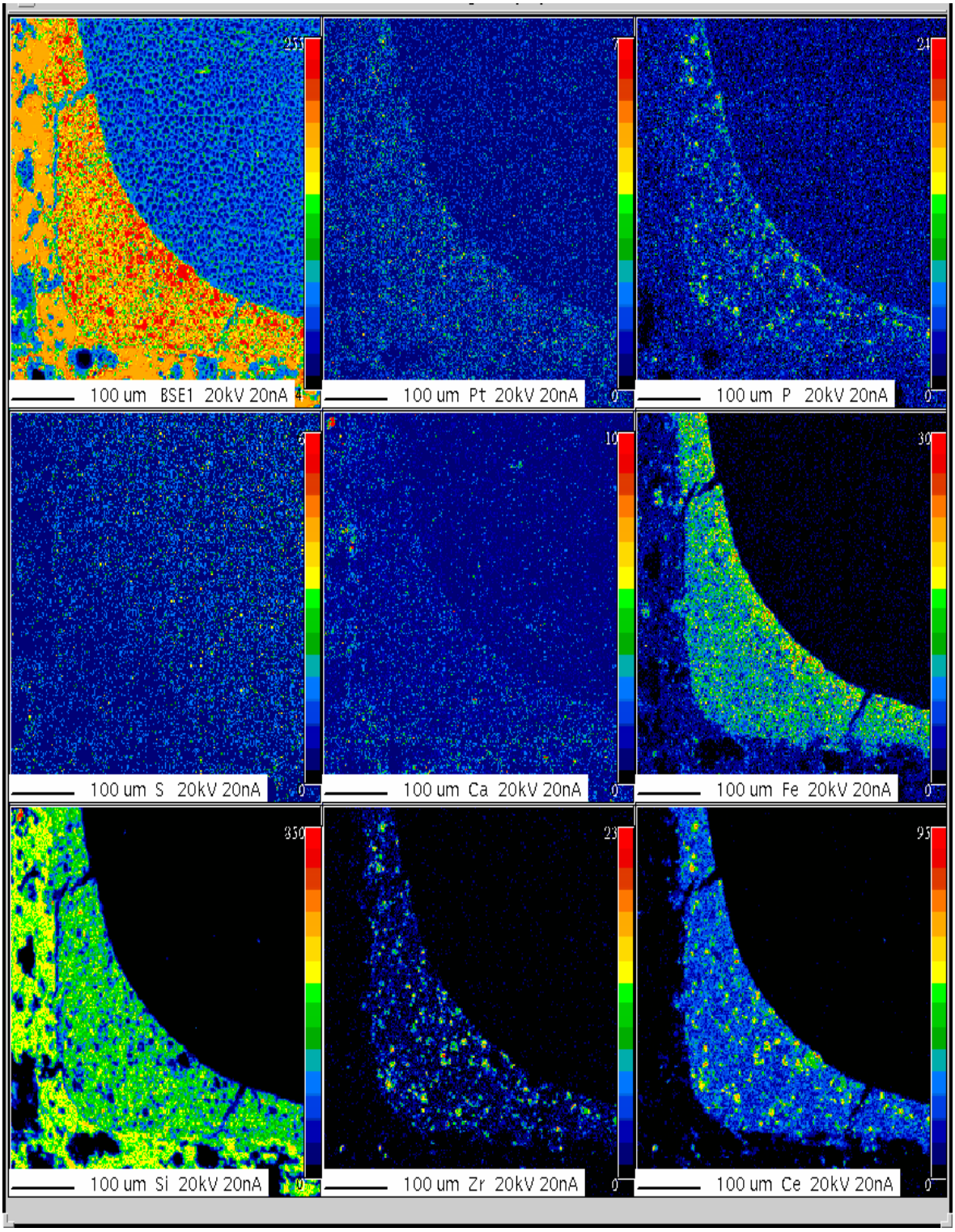

Figure 4-54. Element maps of front section of Fe-SCR-2 catalyst aged at 750°C for 50 cycles

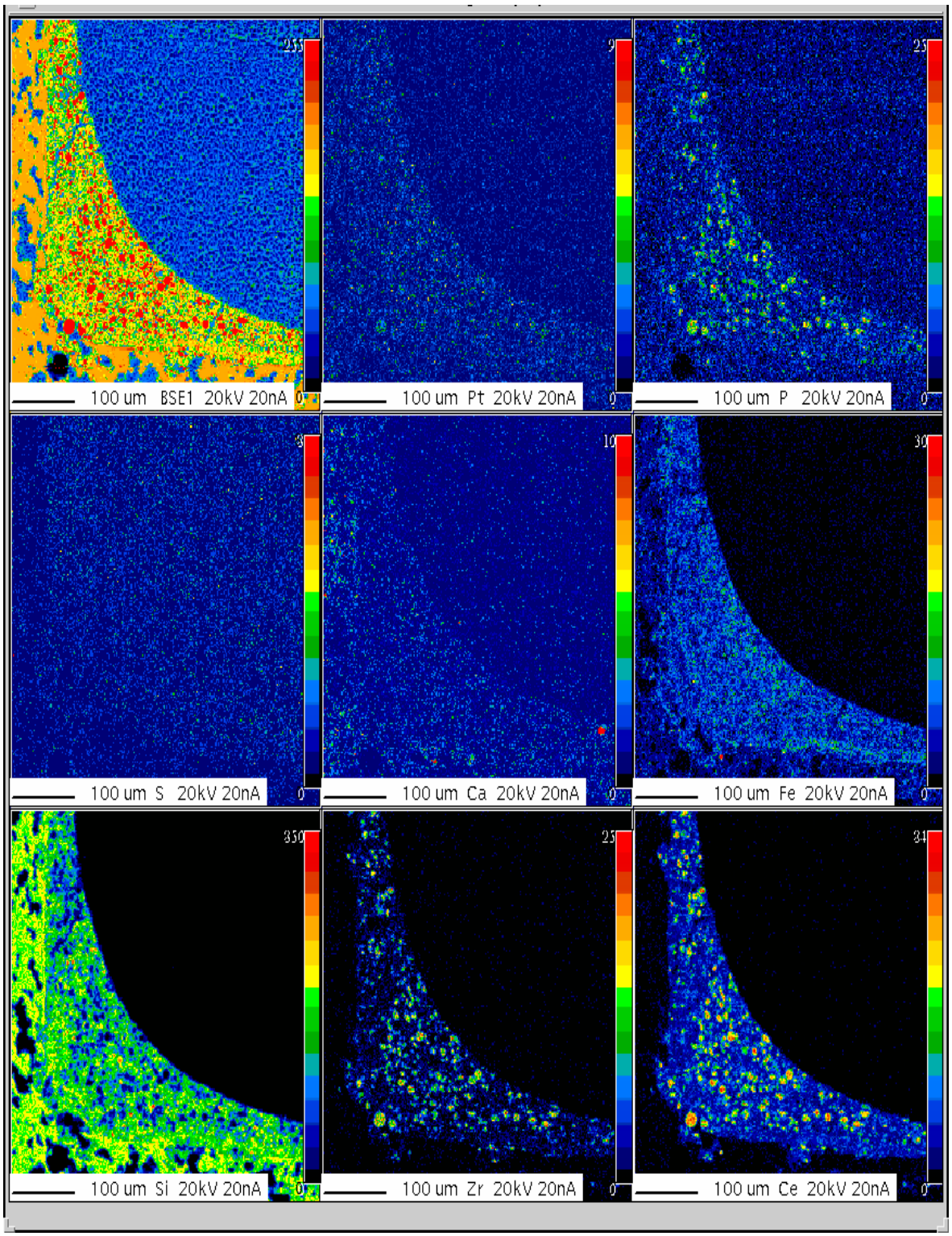

Figure 4-55. Element maps of rear section of Fe-SCR-2 catalyst aged at 750°C for 50 cycles

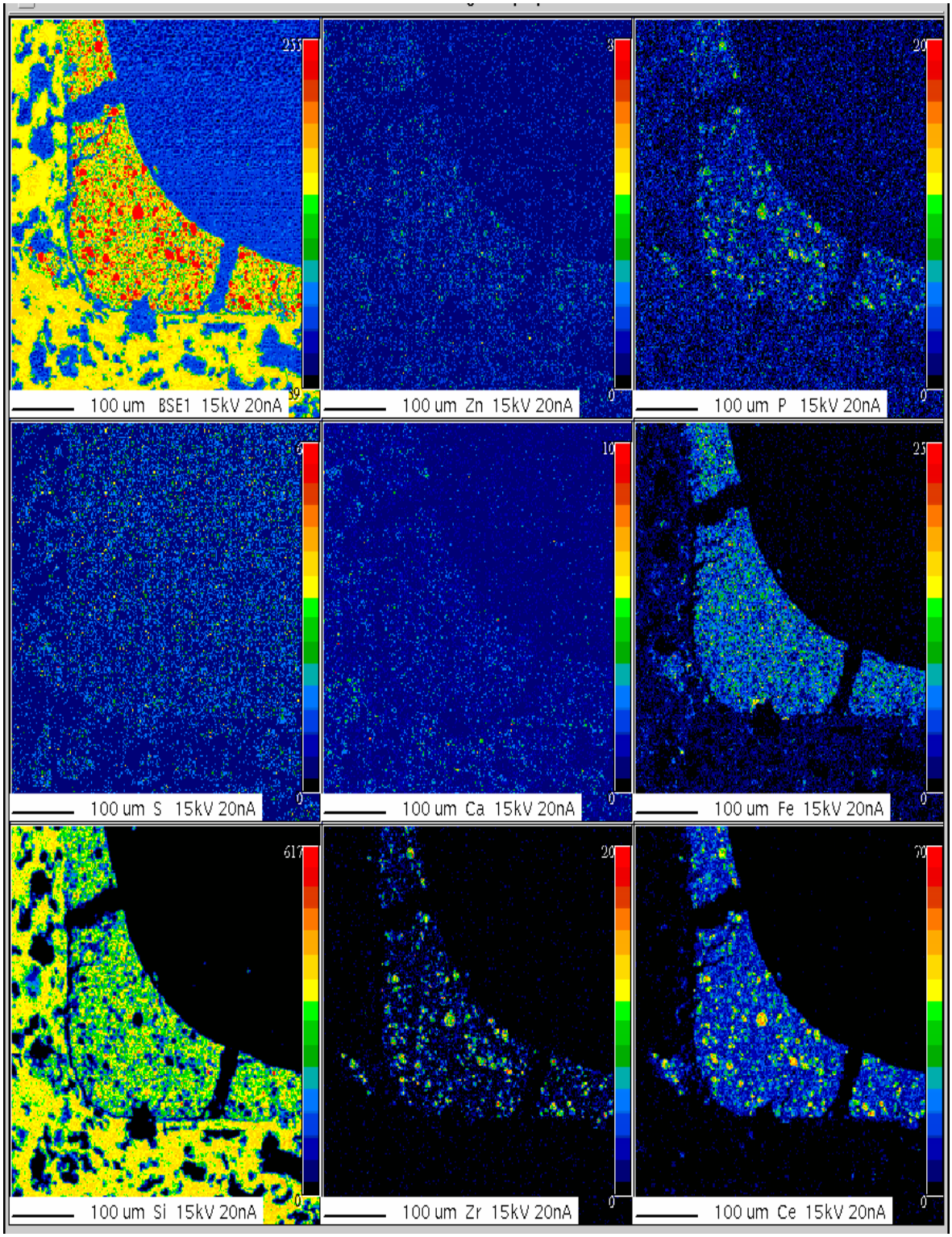

Figure 4-56. Element maps of front section of Fe-SCR-2 catalyst aged at 850°C for 13 cycles

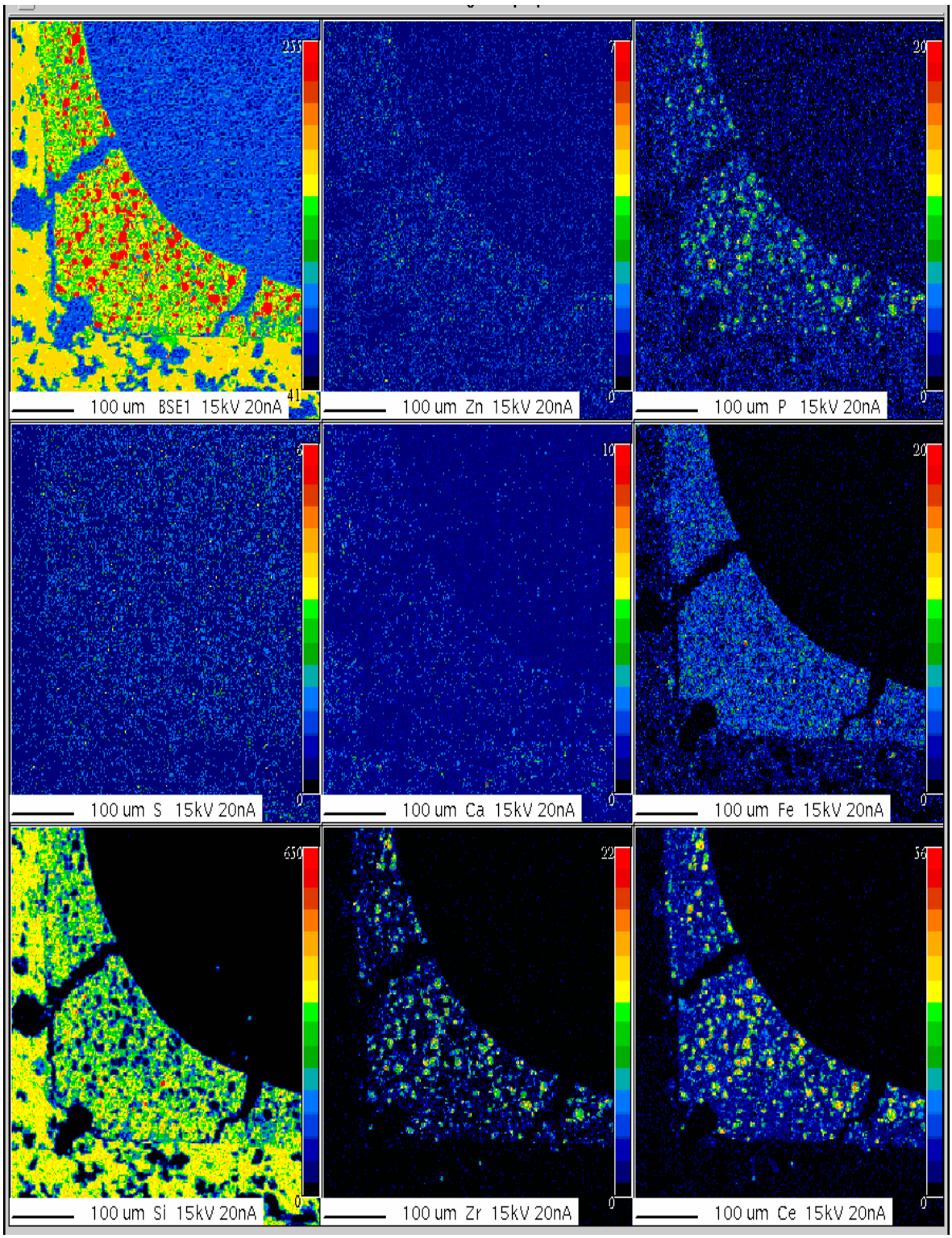

Figure 4-57. Element maps of rear section of Fe-SCR-2 catalyst aged at 850°C for 13 cycles

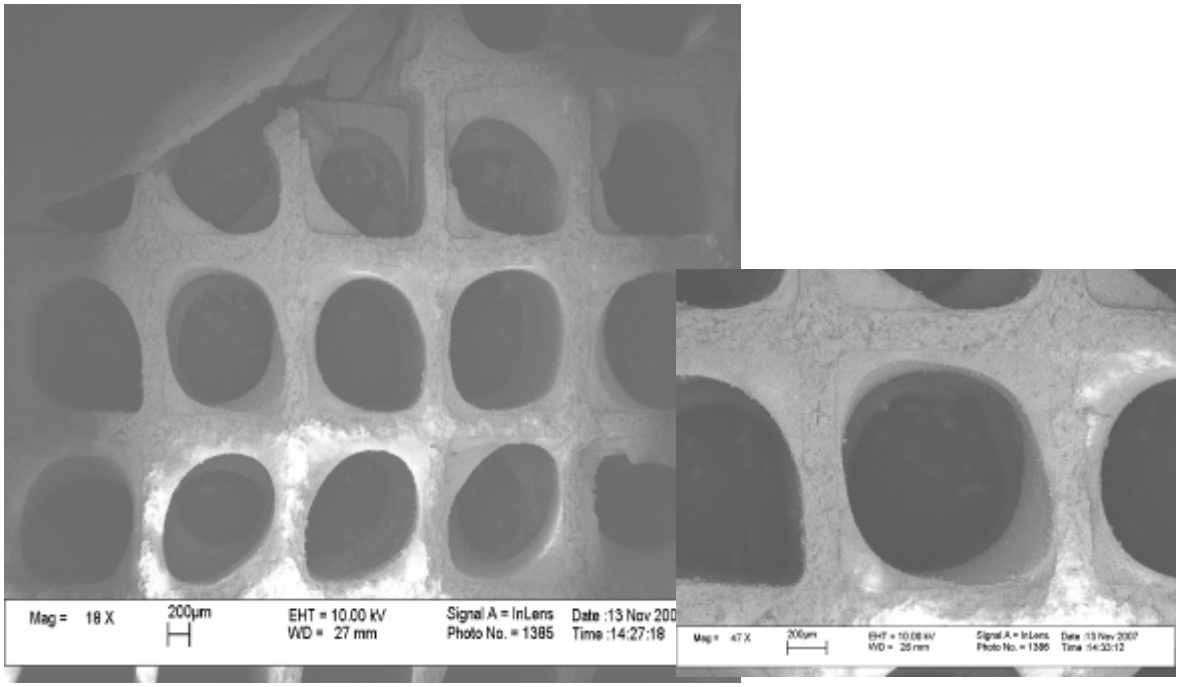

Figure 4-58. SEM micrographs of fresh Fe-SCR-2 catalyst

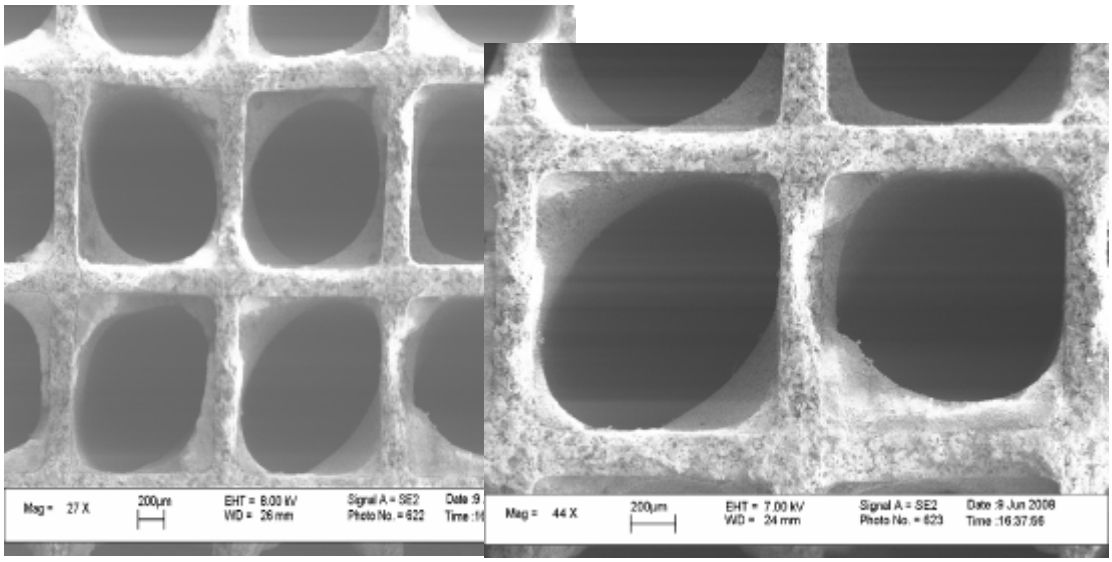

Figure 4-59. SEM micrographs of hydrothermally-aged Fe-SCR-2 catalyst

(Figure 4.57). No cracking or delamination are visible in the micrographs. There are also no visible signs of cracking and delamination in the SEM micrographs of the front and rear sections of engine-aged catalyst at 650°C shown in Figures 4.60 and 4.61. The micrographs appear to be similar to those of the fresh catalyst. All of these micrographs show variation in washcoat thickness, because these catalysts were laboratory-prepared. The micrographs of the catalyst aged at 750°C show cracking and the beginning of washcoat delamination, which can be seen in Figures 4.62 and 4.63. The damage to the washcoat is more prominent in the front section of the catalyst than the rear. Finally, the micrographs of the catalyst aged at 850°C show severe damage to the catalyst washcoat, especially in the front section of the catalyst as seen in Figures 4.64 and 4.65. Cracking and delamination of the washcoat become more visible with increasing aging temperature. Also, the effects of aging, such as cracking and delamination, are more visible in the front sections of the engine-aged catalysts. The high SCR performance of the rear sections of the engine-aged catalysts is due to the integrity of the zeolite washcoat shown in the SEM micrographs.

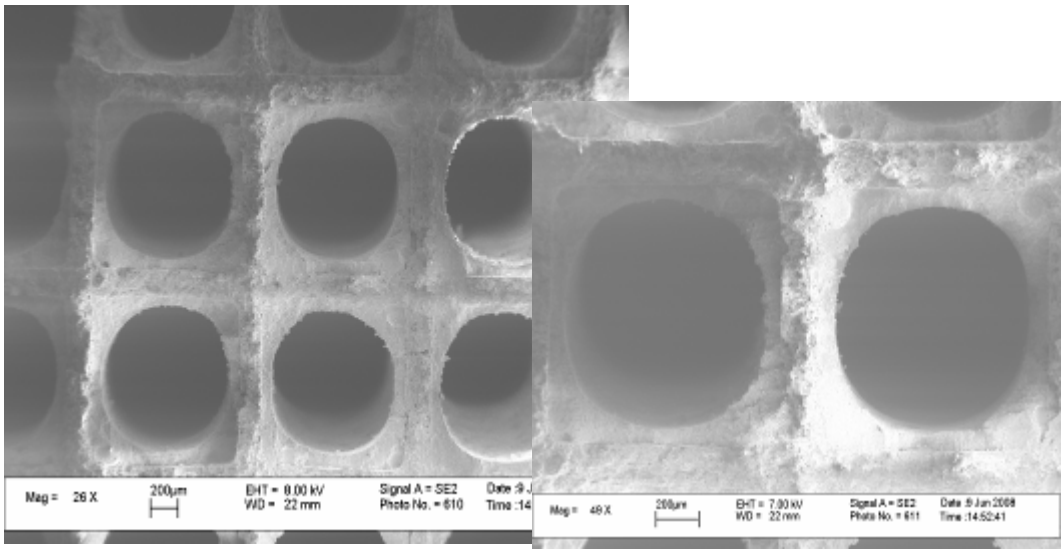

Figure 4-60. SEM micrographs of front section of Fe-SCR-2 catalyst engine-aged at 650°C for 31 cycles

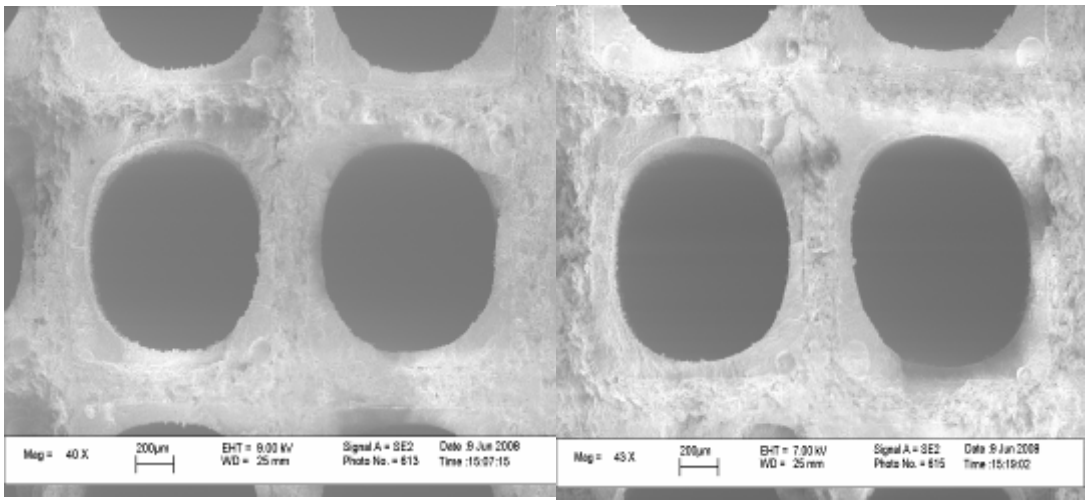

Figure 4-61. SEM micrographs of rear section of Fe-SCR-2 catalyst engine-aged at 650°C for 31 cycles

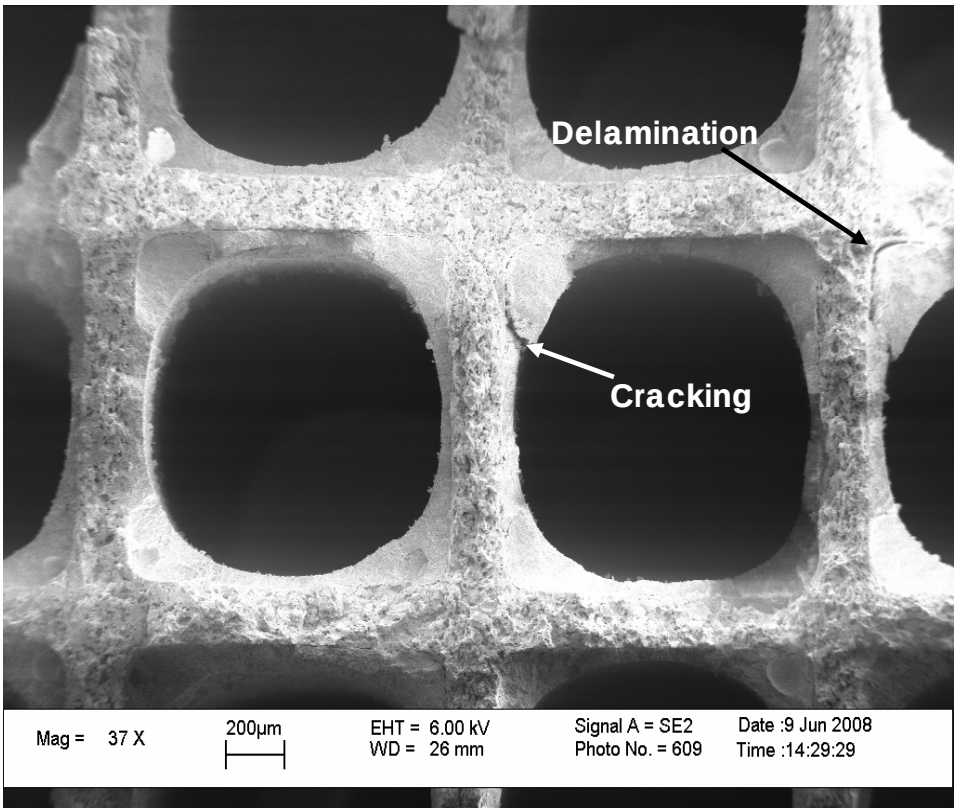

Figure 4-62. SEM micrograph of front section of Fe-SCR-2 catalyst engine-aged at 750°C for 50 cycles

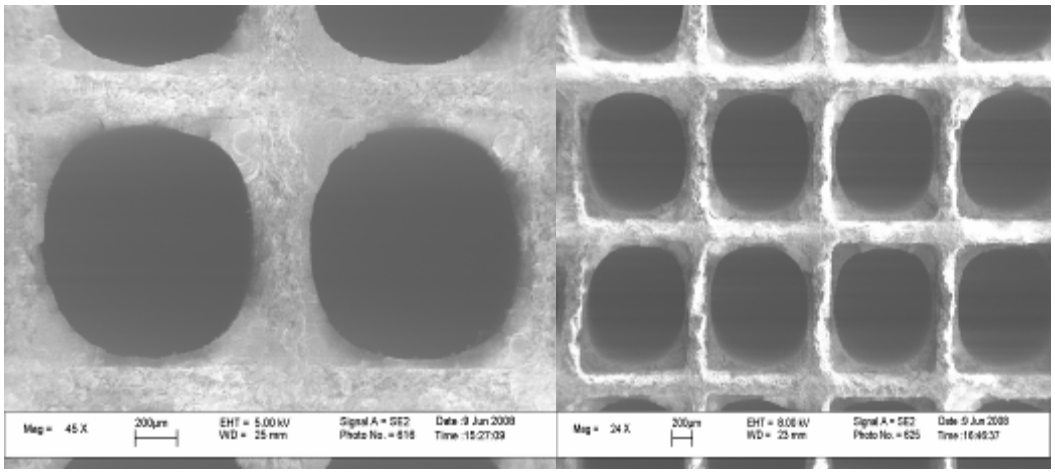

Figure 4-63. SEM micrographs of rear section of Fe-SCR-2 catalyst engine-aged at 750°C for 50 cycles

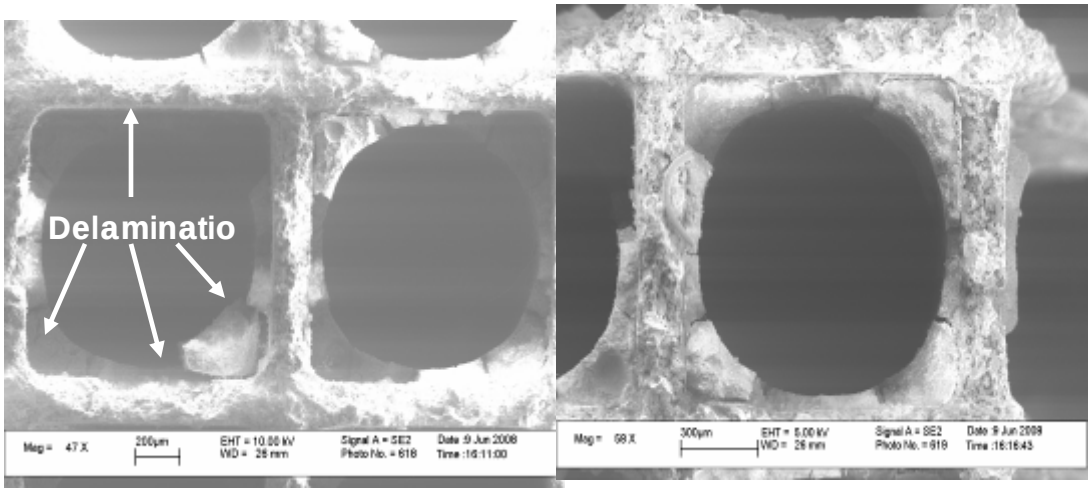

Figure 4-64. SEM micrographs of front section of Fe-SCR-2 catalyst engine-aged at 850°C for 13 cycles

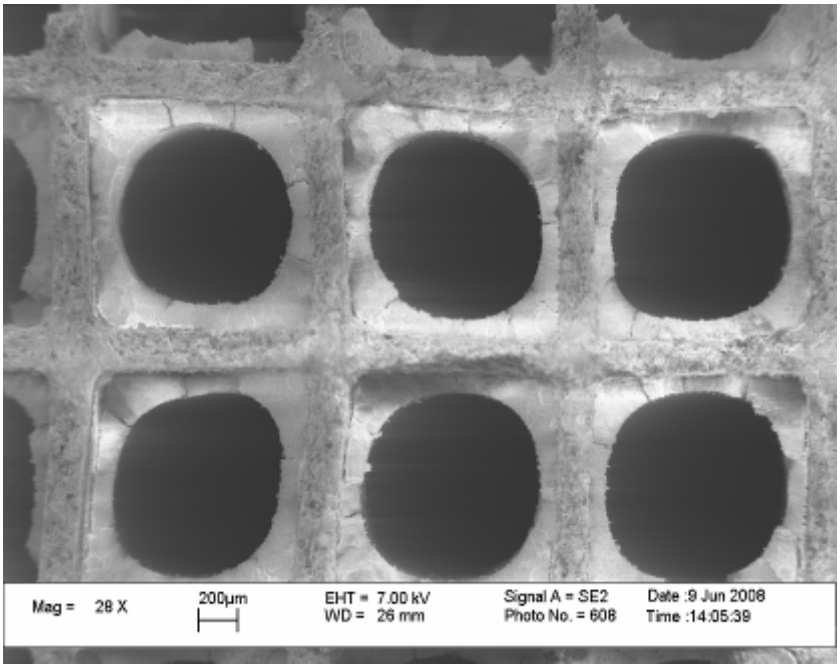

Figure 4-65.SEM picturs of rear section of Fe-SCR-2 catalyst engine-aged at 850°C for 13 cycles

BET surface area measurements presented in Figure 4.66 show a good relationship between catalyst surface area and aging temperature. SCR catalyst temperatures during enging-aging are defined in Table 5. The approximated SCR catalyst temperatures were found by adding and subtracting ¼ of the temperature difference across the SCR catalyst to the exit and inlet gas temperatures, respectively. A linear relationship between catalyst aging temperature and surface area is shown in Figure 4.67. The linear relationship has a correlation coefficient of 0.957. Catalyst surface area decreases with increasing aging temperature. The catalyst aged at 650°C shows surface areas of 60 m^2/g and 59 m^2/g in the front and rear sections, respectively, which is as high as that of the fresh catalyst. Aging at 650°C for 31 cycles appears to have no great effect on the Fe-SCR-2 catalyst, however, there is a small drop in activity (≈10%) measured during BFR evaluation at 400, 450 and 500°C in the rear section of this catalyst and a significant drop in NO_x conversion for the front section. Judging by the decrease of 10 m^2/g seen in the rear section of the catalyst aged at 750°C, it is expected to see a small drop in activity which is confirmed byBFR evaluation. The large decrease in surface area in the rear section of the catalyst aged at850°C indicates zeolite dealumination, and it is expected to see a decrease in SCR activity, which is also confirmed by BFR evaluation.

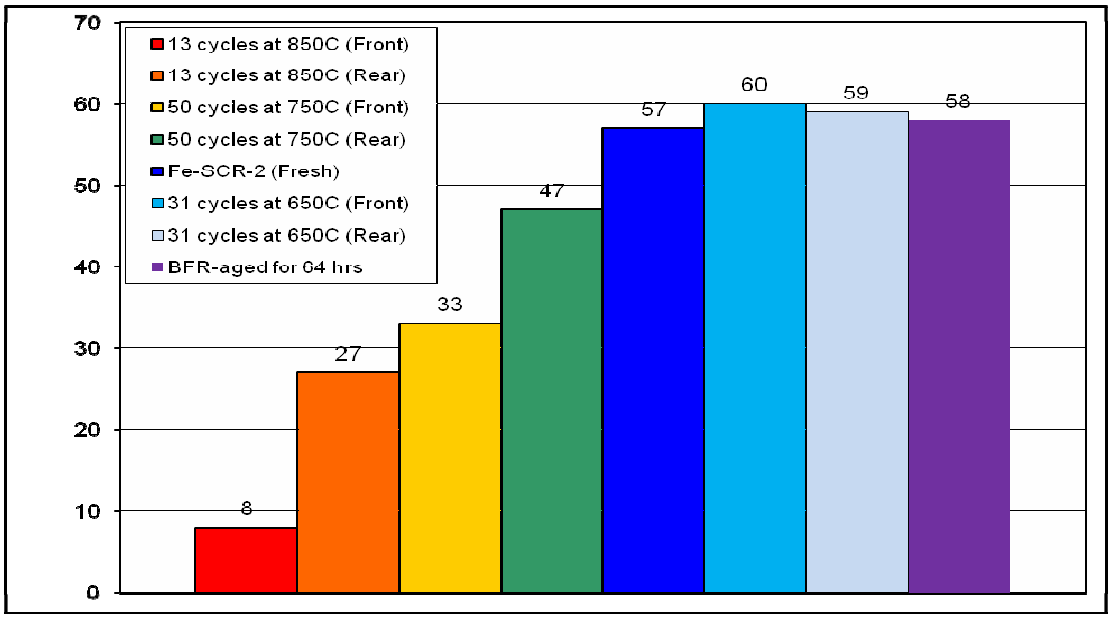

Figure 4-66. BET surface area measurements of fresh and accelerated thermally aged Fe-SCR-2 catalyst

Table 5. SCR catalyst temperatures during accelerated thermal aging on engine bench

	Catalyst Temp C	
Aging Temp C	Front	Rear
650	625	575
750	728	683
850	838	813

The general concensus is that deactivation of Fe-zeolite SCR catalysts is directly related to zeolite dealumination [31-33]. Dealumination leads to reduced acidity of the zeolite, i.e., a loss of Brønsted acid sites and a collapse of the zeolite structure. With the collapse of the zeolite structure, active cations are lost due to the formation of Fe_2O_3 as well as an irreversible reduction of catalyst surface area. The formation of Fe_2O_3 and Al_2O_3 is found in the present study as evidenced in the XRD patterns of the aged Fe-zeolite SCR catalysts, including those aged at low temperatures (650 and 670°C). This indicates that aged catalysts experienced dealumination and a reduction of active iron cations, culminating in a decrease in NO oxidation activity as obtained using the BFR (see Figure 4.43). However, some of the aged catalysts still show good activity for the SCR of NO_X (hydrothermally-aged and rear sections of the engine-aged catalysts at 650 and 750°C). The rear sections of the catalysts engine-aged at 650 and 750°C show NO_x conversions similar to that of a fresh catalyst between evaluation temperatures of 400 and 500°C. Therefore, while the formation of Fe_2O_3 and Al_2O_3 is a good indication of catalyst dealumination, it may not be useful in quantifying the extent of catalyst deactivation. Nevertheless, there is a strong relationship between NO_x performance and catalyst surface area of the rear sections of the engine-aged catalysts as seen in Figure 4.68; as catalyst surface area decreases, so does SCR activity. Figure 4.69 shows a relationship between NO_x conversions of the front sections of the engine-aged catalysts and catalyst surface area. The relationship seen with the rear sections of the engine-aged catalysts is not as strong with the front sections.

It is interesting to see a large amount of deactivation in the front sections of the catalysts aged at 650 and 750°C; while materials characterization and surface studies show little changes

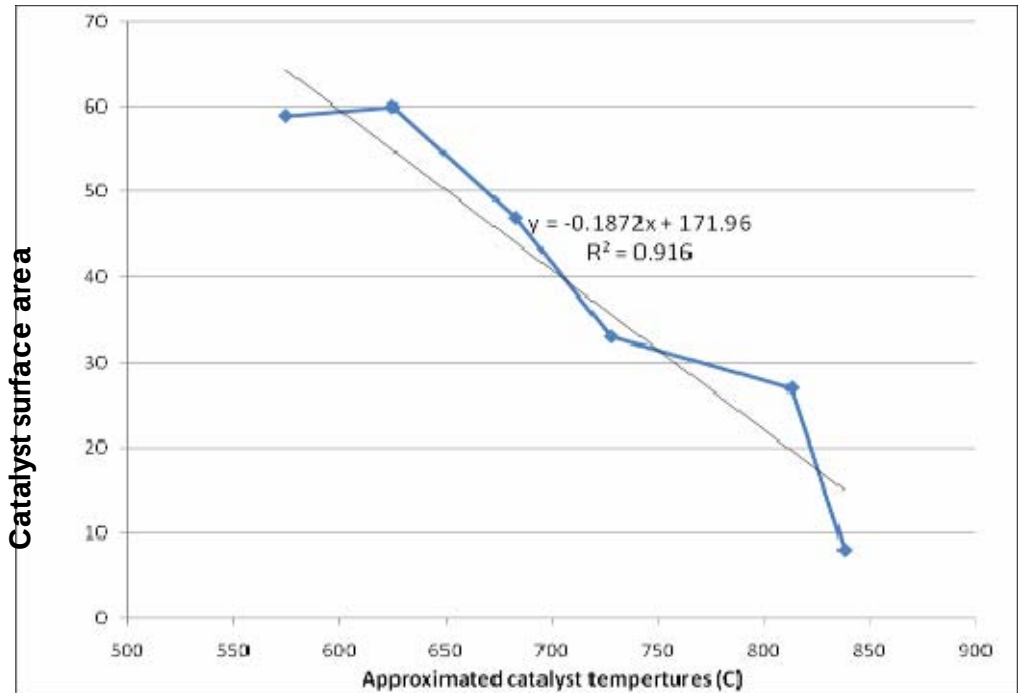

Figure 4-67. Surface area of engine-aged catalysts as a function of catalyst aging temperature

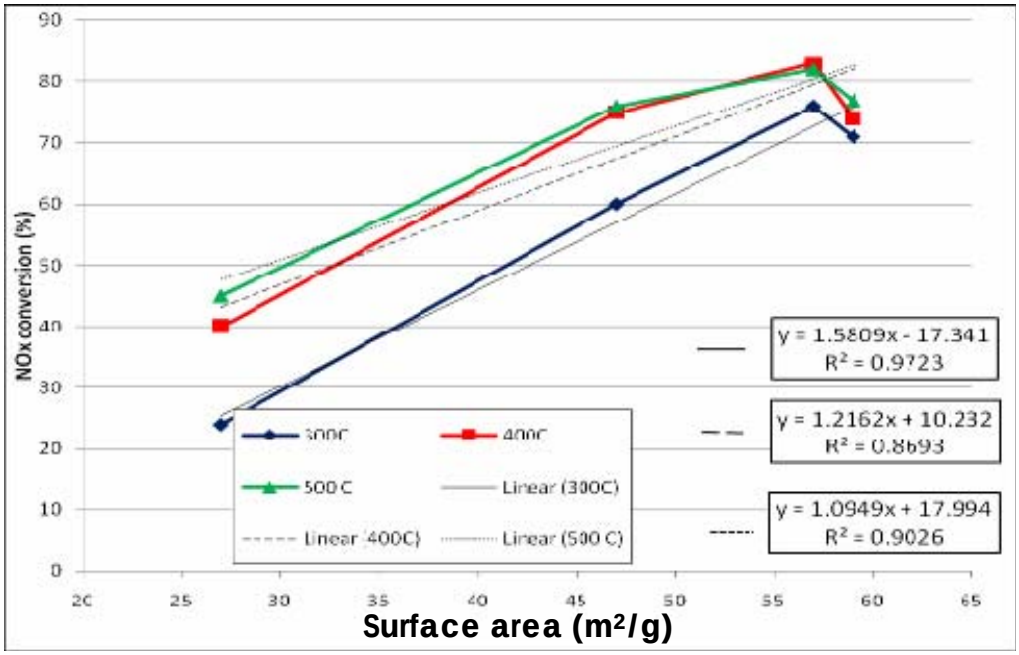

Figure 4-68. NOx conversion of rear sections of engine-aged catalysts with 350 ppm NO as a function of catalyst surface area

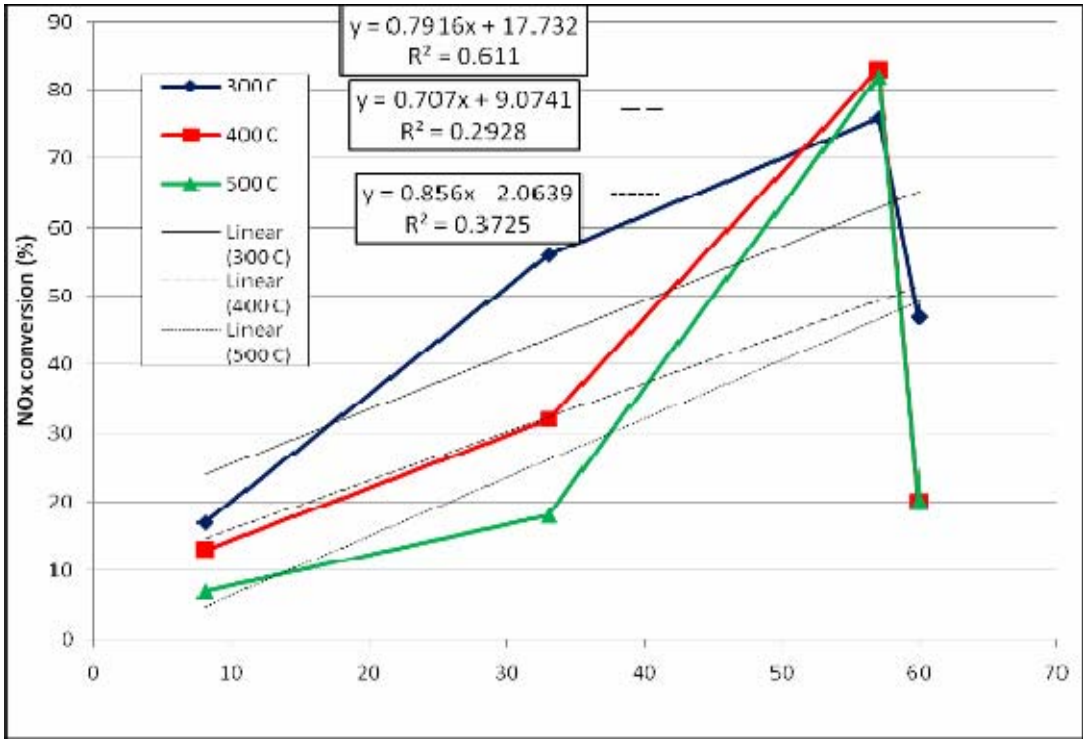

Figure 4-69. NOx conversion of front sections of engine-aged catalysts with 350 ppm NO as a function of catalyst surface area

in these catalyst samples, BFR evaluation reveals severe degradation in NO_x performance. The linear correlations in Figure 4.69 show that there is not a relationship between NO_x performance of these catalyst sections and catalyst surface area. Consequently, the severe reduction in NO_x performance in the front section of engine-aged catalysts may be due to contaminations from the DOC, poisoning from lube-oil derived species and soot deposits.

4.3 Comparison of field-aged and engine-aged Fe-zeolite catalysts

A comparison is made between the NO_x performance of the field-aged and engine-aged catalysts to assess the validity of the implemented accelerated thermal aging protocol in replicating the aging conditions observed in the field-aged catalyst. Figure 4.70 is a comparison in NO_x performance of front and rear sections of field-aged and engine-aged catalysts—the engine-aged catalyst is aged at 650°C for 31 cycles. The front and rear sections of the two

catalysts show similar trends in NO_x conversion at evaluation temperatures of 400, 450 and 600°C. However at an evaluation temperature of 300°C, the engine-aged catalyst exhibits significantly higher NO_x conversion in both sections, i.e., 48% to 30% for the front and 71% to 50% for the rear.

Figure 4.71 is a comparison in NO_x conversion of the front and rear sections of the catalyst engine-aged at 750°C for 50 cycles and those of the field-aged catalyst. The rear sections of the two catalysts show similar NO_x performance with a difference in maximum NO_x conversion of only 3%; i.e., 79% for the field-aged and 76% for engine-aged. In addition the difference in NO_x conversion at an evaluation temperature of 300°C is only 10%, which is much less than the difference obtained with the catalyst engine-aged at 650°C for 31 cycles (Figure 4.70). The front sections of both catalysts show severe degradation in NO_x performance over the entire temperature range for evaluation.

Figure 4.72 shows the NO_x performance of the field-aged catalyst and the catalyst engine-aged at 850°C for 13 cycles. The NO_x performances of these two catalysts do not compare very well. The NO_x performance of both sections of the engine-aged catalyst is significantly lower

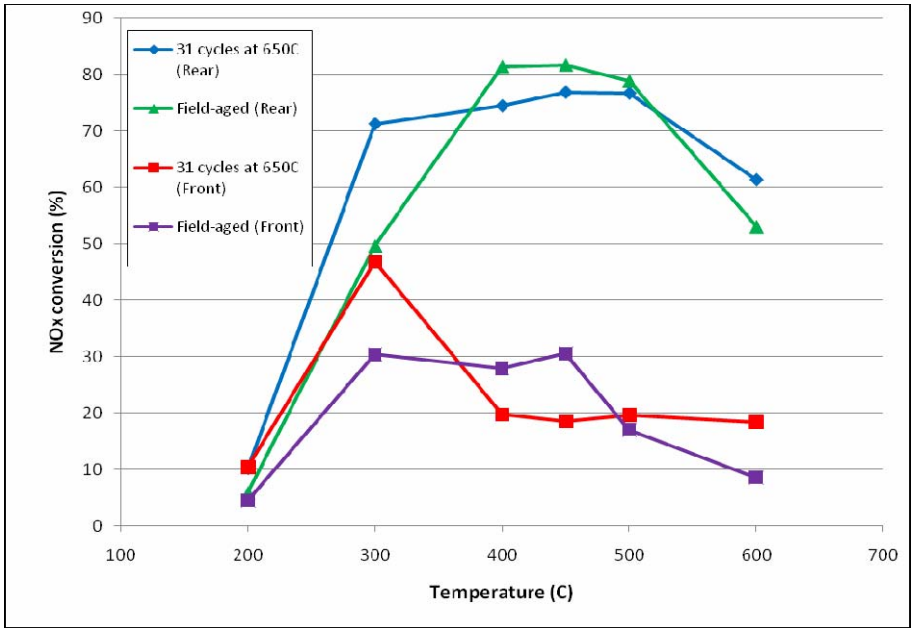

Figure 4-70. NOx conversion of field-aged and engine-aged Fe-SCR-2 catalyst aged at 650°C for 31 cycles; evaluated with 5% CO_2, 5% H_2O, 14% O_2, 350 ppm NO, 350 ppm NH_3 (α = 1.0), N_2 balance, GHSV = 30,000 h^{-1}

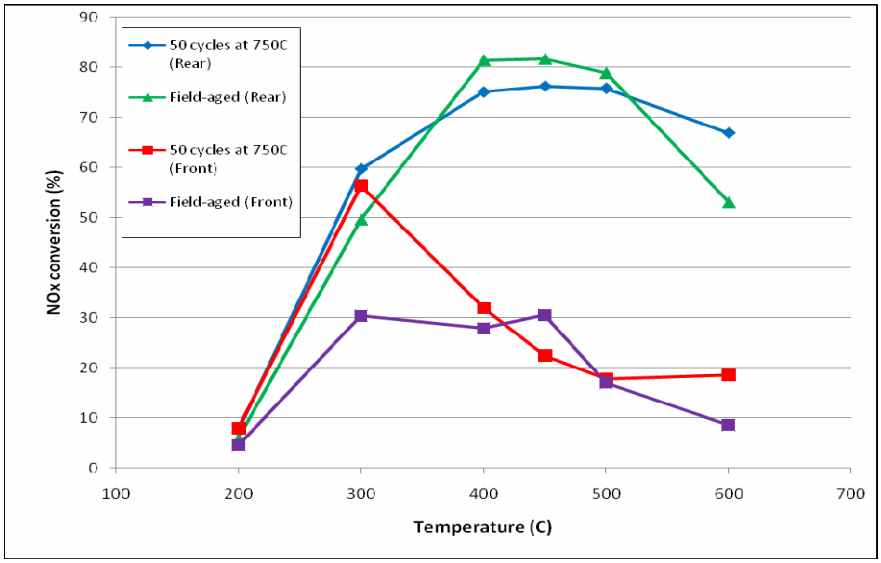

Figure 4-71. NOx conversion of field-aged and engine-aged Fe-SCR-2 catalyst aged at 750°C for 50 cycles; evaluated with 5% CO_2, 5% H_2O, 14% O_2, 350 ppm NO, 350 ppm NH_3 (α = 1.0), N_2 balance, GHSV = 30,000 h^{-1}

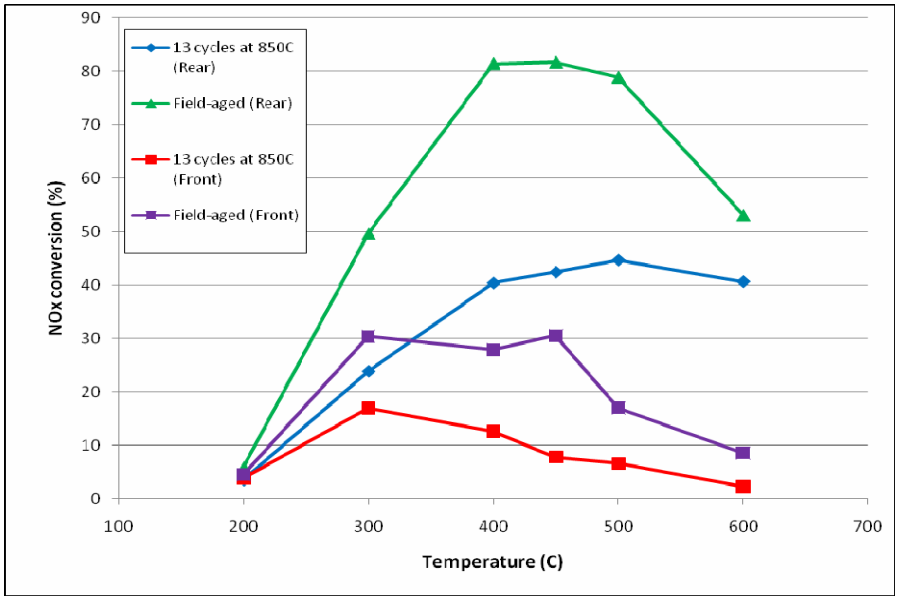

Figure 4-72. NOx conversion of field-aged and engine-aged Fe-SCR-2 catalyst aged at 850°C for 13 cycles; evaluated with 5% CO_2, 5% H_2O, 14% O_2, 350 ppm NO, 350 ppm NH_3 (α = 1.0), N_2 balance, GHSV = 30,000 h^{-1}

than that of field-aged catalyst. The maximum NO_x conversion over the front and rear sections of the engine-aged catalyst are 17% and 45%, respectively.

It is apparent that the NO_x performance of the catalyst engine-aged at 750°C for 50 cycles agrees quite well with that of the field-aged catalyst. Because engine-aging is performed at elevated temperatures to accelerate the aging process, the field-aged catalyst probably experienced more DPF regenerations at slightly lower SCR catalyst temperatures (≈600 to 700°C). The agreement in the NO_x performance of both catalysts is further substantiated in Figure 4.73 when an equimolar amount of NO and NO_2 is used in the evaluation gases. Both the front and rear sections of the two catalysts show very similar NO_x conversion at all evaluation temperatures, except at 600°C where the field-aged catalyst shows more severe deactivation.

Figures 4.74 to 4.81 are the SEM micrographs of the engine-aged and the field-aged catalysts. The superior NO_x performance of the catalyst engine-aged at 650°C would indicate that the washcoat is less degraded than that of the field-aged catalyst. As expected, the micrographs in Figures 4.75 and 4.79 show that the washcoat of the catalyst engine-aged at 650°C resembles that of a fresh catalyst.

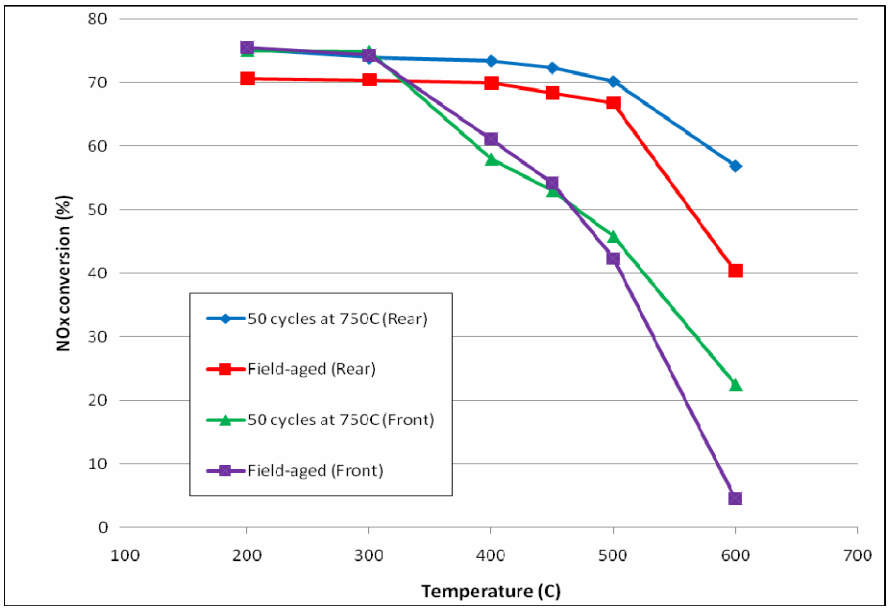

Figure 4-73. NOx conversion of field-aged and engine-aged Fe-SCR catalyst aged at 750°C

for 50 cycles; evaluated with 5% CO_2, 5% H_2O, 14% O_2, 175 ppm NO, 175 ppm NO_2, 350 ppm NH_3 (α = 1.0), N_2 balance, GHSV = 30,000 h^{-1}

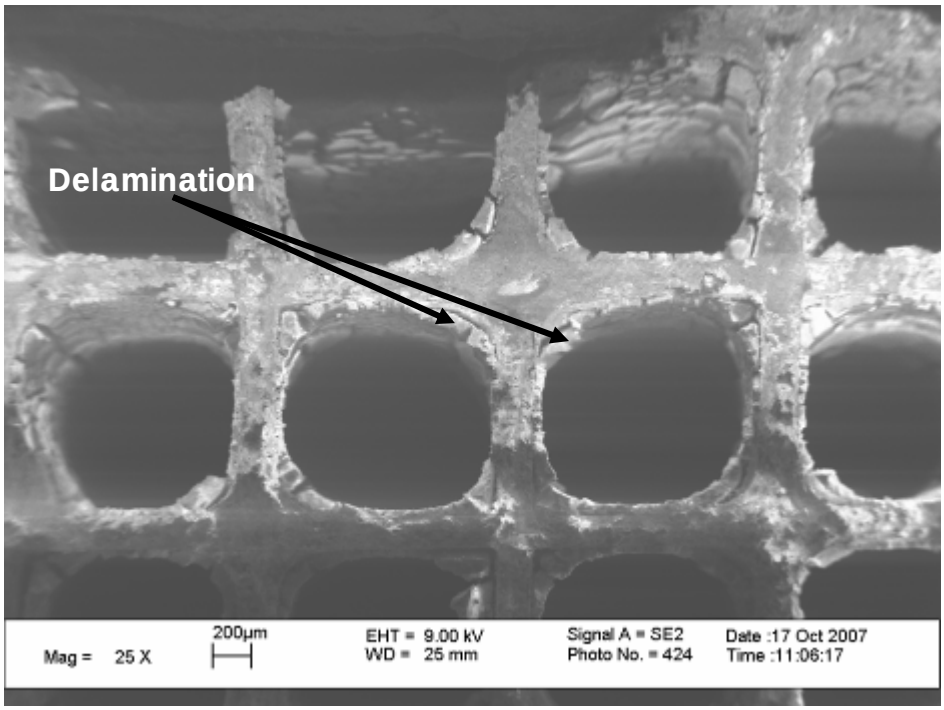

Figure 4-74. SEM micrograph of front section of field-aged Fe-SCR-1 catalyst

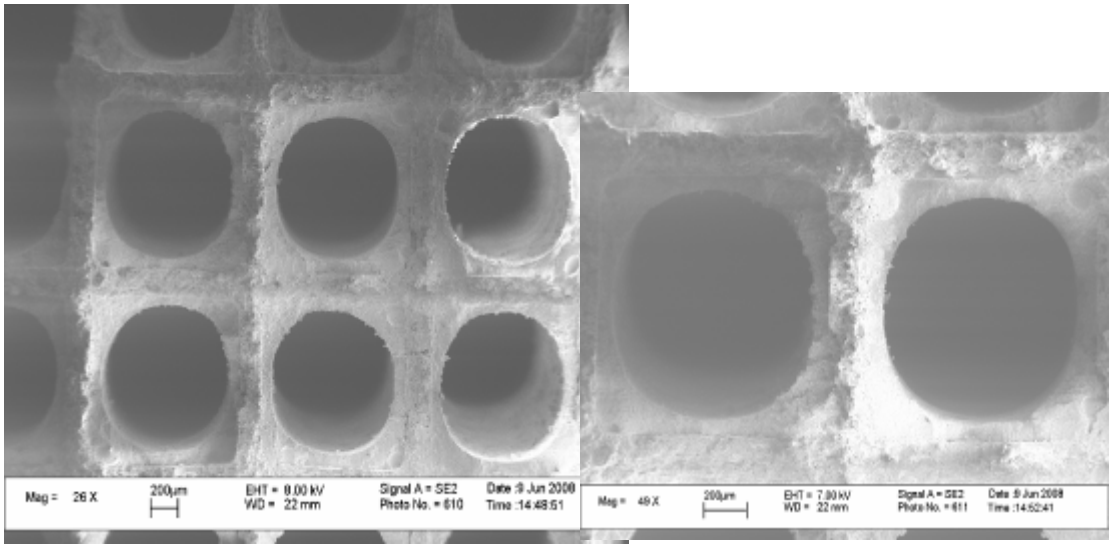

Figure 4-75. SEM micrographs of front section of engine-aged Fe-SCR-2 catalyst aged at 650°C for 31 cycles

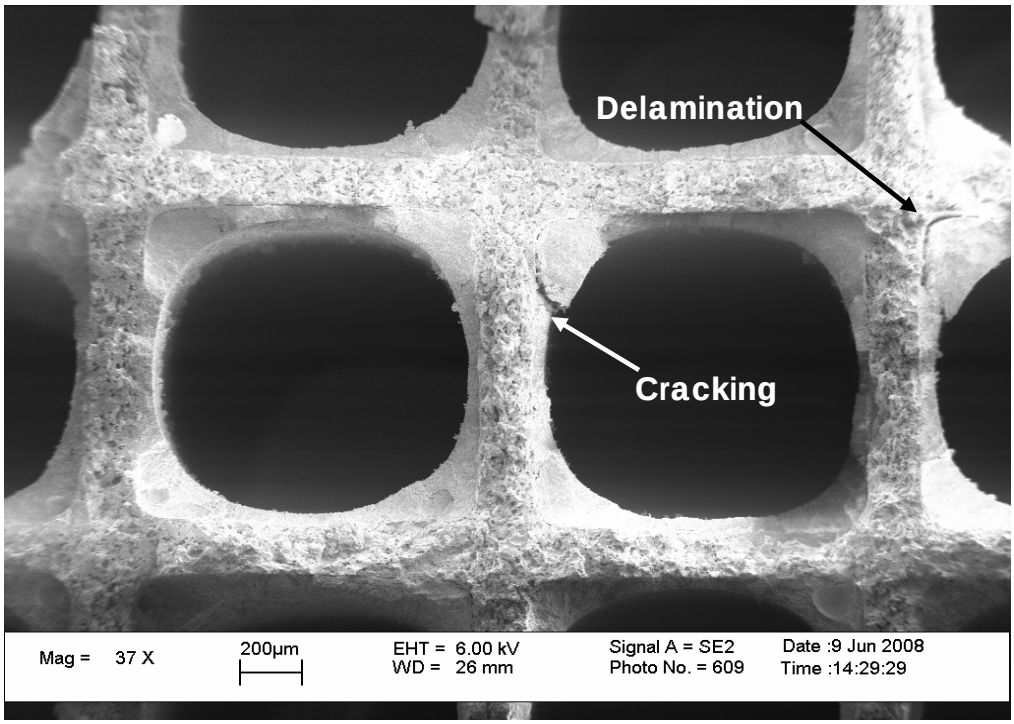

Figure 4-76. SEM micrograph of front section of engine-aged Fe-SCR-2 catalyst aged at 750°C for 50 cycles

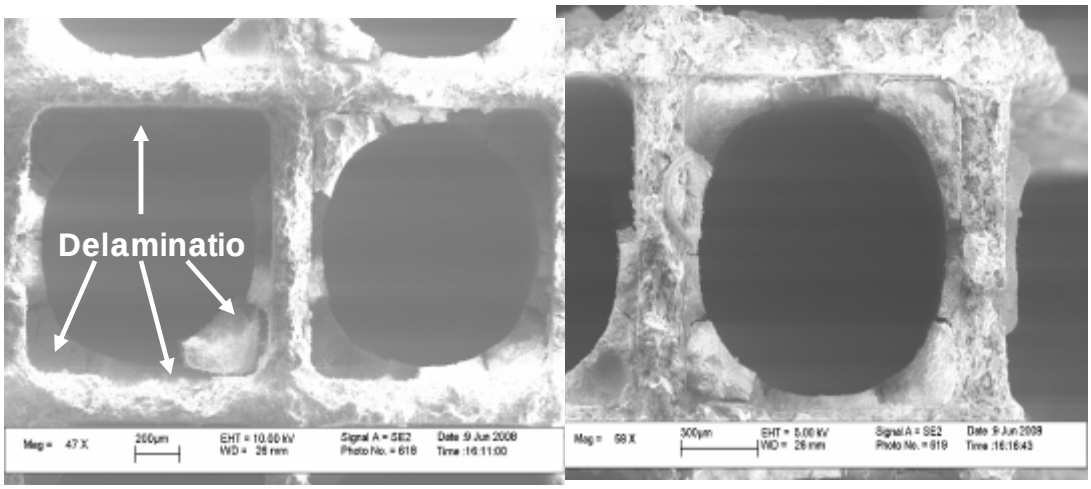

Figure 4-77. SEM micrographs of front section of engine-aged Fe-SCR-2 catalyst aged at 850°C for 13 cycles

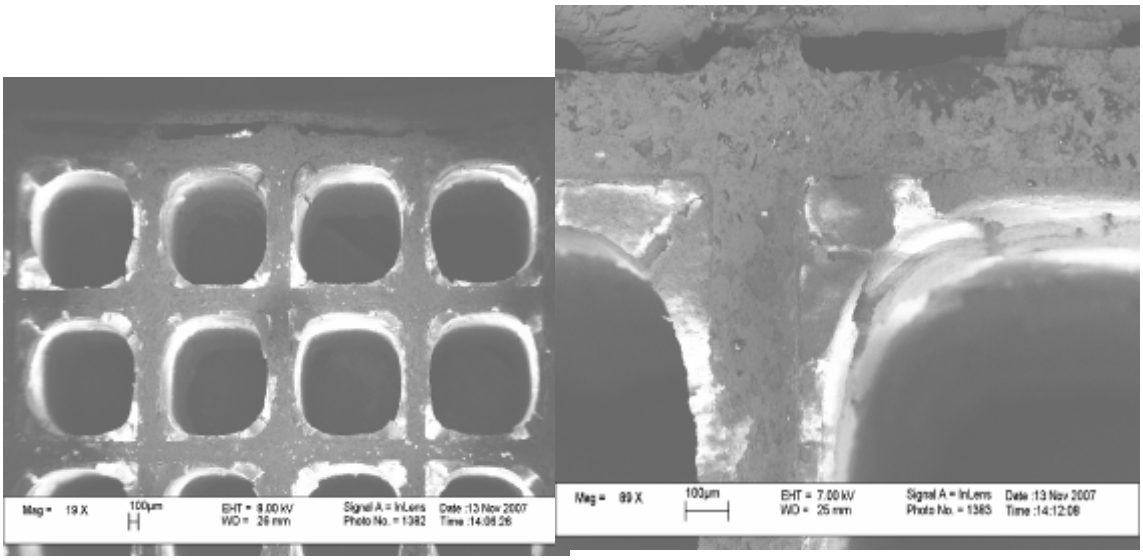

Figure 4-78. SEM micrographs of rear section of field-aged Fe-SCR-1

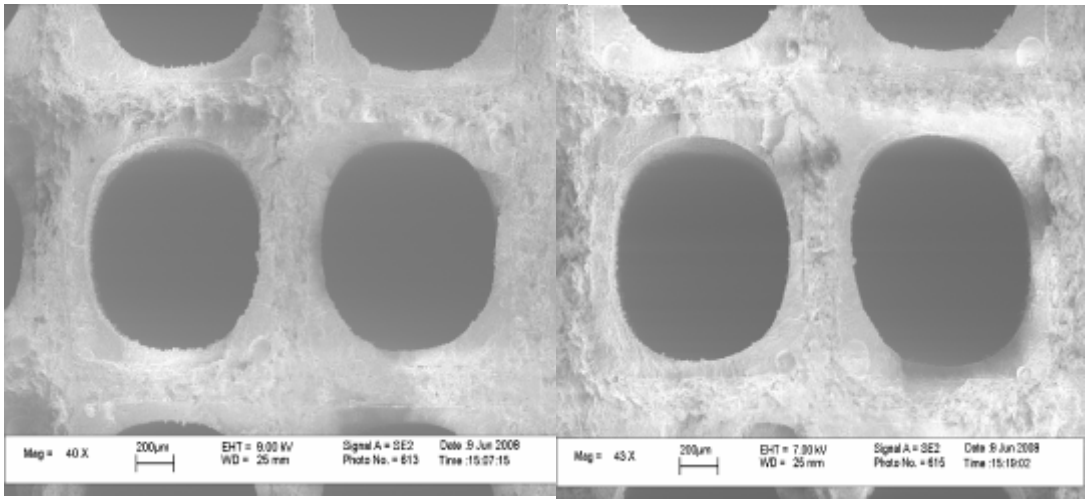

Figure 4-79. SEM micrographs of rear section of engine-aged Fe-SCR-2 catalyst aged at 650°C for 31 cycles

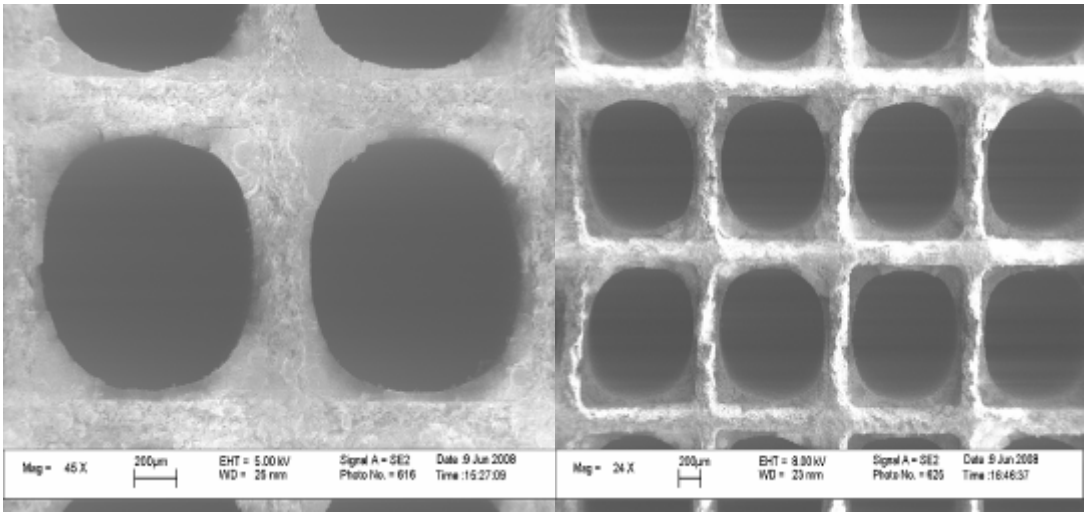

Figure 4-80. SEM micrographs of rear section of engine-aged Fe-SCR-2 catalyst aged at 750°C for 50 cycles

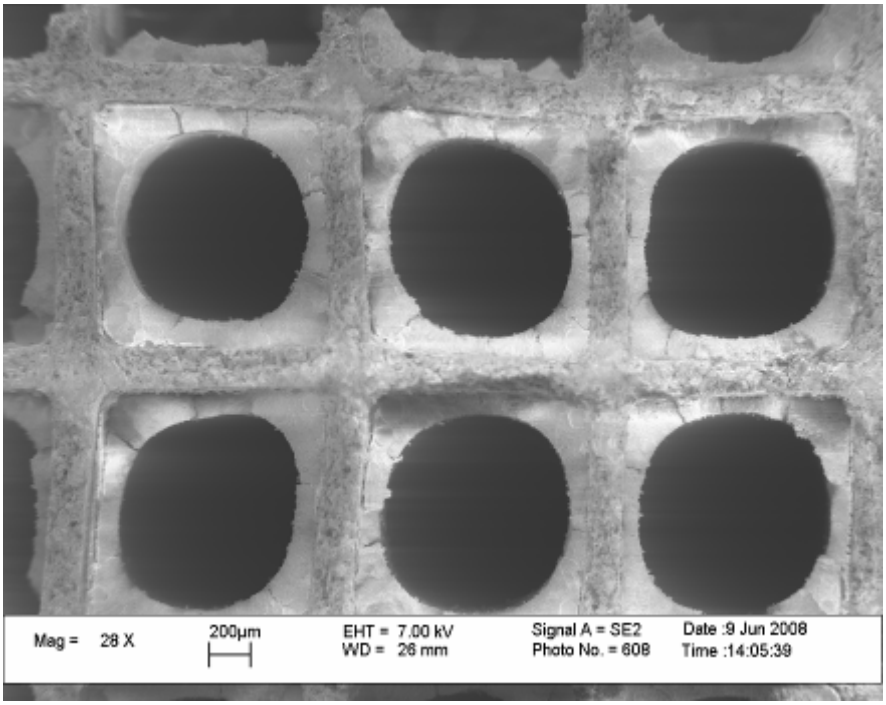

Figure 4-81 SEM picturs of rear section of engine-aged Fe-SCR-2 catalyst aged at 850°C for 13 cycles

aged catalyst has suffered more severe degradation. Conversely, the micrographs of the catalyst engine-aged at 850°C compare very well with the micrographs of the field-aged catalyst. Severe cracking and delamination are seen in the front sections of both catalysts. Plus, the severe cracking observed in the rear section of the field-aged catalyst is also observed in the rear section of the catalyst engine-aged at 850°C. Table 6 shows percent reduction of catalyst surface area for the front and rear sections of the engine-aged catalysts at different aging temperatures and aging cycles, as well as that of the field-aged catalyst. The table shows that the SEM micrographs are somewhat misleading. Percent reduction of catalyst surface area from engine-aging at 750°C compares very well with the field-aged catalyst. The reduction of catalyst surface area from engine-aging at 850°C is much greater that of the field-aged catalyst. Although, the SEM micrographs of the engine-aged catalyst at 750°C do not look similar to those of the field-aged catalyst, the surface area comparison and NO_x performances show that engine-aging at 750°C produces similar catalyst changes to those seen in the field-aged catalyst.

The surface studies and BFR evaluations in the previous sections show that the accelerated

Table 6. Percent reduction of original catalyst surface area

	Reduction of Surface Area (%)	
Aging Conditions	Front	Rear
31 cycles at 650C	0	0
50 cycles at 750C	42	18
13 cycles at 850C		
Field-aged		

thermal aging protocol is successful in bringing about the catalyst changes seen in the field-aged catalyst. For the rear sections of the engin-aged and field-aged catalyst, it is concluded that the deactivation mechanism associated with both types of catalyst aging is primarily physical changes to the washcoat, such as loss of active iron sites and reduction of catalyst surface areas. X-ray diffraction and NO oxidation experiments indicate that zeolite dealumination is the underlying cause of catalyst degradation for both field service and accelerated thermal aging. While similar washcoat changes occur in the front sections of aged catalysts, washcoat deterioration does not appear to be the primary cause of catalyst deactivation. NO_x performance profiles suggest that some type of poisoning is affecting these catalyst sections, however, it is not identified in this study.

It is worth noting that exhaust temperatures of 850°C and higher result in an accelerated destruction of the Fe-SCR-2 catalyst and these temperatures should be avoided in automotive applications. It may be possible to obtain more comparable deactivation if aging at 650 and 750°C was carried out for longer aging times, such as 100 aging cycles or more.

CHAPTER 5 CONCLUSIONS

Accelerated thermal aging of Fe-zeolite SCR catalysts using a small single-cylinder diesel engine as well as hydrothermal aging in a bench-flow reactor are performed in order to investigate the durability and to ascertain the deactivation mechanisms of Fe-zeolite SCR catalysts. The degradation of catalytic performance and changes in surface morphology due to accelerated thermal aging are compared to those of a field-aged SCR catalyst of similar formulation for the purpose of determining accelerated aging conditions that may successfully reproduce catalyst changes resulting from field service. Due to cycle-to-cycle variation, the exhaust temperature and the composition of the engines exhaust gases can vary considerably which necessitates the use of the bench-flow reactor (BFR) to accurately evaluate the NO_x performance of the engine-aged catalysts. Catalyst evaluations are performed in accordance with the CLEERS protocol, which suggests an evaluation gas composition of 5% H_2O, 5% CO_2, 14% O_2, 350 ppm NO_x, 350 ppm NH_3 and N_2 balance at a gas hourly space velocity of 30,000 h^{-1}.

Hydrothermal aging is performed on the BFR with 28ppm SO_2 at a catalyst temperature of 670°C for a total of 64 hours as prescribed by the CLEERS protocol. Hydrothermal aging appears to have minimal effect on the NO_x performance of the Fe-zeolite SCR catalysts. The only observable difference is that the hydrothermally-aged catalyst shows significantly less NO oxidation activity than the fresh catalyst. Because NO oxidation occurs over active Fe sites, the reduction in NO oxidation activity in the hydrothermally-aged catalyst is attributed to a loss of active Fe sites in the zeolite structure. X-ray diffraction patterns of the hydrothermally-aged catalyst reveal the formation of Fe_2O_3 from the oxidation of active iron sites during aging.

The engine-based accelerated thermal aging protocol utilizes high temperature exhaust gases of 650, 750 and 850°C at the SCR inlet during active regeneration of the DPF. The front sections of the engine-aged catalysts show significant catalyst degradation in NO_x performance at all aging temperatures. It could be argued that this is due to a severe reduction of catalyst surface area as seen in the front sections of the catalysts aged at 750 and 850°C. However, the surface area of the engine-aged catalyst aged at 650°C is similar to that of a fresh catalyst, thus ruling out a decrease in catalyst surface area as the sole cause of catalyst deactivation. The similar shape of the NO_x conversion profiles observed with these catalyst sections, even at

different aging temperatures, indicates some type of catalyst poisoning. However, the cause of catalyst degradation in theses catalyst sections is not determined in this study.

There is a good relationship between NO_x performance and aging temperature seen with the rear sections of the engine-aged catalysts. The catalyst aged at 850°C shows significant deactivation during NO_x performance evaluations. The maximum NO_x conversion with 350 ppm NO in the evaluation gases is measured to be 45% in comparison to 85% with a fresh catalyst. The catalysts aged at 650 and 750°C retain good NO_x performance, showing NO_x conversions greater than 70% at evaluation temperatures between 400 and 500°C, when there is 350 ppm NO in the evaluation gases. The catalyst aged at 650°C has the best overall NO_x performance as evidenced by a NO_x conversion of 71% at 300°C in comparison to 60% with the catalyst aged at 750°C. The NO_x performances of the aged catalysts are almost fully recovered to that of a fresh catalyst upon adding NO_2 to the evaluation gases. When a mixture of 175 ppm NO and 175 ppm NO_2 is used in the evaluation gases, the rear sections of the aged catalysts perform like fresh catalysts.

There is a significant decrease of intensity of the zeolite peaks, and formation of both Fe_2O_3 and Al_2O_3 seen in the XRD patterns of the engine-aged catalysts; all of which are indicative of zeolite dealumination. Dealumination is the process in which the Al^{3+} ions migrate out of the zeolite (SiO_2-Al_2O_3) structure. This leads to irreversible deactivation of active acid sites, a partial collapse of the zeolite structure and a decrease of catalyst surface area. As the zeolite structure breaks down active cations are freed from the zeolite and they can form oxide clusters, such as Fe_2O_3.

BET surface area measurements of the rear sections of the engine-aged catalysts provide a good correlation between NO_x performance activity and catalyst surface area. Since there is not a decrease of surface area seen in the catalyst aged at 650°C, the deactivation measured with this catalyst could be attributed to a small amount of dealumination that has not affected the catalyst surface area, but has caused a slight deactivation due to a loss of active iron and Brønsted acid sites.

The surface studies and BFR evaluations of the engine-aged and field-aged catalysts show that the implemented accelerated thermal aging protocol is successful in replicating the aging conditions observed in the field-aged catalyst. Similar to the engine-aged catalysts, bench-

flow reactor evaluation of the field-aged catalyst shows that the front section of the field-aged catalyst is degraded severely, with a maximum NO_x conversion of 31% when 350 ppm NO is used in the evaluation gases. The middle and rear sections retain high NO_x conversions (>70%) between evaluation temperatures of 400 and 500°C, when 350 ppm NO is used in the evaluation gases. As seen with the engine-aged catalysts, the X-ray diffraction patterns of the field-aged catalyst sections reveal the presence of Fe_2O_3 and Al_2O_3, indicating that zeolite dealumination has occurred as a result of field-service. The de-NO_x performance of the front and rear sections of the field-aged catalyst are comparable to that of the catalyst engine-aged for 50 cycles at 750°C. However, SEM micrographs and EPMA elemental maps reveal significantly more cracking and washcoat delamination in the field-aged catalyst. It may be possible to obtain even more comparable results if engine-aging at 650 and 750°C could be carried out for longer aging times, such as 100 aging cycles or more.

The deactivation mechanisms associated with Fe-zeolite catalyst aging are primarily microstructure damage to the zeolite washcoat. BET surface area measurements and SEM micrographs of the engine-aged catalysts show that washcoat degradation intensifies with increasing aging temperature. The NO_x performances of the rear section of the engine-aged catalysts relate very well with catalyst surface area. X-ray diffraction and NO oxidation experiments suggest that dealumination of the zeolite is the cause of the washcoat degradation seen in the aged catalysts. It is known that dealumination causes catalyst deactivation through the loss of active acid sites as well as a collapse of the zeolite structure, causing a decrease of catalyst surface area.

LIST OF REFERENCES

[1] http://www.cleers.org

[2] Mori, K. "Worldwide Trends in Heavy-Duty Diesel Engine Exhaust Emission Legislation and Compliance Technologies." SAE (1997): Paper 970753.

[3] Eaton, S. Accelerated Poisoning of Diesel Oxidation Catalysts by Zinc Dialkyldithiophosphate Derived Phosphorus. Thesis. Knoxville: Univesity of Tennessee, 2006.

[4] Schaeffer, A. "The Advantage of Diesel Technology." Diesel Technology Forum. Washington DC, 2001. 1-20.

[5] E.P.A., U.S. Climate Change - Greenhouse Gas Emissions. 25 February 2008. 6 March 2008 <http://www.epa.gov/climatechange/emissions/usinventoryreport.html>.

[6] E.P.A., U.S. Climate Change - Science. 20 December 2007. 6 March 2008 <http://www.epa.gov/climatechange/science/recenttc.html>.

[7] E.P.A., U.S. Six Common Air Pollutants. 23 July 2007. 6 March 2008 <http://www.epa.gov/air/urbanair/nox/hlth.html>.

[8] E.P.A., U.S. Health and Enviromental Effects Research. 20 July 2007. 6 March 2008 <http://www.epa.gov/NHEERL/research/pm/>.

[9] DieselNet. U.S. Emissions Standards:. 2008. 12 March 2008 <http://www.dieselnet.com/standards/us/hd.html#y2004>.

[10] Emissions Advantage. "Lean NOx Catalyst (LNC)." WRAP Offroad Diesel Retrofit Guidance Document 18 November 2005: 2.IV (1-4).

[11] University of Kentucky Center for Applied Energy Research. "Investigation of Aging Mechanisms in Lean NOx Trap Catalysts." Biofuels and Enviromental Catalysis (2007).

[12] Guo, X. "Poisoning and Sulfation on Vanadia SCR Catalyst." Thesis. 2006.

[13] Miller, T. W. Investigation of the Kinetics of NO Reduction by Ammonia on an

Automotive catalyst. Thesis. Knoxville: University of Tennessee, 2005.

[14] Koebel, M. and Elsener, M. “Selective Catalytic Reduction of NO over Commercial $DeNO_x$-Catalysts: Experimental Determination of Kinetic and Thermodynamic Parameters.” Chemical Engineering Science (1997): 657-669

[15] Marangozis, J. “Comparison and Analysis of Intrinsic Kinetics and Effectiveness Factors for the Catalytic Reduction of NO with Ammonia in the Presence of Oxygen.” Industrial and Engineering Chemical Research (1992): 987-994

[16] Cundy, C., Cox, P. A. "The Hydrothermal Synthesis of Zeolites." Chemistry Review (2003): 663-702.

[17] Wickepedia. Zeolite. 13 March 2008. 28 March 2008 <http://en.wikipedia.org/wiki/Zeolite>.

[18] Delahay, G., Valade, D., Guzman-Vargas, A. and Coq, B. "Selective catalytic reduction of nitric oxide with ammonia on Fe-ZSM-5 catalysts prepared by different methods." Applied Catalysis B (2002): 149-155.

[19] Devadas, M., Krocher, O. and Wokaun, A. "Catalytic Investigation of Fe-ZSM5 in the Selective Catalytic Reduction of NOx with NH3." Reaction Kinetics Catalysis Letters (2005): 347-354.

[20] Rahkamaa-Toloen, K., Maunula, M.L., Huuhtanen, M and Keiski, R.L. "The effect of NO2 on the activity of fresh and aged zeolite catalysts in the NH3-SCR reaction." Catalysis Today (2005): 217-222.

[21] Malmberg, S., Votsmeier, M., Gieshoff,J., Soger, N., Mubmann, L., Schuler,A. and Drochner, A. "Dynamic phenomena of SCR-catalysts containing Fe-exchanged zeolites - experiments and computer simulations." Topics in Catlysis (2007): 33-36.

[22] Devadas, M., Krocher, O., Elsener, M., Wokaun, A., Mitrikas, G., Soger, N., Pfeifer, M., Demel, Y., Mussmann, L. "Characterization and catalytic investigation of Fe-ZSM5 for

urea-SCR." Catalysis Today (2007): 137-144.

[23] Sun, Q., Gao, Z., Wen, B., Sachtler, W.M.H. "Spectroscopic evidence for a nitrite intermediate in the catalytic reduction of NOx with ammonia on Fe/MFI." Catalysis Letters (2002): 1-5.

[24] Sun, Q., Gao, Z., Chen, H., Sachtler, W.M.H. "Reduction of NOx with Ammonia over Fe/MFI: Reaction Mechanism Based on Isotopic Labeling." Journal of Catalysis (2001): 89-99.

[25] Gao, Z., Sun, Q., Sachtler, W.M.H. "Adsorption complexes of O2 on Fe/MFI and their role in the catalytic reduction of NOx." Applied Catalysis (2001): 9-23.

[26] Sjovall, H., Olsson, L., Firdell, E., Blint, R.J. " Selective catalytic reduction of NOx with NH3 over Cu-ZSM-5 - The effect of changing the gas composition." Applied Catalysis (2006): 180-188.

[27] Prikhodko, V. Y. Effect of Length on Performance of Lean NOx Traps. Thesis. Knoxville: University of Tennessee, 2007.

[28] Hayes, R. E. and S.T. Kolaczkowski. Introduction to Catalytic Combustion. Gordon and Breah Science Publishers, 1997.

[29] Chen, H., Sachtler, W. M.H. "Promoted Fe/ZSM-5 catalysts prepared by sublimation: de-NOx activity and durability in H2O-rich streams." Catalysis Letters (1998): 125-130.

[30] Herman, R.G., Sale, J.W., Stenger, H.G. Jr., Lyman, C.E., Agogliati, J.E., Cai,Y., Ramachandran, B. and Choi, S."Monitoring aging and deactivation of emission abatement catalysts for selective catalytic reduction of NOx." Topics in Catalysis (2002): 251-257.

[31] Liu, Z., Yezerets, A. And Currier, N. Hydrothermal Stability of Fe/Zeolite SCR Catalyst for NOx reduction of Diesel Engine Exhaust Gas. Columbus, IN: Cummins Inc.

[32] Park, J., Park, H.J., Biak, J.H., Nam, I., Shin, C., Lee, J., Cho, B.K., O, S.H.

"Hydrothermal stability of CuZSM5 catalyst in reducing NO by NH3 for the urea selective catalytic reduction process." Journal of Catalysis (2006): 47-57.

[33] Ham, S., Nam, I. and Kim, Y. G. "Activity and Durability of Iron-exchanged Mordenite type Zeolite Catalysts for the Reduction of NO by NH3" Journal of Chemical Engineering (2000): 318-324.

[34] Guisnet, M., Ayrault, P., Countanceau, Christophe., Alvarez, Maria F., and Datka, Jerzy. "Acid properties of dealuminated beta zeolites studied by IR spectroscopy" Journal of the Chemical Society (1997): 1661-1665

[35] Zhdanov, S.P., Feoktistova, N. N., Kozlova, N. I., and Polyakova, I. G., "Thermal Stability of High-Silica zeolites of the ZSM-5 family." Plenum Publishing Corp. 1986.

[36] Kim, H., Nguyen, K., Bunting, B. G., Toops, T. and Yoon, C. S. "Rapid Aging of Lean NO_x Traps by High-Temperature Thermal Cycling" SAE (2007): Paper 2007-01-0470

[37] Smith, S. S. Reverse-Flow Oxidation Catalysts with Supplemental Fuel Injection for Lean-Burn Natural Gas Engines. Thesis. Knoxville: University of Tennessee, 2005.

[38] Youngquist, A. Development of a Rapid Ash Loading Protocol for Rapid Performance Evaluation of Diesel Particulate Filters Including Comprehensive Characterization Ash-Loaded Substrates. Thesis. Knoxville: Univeristy of Tennessee, 2008.

[39] Macdonald, R.J.,Tagleur, E.C., Wandelt, K.R.eds. Surface Science Principles and Current Applications. Berlin: Springer-Verlag, 1996.

[40] Niemantsverdriet, J.W. Spectrocopy in Catalysis an Introduction. 2nd ed. Weinheim: Wiley-VCH Verlag GmbH, 2000.

[41] Riviere, J.C. Surface Analytical Techniques. NY: Oxford UP, 1990.

[42] Brunauer, S., Emmett, P.H., Teller, E. "Adsorption of Gases in Multimolecular Layers" Journal of the American Chemical Society (1938): 309-319

[43] Batista, M.S., Morales, M.A., Baggio-Saitovich, E. and Urquieta-Gonzalez, E.A.. "Iron

Species Present in Fe/ZSM-5 Catalysts - Influence of the Preparation Method." Hyperfine Interactions (2001): 161-166.

APPENDIX

Appendix A: Temperature Histories

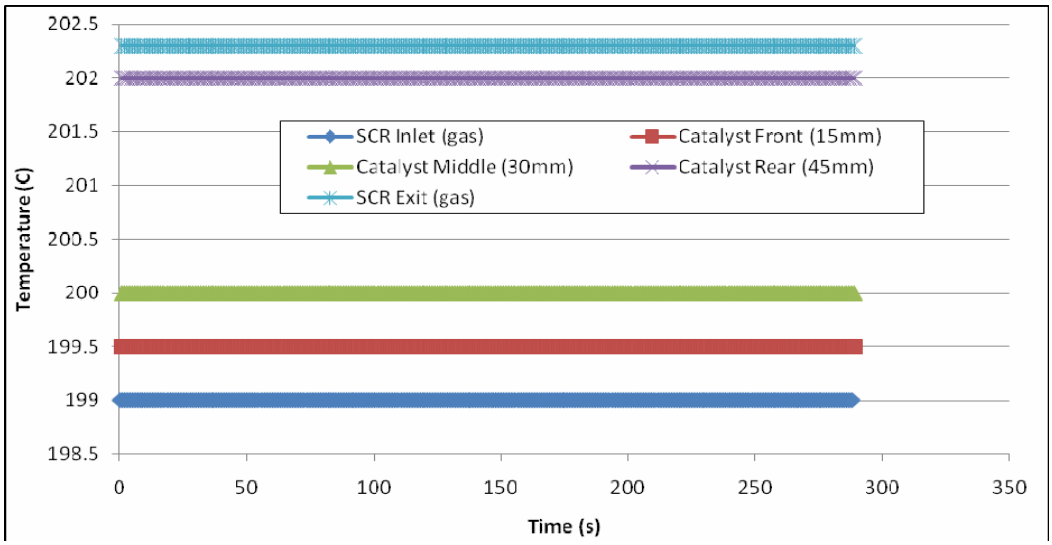

Figure AA 1. Fresh Fe-SCR-2 catalyst temperatures during NOx performance evaluation at 200°C; evaluated with 5% H_2O, 5% CO_2, 14% O_2, 350 ppm NO, 350 ppm NH_3 ($\alpha = 1$), N_2 balance, GHSV = 30,000 h^{-1}

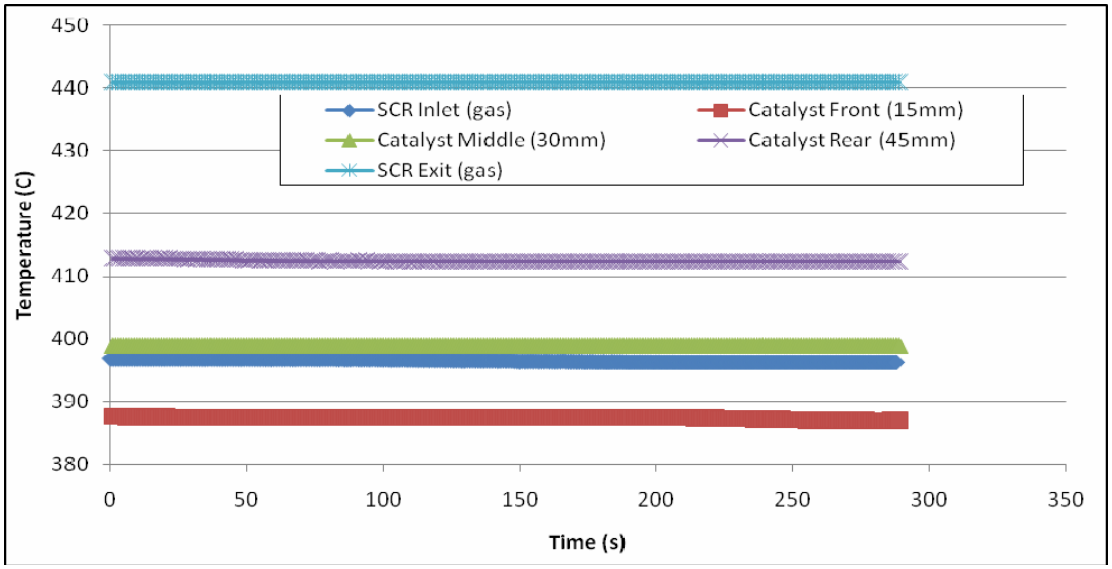

Figure AA 2. Fresh Fe-SCR-2 catalyst temperatures during NOx performance evaluation at 400°C; evaluated with 5% H_2O, 5% CO_2, 14% O_2, 350 ppm NO, 350 ppm NH_3 ($\alpha = 1$), N_2 balance, GHSV = 30,000 h^{-1}

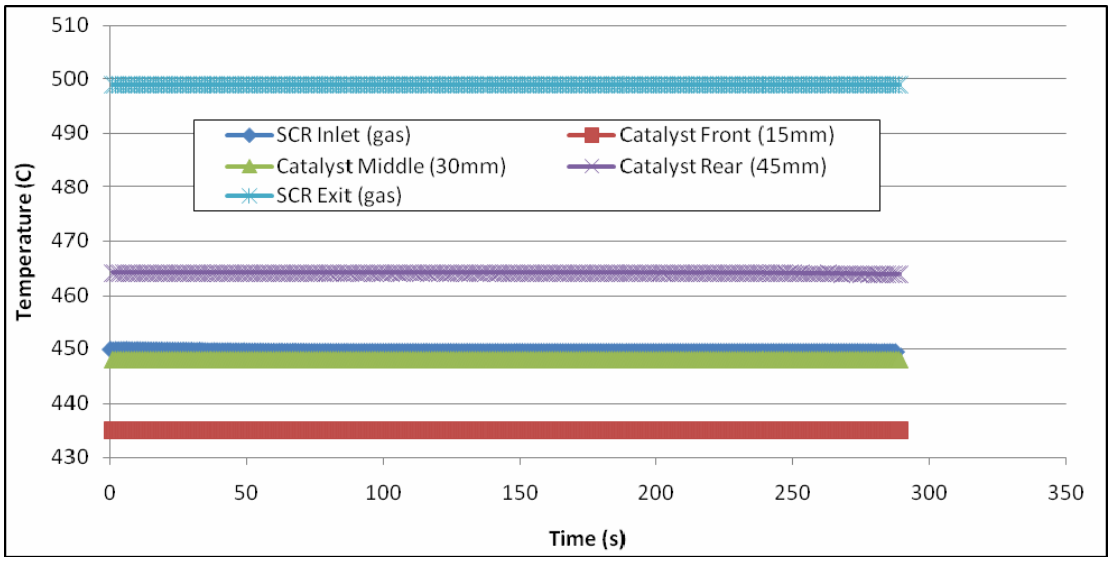

Figure AA 3. Fresh Fe-SCR-2 catalyst temperatures during NOx performance evaluation at 450°C; evaluated with 5% H_2O, 5% CO_2, 14% O_2, 350 ppm NO, 350 ppm NH_3 (α = 1), N_2 balance, GHSV = 30,000 h^{-1}

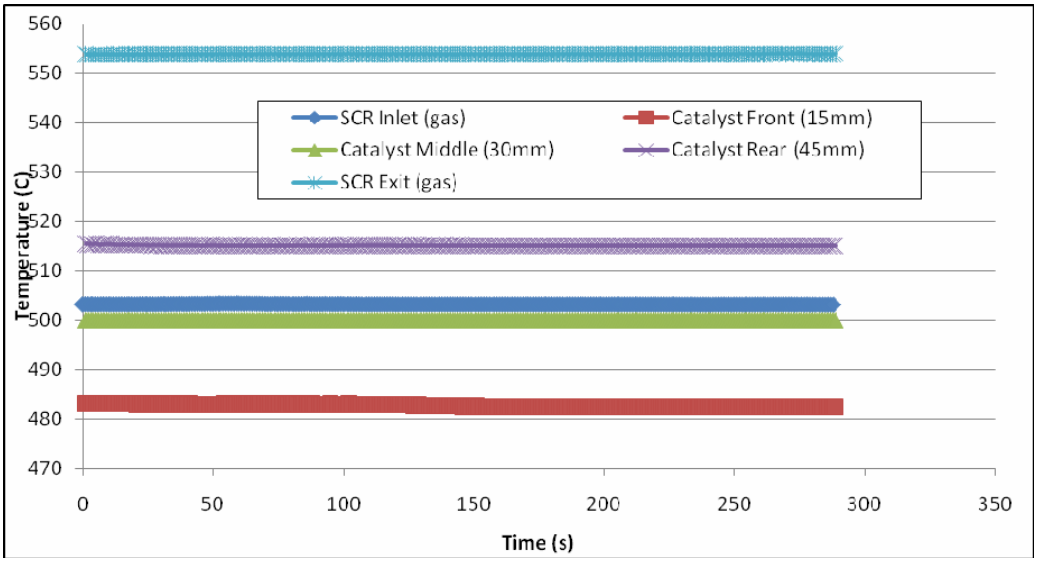

Figure AA 4. Fresh Fe-SCR-2 catalyst temperatures during NOx performance evaluation at 500°C; evaluated with 5% H_2O, 5% CO_2, 14% O_2, 350 ppm NO, 350 ppm NH_3 (α = 1), N_2 balance, GHSV = 30,000 h^{-1}

Appendix B: NH_3 Oxidation Issues

Originally, the NH_3 injection line was pointed upstream in the exhaust aftertreatement system on the engine bench. This was done to increase mixing. FTIR measurements were taken to quantify the amount of NH_3 slip that was occurring in the system at different NH_3 concentrations and determine the necessary amount of NH_3 to use during NO_x peformance evaluation on the engine bench. No NH_3 slip was measured at α ratios of 0.8 and above; however, NO_x conversion was measured to be about 50%. This meant that approximately 30% of the injected NH_3 was not accouned for. A closer look at the FTIR measurments revealed that the aftertreatment system was producing a significant amount of N_2O (≈70 ppm). It was decided that some NH_3 was reaching the DOC and catalytically oxidizing to form N_2O. The NH_3 injection line was turned around to point downstream, away from the DOC and towards the SCR catalyst. Futher FTIR measurements showed a NH_3 slip of approximately 100 ppm and no N_2O. Consequently the NO_x conversion increased to about 60%. An α ratio of 0.6 was used during NO_x performance evaluations on the engine bench, because there was no NH_3 slip at this concentration of ammonia.

VITA

Adam Foster was born in Chattanooga, TN on 3 June 1983. He graduated from the McCallie school for boys in May of 2002. Later, he graduated Summa Cum Laude from the University of Tennessee – Knoxville May 2007 with a degree in Mechanical Engineering. While in attendance, Adam became a member of Lambda Chi Alpha, Pi Tau Sigma and Tau Beta Pi. In the Summer of 2007, he attended the University of Tennessee – Knoxville where he earned his Master of Science degree of Mechanical Engineering in August of 2008.